frontiers | Research Topics

Epigenetic and genetic mechanisms underlying cardiovascular diseases and neurodevelopmental disorders

Edited by
Lingshan Gou, Dharmani Devi Murugan, Hongsong Zhang and Peng Zhang

Published in
Frontiers in Cardiovascular Medicine
Frontiers in Genetics
Frontiers in Cell and Developmental Biology
Frontiers in Neurology

ISSN 1664-8714
ISBN 978-2-8325-4767-0
DOI 10.3389/978-2-8325-4767-0

About Frontiers

Frontiers is more than just an open access publisher of scholarly articles: it is a pioneering approach to the world of academia, radically improving the way scholarly research is managed. The grand vision of Frontiers is a world where all people have an equal opportunity to seek, share and generate knowledge. Frontiers provides immediate and permanent online open access to all its publications, but this alone is not enough to realize our grand goals.

Frontiers journal series

The Frontiers journal series is a multi-tier and interdisciplinary set of open-access, online journals, promising a paradigm shift from the current review, selection and dissemination processes in academic publishing. All Frontiers journals are driven by researchers for researchers; therefore, they constitute a service to the scholarly community. At the same time, the *Frontiers journal series* operates on a revolutionary invention, the tiered publishing system, initially addressing specific communities of scholars, and gradually climbing up to broader public understanding, thus serving the interests of the lay society, too.

Dedication to quality

Each Frontiers article is a landmark of the highest quality, thanks to genuinely collaborative interactions between authors and review editors, who include some of the world's best academicians. Research must be certified by peers before entering a stream of knowledge that may eventually reach the public - and shape society; therefore, Frontiers only applies the most rigorous and unbiased reviews. Frontiers revolutionizes research publishing by freely delivering the most outstanding research, evaluated with no bias from both the academic and social point of view. By applying the most advanced information technologies, Frontiers is catapulting scholarly publishing into a new generation.

What are Frontiers Research Topics?

Frontiers Research Topics are very popular trademarks of the *Frontiers journals series*: they are collections of at least ten articles, all centered on a particular subject. With their unique mix of varied contributions from Original Research to Review Articles, Frontiers Research Topics unify the most influential researchers, the latest key findings and historical advances in a hot research area.

Find out more on how to host your own Frontiers Research Topic or contribute to one as an author by contacting the Frontiers editorial office: frontiersin.org/about/contact

Epigenetic and genetic mechanisms underlying cardiovascular diseases and neurodevelopmental disorders

Topic editors

Lingshan Gou – Xuzhou Maternity and Child Health Care Hospital Affiliated to Xuzhou Medical University, China

Dharmani Devi Murugan – University of Malaya, Malaysia

Hongsong Zhang – Nanjing Medical University, China

Peng Zhang – Longgang ENT Hospital, Institute of ENT and Shenzhen Key Laboratory of ENT, China

Citation

Gou, L., Murugan, D. D., Zhang, H., Zhang, P., eds. (2024). *Epigenetic and genetic mechanisms underlying cardiovascular diseases and neurodevelopmental disorders*. Lausanne: Frontiers Media SA. doi: 10.3389/978-2-8325-4767-0

Table of contents

frontiers | Frontiers in Genetics

TYPE Editorial
PUBLISHED 03 April 2024
DOI 10.3389/fgene.2024.1401354

OPEN ACCESS

EDITED AND REVIEWED BY
Michael E. Symonds,
University of Nottingham, United Kingdom

*CORRESPONDENCE
Hongsong Zhang,
hustzhs@alumni.hust.edu.cn
Lingshan Gou,
jifeng0241527@163.com
Peng Zhang,
zhangpeng831226@gmail.com

RECEIVED 15 March 2024
ACCEPTED 21 March 2024
PUBLISHED 03 April 2024

CITATION
Zhang P, Gou L, Murugan DD and Zhang H (2024), Editorial: Epigenetic and genetic mechanisms underlying cardiovascular diseases and neurodevelopmental disorders.
Front. Genet. 15:1401354.
doi: 10.3389/fgene.2024.1401354

Editorial: Epigenetic and genetic mechanisms underlying cardiovascular diseases and neurodevelopmental disorders

Peng Zhang[1]*, Lingshan Gou[2]*, Dharmani Devi Murugan[3] and Hongsong Zhang[4]*

[1]Shenzhen Key Laboratory of ENT, Institute of ENT and Longgang ENT Hospital, Shenzhen, China, [2]Center for Genetic Medicine, Xuzhou Maternity and Child Healthcare Hospital Affiliated to Xuzhou Medical University, Xuzhou, China, [3]Department of Pharmacology, Faculty of Medicine, Universiti of Malaya, Kuala Lumpur, Malaysia, [4]Department of Cardiology, Nanjing First Hospital, Nanjing Medical University, Nanjing, Jiangsu, China

KEYWORDS

genetics, cardiovascular disease, neurodevelopmental disorder, epigenetics, coronary artery disease

Editorial on the Research Topic
Epigenetic and genetic mechanisms underlying cardiovascular diseases and neurodevelopmental disorders

Cardiovascular diseases (CVD) and neurodevelopmental disorders (NDD) represent significant health challenges, posing severe threats to human health and quality of life. Emerging as the foremost cause of mortality and disability globally, CVD is intricately linked with a variety of factors such as chronic inflammation and genetic predispositions (Dzau and Hodgkinson, 2024). Similarly, NDD, characterized by deficits in cognitive functions, social interactions, and learning capabilities (Olson et al., 2024), demands deeper understanding of their genetic and epigenetic underpinnings. The complexities of these diseases stem from a multifaceted etiology involving DNA variants, epigenetic modifications, and environmental influences, a narrative supported by research from Srour and Shevell (2014), Homberg et al. (2016), and Hartiala et al. (2021).

Chronic inflammation plays a pivotal role in CVD, such as acute myocardial infarction (AMI) and coronary artery disease (CAD) (Liu C. et al., 2022; Lopez-Candales et al., 2017). Macrophage migration inhibitory factor (MIF) is an important pro-inflammatory cytokine implicated in the pathogenesis of CVD (Zernecke et al., 2008). *MIF* gene, located at 22q11.2, features polymorphisms such as −173 G/C polymorphism (rs755622), and −974 CATT tetranucleotide repeat (rs5844572), which may influence gene transcription and inflammatory processes. Fouda et al. conducted a meta-analysis of the MIF -173G/C variant's impact on CVD risk in 9,047 participants, revealing its association with increased CVD risk in specific populations, highlighting the genetic underpinnings of inflammation in CVD.

AMI is a life-threatening disease involving thrombosis, fibrinolysis, inflammation, and lipid metabolism. Jeon et al. identified six early-onset AMI-associated variants, notably rs12639023 as a prognostic marker for cardiac mortality. This genetic perspective is crucial for understanding AMI's complex pathogenesis. Despite extensive research, the

understanding of epigenetic alterations in endothelial cells and their implication in the etiopathology of AMI remains incomplete. Tang et al. addressed this gap by investigating DNA methylation alterations and altered gene expression profile in endothelial cells exposed to oxygen-glucose deprivation. Their findings shed light on oxygen-glucose deprivation-specific genes implicated in coronary endothelial cell injury during AMI.

CAD comprised a broad spectrum of clinical syndromes induced by inadequate blood flow to the myocardium, primarily attributed to subintimal atheroma deposition resulting in arterial stenosis, occlusion and wall thickening (Knuuti et al., 2020). MicroRNA (miRNA) orchestrate multiple crucial processes such as angiogenesis, cell proliferation, differentiation, migration, and apoptosis within the circulatory system. MiRNAs have the potential in facilitating early detection, assessing disease severity, and predicting outcomes in CAD. Lv et al. reported significantly elevated miR-183-5p levels in CAD patients across varying disease severities compared to non-CAD individuals. These results underscore the potential of serum miR-183-5p levels as a predictive biomarker for CAD presence and severity, offering valuable insights into disease progression and prognosis.

Sick Sinus Syndrome (SSS), atrial fibrillation (AF), and pulmonary arterial hypertension (PAH), also represent significant challenges within the realm of CVD. SSS arises from the sinus node dysfunction or impaired electrical impulse conduction, culminating in sinus bradycardia, sinus block, or sinus arrest (De Ponti et al., 2018). Genetic mutations have been linked to familial SSS. Liang et al., identified heterozygous mutations of *SCN5A* gene in three young familial SSS females, including novel mutation sites not previously reported in Asian patients. Advancements in genetic research have elucidated the genetic substrates of AF, with early-onset AF potentially indicating genetic atrial myopathy (Kany et al., 2021). Silva Cunha et al. reported a young AF patient with extensive atrial fibrosis and extensive areas of low voltage. Genetic analysis unveiled a homozygous pathogenic variant in *NPPA*, which was parentally inherited. This case underscores the role of genetic predispositions, particularly NPPA mutations, in AF pathogenesis and atrial fibrosis development.

Epigenetic modifications and abnormal immune microenvironment are key factors in PAH pathogenesis (Kim et al., 2015; Liu J. et al., 2022). N6-methyladenosine (m6A) RNA modification, a critical epitranscriptomic mechanism, regulates RNA biology. Gao et al. analyzed the data from the GSE117261 dataset, identifying differential expression of genes (DEGs) and m6A regulators in idiopathic PAH (IPAH) samples. Functional and pathway enrichment analyses incorporating 77 DEGs further underscored aberrant immune activity implicated in IPAH pathogenesis. Notably, histone lactylation, a novel post-translational modification, also assumes significance in PAH. Zhao et al. reviewed the role of histone lactylation in PAH, and its effects on N6-methyladenosine (m6A) and immune microenvironment. These insights offer novel perspectives into PAH diagnosis and pathogenesis.

Benign familial infantile epilepsy (BFIE), late-stage mild cognitive impairment (LMCI) and Alzheimer's disease (AD) represent critical areas of concern within neurodevelopmental and neurodegenerative disorders (Vigevano, 2005; Dakterzada et al., 2023; Sun et al., 2023). BFIE is a familial epileptic syndrome, characterized with focal seizures that may evolve to secondary generalized tonic-clonic seizures. *PRRT2* gene, encoding the proline-rich transmembrane protein 2, is a major causative gene for BFIE (Massimino et al., 2023). Gu et al. reported seven cases of BFIE effectively managed with anti-seizure medication, all stemming from pathogenic PRRT2 variants. Notably, among these variants, the frameshift variant c.397delG was novel, highlighting the importance of whole-exome sequencing in BFIE diagnosis.

In the realm of neurodegenerative diseases, the transition from late-stage mild cognitive impairment (LMCI) to AD poses a significant risk for cognitive decline (Tábuas-Pereira et al., 2016). Zhang et al. explored the association of peripheral blood methylation profiles between individuals experiencing cognitive aging and those diagnosed with LMCI. Abnormal methylation signal intensities for some genes have been identified to be related to an enhanced susceptibility to AD. These findings illuminate the complex interplay between DNA methylation patterns and gene expression regulation in the context of cognitive impairment and Alzheimer's disease progression, providing potential avenues for further exploration in diagnostic and therapeutic interventions.

In summary, the understanding of the pathogenic mechanisms underlying CVD and NDD remain incomplete due to their complex etiologies. However, the studies featured in the current Research Topic have made significant strides in unraveling these complexities. Primarily focusing on epigenetic and genetic factors, the investigations delved into the intricate etiologies and potential biomarkers crucial for diagnosing these conditions. The findings presented in these studies represent valuable contributions to the existing body of knowledge regarding the origins, progression, and diagnostic strategies for these diseases.

Author contributions

PZ: Conceptualization, Funding acquisition, Writing–original draft, Writing–review and editing, Formal Analysis, Visualization. LG: Conceptualization, Funding acquisition, Writing–original draft, Writing–review and editing. DM: Writing–original draft, Writing–review and editing. HZ: Funding acquisition, Supervision, Writing–original draft, Writing–review and editing, Formal Analysis.

Funding

The author(s) declare that financial support was received for the research, authorship, and/or publication of this article. This project was supported by grants from Nanjing Medical Science and Technology Development Project (YKK 22105); Key Medical Talents Training Project of Xuzhou (XWRCHT20220060); Shenzhen Key Medical Discipline Construction Fund (No. SZXK039).

Conflict of interest

The authors declare that the research was conducted in the absence of any commercial or financial relationships that could be construed as a potential conflict of interest.

Publisher's note

References

Dakterzada, F., Jové, M., Huerto, R., Carnes, A., Sol, J., Pamplona, R., et al. (2023). Changes in plasma neutral and ether-linked lipids are associated with the pathology and progression of Alzheimer's disease. *Aging Dis.* 14 (5), 1728–1738. doi:10.14336/AD.2023.0221

De Ponti, R., Marazzato, J., Bagliani, G., Leonelli, F. M., and Padeletti, L. (2018). Sick sinus syndrome. *Card. Electrophysiol. Clin.* 10, 183–195. doi:10.1016/j.ccep.2018.02.002

Dzau, V. J., and Hodgkinson, C. P. (2024). RNA therapeutics for the cardiovascular system. *Circulation* 149 (9), 707–716. doi:10.1161/CIRCULATIONAHA.123.067373

Hartiala, J. A., Hilser, J. R., Biswas, S., Lusis, A. J., and Allayee, H. (2021). Gene-environment interactions for cardiovascular disease. *Curr. Atheroscler. Rep.* 23 (12), 75. doi:10.1007/s11883-021-00974-9

Homberg, J. R., Kyzar, E. J., Scattoni, M. L., Norton, W. H., Pittman, J., Gaikwad, S., et al. (2016). Genetic and environmental modulation of neurodevelopmental disorders: translational insights from labs to beds. *Brain. Res. Bull.* 125, 79–91. doi:10.1016/j.brainresbull.2016.04.015

Kany, S., Reissmann, B., Metzner, A., Kirchhof, P., Darbar, D., and Schnabel, R. B. (2021). Genetics of atrial fibrillation-practical applications for clinical management: if not now, when and how? *Cardiovasc. Res.* 117 (7), 1718–1731. doi:10.1093/cvr/cvab153

Kim, J. D., Lee, A., Choi, J., Park, Y., Kang, H., Chang, W., et al. (2015). Epigenetic modulation as a therapeutic approach for pulmonary arterial hypertension. *Exp. Mol. Med.* 47 (7), e175. doi:10.1038/emm.2015.45

Knuuti, J., Wijns, W., Saraste, A., Capodanno, D., Barbato, E., Funck-Brentano, C., et al. (2020). 2019 ESC Guidelines for the diagnosis and management of chronic coronary syndromes. *Eur. Heart. J.* 41 (3), 407–477. doi:10.1093/eurheartj/ehz425

Liu, C., Sun, Z., Shali, S., Mei, Z., Chang, S., Mo, H., et al. (2022a). The gut microbiome and microbial metabolites in acute myocardial infarction. *J. Genet. Genomics.* 49 (6), 569–578. doi:10.1016/j.jgg.2021.12.007

Liu, J., Yang, P., Tian, H., Zhen, K., McCabe, C., Zhao, L., et al. (2022b). Right ventricle remodeling in chronic thromboembolic pulmonary hypertension. *J. Transl. Int. Med.* 10 (2), 125–133. doi:10.2478/jtim-2022-0027

Lopez-Candales, A., Hernández Burgos, P. M., Hernandez-Suarez, D. F., and Harris, D. (2017). Linking Chronic Inflammation with Cardiovascular Disease: From Normal Aging to the Metabolic Syndrome. *J. Nat. Sci.* 3 (4), e341.

Massimino, C. R., Portale, L., Sapuppo, A., Pizzo, F., Sciuto, L., Romano, C., et al. (2023). RRT2 related epilepsies: a gene review. *J. Pediatr. Neurol.* 21 (04), 264–272. doi:10.1055/s-0041-1728683

Olson, L., Bishop, S., and Thurm, A. (2024). Differential diagnosis of autism and other neurodevelopmental disorders. *Pediatr. Clin. North. Am.* 71 (2), 157–177. doi:10.1016/j.pcl.2023.12.004

Srour, M., and Shevell, M. (2014). Genetics and the investigation of developmental delay/intellectual disability. *Arch. Dis. Child.* 99 (4), 386–389. doi:10.1136/archdischild-2013-304063

Sun, Y., Hefu, Z., Li, B., Lifang, W., Zhijie, S., Zhou, L., et al. (2023). Plasma extracellular vesicle microRNA analysis of Alzheimer's disease reveals dysfunction of a neural correlation network. *Research* 6, 0114. doi:10.34133/research.0114

Tábuas-Pereira, M., Baldeiras, I., Duro, D., Santiago, B., Ribeiro, M. H., Leitão, M. J., et al. (2016). Prognosis of early-onset vs late-onset mild cognitive impairment: comparison of conversion rates and its predictors. *Geriatrics* 1 (2), 11. doi:10.3390/geriatrics1020011

Vigevano, F. (2005). Benign familial infantile seizures. *Brain Dev.* 27 (3), 172–177. doi:10.1016/j.braindev.2003.12.012

Zernecke, A., Bernhagen, J., and Weber, C. (2008). Macrophage migration inhibitory factor in cardiovascular disease. *Circulation* 117 (12), 1594–1602. doi:10.1161/CIRCULATIONAHA.107.729125

frontiers | Frontiers in Neurology

TYPE Original Research
PUBLISHED 09 May 2023
DOI 10.3389/fneur.2023.1135044

OPEN ACCESS

EDITED BY
Carl E. Stafstrom,
Johns Hopkins University, United States

REVIEWED BY
Cybel Mehawej,
Lebanese American University, Lebanon
André Mégarbané,
Lebanese American University, Lebanon

*CORRESPONDENCE
Daoqi Mei
✉ mdq3755@163.com
Xiaona Wang
✉ xiaonawang2015@163.com
Yaodong Zhang
✉ syek@163.com

†These authors have contributed equally to this work and share first authorship

RECEIVED 04 January 2023
ACCEPTED 18 April 2023
PUBLISHED 09 May 2023

CITATION
Gu Y, Mei D, Wang X, Ma A, Kong J, and Zhang Y (2023) Clinical and genetic analysis of benign familial infantile epilepsy caused by *PRRT2* gene variant.
Front. Neurol. 14:1135044.
doi: 10.3389/fneur.2023.1135044

Clinical and genetic analysis of benign familial infantile epilepsy caused by *PRRT2* gene variant

Yu Gu[1†], Daoqi Mei[2*†], Xiaona Wang[3*], Ang Ma[1], Jinghui Kong[3] and Yaodong Zhang[3*]

[1]Department of Pediatrics, Children's Hospital Affiliated to Zhengzhou University, Henan Children's Hospital, Zhengzhou Children's Hospital, Zhengzhou, China, [2]Department of Neurology, Children's Hospital Affiliated to Zhengzhou University, Henan Children's Hospital, Zhengzhou Children's Hospital, Zhengzhou, China, [3]Zhengzhou Key Laboratory of Pediatric Neurobehavioral, Henan Neural Development Engineering Research Center, Children's Hospital Affiliated to Zhengzhou University, Zhengzhou, China

Objective: This study presents the clinical phenotypes and genetic analysis of seven patients with benign familial infantile epilepsy (BFIE) diagnosed by whole-exome sequencing.

Methods: The clinical data of seven children with BFIE diagnosed at the Department of Neurology, Children's Hospital Affiliated to Zhengzhou University between December 2017 and April 2022 were retrospectively analyzed. Whole-exome sequencing was used to identify the genetic causes, and the variants were verified by Sanger sequencing in other family members.

Results: The seven patients with BFIE included two males and five females ranging in age between 3 and 7months old. The main clinical phenotype of the seven affected children was the presence of focal or generalized tonic–clonic seizures, which was well controlled by anti-seizure medication. Cases 1 and 5 exhibited predominantly generalized tonic–clonic seizures accompanied by focal seizures while cases 2, 3, and 7 displayed generalized tonic–clonic seizures, and cases 4 and 6 had focal seizures. The grandmother and father of cases 2, 6, and 7 had histories of seizures. However, there was no family history of seizures in the remaining cases. Case 1 carried a *de novo* frameshift variant c.397delG (p.E133Nfs*43) in the proline-rich transmembrane protein 2 (*PRRT2*) gene while case 2 had a nonsense variant c.46G>T (p.Glu16*) inherited from the father, and cases 3–7 carried a heterozygous frameshift variant c.649dup (p.R217Pfs*8) in the same gene. In cases 3 and 4, the frameshift variant was *de novo*, while in cases 5–7, the variant was paternally inherited. The c.397delG (p.E133Nfs*43) variant is previously unreported.

Conclusion: This study demonstrated the effectiveness of whole-exome sequencing in the diagnosis of BFIE. Moreover, our findings revealed a novel pathogenic variant c.397delG (p.E133Nfs*43) in the *PRRT2* gene that causes BFIE, expanding the mutation spectrum of *PRRT2*.

KEYWORDS

benign familial infantile epilepsy (BFIE), *PRRT2* gene, epilepsy syndrome, heterozygous mutations, anti-seizure medication

Introduction

Benign familial infantile epilepsy [BFIE; pyridoxine dependent epilepsy, Online Mendelian Inheritance in Man (OMIM) # 605751] is a benign familial neurological disorder with an incidence of 1 in 10,000 (1). Inheritance is autosomal dominant, and the condition is characterized by focal seizures that may progress to secondary generalized tonic–clonic seizures. The age of seizure onset in affected children usually ranges between 4 and 6 months old. The seizures usually occur in clusters and have a good prognosis and usually resolve by 2 years old (2, 3).

Benign familial infantile epilepsy is recognized as a genetically heterogeneous disorder. The *PRRT2* gene, encoding proline-rich transmembrane protein 2, is a major causative gene for BFIE. *PRRT2* located on the short arm 11.2 of chromosome 16, is mainly expressed in the nervous system, especially in the cerebral cortex, hippocampus, basal ganglia, and cerebellum (4, 5). Mutations in *PRRT2* are associated with multiple childhood-onset neurological disorders, including BFIE [(OMIM) # 605751], paroxysmal kinesigenic dyskinesia [PKD; (OMIM) # 128200], and infantile convulsions and choreoathetosis [ICCA; (OMIM) # 602066]. Other genetic mutations, including mutations in *SCN2A*, *KCNQ2*, *SCN8A*, and *ATP1A2*, have also been found to cause BFIE (6). However, these genes do not account for all cases of BFIE and the causative genes in some patients remain unknown. In this study, we summarized the clinical phenotypes of seven affected children from the Chinese Han population diagnosed with BFIE and analyzed the genetic etiologies underlying the disease in these cases.

Materials and methods

The present study was a case series study and was approved by the Medical Ethics Committee of the Children's Hospital Affiliated with Zhengzhou University. Informed consent was obtained from the children's guardians. We retrospectively analyzed the clinical data of seven children diagnosed with BFIE in the neurology outpatient ward of our hospital from December 2017 to April 2022. The diagnosis of BFIE was confirmed by clinical features and genetic diagnosis in all these patients.

The clinical data of seven children were collected. The laboratory tests included routine blood tests, tests for liver, kidney, and thyroid function, blood ammonia, pyruvate, lactate, inorganic elements, nine vitamins, ceruloplasmin, and genetic metabolic screening of the blood and urine. Scale examinations included the pediatric neuropsychological screening scale (DQ), imaging tests included cranial computed tomography (CT), and magnetic resonance imaging (MRI), and electrophysiological tests included long-range video electroencephalogram monitoring.

After obtaining informed consent from the children's guardians, 2 mL of peripheral venous blood was collected from each child and the parents into ethylenediaminetetraacetic acid tubes. Whole-exome sequencing was performed on the three members of each family and the suspected variants with clinical significance were verified in the family members using Sanger sequencing. Genetic sequencing was performed by the Beijing Zhiyin Oriental Translational Medicine Research Center Co., Ltd., and the relevant data analysis was conducted by Henan Provincial Key Laboratory of Children's Genetics and Metabolic Diseases in our hospital.

Results

Clinical characteristics

All the children experienced seizures of varying severity during infancy; details of the clinical manifestations of the children are listed in Table 1. Cases 1 and 5 mainly displayed generalized tonic–clonic seizures accompanied by focal seizures, cases 2, 3, and 7 mainly experienced generalized tonic–clonic seizures, and cases 4 and 6 showed mainly focal seizures. All the cases were effectively controlled by anti-epileptic drug treatment. The parents of the seven children were non-consanguineous. None of the parents of cases 1, 3, 4, or 5 had a history of seizures, whereas the grandmother and father of cases 2, 6, and 7 had a history of seizures. In addition, cases 3 and 5 each had a sister, and cases 2 and 6 brothers, and none of these siblings had a history of seizures (Figure 1).

Cranial MRI showed varying degrees of cerebral white matter hemi-oval central myelin hypoplasia at 6 months old in cases 1 and 4, indicating a delay in neuronal development. On the other hand, the cranial MRI showed varying degrees of frontotemporal subarachnoid widening in cases 1, 2, and 6 (Figure 2). No developmental delays in terms of growth and cognitive function compared with normal children of the same age were observed in any of the seven cases. Video electroencephalograph (EEG) testing in cases 1, 2, 4, and 5 showed varying degrees of abnormal discharge (Figure 3).

Genetic analysis

Table 2 summarizes variants observed in the *PRRT2* (NM_145239.2) gene in the seven children. Whole-exome sequencing analysis showed that among the seven probands, cases 2, 5, 6, and 7 carried variants inherited from the father, while the variants in cases 1, 3, and 4 were *de novo*. Case 1 carried a *de novo* frameshift shift variant c.397delG (p.E133Nfs*43; Figure 4), case 2 carried a nonsense variant c.46G > T (p.Glu16*), cases 3 and 4 had *de novo* frameshift variants c.649dup (p.R217Pfs*8), and all the variants in cases 5, 6, and 7 were frameshift variants c.649dup (p.R217Pfs*8). The c.397delG (p.E133Nfs*43) frameshift variant was novel and has not been reported previously. The evidence for the pathogenicity of c.397delG (p.E133Nfs*43) included PVS1, PS2, PM2, and PP3. The variant was predicted to be deleterious by multiple software programs including SIFT, Polyphen-2, and MutationTaster. According to the standards and guidelines of the ACMG (7), c.397delG (p.E133Nfs*43) was classified as a pathogenic variant. The c.649dup (p.R217Pfs*8) and c.46G > T(p.Glu16*) variants are known pathogenic variants, as reported in previous studies (8–10).

Discussion

Benign familial infantile epilepsy is an autosomal dominant epilepsy that was first reported by Vigevano et al. (11) and was named BFIE in 2010 by the International League Against Epilepsy (ILAE)

TABLE 1 Clinical data of seven children with benign familial infantile convulsions.

ID/ Sex	Age[1]	Birth history	Age[2] of onset	Types of seizures	Initial physical examination	Video EEG[3]	Head MRI[4]	Efficacy and follow-up	Evolution
1F[5]	6 months 15 days	G1P1, full term cesarean section, W: 2.8 kg, no history of asphyxia or resuscitation	4 months	(1) GTCS[6]; (2) focal seizures	W: 7 kg, HC[7]: 42 cm, fontanelle 1.5 × 2.0 cm; normal pursuit of vision and hearing; vertical head stability; and unable to sit alone	Abnormal	Delayed myelination, and bilateral frontotemporal subarachnoid space widened	LEV[8]	Control
2M[9]	4 months 13 days	G2P2 full term cesarean section, W: 3.0 kg, no history of hypoxia or asphyxia	3 months and 13 days	GTCS	W: 6 kg, HC: 39 cm, vertical head stability; poor pursuit response	Abnormal	Bilateral frontotemporal subarachnoid space widened	LEV, vitamin B6	Improvement (seizures reduced)
3F	4 months 20 days	G2P2, 38^{+5} weeks, cesarean section, W: 3.9 kg, no history of asphyxia or resuscitation	4 months and 9 days	Generalized seizure on awakening	W: 7 kg, HC: 40.5 cm, fontanelle 0.5 × 0.5 cm, head raised steadily; normal muscle strength and tone	Normal	Normal	VPA[10] → PB[11]	Control
4F	6 months 5 days	G1P1, 39 weeks normal delivery, W: 3.2 kg, no history of asphyxia or choking	6 months	Focal seizures	W: 8 kg, fontanelle 1.5 × 1.5 cm, head raised steadily; unstable sit; normal pursuit of vision and hearing; normal muscle strength and tone	Abnormal	Delayed myelination	OXC[12]	Control
5 M	5 months	G2P2, delivered at 39^{+3} weeks, W: 3.85 kg, no history of perinatal hypoxic asphyxia	4 months 10 days	(1) GTCS; (2) Focal seizures	W: 7 kg, HC: 41 cm, fontanelle 1.5 × 1.5 cm, poor tracking vision and hearing; head raised steadily at 3 months, turn over at 4 months	Abnormal	Normal	LEV, vitamin B6 tablets → OXC	Control
6F	4 months 9 days	G2P2, full term cesarean section, W: 3.85 kg, no history of perinatal hypoxic asphyxia	4 months and 3 days	Focal seizures	W: 7.5 kg, HC: 40 cm, fontanelle 1.0 × 1.0 cm	Normal	Bilateral frontotemporal subarachnoid space widened	LEV, vitamin B6 tablets → OXC	Control
7F	5 months 15 days	G2P2, full term normal birth, W: 3.6 kg, no history of asphyxia or resuscitation	5 months 10 days	GTCS	W: 7 kg, HC: 43 cm, fontanelle 2.0 × 1.5 cm, head raised steadily, normal hearing and smiling, normal muscle strength and tone	Normal	Normal	LEV, PB	Control

[1]Age, current age; [2]Age of onset, Age of first onset; [3]Video EEG, Video EEG features; [4]Head MRI, Head magnetic Resonance Imaging; [5]Female; [6]GTCS, generalized tonic–clonic seizure; [7]HC, head circumference; [8]LEV, levetiracetam; [9]M, Male; [10]VPA, valproic acid; [11]PB, phcnobarbital; and [12]OXC, oxcarbazepine.

(12). The main clinical criteria for diagnosis (13) include (1) first onset at 3–12 months old, (2) family history of benign infantile epilepsy, (3) normal psychomotor development before and after onset, (4) focal seizures, alone or followed by generalized seizures, with ≥2 seizures within 24 h, mostly cluster seizures, usually without persistent status epilepticus, (5) normal EEG background during interictal periods with Rolandic epilepsy, (6) no abnormalities in cranial imaging, (7) exclusion of convulsions due to metabolic disorders such as hypocalcemia and hypoglycemia, and (8) self-limiting seizures or seizures that respond well to antiepileptic drugs, with resolution before the age of 2 years old (14, 15). In this study, all the seven affected children were within 3–7 months old, and some of them had a family history of seizure disorders. Moreover, cases 1 and 5 mainly displayed generalized tonic—clonic seizures accompanied by focal seizures,

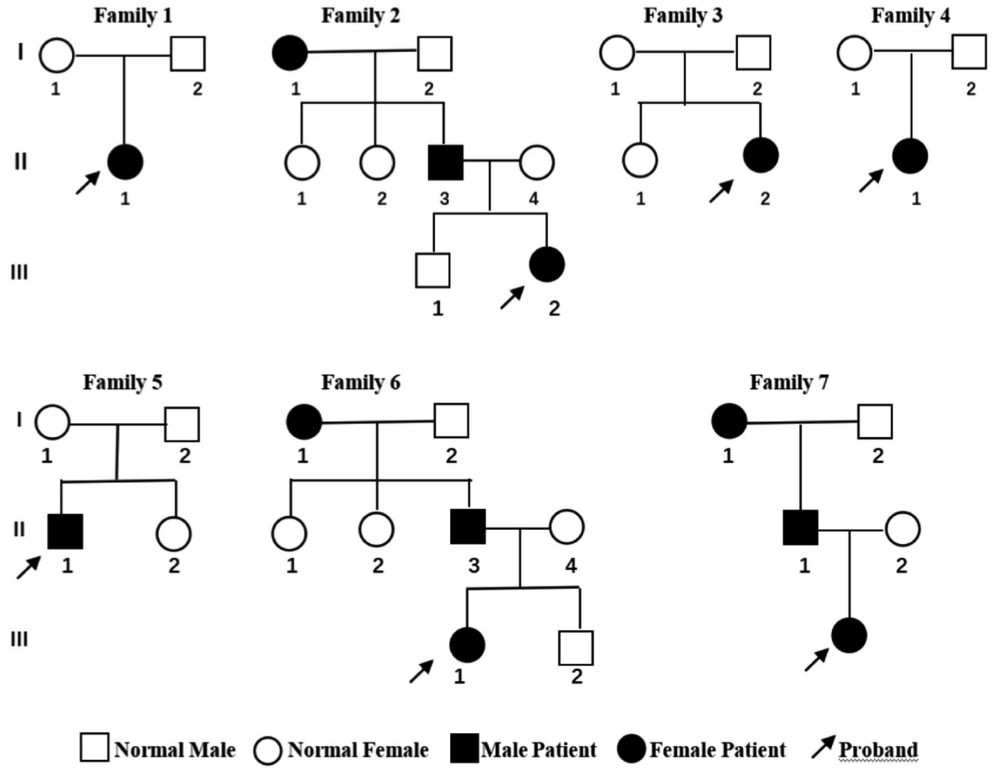

FIGURE 1
Genetic pedigree of the seven children with benign familial infantile epilepsy. Squares represent males. Circles indicate females. Black indicates a history of epilepsy. The arrows indicate the proband in the family.

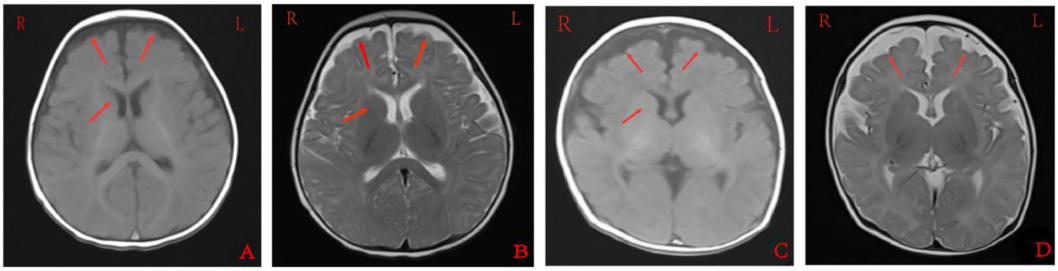

FIGURE 2
Cranial magnetic resonance imaging findings of case 1 **(A,B)** and case 2 **(C,D)**. **A** and **C** were T1 sequences, showed low signal in the widening of bilateral frontotemporal subarachnoid space, high signal in T1WI of the bilateral inner capsule forelimb, and delayed myelin sheath development compared to children of the same age. **B** and **D** were T2 sequences that showed high signal in the widening of the bilateral frontotemporal subarachnoid space, and low and fuzzy signal on T2WI of the bilateral inner capsule forelimbs. EEG: 155 new1; Amplitude: 100μV/cm; Low frequency: 0.3s; High frequency: 15Hz; Trapped wave: 50Hz; and Multi speed: 3.0cm/s.

cases 2, 3, and 7 mainly exhibited generalized tonic—clonic seizures, and cases 4 and 6 mainly displayed focal seizures. However, several of the cases in this study were found to have varying degrees of myelin dysplasia and widening of the frontotemporal subarachnoid space on cranial MRI testing.

Multiple causative genes associated with BFIE have been reported, including *PRRT2*, *SCN2A*, *KCNQ2*, *SCN8A*, *ATP1A2*, *KCNA1*, *KCNMA1*, *BFIE1*, and *BFIE4* (2, 6). *PRRT2* encodes an ion channel and was found to be a major causative gene for BFIE by Heron et al. (16). The *PRRT2* gene, located on chromosome 16p11.2, consists of four exons and encodes a protein containing 340 amino acids (17, 18). The PRRT2 protein consists of a proline-rich N-terminal sequence (N-glycosylation site), two transmembrane structural domains, and a C-terminal sequence. The transmembrane region is highly conserved and has important physiological functions (4, 19–21). *PRRT2* is mainly expressed in the presynaptic membrane and cytoplasm of neurons in the cerebral cortex, basal ganglia, cerebellum, and hippocampus. The PRRT2 protein plays a key role in neurotransmitter release by interacting with fusion complexes and calcium sensor proteins involved in synaptic vesicle cytokinesis and calcium sensitivity. Functional analysis showed that *PRRT2* knockout in excitatory neurons resulted in slowed cytokinesis kinetics, reduced

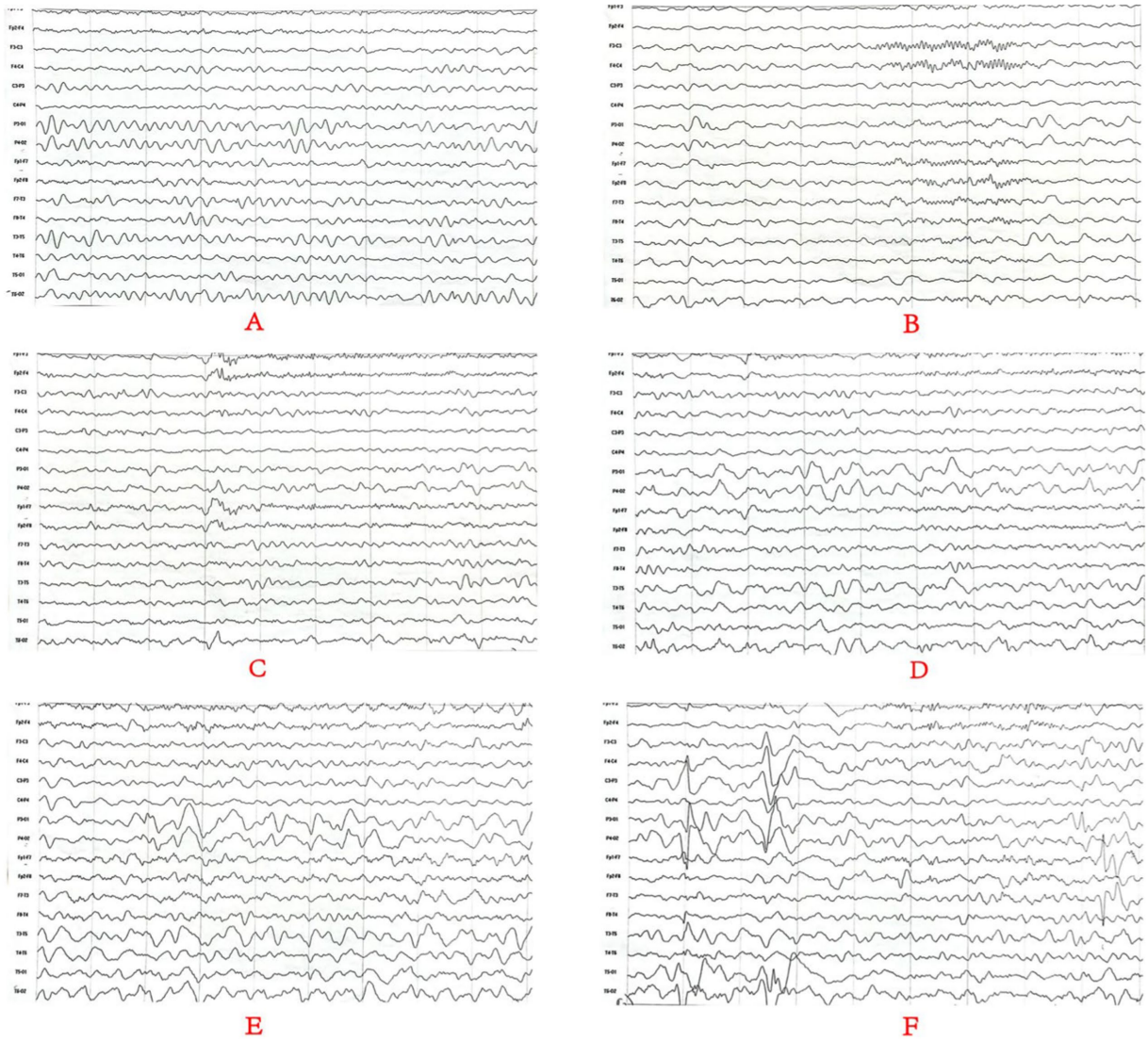

FIGURE 3
Monitoring results for the long-range video electroencephalogram of case 4. Panel **(A)** is background EEG with low-medium amplitude θ activity in the bilateral occipital area at 5–6Hz; Panel **(B)** is the EEG in the sleep stage; Panels **(C–E)** is the EEG in the attack stage and **(F)** is the EEG at the end of the attack stage. Two focal onset attacks were recorded in waking stage with a simultaneous abnormal low-medium sharp wave and sharp slow waves well as a simultaneous amplitude sharp wave and sharp slow wave.

synaptic transmission, and significantly increased susceptibility to chemotaxis. In neuronal networks, deletion of *PRRT2* was found to lead to increased spontaneous and evoked activity, resulting in dysregulation of neuronal excitability in various regions of the brain, ultimately triggering paroxysmal movement disorders and seizures (8). All of the seven patients in the present study showed seizures of varying degrees. Cases 1 and 5 had predominantly generalized tonic–clonic seizures together with focal seizures, cases 2, 3, and 7 had generalized tonic–clonic seizures, while cases 4 and 6 had focal seizures. While the grandmother and father of cases 2, 6, and 7 had a history of seizures, there was no family history of seizures in the remaining cases (Figure 1).

According to the Human Genome Variation Society (HGVS), nearly 100 variants have been reported in the *PRRT2* gene, including missense, nonsense, frameshift, splice site, deletion, and insertion variants, with the highest proportion of frameshift variants occurring mainly in exon 2, resulting in truncation and decay of the expressed protein (2). Among the *PRRT2* variants, c.649dupC is by far the most common cause of BFIE, accounting for nearly 80% of cases (8, 9, 22). In this study, all seven affected children carried heterozygous variants in exon 2 with one of the known pathogenic variants, c.649dup (p.R217Pfs*8), accounting for 71.4% (5/7) of the cases, consistent with previous reports (8, 9). Case 1 carried an unreported variant, c.397delG (p.E133Nfs*43), which was predicted to be deleterious and pathogenic by multiple software programs. Luo et al. (3) reported that seven family members carrying heterozygous mutations in the *PRRT2* gene had no clinical symptoms associated with *PRRT2*-related disorders, suggesting incomplete penetrance of the *PRRT2* mutations. In the current study, the variant in case 5 was inherited from the father who showed no clinical phenotype, also suggesting incomplete penetrance.

TABLE 2 Analysis of the PRRT2 gene variants in seven cases as follows.

Sequence	1	2	3	4	5	6	7
PRRT2 mutation	c.397delG (p.E133Nfs*43)	c.46G > T (p.Glu16*)	c.649dup(p.R217Pfs*8)	c.649dup(p.R217Pfs*8)	c.649dup(p.R217Pfs*8)	c.649dup(p.R217Pfs*8)	c.649dup(p.R217Pfs*8)
ACMG Rating	PVS1 + PS2 + PM2	PVS1 + PS2 + PM2	PVS1 + PS2 + PS4 + PP1_Strong	PVS1 + PS2 + PS4 + PP1_Strong	PVS1 + PS4 + PP1_Strong	PVS1 + PS4 + PP1_Strong	PVS1 + PS4 + PP1_Strong
Pathogenicity analysis	Pathogenic	Pathogenic	Pathogenic	Pathogenic	Pathogenic	Pathogenic	Pathogenic
Type of variation	Shift code *de novo* variant, wild type parents	Nonsense variant, source father heterozygous	Shift code *de novo* variant, wild type parents	Shift code *de novo* variant, wild type parents	Shift code variation, source father heterozygosity	Shift code variation, source father heterozygosity	Shift code variation, source father heterozygosity
Source, Phenotype	Parents without phenotype	Father has phenotype	Parents without phenotype	Parents without phenotype	Parents without phenotype	Father has phenotype	Father has phenotype

ACMG, American College of Medical Genetics and Genomics; PVS1, very strong evidence of pathogenicity; PS1, strong evidence 1 of pathogenicity; PS2, strong evidence 2 of pathogenicity; PM1, moderate evidence 1 of pathogenicity; PM2, moderate evidence 2 of pathogenicity; PP3, supporting evidence 3 of pathogenicity; and PP5, supporting evidence 5 of pathogenicity.

Proline-rich transmembrane protein 2 has analogs in various vertebrate species, such as humans, gorillas, macaques, and mice, whereas no homologs have been found in invertebrates such as nematodes (2, 4). In humans and rodents, PRRT2 is a neuroprotein that is most abundantly expressed in the cerebellum, basal ganglia, and neocortex. Mutations in *PRRT2* are associated with a variety of neurological disorders, such as BFIE, paroxysmal kinesigenic dyskinesia, and infantile convulsions and choreoathetosis, which account for more than 90% of all cases (3, 23). Other rare phenotypes, including seizures, ictal ataxia, and hemiplegic migraine, have also been reported, suggesting significant phenotypic heterogeneity resulting from *PRRT2* mutations (24–26). To date, most *PRRT2* mutations have been labeled "benign" and lead to self-limited familial infantile epilepsy. However, a small number of patients with *PRRT2* variants have been reported to exhibit severe neurological deficits, such as focal seizures and epileptic spasms, severe seizures, cognitive impairment, or complex malformations (27, 28). In general, the genotype—phenotype correlation of *PRRT2* mutations remains unclear, and there are numerous genetic variants and loci with no direct correlation between genotype and clinical phenotype. In addition to BFIE, mutations in *PRRT2* also cause paroxysmal kinesigenic dyskinesia (PKD), with a prevalence estimated at 1:150,000, characterized by recurrent episodes, transient chorea, dystonia, and/or ballismus (18). In the present study, none of the seven affected children or their family members showed any signs of PKD. Nevertheless, the development of PKD at a later stage cannot be ruled out, as the children are young. Long-term follow-up might be required to monitor the possible development of PKD.

Cranial MRI is usually nonspecific for BFIE as some patients appear normal while others show diffuse hypomyelination, a thin corpus callosum, or high signals in the basal ganglia, thalamus, or hippocampus (29). In this study, cranial MRI showed no abnormal brain changes in cases 3, 5, and 7 while in cases 1 and 4, the development of white-matter myelination was delayed. Moreover, cases 2 and 6 displayed varying degrees of widening of the subarachnoid space (Figure 2). Furthermore, previous studies have shown that interictal EEGs in BFIE are usually normal, though some BFIEs may exhibit interictal focal epileptiform discharges, mostly originating in the parieto-occipital lobe and located in the frontotemporal region (12, 30, 31). Here, we found that cases 3, 6, and 7 had no abnormal discharges on long-range video in EEG monitoring, whereas cases 1, 2, 4, and 5 displayed focal discharges of varying degrees during the interictal period. Cases 1, 2, and 5 had discharges in the frontotemporal region, consistent with previous studies (31).

In terms of treatment, most children with BFIE respond well to antiepileptic drugs, and seizures are usually completely controlled by 2 years old (9). Several studies (32) have shown that in some BFIE patients, initial treatment regimens of levetiracetam were not effective, and seizures were controlled by switching to oxcarbazepine or sodium valproate. Additionally, oxcarbazepine has fewer adverse effects and no effect on cognitive function. In the present study, the seven affected children underwent treatment and follow-up. Case 1 was well-controlled with levetiracetam while case 4 was treated with oxcarbazepine alone and remained seizure-free. Seizure control was achieved in case 3 using sodium valproate combined with phenobarbital. Although treatment with levetiracetam resulted in

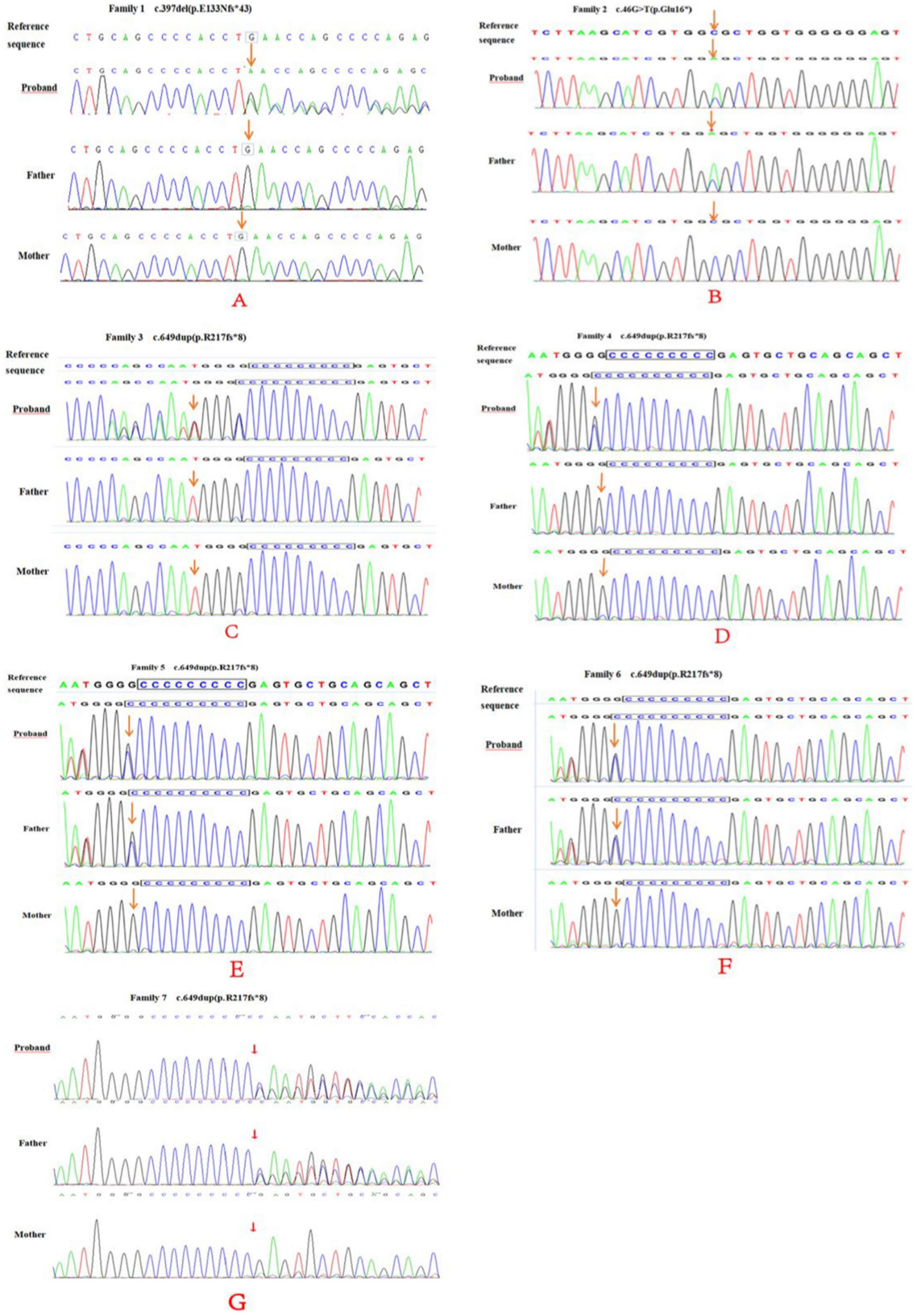

FIGURE 4
PRRT2 gene sequencing of family 1–7 **(A–E)** and their parents. Family 1 **(A)** was c.397del (p.E133Nfs*43), a frame-shift newborn mutation (arrow). No mutation was found in either parents (arrow). Family 2 **(B)** had a c.46G>T (p.Glu16*) nonsense mutation (arrow) and the father had a heterozygous mutation (arrow). Family 3 **(C)** and 4 **(D)** and 4 were c.649dup (p.R217fs*8) newborn frame-shift variation (arrow), and no mutations were found in either parents (arrow). Family 5–7 **(E–G)** and their parents showed a c.649dup (p.R217fs*8) frame-shift variation (arrow), and heterozygous variation locus for the father (arrow).

poor control in the remaining four cases, complete control was achieved after switching to oxcarbazepine, which is consistent with the findings of previous studies (32).

Early epilepsy (whether secondary or systemic) is representative of a number of disorders, often with devastating and persistent adverse consequences. Many brain malformations and inborn metabolic disorders are caused by genetic factors, such as ion channel disease, which may be associated with abnormalities in brain structure. Most children with neurometabolic disorders show some signs of disordered metabolism, which can be differentially diagnosed by genetic testing. When the diagnostic criteria are unclear, genetic testing may be the most effective means of diagnosing these diseases. Moreover, genetic testing can also guide the application of appropriate antiepileptic drugs and clinical management (33, 34). In the current study, the seizures were controlled within 2 years of age and there has been no recurrence so far in the seven affected children. In addition, the growth and language development of the seven children have been normal, and their muscle tone is normal. These results indicate that genetic testing is beneficial in the clinical diagnosis and treatment of BFIE.

Conclusion

In summary, BFIE is a genetic epilepsy with onset in the first year of life. *PRRT2* is a major causative gene of BFIE, with mutations in the gene showing an expanding clinical spectrum and incomplete penetrance. Genetic testing is critical for the diagnosis and clinical management of BFIE patients and is beneficial for prognostic prediction. Moreover, the current study identified a novel BFIE-associated variant, c.397delG (p.E133Nfs*43), in the *PRRT2* gene, thereby expanding the genetic spectrum of BFIE.

Data availability statement

The datasets presented in this study can be found in online repositories. The names of the repository/repositories and accession number(s) can be found at: https://www.ncbi.nlm.nih.gov/, SCV002760034.

Ethics statement

Written informed consent was obtained from the minor(s)' legal guardian/next of kin for the publication of any potentially identifiable images or data included in this article.

Author contributions

YG, DM, YZ, XW, AM, and JK contributed to the study conception and design and performed material preparation and data collection and analysis. The first draft of the manuscript was written by YG, DM, and YZ. XW and YZ critically revised the manuscript. All authors contributed to the article and approved the submitted version.

Funding

This work was supported by Joint Construction Project of Henan Medical Science and Technology Project (LHGJ20200618, 2018020633, and LHGJ20200640), Scientific and Technological Project of Henan (212102310034, 232102311006, and 232102310077), Henan Engineering Research Center of Childhood Neurodevelopment Open Project (SG201907), and National Natural Science Foundation of China (81901387).

Conflict of interest

The authors declare that the research was conducted in the absence of any commercial or financial relationships that could be construed as a potential conflict of interest.

Publisher's note

References

1. Symonds JD, Zuberi SM, Stewart K, McLellan A, O'Regan M, MacLeod S, et al. Incidence and phenotypes of childhood-onset genetic epilepsies: a prospective population-based national cohort. *Brain*. (2019) 142:2303–18. doi: 10.1093/brain/awz195

2. He J, Tang H, Liu C, Tan L, Xiao W, Xiao B, et al. Novel PRRT2 gene variants identified in paroxysmal kinesigenic dyskinesia and benign familial infantile epilepsy in Chinese families. *Exp Ther Med*. (2021) 21:504. doi: 10.3892/etm.2021.9935

3. Luo HY, Xie LL, Hong SQ, Li XJ, Li M, Hu Y, et al. The genotype and phenotype of proline-rich transmembrane protein 2 associated disorders in chinese children. *Front Pediatr*. (2021) 9:676616. doi: 10.3389/fped.2021.676616

4. Yang L, You C, Qiu S, Yang X, Li Y, Liu F, et al. Novel and de novo point and large microdeletion mutation in PRRT2-related epilepsy. *Brain Behav*. (2020) 10:e01597. doi: 10.1002/brb3.1597

5. Vlaskamp DRM, Callenbach PMC, Rump P, Giannini LAA, Brilstra EH, Dijkhuizen T, et al. PRRT2-related phenotypes in patients with a 16p11.2 deletion. *Eur J Med Genet*. (2019) 62:265–9. doi: 10.1016/j.ejmg.2018.08.002

6. Zara F, Specchio N, Striano P, Robbiano A, Gennaro E, Paravidino R, et al. Genetic testing in benign familial epilepsies of the first year of life: clinical and diagnostic significance. *Epilepsia*. (2013) 54:425–36. doi: 10.1111/epi.12089

7. Richards S, Aziz N, Bale S, Bick D, das S, Gastier-Foster J, et al. Standards and guidelines for the interpretation of sequence variants: a joint consensus recommendation of the American college of medical genetics and genomics and the association for molecular pathology. *Genet Med*. (2015) 17:405–24. doi: 10.1038/gim.2015.30

8. Döring JH, Saffari A, Bast T, Brockmann K, Ehrhardt L, Fazeli W, et al. The phenotypic spectrum of PRRT2-associated paroxysmal neurologic disorders in childhood. *Biomedicine*. (2020) 8:456. doi: 10.3390/biomedicines8110456

9. Zhao Q, Liu Z, Hu Y, Fang S, Zheng F, Li X, et al. Different experiences of two PRRT2-associated self-limited familial infantile epilepsy. *Acta Neurol Belg*. (2020) 120:1025–8. doi: 10.1007/s13760-020-01348-9

10. Kita M, Kuwata Y, Murase N, Akiyama Y, Usui T. A novel truncation mutation of the PRRT2 gene resulting in a 16-amino-acid protein causes self-inducible paroxysmal kinesigenic dyskinesia. *Mov Disord Clin Pract*. (2017) 4:625–8. doi: 10.1002/mdc3.12500

11. Vigevano F, Fusco L, Di Capua M, Ricci S, Sebastianelli R, Lucchini P. Benign infantile familial convulsions. *Eur J Pediatr*. (1992) 151:608–12. doi: 10.1007/bf01957732

12. Berg AT, Berkovic SF, Brodie MJ, Buchhalter J, Cross JH, van Emde BW, et al. Revised terminology and concepts for organization of seizures and epilepsies: report of

the ILAE commission on classification and terminology, 2005-2009. *Epilepsia*. (2010) 51:676–85. doi: 10.1111/j.1528-1167.2010.02522.x

13. Vigevano F. Benign familial infantile seizures. *Brain Dev*. (2005) 27:172–7. doi: 10.1016/j.braindev.2003.12.012

14. Lu JG, Bishop J, Cheyette S, Zhulin IB, Guo S, Sobreira N, et al. A novel PRRT2 pathogenic variant in a family with paroxysmal kinesigenic dyskinesia and benign familial infantile seizures. *Cold Spring Harb Mol Case Stud*. (2018) 4:a002287. doi: 10.1101/mcs.a002287

15. Zhao SY, Li LX, Chen YL, Chen YJ, Liu GL, Dong HL, et al. Functional study and pathogenicity classification of PRRT2 missense variants in PRRT2-related disorders. *CNS Neurosci Ther*. (2020) 26:39–46. doi: 10.1111/cns.13147

16. Heron SE, Grinton BE, Kivity S, Afawi Z, Zuberi SM, Hughes JN, et al. PRRT2 mutations cause benign familial infantile epilepsy and infantile convulsions with choreoathetosis syndrome. *Am J Hum Genet*. (2012) 90:152–60. doi: 10.1016/j.ajhg.2011.12.003

17. Lee EH. Epilepsy syndromes during the first year of life and the usefulness of an epilepsy gene panel. *Kor J Pediatr*. (2018) 61:101–7. doi: 10.3345/kjp.2018.61.4.101

18. Hatta D, Shirotani K, Hori Y, Kurotaki N, Iwata N. Activity-dependent cleavage of dyskinesia-related proline-rich transmembrane protein 2 (PRRT2) by calpain in mouse primary cortical neurons. *FASEB J*. (2020) 34:180–91. doi: 10.1096/fj.201902148R

19. Landolfi A, Barone P, Erro R. The spectrum of PRRT2-associated disorders: update on clinical features and pathophysiology. *Front Neurol*. (2021) 12:629747. doi: 10.3389/fneur.2021.629747

20. El Achkar CM, Rosen Sheidley B, O'Rourke D, Takeoka M, Poduri A. Compound heterozygosity with PRRT2: pushing the phenotypic envelope in genetic epilepsies. *Epilepsy Behav Case Rep*. (2019) 11:125–8. doi: 10.1016/j.ebcr.2016.12.001

21. Baldi S, Zhu JL, Hu QY, Wang JL, Zhang JB, Zhang SH. A novel PRRT2 variant in chinese patients suffering from paroxysmal kinesigenic dyskinesia with infantile convulsion. *Behav Neurol*. (2020) 2020:2097059. doi: 10.1155/2020/2097059

22. Heron SE, Dibbens LM. Role of PRRT2 in common paroxysmal neurological disorders: a gene with remarkable pleiotropy. *J Med Genet*. (2013) 50:133–9. doi: 10.1136/jmedgenet-2012-101406

23. Zeng Q, Yang X, Zhang J, Liu A, Yang Z, Liu X, et al. Genetic analysis of benign familial epilepsies in the first year of life in a Chinese cohort. *J Hum Genet*. (2018) 63:9–18. doi: 10.1038/s10038-017-0359-x

24. Fay AJ, McMahon T, Ima C, Bair-Marshall C, Niesner KJ, Li H, et al. Age-dependent neurological phenotypes in a mouse model of PRRT2-related diseases. *Neurogenetics*. (2021) 22:171–85. doi: 10.1007/s10048-021-00645-6

25. Rochette J, Roll P, Fu YH, Lemoing AG, Royer B, Roubertie A, et al. Novel familial cases of ICCA (infantile convulsions with paroxysmal choreoathetosis) syndrome. *Epileptic Disord*. (2010) 12:199–204. doi: 10.1684/epd.2010.0328

26. Becker F, Schubert J, Striano P, Anttonen AK, Liukkonen E, Gaily E, et al. PRRT2-related disorders: further PKD and ICCA cases and review of the literature. *J Neurol*. (2013) 260:1234–44. doi: 10.1007/s00415-012-6777-y

27. Pavone P, Corsello G, Cho SY, Pappalardo XG, Ruggieri M, Marino SD, et al. PRRT2 gene variant in a child with dysmorphic features, congenital microcephaly, and severe epileptic seizures: genotype-phenotype correlation? *Ital J Pediatr*. (2019) 45:159. doi: 10.1186/s13052-019-0755-2

28. Ebrahimi-Fakhari D, Saffari A, Westenberger A, Klein C. The evolving spectrum of PRRT2-associated paroxysmal diseases. *Brain*. (2015) 138:3476–95. doi: 10.1093/brain/awv317

29. Pisano T, Numis AL, Heavin SB, Weckhuysen S, Angriman M, Suls A, et al. Early and effective treatment of KCNQ2 encephalopathy. *Epilepsia*. (2015) 56:685–91. doi: 10.1111/epi.12984

30. Zorzi G, Conti C, Erba A, Granata T, Angelini L, Nardocci N. Paroxysmal dyskinesias in childhood. *Pediatr Neurol*. (2003) 28:168–72. doi: 10.1016/s0887-8994(02)00512-x

31. van Strien TW, van Rootselaar AF, Hilgevoord AA, Linssen WH, Groffen AJ, Tijssen MA. Paroxysmal kinesigenic dyskinesia: cortical or non-cortical origin. *Parkinsonism Relat Disord*. (2012) 18:645–8. doi: 10.1016/j.parkreldis.2012.03.006

32. Callenbach PM, de Coo RF, Vein AA, Arts WF, Oosterwijk J, Hageman G, et al. Benign familial infantile convulsions: a clinical study of seven dutch families. *Eur J Paediatr Neurol*. (2002) 6:269–83. doi: 10.1053/ejpn.2002.0609

33. Berg AT, Coryell J, Saneto RP, Grinspan ZM, Alexander JJ, Kekis M, et al. Early-life epilepsies and the emerging role of genetic testing. *JAMA Pediatr*. (2017) 171:863–71. doi: 10.1001/jamapediatrics.2017.1743

34. McKnight D, Morales A, Hatchell KE, Bristow SL, Bonkowsky JL, Perry MS, et al. Genetic testing to inform epilepsy treatment management from an international study of clinical practice. *JAMA Neurol*. (2022) 79:1267–76. doi: 10.1001/jamaneurol.2022.3651

frontiers | Frontiers in Cardiovascular Medicine

TYPE Case Report
PUBLISHED 08 June 2023
DOI 10.3389/fcvm.2023.1149717

OPEN ACCESS

EDITED BY
Lingshan Gou,
Xuzhou Maternity and Child Health Care Hospital Affiliated to Xuzhou Medical University, China

REVIEWED BY
Elena V. Zaklyazminskaya,
Russian National Research Center of Surgery named after B.V. Petrovsky, Russia
Cagri Gulec,
Istanbul University, Türkiye

*CORRESPONDENCE
Pedro Silva Cunha
✉ pedro.cunha@chlc.min-saude.pt

RECEIVED 22 January 2023
ACCEPTED 19 May 2023
PUBLISHED 08 June 2023

CITATION
Silva Cunha P, Antunes DO, Laranjo S, Coutinho A, Abecasis J and Oliveira MM (2023) Case report: Mutation in *NPPA* gene as a cause of fibrotic atrial myopathy.
Front. Cardiovasc. Med. 10:1149717.
doi: 10.3389/fcvm.2023.1149717

Case report: Mutation in *NPPA* gene as a cause of fibrotic atrial myopathy

Pedro Silva Cunha[1,2,3]*, Diana Oliveira Antunes[4,5], Sérgio Laranjo[1,6], Ana Coutinho[5], João Abecasis[3,6] and Mário Martins Oliveira[1,2]

[1]Arrhythmology, Pacing and Electrophysiology Unit, Cardiology Service, Santa Marta Hospital, Centro Hospitalar Universitário Lisboa Central, Lisbon, Portugal, [2]Faculdade de Medicina, Universidade de Lisboa, Lisbon, Portugal, [3]Cardiovascular Department, Hospital Lusíadas Lisboa, Lisbon, Portugal, [4]Genetics Department, Hospital Dona Estefânia, Centro Hospitalar Universitário Lisboa Central, Lisbon, Portugal, [5]GenoMed Diagnóstico Medicina Molecular, Instituto de Medicina Molecular, Lisbon, Portugal, [6]NOVA Medical School, Universidade NOVA de Lisboa, Lisbon, Portugal

Early-onset atrial fibrillation (AF) can be the manifestation of a genetic atrial myopathy. However, specific genetic identification of a mutation causing atrial fibrosis is rare. We report a case of a young patient with an asymptomatic AF, diagnosed during a routine examination. The cardiac MRI revealed extensive atrial fibrosis and the electrophysiology study showed extensive areas of low voltage. The genetic investigation identified a homozygous pathogenic variant in the *NPPA* gene in the index case and the presence of the variant in heterozygosity in both parents.

KEYWORDS

atrial fibrillation, *NPPA* gene, mutation—genetics, fibrosis, atrial myopathy

Introduction

Atrial fibrillation (AF) is a complex disease where several environmental and genetic risk factors contribute to its genesis. In recent years, rapid progress has been made in identifying the genetic basis for this highly prevalent arrhythmia.

Early-onset AF can be the manifestation of an atrial myopathy. However, specific genetic identification of a mutation causing atrial fibrosis is rare.

Here, we report a case of a young patient with atrial fibrillation and absence of previously known cardiovascular disease or cardiovascular risk factors, in which we identified a homozygous pathogenic variant in *NPPA* gene (by targeted gene panel for inherited cardiac diseases from whole-exome sequencing) and a phenotype characterised by persistent atrial fibrillation and bi-atrial extensive areas of low voltage (generalised fibrosis). This case report is exemplary of a genetic arrhythmogenic atrial cardiomyopathy.

Case report

A 31-year-old man, asymptomatic with an unremarkable medical history and regularly observed by occupational medicine, was diagnosed with atrial fibrillation (of unknown duration since a previous ECG performed 24 months before presented normal sinus rhythm) during his routine health check. He was subsequently referred to our arrhythmia department for evaluation.

The patient had no history of structural heart disease or tobacco or alcohol use. Except for irregular pulse, the physical findings were within the normal range on the baseline

examination. The surface ECG presented atrial fibrillation—with a very low voltage (**Figure 1**) -and the transthoracic echocardiography estimated the LV ejection fraction to be 65%. The left atrial dimension was 35 ml/m2.

The patient was started on oral flecainide (weight-adjusted), bisoprolol, and non-vitamin K oral anticoagulant, and four weeks later, was submitted to electrical cardioversion with success. However, one week after cardioversion, the patient resumed atrial fibrillation. The medical team discussed with the patient the state of the illness and the possible benefits and risks of various treatments. Pulmonary vein isolation was addressed in the face of the results of the EAST-AFNET 4 trial (1) that indicate a rhythm-control strategy is superior to usual care (rate control in the majority of cases) in improving CV outcomes at five years and also the results of the author's centre that reported that a single ablation procedure in patients with persistent AF, resulted in 62.2% freedom from AF at a 22-month follow-up (2). Therefore, the option for catheter ablation treatment was chosen.

Cardiac computed tomography (CT) evaluation before the electrophysiological study revealed no significant stenotic lesions in the coronary arteries and no structural heart disease, with a left atrial volume of 70 ml and a left pulmonary venous drainage pattern R2a/L1 (**Figure 2**) (3).

Ablation procedure

A three-dimensional (3D) mapping system (Carto, Biosense Webster, Diamond Bar, California) was used for electro-anatomical mapping and ablation. First, a transseptal puncture from the right atrium to the LA was completed under fluoroscopic guidance. Next, the patient underwent high-density

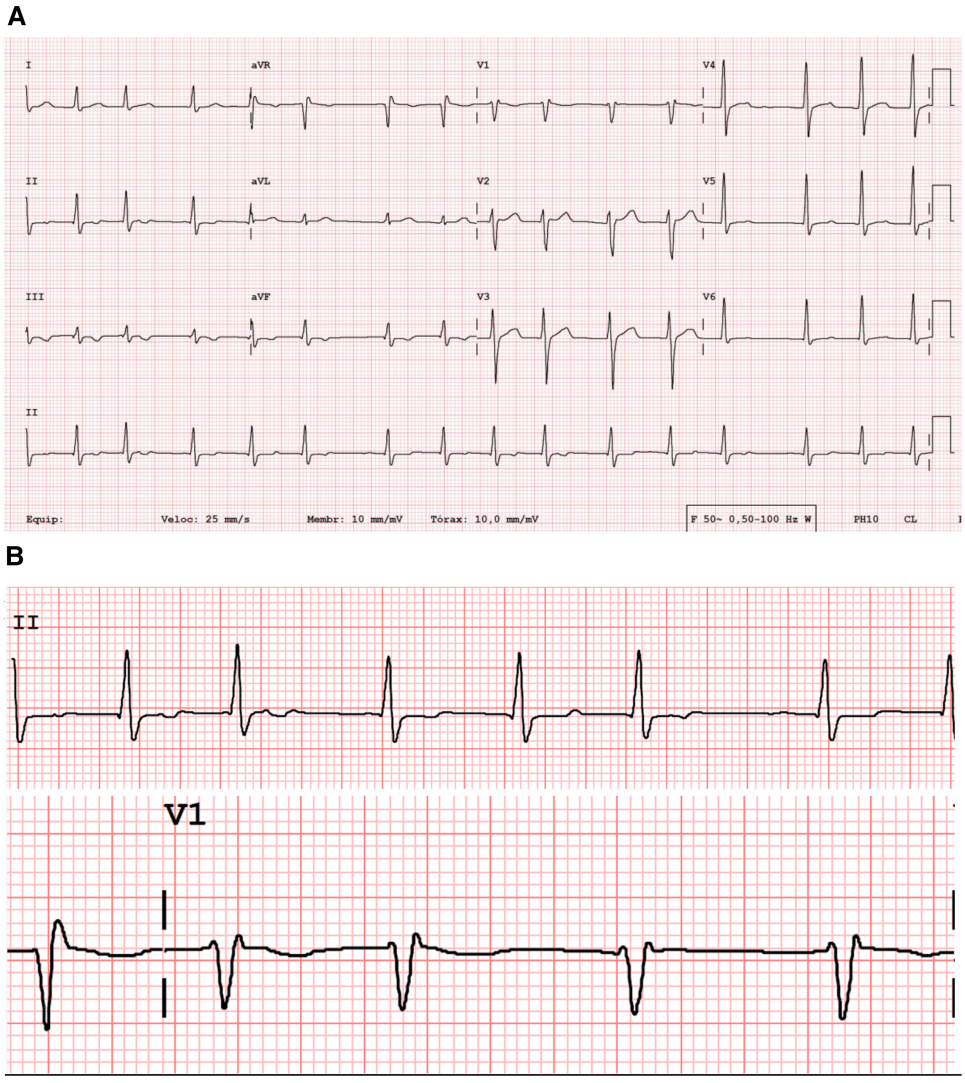

FIGURE 1
Standard 12-lead surface ECG (**A**), with a very low voltage atrial activity and irregularly irregular (with no pattern to the RR intervals) ventricular response with a rate of 92 beats/mi. QRS width of 100 msec; QTc 463 msec. Magnification of leads DII and V1 (**B**), showing almost undetectable atrial electrical activity.

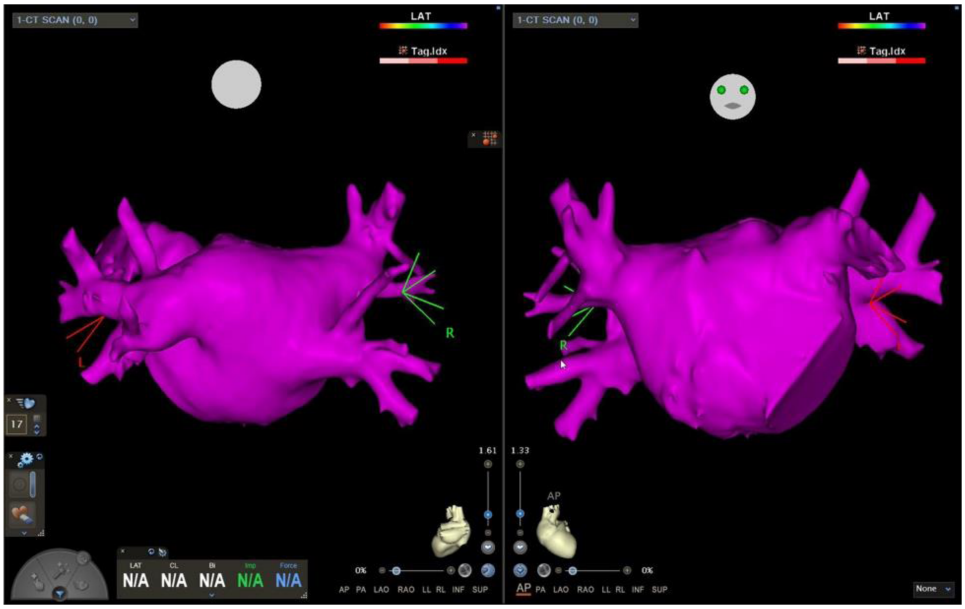

FIGURE 2
Left atrial CT scan segmentation. Cardiac computed tomography, with a left atrial volume of 70 ml and a left pulmonary venous drainage pattern R2a/L1.

mapping of bi-atrial voltage using the PentaRay multipolar catheter (Biosense Webster, Inc). In the mapping system, the cut-off values for defining low-voltage areas (LVAs) were <0.5 mV for low voltage, <0.2 mV for dense scar, and >0.5 mV for normal voltage. The voltage mapping points were obtained in atrial fibrillation before the pulmonary veins' ablation. Here, the number of points was >1,500. The right and left atrial maps revealed extensive LVAs (**Figure 3**). Wide antral pulmonary vein isolation was performed, and the patient was cardioverted at the end of the procedure. Twelve hours after the PVI and cardioversion, the AF returned. In the face of the extensive LVA, the medical team opted not to convert the arrhythmia.

Considering the clinical context of AF at a young age and extensive LVA in invasive 3D mapping, we decided to perform a genetic study.

Genetic study and results

DNA was obtained from the peripheral blood of the patient. Whole exome sequencing was performed through Next-generation sequencing with Twist human core exome plus RefSeq extension (Twist Bioscience) in Illumina NovaSeq 6,000 platform. A targeted panel for the inherited cardiac disease were analysed (in **Supplementary Material**), which revealed the variant c.449G > A, p.(Arg150Gln) in homozygosity in NPPA gene (**Figure 4**) classified as pathogenic, according to guidelines ACMG/ACGS 2020 (P—PM3_vstr, PP1_str).

Familiar segregation studies reveal the consanguinity of the parents, and the presence of the variant in heterozygosity (**Figure 5**) in both parents was confirmed. Furthermore, the asymptomatic brother was also proved to be a carrier of the variant in heterozygosity.

Follow-up

Eight months after the ablation procedure, the patient remained asymptomatic without physical activity limitation and under oral anticoagulation and bisoprolol. The rhythm recorded on the routine Holter was atrial fibrillation, confirmed by a surface electrocardiogram. In addition, cardiac magnetic resonance imaging was performed (**Figure 6**), where extensive areas of fibrosis could be identified. Eighteen months after the ablation procedure, according to the European Heart Rhythm Association (EHRA) score of AF-related symptoms, the patient classifies as score I (4, 5). Integrating the clinical context and the results of the cardiac MRI, the patient and physician accepted the presence of AF, and no further attempts to restore/maintain sinus rhythm were undertaken.

Discussion

Atrial natriuretic peptides (ANP) establish a relationship between the heart and the kidneys. ANP is a powerful hormone with natriuretic, diuretic, and hypotensive actions (6). Its secretion occurs in the right atrium as a reaction to atrial stretching due to factors like hypervolemia or hypertension. Furthermore, this hormone regulates sodium homeostasis (7), vascular remodelling, and energy metabolism (8). In addition to the functions mentioned above, ANP and B-type natriuretic

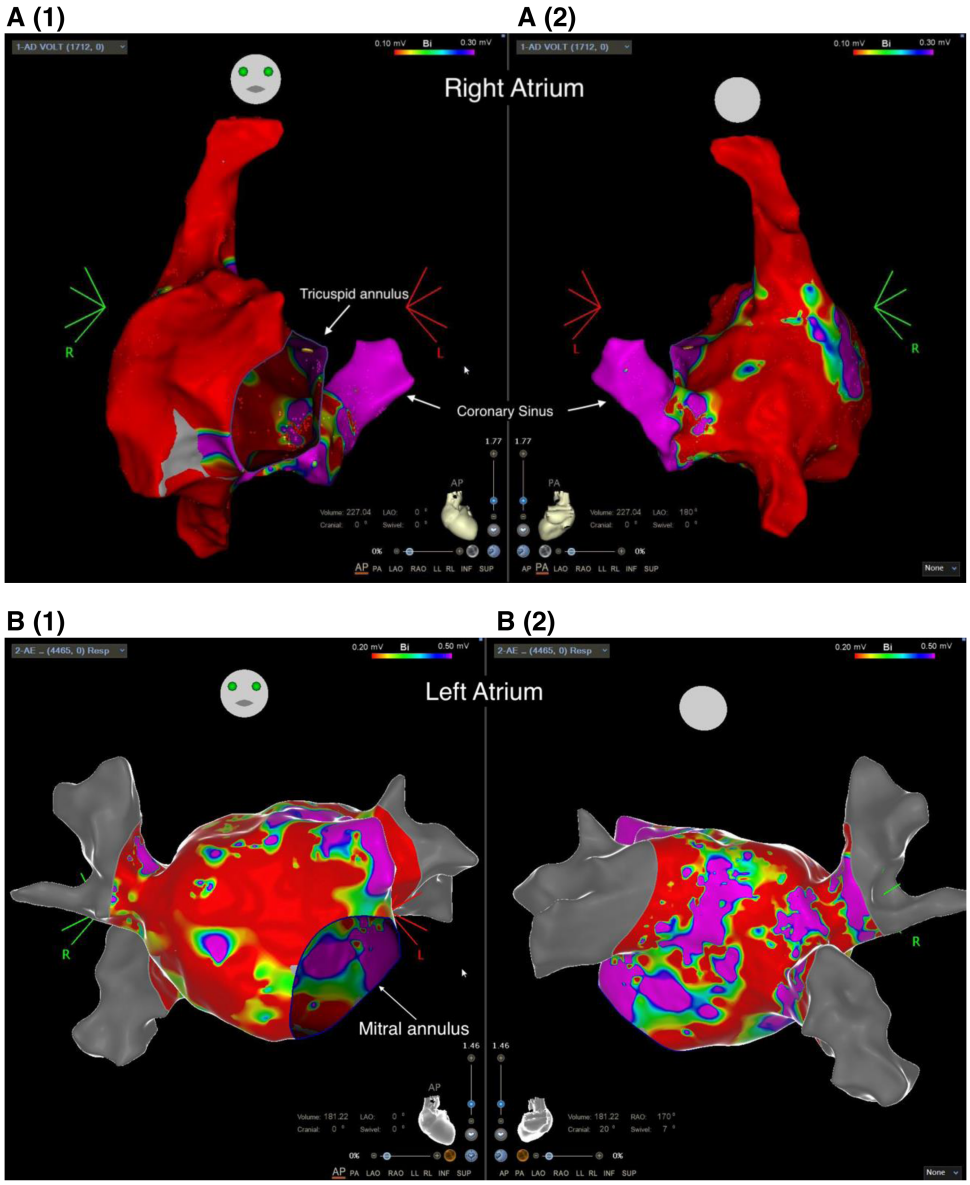

FIGURE 3
Voltage map of the right (A) and the left atrium (B), depicting extensive areas of low voltage (red) (cut-off 0.20–0.50 mV). (A1 and B1) Antero-Posterior view; (A2 and B2) posteroanterior view.

peptide (BNP) have also been shown to exert antifibrotic and antihypertrophic effects within the heart (8, 9).

ANP is encoded by the *NPPA* gene (10) located on chromosome 1 in the human genome and is primarily expressed by atrial myocytes. ANP derives from its precursors pre-pro-ANP and pro-ANP (11).

The *NPPA* gene encodes a 151-amino acid polypeptide known as preproANP. A post-translational modification process cleaves the 25 amino acid signal sequence to produce proANP, a 126 amino acid peptide stored in intracellular granules of atrial myocytes (12).

In 2008 Hodgson-Zingman et al. (13) first identified a truncating frameshift mutation in *NPPA* in a family with an autosomal dominant inheritance pattern of AF. This specific mutation caused a two-base pair deletion in exon three that eliminated the original stop codon, giving origin to 12 new amino acids to be appended to the C terminus of the mature peptide. Later, Disertori et al. (14) identified by linkage analysis a locus at 1p36.22 that contained the Natriuretic Peptide Precursor A gene and, by sequencing, identified the homozygous missense mutation (p.Arg150Gln). The same authors (14, 15) described a population of patients in whom the following clinical characteristics were observed: clinical onset in adulthood; biatrial dilatation (up to giant size); early supraventricular arrhythmias with progressive loss of atrial electric activity to an atrial standstill; thromboembolic complications; and during the long-term course of the disease a stable, normal left ventricular function.

A population-based association study in China (16) with a case-control design supported that variants in *NPPA* confer the

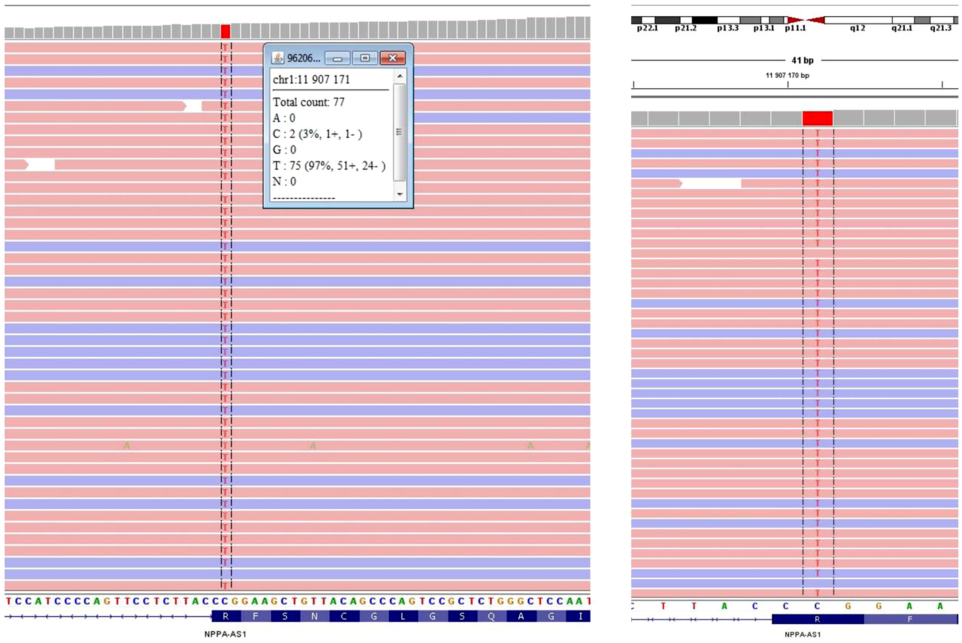

FIGURE 4
Visualization of next-generation sequencing results, showing the variant c.449G > A, p.(Arg150Gln) in the NPPA gene as homozygous in the index case.

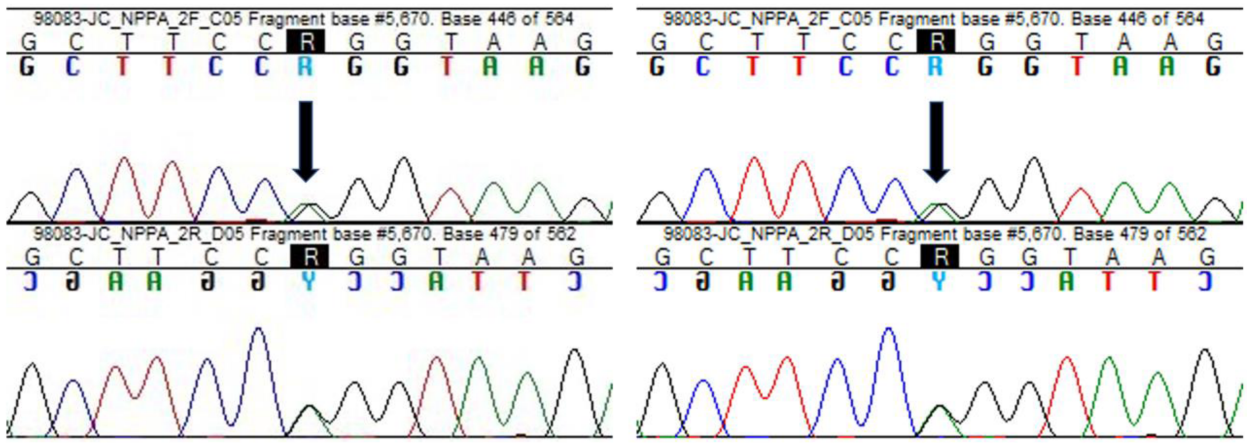

FIGURE 5
Sanger sequencing showing the variant c.449G > A, p.(Arg150Gln) in NPPA gene, identified in heterozygosity both in the father and the mother of the patient. Black arrows indicate the point mutation.

risk of lone AF. These results establish the association between a common variant (a heterozygous variant p.Ile138Thr) in *NPPA* and lone AF. Several other variants in *NPPA*, including p.Ser64Arg, p.Gln93Glu, and p.Ala117Val, were later also linked to AF (17, 18).

A study that comprehensively examined the functional consequences of the frameshift mutation of ANP (19) found data that indicate that the familial ANP mutation associated with atrial fibrillation has only minor effects on natriuretic peptide receptor interactions but markedly modifies peptide proteolysis. The authors conclude that this mutation increased the resistance of ANP to degradation, in essence causing an increase in ANP-mediated signalling. ANP exerts its effects by increasing the amounts of cyclic guanosine monophosphate (cGMP) circulating in target tissues (20).

To further study the biological implications, a group of researchers have conducted studies in mice that knocked out either the gene for ANP or the gene for natriuretic peptide receptor-A (NPR-A). Cheng et al. (21) demonstrated that AF-associated human variant p.Ile138Thr in natriuretic peptide A (*NPPA*) encoding the atrial natriuretic peptide (ANP) causes inflammation, fibroblast activation, atrial fibrosis, and AF in knock-in (KI) rats. This variant inhibits the interaction between ANP and its receptor and reduces intracellular cGMP levels. Although the exact molecular mechanisms are still unclear, this

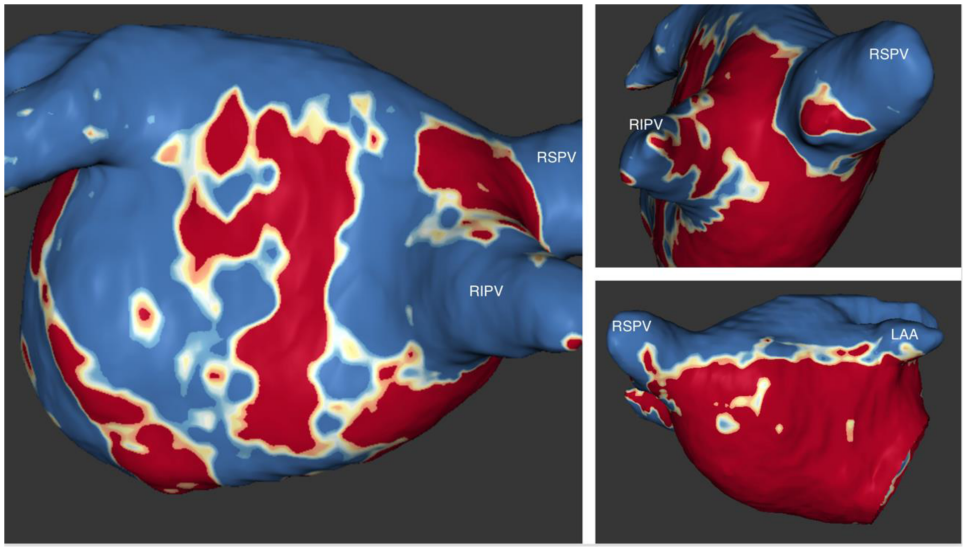

FIGURE 6
Images from late gadolinium enhancement (LGE) MRI. Fibrosis assessment with the ADAS 3 D software. The three-dimensional LA model from MRI shows extensive areas of fibrosis (dense scar) involving the posterior wall and the anterior and septal walls. LAA, left atrial appendage; RSVP, right superior pulmonary vein; RIPV, right inferior pulmonary vein.

study observed that mutant ANP activates multiple innate immunity pathways, including TNF-α, NF-κB, and IL-1β signalling. In addition, the mutant ANP induces cardiac fibroblast (CFs) differentiation to myofibroblasts and promotes CF proliferation and fibrosis. These results suggest that *NPPA* variant p.Ile138Thr causes AF by starting innate immunity by inflammasome activation (22).

In the above-described clinical case, the knowledge of the genetic variant is essential, leading us to make therapeutic options based on similar variants reported in the literature. For instance, even though the patient had a CHADS-VASC risk score of 0, it was decided to maintain life-long oral anticoagulation given the information from the study by Disertori et al. (14), in which 13 members of a family were followed for 37 years, and one of the complications reported was the occurrence of thromboembolic events.

Our clinical case is unique since it has extensive documentation of atrial myopathy through invasive intracavitary tissue voltage assessment (endocavitary mapping with the 3D CARTO system) and the evaluation by magnetic resonance imaging displaying fibrotic areas. The recognition of extensive atrial fibrosis represents essential data in the clinical decision since the dependence of marked disease on the substrate is apparent as the cause of atrial fibrillation. Therefore, the repetition of the catheter ablation would be superfluous in the approach of this specific case.

This case report highlights two fundamental aspects of the approach to the patient with atrial fibrillation. The first is the need to assess the presence of structural atrial disease, and the second is the etiological investigation.

In persistent AF pathogenesis, atrial structural remodelling is essential and mainly involves fibrosis (23, 24). Therefore, assessing the extension and degree of atrial fibrosis is crucial in determining treatment options, predicting long-term evolution, and evaluating the substrate critical in the pathophysiology of atrial thrombogenesis.

The exposed clinical case also represents an example of deep etiological investigation, leading to identifying a rare genetic cause. This identification is essential in the genetic counselling of the patient and the broader contribution to the knowledge of the etiopathogenesis of atrial fibrillation.

In the upcoming years, it is expected to identify other AF-related genes in more extensive association studies, exome sequencing, and genome sequencing studies (25).

Not only the investigation of large populations will form the basis for the advancement of knowledge in this area, but we also believe that the reporting of clinical cases, such as the one we carry out in this article, also represents a contribution to advance in medical knowledge since a large part of the phenotype of specific genes is uncertain. Furthermore, retrospective information on other patients with the same genetic alterations is essential for prognosis.

Data availability statement

The datasets for this article are not publicly available due to concerns regarding participant/patient anonymity. Requests to access the datasets should be directed to the corresponding author.

Ethics statement

Written informed consent was obtained from the individual(s) for the publication of any potentially identifiable images or data included in this article.

Author contributions

PS, DA, AC, and MO: conceived the study. PS and DA: drafted the manuscript. MO: checked it and performed critical revision. All authors contributed to the article and approved the submitted version.

Conflict of interest

The authors declare that the research was conducted in the absence of any commercial or financial relationships that could be construed as a potential conflict of interest.

Publisher's note

Supplementary material

The Supplementary Material for this article can be found online at: https://www.frontiersin.org/articles/10.3389/fcvm.2023.1149717/full#supplementary-material

References

1. Kirchhof P, Camm AJ, Goette A, Brandes A, Eckardt L, Elvan A, et al. Breithardt G; EAST-AFNET 4 trial investigators. Early rhythm-control therapy in patients with atrial fibrillation. *N Engl J Med*. (2020) 383(14):1305–16. doi: 10.1056/NEJMoa2019422

2. Silva Cunha P, Fonseca P, Laranjo S, Montenegro Sá F, Tereno Valente B, Portugal G, et al. Clinical outcome of a single procedure cryoballoon ablation for the treatment of atrial fibrillation: a real-world multicenter experience in Portugal. *Rev Port Cardiol*. (2023) 42(4):363–70. English, Portuguese. doi: 10.1016/j.repc.2022.02.012

3. Marom EM, Herndon JE, Kim YH, McAdams HP. Variations in pulmonary venous drainage to the left atrium: implications for radiofrequency ablation. *Radiology*. (2004) 230(3):824–9. doi: 10.1148/radiol.2303030315

4. Kirchhof P, Auricchio A, Bax J, Crijns H, Camm J, Diener HC, et al. Outcome parameters for trials in atrial fibrillation: recommendations from a consensus conference organized by the German atrial fibrillation competence NETwork and the European heart rhythm association. *Europace*. (2007) 9:1006–23. doi: 10.1093/europace/eum191

5. Wynn GJ, Todd DM, Webber M, Bonnett L, McShane J, Kirchhof P, et al. The European Heart Rhythm Association symptom classification for atrial fibrillation: validation and improvement through a simple modification. *EP Europace*. (2014) 16(7):965–72. doi: 10.1093/europace/eut395

6. Tsukada T, Takei Y. Integrative approach to osmoregulatory action of atrial natriuretic peptide in seawater eels. *Gen Comp Endocrinol*. (2006) 147(1):31–8. doi: 10.1016/j.ygcen.2005.09.009

7. Birkenfeld AL, Boschmann M, Moro C, Adams F, Heusser K, Franke G, et al. Lipid mobilisation with physiological atrial natriuretic peptide concentrations in humans. *J Clin Endocrinol Metab*. (2005) 90(6):3622–8. doi: 10.1210/jc.2004-1953

8. Nakagawa Y, Nishikimi T, Kuwahara K. Atrial and brain natriuretic peptides: hormones secreted from the heart. *Peptides*. (2019) 111:18–25. doi: 10.1016/j.peptides.2018.05.012

9. Potter LR, Abbey-Hosch S, Dickey DM. Natriuretic peptides, their receptors, and cyclic guanosine monophosphate-dependent signalling functions. *Endocr Rev*. (2006) 27(1):47–72. doi: 10.1210/er.2005-0014

10. Song W, Wang H, Wu Q. Atrial natriuretic peptide in cardiovascular biology and disease (NPPA). *Gene*. (2015) 569(1):1–6. doi: 10.1016/j.gene.2015.06.029

11. Da Silva GJJ, Altara R, Booz GW, Cataliotti A. Atrial natriuretic peptide: a novel therapeutic factor for cardiovascular diseases. *Front Physiol*. (2021) 12:691407. doi: 10.3389/fphys.2021.691407

12. Fu S, Ping P, Wang F, Luo L. Synthesis, secretion, function, metabolism and application of natriuretic peptides in heart failure. *J Biol Eng*. (2018) 12:2. doi: 10.1186/s13036-017-0093-0

13. Hodgson-Zingman DM, Karst ML, Zingman LV, Heublein DM, Darbar D, Herron KJ, et al. An atrial natriuretic peptide frameshift mutation in familial atrial fibrillation. *N Engl J Med*. (2008) 359:158–65. doi: 10.1056/NEJMoa0706300

14. Disertori M, Quintarelli S, Grasso M, Pilotto A, Narula N, Favalli V, et al. Autosomal recessive atrial dilated cardiomyopathy with standstill evolution associated with mutation of natriuretic peptide precursor A. *Circ Cardiovasc Genet*. (2013) 6:27–36. doi: 10.1161/CIRCGENETICS.112.963520

15. Disertori M, Guarnerio M, Vergara G, Del Favero A, Bettini R, Inama G, et al. Familial endemic persistent atrial standstill in a small mountain community: a review of eight cases. *Eur Heart J*. (1983) 4(5):354–61. doi: 10.1093/oxfordjournals.eurheartj.a061473

16. Ren X, Xu C, Zhan C, Yang Y, Shi L, Wang F, et al. Identification of NPPA variants associated with atrial fibrillation in a Chinese GeneID population. *Clin Chim Acta*. (2010) 411(7-8):481–5. doi: 10.1016/j.cca.2009.12.019

17. Olesen MS, Andreasen L, Jabbari J, Refsgaard L, Haunsø S, Olesen SP, et al. Very early-onset lone atrial fibrillation patients have a high prevalence of rare variants in genes previously associated with atrial fibrillation. *Heart Rhythm*. (2014) 11(2):246–51. doi: 10.1016/j.hrthm.2013.10.034

18. Ritchie MD, Rowan S, Kucera G, Stubblefield T, Blair M, Carter S, et al. Chromosome 4q25 variants are genetic modifiers of rare ion channel mutations associated with familial atrial fibrillation. *J Am Coll Cardiol*. (2012) 60:1173–81. doi: 10.1016/j.jacc.2012.04.030

19. Dickey DM, Yoder AR, Potter LR. A familial mutation renders atrial natriuretic peptide resistant to proteolytic degradation. *J Biol Chem*. (2009) 284:19196–202. doi: 10.1074/jbc.M109.010777

20. Yan W, Wu F, Morser J, Wu Q. Corin, a transmembrane cardiac serine protease, acts as a pro-atrial natriuretic peptide-converting enzyme. *Proc Natl Acad Sci U S A*. (2000) 97:8525–9. doi: 10.1073/pnas.150149097

21. Cheng C, Liu H, Tan C, Tong D, Zhao Y, Liu X, et al. Mutation in NPPA causes atrial fibrillation by activating inflammation and cardiac fibrosis in a knock-in rat model. *FASEB J*. (2019) 33(8):8878–91. doi: 10.1096/fj.201802455RRR

22. Iwasaki YK, Nishida K, Kato T, Nattel S. Atrial fibrillation pathophysiology: implications for management. *Circulation*. (2011) 124:2264–74. 14. doi: 10.1161/CIRCULATIONAHA.111.019893

23. Lo LW, Chen SA. Role of atrial remodeling in patients with atrial fibrillation. *J Chin Med Assoc*. (2007) 70:303–9. doi: 10.1016/S1726-4901(08)70010-8

24. Cunha PS, Laranjo S, Heijman J, Oliveira MM. The atrium in atrial fibrillation—a clinical review on how to manage atrial fibrotic substrates. *Front Cardiovasc Med*. (2022) 9:879984. doi: 10.3389/fcvm.2022.879984

25. Christophersen I, Ellinor P. Genetics of atrial fibrillation: from families to genomes. *J Hum Genet*. (2016) 61:61–70. doi: 10.1038/jhg.2015.44

frontiers | Frontiers in Cardiovascular Medicine

TYPE Original Research
PUBLISHED 15 June 2023
DOI 10.3389/fcvm.2023.1196348

OPEN ACCESS

EDITED BY
Hongsong Zhang,
Nanjing Medical University, China

REVIEWED BY
Yu Du,
Capital Medical University, China
Yake Lou,
Second Affiliated Hospital of Chongqing Medical University, China
Ruiyan Pan,
Weifang Medical University, China

*CORRESPONDENCE
Guangping Li
✉ tic_tjcardiol@126.com

†These authors have contributed equally to this work

RECEIVED 29 March 2023
ACCEPTED 10 May 2023
PUBLISHED 15 June 2023

CITATION
Lv D, Guo Y, Zhang L, Li X and Li G (2023) Circulating miR-183-5p levels are positively associated with the presence and severity of coronary artery disease.
Front. Cardiovasc. Med. 10:1196348.
doi: 10.3389/fcvm.2023.1196348

Circulating miR-183-5p levels are positively associated with the presence and severity of coronary artery disease

Dong Lv[1,2†], Yanfu Guo[3,4†], Li Zhang[5], Xia Li[2] and Guangping Li[1*]

[1]Department of Cardiology, Tianjin Key Laboratory of Lonic-Molecular Function of Cardiovascular Disease, Tianjin Institute of Cardiology, The Second Hospital of Tianjin Medical University, Tianjin, China, [2]Department of Cardiology, Beijing Renhe Hospital, Beijing, China, [3]Department of Clinical Medicine, Graduate School of Jiamusi University, Heilongjiang, China, [4]Department of Cardiology, Hegang People's Hospital, Heilongjiang, China, [5]Department of Clinical Medicine, Jiamusi University, Heilongjiang, China

Background: Serum miR-183-5p levels are associated with carotid atherosclerosis, while less is known about the relationship between circulating miR-183-5p levels and stable coronary artery disease (CAD).
Methods: In this cross-sectional study, consecutive patients with chest pain who underwent coronary angiograms from January 2022 to March 2022 at our center were enrolled. Those presenting acute coronary syndrome or had a prior CAD were excluded. Clinical presentations, laboratory parameters, and angiographic findings were collected. Serum miR-183-5p levels were measured using quantitative real-time polymerase chain reaction. CAD severity was displayed as the number of diseased vessels and further evaluated by the Gensini score system.
Results: Overall, 135 patients (median age, 62.0 years; male, 52.6%) were included in the present study. Stable CAD was identified in 85.2% of the study population, with 45.9% having 1-vessel disease, 21.5% having 2-vessel disease, and 17.8% having 3-vessel or left main disease. Serum miR-183-5p levels were significantly increased in CAD patients with different severities than non-CAD patients (all adjusted $p < 0.05$). Serum miR-183-5p levels increased as tertiles of the Gensini score progressed (all adjusted $p < 0.05$). Importantly, serum miR-183-5p levels could predict the presence of CAD and 3-vessel or left main disease in the receiver operating characteristic curve analysis (both $p < 0.01$), and also in multivariate analysis adjusting for age, sex, body mass index, diabetes, hypersensitive-C-reactive protein (both $p < 0.05$).
Conclusion: Serum miR-183-5p levels are independently and positively correlated with CAD presence and severity.

KEYWORDS

miR-183-5p, coronary artery disease, severity, Gensini score, association

Introduction

Coronary artery disease (CAD) remains a major cause of mortalities and morbidities worldwide (1). Approximately 11% of adults ≥ 45 years and 17% of adults ≥ 65 years are probably to have CAD, and around 800,000 suffer a myocardial infarction (MI) every year in the U.S. (2). In 2018, CAD mortality was 365,744 and MI mortality was 108,610 in the U.S. (2). These lead to a significant healthcare burden, expected to increase to > $177 billion by 2040 in the U.S. (3). Importantly, in-hospital mortality did not improve in patients with ST-segment elevation MI (STEMI) undergoing percutaneous coronary intervention (PCI) (4). Similarly, overall mortality of acute MI continued to increase since

2002 in both the urban and rural area of China. Given the increasing prevalence of CAD and its risk factors (e.g., advanced age, obesity), there is an unmet need to discover an optimal biomarker predicting the presence and severity of CAD.

MicroRNA (miRNA or miR) has been known to regulate gene expression at the post-transcriptional level (5). More than half of human protein-coding genes are estimated to be modulated by miRNA, given one miRNA can regulate the expression of several transcripts (6). Moreover, miRNA can influence cell proliferation, differentiation, and death in the circulatory system (7). Meanwhile, several circulating miRNAs have shown promising for early detection, severity evaluation, and outcome prediction of CAD (8).

miR-183-5p is already known as an oncomir, highly expressed in tumor tissues (9–11). Recently publications revealed that patients with carotid atherosclerosis had higher serum miR-183-5p levels compared with health individuals (12, 13). Meanwhile, elevated expression of circulating miR-183-5p was also detected in both patients with acute coronary syndrome (ACS) and non-ST-segment elevation MI (NSTEMI) (14, 15). Thus, circulating miR-183-5p could potentially be a promising biomarker for atherosclerotic and/or thrombotic disease. However, serum miR-183-5p levels have never been investigated in patients with stable CAD, the most common category of CAD. To fill this gap, we performed this cross-sectional study to examine the relationship between serum miR-183-5p levels and the presence of CAD, as well as the severity of CAD.

Material and methods

Study population and sample

We prospectively enrolled consecutive patients with chest pain who underwent invasive coronary angiograms to determine the presence of stable CAD from January 2022 to March 2022 at Beijing Renhe Hospital, Beijing, China. Patients were excluded from the present study if they had: (1) age < 18 or ≥ 80 years old; (2) history of established arteriosclerotic cardiovascular disease (ASCVD) or vascular revascularization; (3) ACS at this admission; (4) major organ failure (e.g., heart, liver, kidney); (5) active infectious disease, autoimmune diseases, and malignancy.

Fasting venous blood was collected for measuring plasma total triglyceride, total cholesterol, low-density lipoprotein cholesterol (LDL-C), glycosylated hemoglobin, creatinine, and hypersensitive-C-reactive protein (hs-CRP). The blood serum was isolated and stored at −80°C. We also collected the patient's clinical characteristics and risk factors for CAD. Body mass index (BMI) was calculated as weight divided by the square height. Echocardiography was used to evaluate cardiac function and structure using a GE ViVid E7 ultrasonography (GE Healthcare, USA). This study was approved by the Ethics Committee of Beijing Renhe Hospital (RH20220103), and performed following the Declaration of Helsinki. Written informed consent was obtained from all participants.

Quantitative real-time polymerase chain reaction

Total RNA was extracted from the preserved serum samples using Trizol reagent (Invitrogen, USA). RNA (0.5 μg) was reverse transcribed with PrimeScript RT Reagent Kit (Takara, Japan). Then, quantitative real-time polymerase chain reaction (qRT-PCR) was performed using the CFX Real-Time PCR Detection System (Bio-Rad, USA). The thermocycling amplification protocol was as follows: denaturation at 95°C for 3 min, followed by 40 cycles of 95°C for 15 s and 30 s at 60°C. Expression of miR-183-5p was calculated based on the $2^{-\Delta\Delta Ct}$ method. The primer sequences were as follows: miR-183-5p, forward 5′-CGCGGTATGGCACT GGTAGA-3′, reverse 5′-AGTGCAGGGTCCGAGGTATTC-3′; U6 (internal control), forward 5′-CTCGCTTCGGCAGCACAT-3′, reverse 5′-TTTGCGTGTCATCCTTGCG-3′.

Coronary angiography and intervention

Invasive coronary procedures and periprocedural management were performed by international guidelines (16). Briefly, diagnostic coronary angiography was performed by experienced interventionists, who were blind to the patient's serum miR-183-5p levels, using the transradial or transfemoral approach. The location and severity of each coronary artery stenosis were assessed by two independent interventionists, and discrepancies were solved with discussion.

CAD was defined as any major epicardial coronary stenosis $\geq$ 50%. Thus, patients were divided according to the number of diseased vessels: 0-vessel disease (i.e., non-CAD), 1-vessel disease, 2-vessel disease, 3-vessel or left main (LM) disease. In addition, we quantified the severity of CAD using the Gensini score system (17). Thus, in the current study, CAD severity was presented using either the different numbers of diseased vessels or the tertiles of Gensini score. Finally, the decision of coronary intervention was made at the discretion of the interventionist.

Statistical analysis

Continuous variables were shown as median (interquartile range), and compared using the Kruskal-Wallis H test. The Bonferroni correction was used to adjust the p value in multiple-comparison analysis. Categorical variables were expressed as numbers (percentages), and compared using the Chi-square test or Fisher's exact test. To investigate the relationship between serum miR-183-5p levels and CAD severity, we firstly compared serum miR-183-5p levels among a varied number of diseased vessels and tertiles of Gensini score (low tertile, <15.3; middle tertile, 15.3-30.0; high tertile, >30.0). Then, this relationship was examined using Spearman's correlation analysis, shown as r and its 95% confidence interval (CI). Meanwhile, we also determined different CAD severity and extent across the tertile of serum miR-183-5p levels. The receiver operating characteristic (ROC)

curve was performed to explore the diagnostic value of the serum miR-183-5p level for the presence and severity of CAD. The area under the ROC curve (AUC) with its 95% CI was used to measure the predictive ability of miR-183-5p. The Youden index was used to determine the optimal diagnostic threshold of miR-183-5p, and its corresponding sensitivity and specificity. Finally, the predictive value of miR-183-5p on the presence and severity of CAD was investigated in a multivariate model using logistical regression analysis, in which co-variables included age, sex, BMI, and those with a p -value < 0.1 in the univariate analysis. A two-sided p-value < 0.05 was considered statistically significant. All statistical analyzes were conducted using SPSS 20.0 software (IBM, Armonk, New York).

Results

Patient characteristics and angiographic findings

Overall, 135 patients (median age, 62.0 years; male, 52.6%) were included in the present study, who underwent invasive coronary artery angiogram to determine whether CAD was the origin of chest pain (Table 1). Hypertension (71.9%), hyperlipidemia (54.1%) and, current smoking (45.2%) were common risk factors for CAD. Notably, baseline total cholesterol (median, 5.1 mmol/L) and LDL-C (median, 3.2 mmol/L) levels were relatively high (Table 1), resulting in 92.6% of patients prescribed statins (Table 2). In addition, left ventricular systolic function (median left ventricular ejection fraction, 66.0%) and structure (median left ventricular end-diastolic diameter, 46.0 mm) were preserved (Table 1). Importantly, baseline characteristics were comparable across different CAD severities ($p > 0.05$), except for hs-CRP levels ($p = 0.005$). In particular, higher hs-CRP levels were observed in 3-vessel or LM disease (adjusted $p < 0.05$) and 2-vessel disease subgroups (adjusted $p < 0.05$), compared to non-CAD patients (Table 1).

After coronary angiography, CAD was identified in 115 patients (85.2%), with 45.9% of patients having 1-vessel disease, 21.5% of 2-vessel disease, and 17.8% of 3-vessel or LM disease (Table 1). These findings were consistent with an increased overall Gensini score (median, 20.0) (Table 2). Coronary artery stenosis was most likely to present in the left anterior descending artery (78.3%), followed by the right coronary artery (44.3%) and left circumflex artery (43.5%). Three patients (2.6%) had LM disease, which represented a severe type of CAD. Therefore, PCI

TABLE 1 Baseline characteristics of the study population.

	Overall $N = 135$	Non-CAD $N = 20$	CAD			p-value
			1-vessel disease $N = 62$	2-vessel disease $N = 29$	3-vessel/LM disease $N = 24$	
Demographics						
Age, years	62.0 (56.0–69.0)	58.5 (53.5–66.8)	61.5 (55.8–68.0)	62.0 (55.5–70.0)	65.0 (60.0–69.5)	0.170
Male, %	71 (52.6)	10 (50.0)	31 (50.0)	16 (55.2)	14 (58.3)	0.902
Body mass index, kg/m^2	25.0 (23.0–27.0)	26.0 (24.3–26.9)	25.0 (23.0–27.0)	26.0 (24.0–27.5)	24.0 (22.0–27.0)	0.282
Risk factors						
Current smoking, %	61 (45.2)	8 (40.0)	26 (41.9)	15 (51.7)	12 (50.0)	0.753
Hypertension, %	97 (71.9)	13 (65.0)	46 (74.2)	21 (72.4)	17 (70.8)	0.895
Diabetes, %	45 (33.3)	3 (15.0)	25 (40.3)	7 (24.1)	10 (41.7)	0.102
Hyperlipidemia, %	73 (54.1)	8 (40.0)	38 (61.3)	14 (48.3)	13 (54.2)	0.360
Family history, %	38 (28.1)	9 (45.0)	13 (21.0)	8 (27.6)	8 (33.3)	0.196
Lab examinations						
Total triglyceride, mmol/L	1.6 (1.2–2.5)	2.0 (1.3–3.2)	1.7 (1.2–2.4)	1.5 (1.2–2.4)	1.4 (0.9–2.6)	0.316
Total cholesterol, mmol/L	5.1 (4.1–5.9)	5.2 (4.7–5.8)	5.1 (4.1–5.9)	5.2 (4.0–5.7)	4.7 (3.8–6.1)	0.680
LDL-C, mmol/L	3.2 (2.6–3.7)	3.0 (2.6–3.5)	3.2 (2.6–3.8)	3.2 (2.5–3.5)	3.3 (2.4–3.9)	0.903
Glycosylated hemoglobin, %	6.0 (5.6–6.8)	6.2 (5.7–6.9)	5.9 (5.6–6.7)	6.0 (5.5–6.6)	6.2 (5.6–7.7)	0.540
Creatinine, umol/L	63.0 (53.0–73.0)	58.0 (50.3–68.0)	66.0 (55.0–74.0)	65.0 (53.0–74.0)	61.5 (47.8–72.8)	0.216
hs-CRP, mg/L	1.6 (0.8–3.5)	0.9 (0.3–1.7)	1.6 (0.6–3.1)	2.0 (1.0–4.2)*	2.7 (1.2–4.5)*	0.005
White blood cell, *10^9/L	6.2 (5.4–7.4)	6.1 (5.4–7.1)	6.2 (5.4–7.3)	6.4 (5.4–8.6)	5.7 (5.4–6.5)	0.610
Hemoglobin, g/L	132.0 (124.0–143.0)	132.0 (126.0–143.0)	134.0 (123.0–144.3)	130.0 (124.0–144.0)	133.5 (125.3–145.0)	0.915
Platelet, *10^9/L	202.0 (161.0–245.0)	212.0 (175.8–229.0)	192.0 (145.5–233.5)	222.0 (168.5–256.0)	214.0 (155.8–251.8)	0.191
Echocardiography						
LVEF, %	66.0 (61.0–71.0)	65.5 (61.3–69.5)	66.0 (61.0–72.0)	67.0 (61.0–72.5)	63.5 (60.5–68.0)	0.754
LVEDD, mm	46.0 (44.0–49.0)	46.5 (44.0–49.0)	46.0 (44.0–49.0)	44.0 (42.0–46.0)	46.0 (44.0–48.8)	0.112
IVSD, mm	9.0 (8.0–10.0)	9.0 (8.1–9.8)	9.0 (8.0–10.0)	8.0 (7.0–9.5)	9.0 (8.0–10.0)	0.285

Data shown as median (interquartile range), or number (percent) as appropriate.
A p-value was calculated by the Kruskal-Wallis H test.
CAD, coronary artery disease; hs-CRP, hypersensitive-C-reactive protein; IVSD, interventricular septal thickness at diastole; LM, left main; LDL-C, low density lipoprotein cholesterol; LVEF, left ventricular ejection fraction; LVEDD, left ventricular end diastolic diameter.
*Indicated Bonferroni adjusted $p < 0.05$ compared to Non-CAD group.

TABLE 2 Medications and coronary intervention of the study population.

	Overall $N = 135$	Non-CAD $N = 20$	CAD $N = 115$
Disease severity			
Gensini score	20.0 (13.0–36.0)	7.5 (6.0–15.0)	23.0 (16.0–39.0)
Disease location, %			
Left main	–	–	3 (2.6)
Left anterior descending	–	–	90 (78.3)
Left circumflex	–	–	50 (43.5)
Right coronary artery	–	–	51 (44.3)
Medication, %			
Antiplatelet	130 (96.3)	15 (75.0)	115 (100.0)
Statins	125 (92.6)	13 (65.0)	112 (97.4)
ACEI/ARB	65 (48.1)	8 (40.0)	57 (49.6)
Intervention, %			
Any intervention	98 (72.6)	–	98 (85.2)
Stent implantation	87 (64.4)	–	87 (75.7)

Data shown as median (interquartile range), or number (percent) as appropriate. ACEI, angiotensin-converting enzyme inhibitor; ARB, angiotensin receptor blocker; CAD, coronary artery disease.

was performed in 85.2% of CAD patients, with 75.7% having stent implantation (Table 2).

Correlation of serum miR-183-5p with CAD severity

Firstly, we found that serum miR-183-5p levels in any CAD subgroup were significantly increased than non-CAD patients (all adjusted $p < 0.05$) (Figure 1A). Among CAD subgroups, significantly increased miR-183-5p levels were observed in 3-vessel or LM than 1-vessel disease [3.75 [interquartile range (IQR): 2.45–4.90] vs. 2.25 (IQR: 1.45–3.20), adjusted $p = 0.002$] (Figure 1A). Moreover, a significant step-wise increased pattern between the Gensini score tertiles and miR-183-5p was showed [middle vs. low tertile: 2.10 (IQR: 1.60–2.80) vs. 1.20 (IQR: 0.80–2.55), adjusted $p = 0.044$], [high vs. middle tertile: 3.50 (IQR: 2.60–5.50) vs. 2.10 (IQR: 1.60–2.80), adjusted $p < 0.01$], [high vs. low tertile: 3.50 (IQR: 2.60–5.50) vs. 1.20 (IQR: 0.80–2.55), adjusted $p < 0.01$] (Figure 1B).

CAD severity in tertile of serum miR-183-5p levels

Firstly, we found that, across tertiles of serum miR-183-5p levels, the proportion of multiple vessel disease increased, while single or none vessel disease decreased (all $p < 0.05$) (Figure 2A). Similarly, a significant step-wise increased pattern between miR-183-5p tertiles and the Gensini score was observed [middle vs. low tertile: 20.0 (IQR: 15.0–34.5) vs. 12.0 (IQR: 7.0–20.0), adjusted $p = 0.003$] [high vs. middle tertile: 36.0 (IQR: 25.0–52.0) vs. 20.0 (IQR: 15.0–34.5), adjusted $p = 0.007$] [high vs. middle tertile: 36.0 (IQR: 25.0–52.0) vs. 12.0 (IQR: 7.0–20.0), adjusted $p < 0.01$] (Figure 2B). Moreover, serum miR-183-5p levels were positively correlated with the Gensini score ($r = 0.65$, 95% CI: 0.54–0.74, $p < 0.01$) (Figure 3A) and hs-CRP ($r = 0.63$, 95% CI: 0.51–0.73, $p < 0.01$) (Figure 3B).

Predictive value of serum miR-183-5p levels on CAD

The predictive values of serum miR-183-5p levels on the presence of CAD (AUC 0.82, 95% CI 0.71–0.92, $p < 0.01$) and 3-vessel or LM disease (AUC 0.76, 95% CI 0.65–0.86, $p < 0.01$) were confirmed in the ROC curve analysis, respectively (Figure 4A). The optimal cut-off values of miR-183-5p predicting CAD presence and severity were 1.40 (sensitivity 82.6%, specificity 70.0%) and 3.65 (sensitivity 54.2%, specificity 88.3%), respectively (Figure 4B).

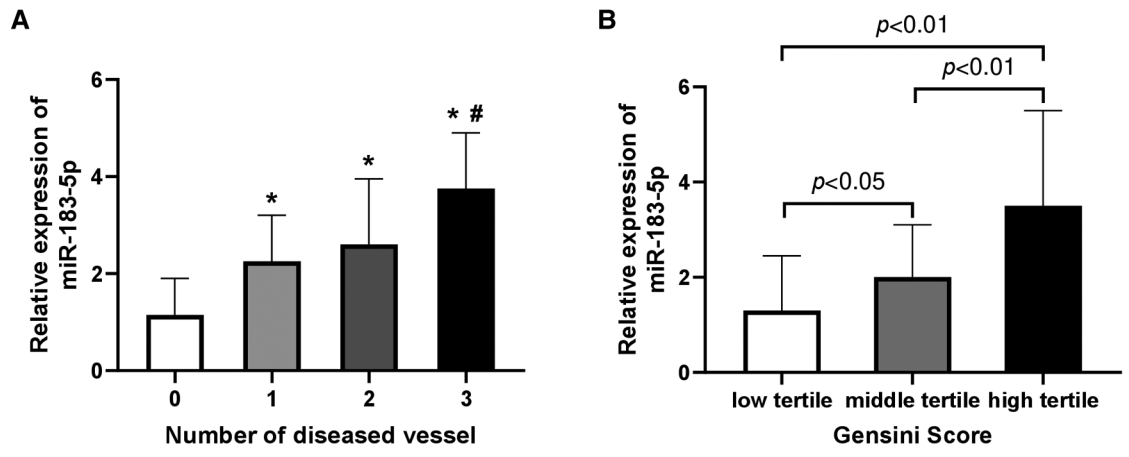

FIGURE 1
Relative expression of serum miR-183-5p levels according to number of diseased vessel (A) and gensini score tertiles (B). (A) *indicated Bonferroni adjusted $p < 0.05$ when compared to 0-vessel disease; #indicated Bonferroni adjusted $p < 0.01$ when compared to 1-vessel disease. (B) all p-values adjusted by Bonferroni correction.

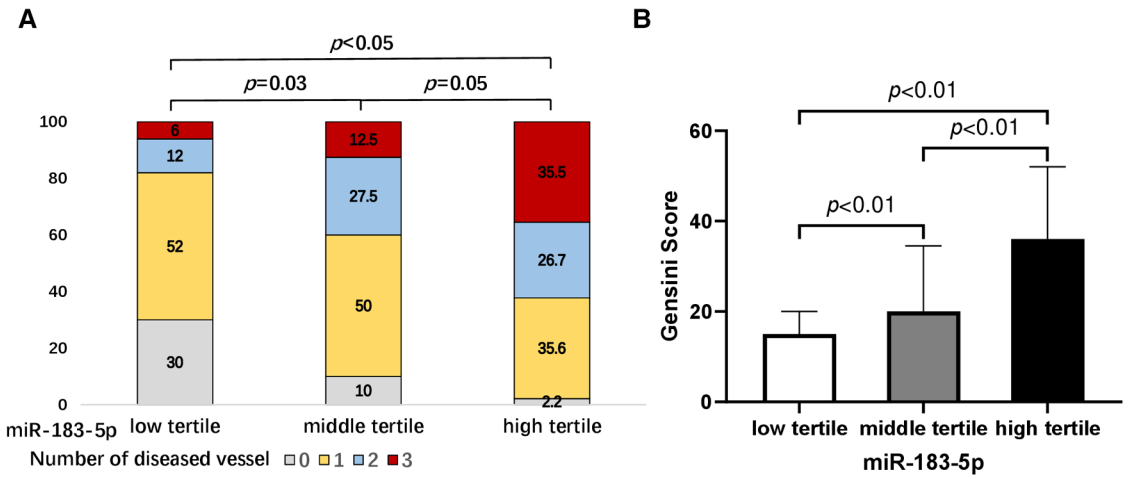

FIGURE 2
Proportions of number of diseased vessel (A) and gensini score (B) according to tertiles of serum miR-183-5p levels. All *p*-values adjusted by Bonferroni correction.

Furthermore, in multivariate analysis adjusting for age, sex, BMI, diabetes, hs-CRP, tertile of serum miR-183-5p levels showed increased predictive value on the presence of CAD (middle vs. low tertile, HR 3.81, 95% CI 1.07–13.56, $p = 0.039$; high vs. low tertile, HR 14.57, 95% CI 1.38–153.65, $p = 0.026$; p for trend = 0.024) and 3-vessel or LM disease (middle vs. low tertile, HR 2.11, 95% CI 0.46–9.70, $p = 0.34$; high vs. low tertile, HR 6.59, 95% CI 1.59–27.25, $p = 0.009$; p for trend = 0.020) (Table 3).

Discussion

To the best of our knowledge, this is the first study investigating the relationship between serum miR-183-5p and stable CAD. The main findings of the present study included: (1) a significant stepwise increased pattern existed between the Gensini score tertiles and serum miR-183-5p levels; (2) serum miR-183-5p levels were positively correlated with the Gensini score and hs-CRP; (3) serum miR-183-5p levels could predict CAD presence and severity, with optimal cut-off values of 1.40 (sensitivity 82.6%, specificity 70.0%) and 3.65 (sensitivity 54.2%, specificity 88.3%), respectively; (4) the predictive value of serum miR-183-5p levels on CAD presence and severity were confirmed in multivariable analysis.

MiR-183 belongs to the miR-183 cluster, consisting of three microRNAs: miR-183, miR-96 and, miR-182. These homologous microRNAs are highly co-expressed in the murine retina, and their chromosomal loci are quite close (18). Increased miR-183 cluster members have been found in autoimmune diseases, neuronal and psychiatric disorders, and various malignancies (19). MiR-183 was identified in 2003 by cloning from the human Saos-2 cell line and mouse tissues (20). MiR-183-5p is known to overexpress in the peripheral blood mononuclear cells (PBMCs)

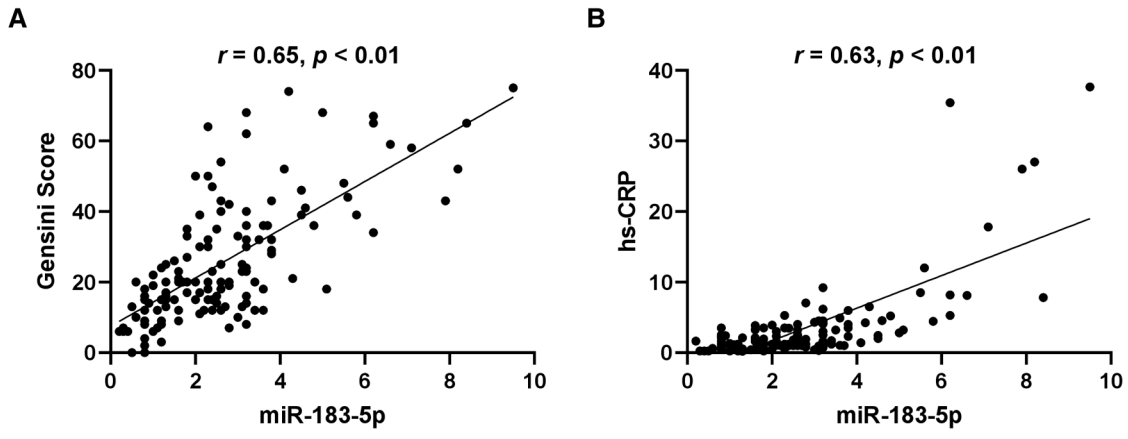

FIGURE 3
Correlation of serum miR-183-5p levels with gensini score (A) and hypersensitive-C-reactive protein (hs-CRP) (B).

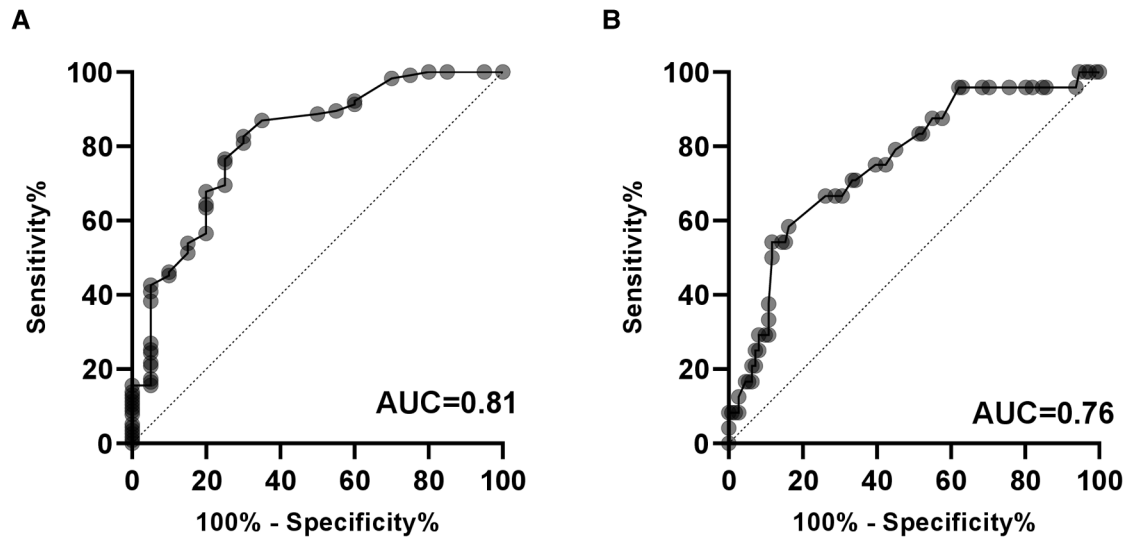

FIGURE 4
Diagnostic value of serum miR-183-5p levels on the presence of CAD (A) and severe CAD (i.e., 3-vessel or LM disease). (B) AUC, area under the receiver operating characteristic curve; CAD, coronary artery disease.

(21) of breast cancer, in the tumor tissue of breast cancer (9), primary nasopharyngeal carcinoma (11), and hepatocellular carcinoma (10). In addition, elevated miR-183-5p is observed in PBMCs from patients with systemic lupus erythematosus (22), and in plasma-derived exosomes from patients with intestinal Behçet's syndrome (23).

The main underlying pathophysiology of CAD is atherosclerosis and/or thrombosis, which is a chronic inflammatory disease. Recently, Meerson et al. found that, compared to healthy individuals, plasma miR-183-5p levels were significantly increased in women with early diabetes (an important risk factor of atherosclerosis) (24). Meanwhile, overexpression of miR-183-5p was observed in the serum of patients with carotid atherosclerosis (12, 13), and positively correlated with carotid intima-media thickness (13). Similarly, elevated miR-183 levels were detected in the plasma exosome from patients with MI than in healthy individuals, which positively correlated with the degree of myocardial injury (14). Recently, Liu found that exosomal miR-183-5p from epicardial adipose tissue of patients with CAD were increased compared with those without CAD (25). Interestingly, Tong et al. found that plasma miR-183-5p levels were novel diagnostic markers only for NSTEMI, but not for STEMI (15). These discrepancies probably resulted from different pathophysiology of these two CAD subtypes, but also different sensitivity and specificity of miR-183-5p detecting methods (i.e., RNA-seq and qPCR).

Circulating miR-183-5p might be a promising marker of carotid atherosclerosis and ACS. However, less is known about its level in stable CAD patients. To fill the gap, we performed this cross-sectional study to investigate the relationship between serum miR-183-5p levels and CAD presence and severity. We found that serum miR-183-5p levels were increased in CAD

TABLE 3 Prediction of CAD presence and severe CAD of the study population.

Variables	Prediction of CAD presence						Prediction of 3-vessel or LM disease					
	Univariate			Multivariate			Univariate			Multivariate		
	HR	95% CI	*p*-value	HR	95% CI	*p*-value	HR	95% CI	*p*-value	HR	95% CI	*p*-value
Age	1.04	0.99–1.10	0.161	1.04	0.98–1.10	0.235	1.05	0.99–1.11	0.071	1.05	0.99–1.11	0.092
Male	1.13	0.44–2.92	0.801	1.06	0.37–3.05	0.914	1.33	0.54–3.24	0.535	1.29	0.47–3.54	0.618
BMI	0.93	0.77–1.12	0.448	0.93	0.76–1.14	0.476	0.88	0.73–1.05	0.160	0.85	0.70–1.05	0.124
Diabetes	3.26	0.90–11.78	0.071	3.52	0.91–13.61	0.068	–	–	–	–	–	–
hs-CRP	1.43	0.98–2.06	0.061	1.08	0.76–1.54	0.657	1.08	1.01–1.16	0.019	1.05	0.72–1.12	0.230
miR-183-5p			0.004*			0.024*			0.020*			0.020*
Low tertile	1.00	–	–	1.00	–	–	1.00	–	–	1.00	–	–
Middle tertile	3.86	1.17–12.77	0.027	3.81	1.07–13.56	0.039	2.24	0.50–10.00	0.291	2.11	0.46–9.70	0.34
High tertile	18.86	2.37–149.79	0.005	14.57	1.38–153.65	0.026	8.64	2.32–32.26	0.001	6.59	1.59–27.25	0.009

Variables in the left column included in the logistics regression analysis.
CAD, coronary artery disease; HR, hazard ratio; CI, confidence interval; BMI, body mass index; hs-CRP, hypersensitive-C-reactive protein.
*Indicated *p*-value for trend in the logistics regression analysis.

patients with different severities than in non-CAD control. Serum miR-183-5p levels were positively correlated with the Gensini score, and hs-CRP, respectively. Interestingly, in patients with carotid atherosclerosis, serum miR-183-5p levels were positively correlated with CRP (13) and ox-LDL (12), which are well-known causes of atherosclerosis. Importantly, serum miR-183-5p levels had a relatively high power to diagnose the presence of CAD (AUC 0.82) and 3-vessel or LM disease (AUC 0.76). The optimal cut-off values of miR-183-5p predicting CAD presence and severity were 1.40 and 3.65, respectively, which were higher than its cut-off point predicting the presence of carotid atherosclerosis (0.91) in the study of Sun et al. (13). Moreover, this predictive value of serum miR-183-5p level was independent of age, sex, BMI, diabetes, and hs-CRP, which are well-established risk factors of CAD. Therefore, circulating miR-183-5p level is a marker of all categories of CAD presence, which could be used for early diagnosis of CAD; Meanwhile, serum miR-183-5p level could dynamically reflect CAD severity; More importantly, miR-183-5p might be a therapeutic target after fully elucidating the underlying mechanism between miR-183-5p and atherosclerosis/thrombosis.

Although the detrimental effects of miR-183-5p on vasculature have been reported, its exact mechanism leading to atherosclerosis is not fully understood. Zhang et al. showed that down-regulation of miR-183-5p in ox-LDL-treated human umbilical vascular endothelial cells could attenuate cell injury and inflammation by upregulation of insulin receptor substrate 1 (26). In subarachnoid hemorrhage rats, bone marrow mesenchymal stem cell-derived extracellular vesicles could alleviate endothelial dysfunction by regulating the KLF3-AS1/miR-183-5p/TCF7L2 signaling axis (27). In addition, Sun et al. found that overexpression of miR-183-5p accelerated the proliferation and migration of vascular smooth muscle cells (VSMCs) (13). Similarly, Fan et al. found, in VSMCs treated with ox-LDL, miR-183-5p was overexpressed, which may down-regulate FOXO1, leading to proliferation/apoptosis imbalance in VSMCs (12). Importantly, miR-183-5p might intervene the initiation and development of atherosclerosis by impacting not only vascular endothelial and VSMCs, but macrophages. In bone marrow-derived macrophages (BMDMs) transfected with a miR-183 inhibitor, the foam-cell formation was reduced, and cholesterol efflux increased (28). Furthermore, in BMDMs subjected to ox-LDL, miR-183 knockdown decreased the M1/M2 ratio with attenuated NF-$_k$B activation, via targeting NR4A2 (28). However, exosomal miR-183-5p derived from bone marrow mesenchymal stem cell could protect ischemia/reperfusion injury in cardiomyocytes by targeting FOXO1 (29) or voltage-dependent anion channel 1 (30). These findings illustrated that miR-183-5p could potentially have multiple effects on the cardiovascular system.

The present study has several limitations. (1) study population was restricted to those without ASCVD, which may limit the extrapolation of the study results to a broader population; (2) number of the study population was relatively small, precluding us from finding a statistical difference of miR-183-5p between CAD patients with different numbers of diseased vessels; (3) given the cross-sectional design, a causal relation between miR-183-5p and CAD cannot be determined; (4) although the multivariate analysis was performed, the residual confounders affecting the correlation between miR-183-5p and CAD cannot be excluded; (5) CAD severity was judged by experienced physician visually, which may be improved using intracoronary imaging and functional examination.

Conclusions

In the population with chest pain who have no history of established ASCVD, serum miR-183-5p levels are independently and positively correlated with stable CAD presence and severity. Further studies are needed to elucidate the physiopathologic mechanism between miR-183-5p and atherosclerosis, as well as the outcome predictive value of miR-183-5p.

Data availability statement

The raw data supporting the conclusions of this article will be made available by the authors, without undue reservation.

Ethics statement

The studies involving human participants were reviewed and approved by the Ethics Committee of Beijing Renhe Hospital (RH20220103). The patients/participants provided their written informed consent to participate in this study. Written informed consent was obtained from the individual(s) for the publication of any potentially identifiable images or data included in this article.

Author contributions

The study was designed by GL. The clinical samples and information were collected by XL. The data were analyzed by DL. The experiments were performed by YG. The original manuscript was drafted by DL with comments by LZ. All authors contributed to the article and approved the submitted version.

Conflict of interest

The authors declare that the research was conducted in the absence of any commercial or financial relationships that could be construed as a potential conflict of interest.

Publisher's note

All claims expressed in this article are solely those of the authors and do not necessarily represent those of their affiliated

organizations, or those of the publisher, the editors and the reviewers. Any product that may be evaluated in this article, or claim that may be made by its manufacturer, is not guaranteed or endorsed by the publisher.

References

1. Roth GA, Johnson C, Abajobir A, Abd-Allah F, Abera SF, Abyu G, et al. Global, regional, and national burden of cardiovascular diseases for 10 causes, 1990 to 2015. *J Am Coll Cardiol*. (2017) 70(1):1–25. doi: 10.1016/j.jacc.2017.04.052

2. Virani SS, Alonso A, Aparicio HJ, Benjamin EJ, Bittencourt MS, Callaway CW, et al. Heart disease and stroke statistics-2021 update: a report from the American heart association. *Circulation*. (2021) 143(8):e254–743. doi: 10.1161/CIR.0000000000000950

3. Odden MC, Coxson PG, Moran A, Lightwood JM, Goldman L, Bibbins-Domingo K. The impact of the aging population on coronary heart disease in the United States. *Am J Med*. (2011) 124(9):827–33.e5. doi: 10.1016/j.amjmed.2011.04.010

4. Sugiyama T, Hasegawa K, Kobayashi Y, Takahashi O, Fukui T, Tsugawa Y. Differential time trends of outcomes and costs of care for acute myocardial infarction hospitalizations by ST elevation and type of intervention in the United States, 2001–2011. *J Am Heart Assoc*. (2015) 4(3):e001445. doi: 10.1161/JAHA.114.001445

5. Pasquinelli AE. MicroRNAs and their targets: recognition, regulation and an emerging reciprocal relationship. *Nat Rev Genet*. (2012) 13(4):271–82. doi: 10.1038/nrg3162

6. Bajan S, Hutvagner G. Regulation of miRNA processing and miRNA mediated gene repression in cancer. *MicroRNA*. (2014) 3(1):10–7. doi: 10.2174/2211536602666140110234046

7. Landskroner-Eiger S, Moneke I, Sessa WC. miRNAs as modulators of angiogenesis. *Cold Spring Harbor Perspect Med*. (2013) 3(2):a006643. doi: 10.1101/cshperspect.a006643

8. Melak T, Baynes HW. Circulating microRNAs as possible biomarkers for coronary artery disease: a narrative review. *Ejifcc*. (2019) 30(2):179–94.

9. Cheng Y, Xiang G, Meng Y, Dong R. MiRNA-183-5p promotes cell proliferation and inhibits apoptosis in human breast cancer by targeting the PDCD4. *Reprod Biol*. (2016) 16(3):225–33. doi: 10.1016/j.repbio.2016.07.002

10. Wojcicka A, Swierniak M, Kornasiewicz O, Gierlikowski W, Maciag M, Kolanowska M, et al. Next generation sequencing reveals microRNA isoforms in liver cirrhosis and hepatocellular carcinoma. *Int J Biochem Cell Biol*. (2014) 53:208–17. doi: 10.1016/j.biocel.2014.05.020

11. Tang JF, Yu ZH, Liu T, Lin ZY, Wang YH, Yang LW, et al. Five miRNAs as novel diagnostic biomarker candidates for primary nasopharyngeal carcinoma. *Asian Pac J Cancer Prev*. (2014) 15(18):7575–81. doi: 10.7314/APJCP.2014.15.18.7575

12. Fan M, Huang Y, Li K, Yang X, Bai J, Si Q, et al. ox-LDL regulates proliferation and apoptosis in VSMCs by controlling the miR-183-5p/FOXO1. *Genes Genomics*. (2022) 44(6):671–81. doi: 10.1007/s13258-022-01236-x

13. Sun B, Shan Z, Sun G, Wang X. Micro-RNA-183-5p acts as a potential diagnostic biomarker for atherosclerosis and regulates the growth of vascular smooth muscle cell. *J Chin Med Assoc*. (2021) 84(1):33–7. doi: 10.1097/JCMA.0000000000000433

14. Zhao X, Jia Y, Chen H, Yao H, Guo W. Plasma-derived exosomal miR-183 associates with protein kinase activity and may serve as a novel predictive biomarker of myocardial ischemic injury. *Exp Ther Med*. (2019) 18(1):179–87. doi: 10.3892/etm.2019.7555

15. Tong KL, Mahmood Zuhdi AS, Wan Ahmad WA, Vanhoutte PM, de Magalhaes JP, Mustafa MR, et al. Circulating MicroRNAs in young patients with acute coronary syndrome. *Int J Mol Sci*. (2018) 19(5):1467. doi: 10.3390/ijms19051467

16. Windecker S, Kolh P, Alfonso F, Collet JP, Cremer J, Falk V, et al. 2014 ESC/EACTS guidelines on myocardial revascularization: the task force on myocardial revascularization of the European society of cardiology (ESC) and the European association for cardio-thoracic surgery (EACTS) developed with the special contribution of the European association of percutaneous cardiovascular interventions (EAPCI). *Eur Heart J*. (2014) 35(37):2541–619. doi: 10.1093/eurheartj/ehu278

17. Gensini GG. A more meaningful scoring system for determining the severity of coronary heart disease. *Am J Cardiol*. (1983) 51(3):606. doi: 10.1016/S0002-9149(83)80105-2

18. Lim LP, Glasner ME, Yekta S, Burge CB, Bartel DP. Vertebrate microRNA genes. *Science*. (2003) 299(5612):1540. doi: 10.1126/science.1080372

19. Dambal S, Shah M, Mihelich B, Nonn L. The microRNA-183 cluster: the family that plays together stays together. *Nucleic Acids Res*. (2015) 43(15):7173–88. doi: 10.1093/nar/gkv703

20. Lagos-Quintana M, Rauhut R, Meyer J, Borkhardt A, Tuschl T. New microRNAs from mouse and human. *RNA*. (2003) 9(2):175–9. doi: 10.1261/rna.2146903

21. Chang CW, Wu HC, Terry MB, Santella RM. microRNA expression in prospectively collected blood as a potential biomarker of breast cancer risk in the BCFR. *Anticancer Res*. (2015) 35(7):3969–77.

22. Zhou S, Zhang J, Luan P, Ma Z, Dang J, Zhu H, et al. miR-183-5p is a potential molecular marker of systemic lupus erythematosus. *J Immunol Res*. (2021) 2021:5547635. doi: 10.1155/2021/5547635

23. Hou CC, Bao HF, Shen Y, Ye JF, Ma HF, Guan JL. Expression of miRNAs derived from plasma exosomes in patients with intestinal Behçet's syndrome. *Clin Exp Rheumatol*. (2022) 40(8):1480–90. doi: 10.55563/clinexprheumatol/6xgxzk

24. Meerson A, Najjar A, Saad E, Sbeit W, Barhoum M, Assy N. Sex differences in plasma MicroRNA biomarkers of early and complicated diabetes mellitus in Israeli arab and Jewish patients. *Noncoding RNA*. (2019) 5(2):32. doi: 10.3390/ncrna5020032

25. Liu J, Gao A, Liu Y, Sun Y, Zhang D, Lin X, et al. MicroRNA expression profiles of epicardial adipose tissue-derived exosomes in patients with coronary atherosclerosis. *Rev Cardiovasc Med*. 23(6):206. doi: 10.31083/j.rcm2306206

26. Zhang Y, Zhan Y, Liu D, Yu B. Inhibition of microRNA-183 expression resists human umbilical vascular endothelial cells injury by upregulating expression of IRS1. *Drug Deliv*. (2019) 26(1):612–21. doi: 10.1080/10717544.2019.1628117

27. Cheng M, Liu L, Zhang T, Chen Y, Wang Q, Wu Y. Extracellular vesicles derived from bone marrow mesenchymal stem cells alleviate neurological deficit and endothelial cell dysfunction after subarachnoid hemorrhage via the KLF3-AS1/miR-83-5p/TCF7L2 axis. *Exp Neurol*. (2022) 356:114151. doi: 10.1016/j.expneurol.2022.114151

28. Gong FH, Long L, Yang YS, Shen DH, Zhang YS, Wang XS, et al. Attenuated macrophage activation mediated by microRNA-183 knockdown through targeting NR4A2. *Exp Ther Med*. (2021) 21(4):300. doi: 10.3892/etm.2021.9731

29. Mao S, Zhao J, Zhang ZJ, Zhao Q. MiR-183-5p overexpression in bone mesenchymal stem cell-derived exosomes protects against myocardial ischemia/reperfusion injury by targeting FOXO1. *Immunobiology*. (2022) 227(3):152204. doi: 10.1016/j.imbio.2022.152204

30. Lin D, Cui B, Ma J, Ren J. MiR-183-5p protects rat hearts against myocardial ischemia/reperfusion injury through targeting VDAC1. *Biofactors*. (2020) 46(1):83–93. doi: 10.1002/biof.1571

frontiers | Frontiers in Cardiovascular Medicine

TYPE Original Research
PUBLISHED 03 July 2023
DOI 10.3389/fcvm.2023.1226971

OPEN ACCESS

EDITED BY
Hongsong Zhang,
Nanjing Medical University, China

REVIEWED BY
Guanglin Cui,
Huazhong University of Science and Technology, China
Tao You,
The First Affiliated Hospital of Soochow University, China

*CORRESPONDENCE
Jong Bhak
jongbhak@genomics.org
Eun-Seok Shin
sesim1989@gmail.com

†These authors have contributed equally to this work

RECEIVED 22 May 2023
ACCEPTED 20 June 2023
PUBLISHED 03 July 2023

CITATION
Jeon Y, Jeon S, An K, Kim YJ, Kim B-C, Ryu H, Choi W-H, Choi H, Kim W, Lee SY, Bae J-W, Hwang J-Y, Kang MG, An S, Kim Y, Kang Y, Kim BC, Bhak J and Shin E-S (2023) Identification and validation of six acute myocardial infarction-associated variants, including a novel prognostic marker for cardiac mortality.
Front. Cardiovasc. Med. 10:1226971.
doi: 10.3389/fcvm.2023.1226971

Identification and validation of six acute myocardial infarction-associated variants, including a novel prognostic marker for cardiac mortality

Yeonsu Jeon[1,2†], Sungwon Jeon[2†], Kyungwhan An[1,3], Yeo Jin Kim[2], Byoung-Chul Kim[2], Hyojung Ryu[2], Whan-Hyuk Choi[4], HyunJoo Choi[1,3], Weon Kim[5], Sang Yeub Lee[6], Jang-Whan Bae[7], Jin-Yong Hwang[8], Min Gyu Kang[8], Seolbin An[1,3], Yeonkyung Kim[2], Younghui Kang[2], Byung Chul Kim[2], Jong Bhak[1,2,3,9*] and Eun-Seok Shin[10*]

[1]Korean Genomics Center (KOGIC), Ulsan National Institute of Science and Technology (UNIST), Ulsan, Republic of Korea, [2]Clinomics Inc., Ulsan, Republic of Korea, [3]Department of Biomedical Engineering, College of Information-Bio Convergence Engineering, Ulsan National Institute of Science and Technology (UNIST), Ulsan, Republic of Korea, [4]Department of Mathematics, Kangwon National University, ChunCheon, Republic of Korea, [5]Division of Cardiology, Department of Internal Medicine, Kyung Hee University Hospital, Kyung Hee University, Seoul, Republic of Korea, [6]Division of Cardiology, Department of Internal Medicine, Chung-Ang University College of Medicine, Chung-Ang University Gwangmyeong Hospital, Gwangmyeong, Republic of Korea, [7]Department of Internal Medicine, Chungbuk National University Hospital, College of Medicine, Chungbuk National University, Cheongju, Republic of Korea, [8]Department of Internal Medicine, Gyeongsang National University School of Medicine and Gyeongsang National University Hospital, Jinju, Republic of Korea, [9]Personal Genomics Institute (PGI), Genome Research Foundation (GRF), Osong, Republic of Korea, [10]Department of Cardiology, Ulsan University Hospital, University of Ulsan College of Medicine, Ulsan, Republic of Korea

Background: Acute myocardial infarction (AMI) is one of the leading causes of death worldwide, and approximately half of AMI-related deaths occur before the affected individual reaches the hospital. The present study aimed to identify and validate genetic variants associated with AMI and their role as prognostic markers.

Materials and methods: We conducted a replication study of 29 previously identified novel loci containing 85 genetic variants associated with early-onset AMI using a new independent set of 2,920 Koreans [88 patients with early- and 1,085 patients with late-onset AMI, who underwent percutaneous coronary intervention (PCI), and 1,747 healthy controls].

Results: Of the 85 previously reported early-onset variants, six were confirmed in our genome-wide association study with a false discovery rate of less than 0.05. Notably, rs12639023, a cis-eQTL located in the intergenic region between *LINC02005* and *CNTN3*, significantly increased longitudinal cardiac mortality and recurrent AMI. *CNTN3* is known to play a role in altering vascular permeability. Another variant, rs78631167, located upstream of *PLAUR* and known to function in fibrinolysis, was moderately replicated in this study. By surveying the nearby genomic region around rs78631167, we identified a significant novel locus (rs8109584) located 13 bp downstream of rs78631167. The present study showed that six of the early-onset variants of AMI are applicable to both early- and late-onset cases.

Conclusion: Our results confirm markers that can potentially be utilized to predict, screen, prevent, and treat candidate patients with AMI and highlight the potential of rs12639023 as a prognostic marker for cardiac mortality in AMI.

KEYWORDS

acute myocardial infarction, genome-wide association study, cardiac mortality, genetic marker, prognostic marker

Introduction

Acute myocardial infarction (AMI) is a leading cause of death worldwide, with more than one million deaths per year (1). Elucidating the genetic factors underlying AMI is complex, because environmental factors complicate the etiology of the disease (2). In our previous genome-wide association study (GWAS) (3), we had identified 29 novel genetic loci containing 85 suggestive variants of AMI by targeting 596 patients with early-onset AMI with a high genetic predisposition (4). This study provided evidence to support a genetic association between early-onset AMI and four biochemical pathways: thrombosis, fibrinolysis, inflammation, and lipid metabolism. Our findings showed that an imbalance between thrombosis and fibrinolysis, a conflicting mechanism, may cause AMI. However, it was necessary to validate the replicability of the variants in a new, independent cohort, mainly in the ≥65 years of age cohort, which accounts for most patients with AMI.

Here, we present a replication study of a GWAS using 1,173 new patients with AMI who were eventually treated with percutaneous coronary intervention (PCI) and 1,747 healthy controls from the Korean Genome Project (5). Moreover, we screened for AMI-related variants to determine their association with cardiac mortality and recurrent AMI.

Materials and methods

Data sources and study population

A total of 1,173 patients with AMI from the Chungbuk National University Hospital in Korea were enrolled, and 1,747 healthy individuals from the Korean Genome Project (KGP) were selected as controls (5, 6). Patients with AMI were hospitalized with a diagnosis of ST-segment elevation myocardial infarction or non-ST-segment elevation myocardial infarction caused by atherothrombotic occlusive lesions treated with PCI (3, 7). Of the 1,173 patients with AMI, 88 and 1,085 were early-onset and late-onset patients, respectively. Population-based control individuals were obtained from the KGP (5, 6). The KGP is the largest Korean Genome Project and currently includes approximately 10,000 human genomes sequenced in Korea. Information regarding the KGP data can be found on the Korean Genome Project webpage (http://koreangenome.org). The genomes of these 1,173 patients were compared with those of 1,747 control subjects in Korea. Written informed consent was obtained from all participants in this study. Sample collection and sequencing were approved by the Institutional Review Board (IRB) of the Ulsan National Institute of Science and Technology (UNISTIRB-15-19-A). Analyses were performed using Python version 3.7.7 and R version 3.5.0.

Whole-genome sequencing by MGI T7 sequencer

WGS was performed using the MGI T7 platform, and clinical information from the KGP was matched. A total of 2,920 case and control samples were sequenced for this study in 2020. We filtered and finalized samples according to the following criteria: (i) Case: patients with AMI undergoing PCI surgery and (ii) control: healthy participants without AMI history or stent surgery. In total, 1,129 cases and 1,636 control samples were analyzed for further analysis (**Table 1**). Genomic DNA was isolated from the blood-containing plates using a DNeasy Blood & Tissue kit (Qiagen, Germany) according to the manufacturer's protocol. The extracted DNA was quantified using a Quant-iT BR Assay Kit (Invitrogen, USA). Each gDNA sample (200 ng) was used to construct a genomic DNA library using the MGIEasy FS DNA Library Prep Set (MGI, Shenhzen, China) according to the manufacturer's instructions. DNA was fragmented by enzymatic fragmentation using magnetic beads. DNA end-repair and adapter ligation were conducted using the MGIEasy DNA Adapters-96 Kit (MGI, Shenzhen, China). The products were run on the 4150 TapeStation (Agilent, Santa Clara, CA, USA), using the Agilent D1000 ScreenTape (Agilent, Santa Clara, CA, USA) to assess the size distribution of the libraries. They were quantified using a Quanti-iT HS Assay Kit (Invitrogen, USA). The PCR products (40 fmol) were circularized and amplified using rolling-circle amplification to generate DNA nanoball-based libraries, which were loaded onto a DNBSEQ-T7RS Sequencing flow cell (MGI, Shenzhen, China) with a DNBSEQ-T7RS High-throughput Sequencing Kit (MGI, Shenzhen, China). The library was run on a DNBSEQ-T7RS (MGI, Shenzhen, China) platform at paired-end 150 bp reads. The quality of bases in the reads was checked using FastQC (ver. 0.11.5; www.bioinformatics.babraham.ac.uk/projects/fastqc/) software. Additional details regarding the genomic variant identification are provided in the **Supplementary Methods section of the online Supplementary Information**.

Genome-wide association study (GWAS)

GWAS was performed using logistic regression with an additive genetic model using PLINK (ver. 1.9b) (8). A total of

TABLE 1 Baseline characteristics in this study.

	Discovery dataset		Replication dataset	
	Early-onset AMI ($N = 596$)	Control ($N = 636$)	AMI ($N = 1,129$)	Control ($N = 1,636$)
Male, *n* (%)	486 (81.5)	328 (51.0)	861 (76.3)	718 (43.9)
Age, median (Q1–Q3)	46 (42.0–48.0)	44 (29.5–57.0)	65 (58.0–75.0)	45 (32.0–55.0)
Body mass index, mean ± SD	25.5 ± 3.9	24.0 ± 3.4	30.0 ± 109.7	23.7 ± 3.5
Hypertension, *n* (%)	188 (31.5)	90 (14.0)	576 (51)	276 (16.9)
Diabetes mellitus, *n* (%)	118 (19.8)	33 (5.1)	341 (30.2)	112 (6.8)
Current smoking, *n* (%)	360 (60.4)	82 (12.8)	430 (38.1)	170 (10.4)
Lipid levels, mg/dl				
Total cholesterol, mean ± SD	202.7 ± 49.2	179.6 ± 34.3	177.4 ± 47.3	198.6 ± 38.0
LDL cholesterol, mean ± SD	129.1 ± 43.4	115.8 ± 33.0	110.2 ± 39.2	118.1 ± 34.8
HDL cholesterol, mean ± SD	43.9 ± 13.0	57.4 ± 13.9	43.6 ± 12.2	56.8 ± 14.2
Triglycerides, mean ± SD	209.1 ± 185.1	115.8 ± 77.0	144.6 ± 113.6	118.4 ± 73.4

AMI, acute myocardial infarction; LDL, low-density lipoprotein; HDL, high-density lipoprotein.
Values are mean ± SD, median (interquartile range, 25th–75th), or *n* (%).

3,484 SNPs and indels, which are near the previous genetic variants associated with early-onset AMI, were tested for replication. Sex and the top ten principal components were included as covariates in the model. The statistically significant *P*-value threshold was determined to be 5.88×10^{-4} which is the same as 0.05 FDR value with Bonferroni correction. We assigned significantly replicated variants using the following criteria: (i) variants whose *P*-value was over the significance threshold, and (ii) variants that had a consistent direction of effect in both GWAS results between the discovery and replication datasets.

Survival analysis of genetic effect on cardiac mortality and recurrent AMI

Survival analysis was performed using the Cox multivariate regression model to estimate the risk of composite outcomes of cardiac mortality and recurrent AMI among patients with AMI by genotype. The survival package in R software (ver. 4.2.2) was used for the analysis (9). Age and sex were also included as covariates in the model. The follow-up period was restricted to 2,000 days (5.5 years). Wild-type genotype carriers were assigned a value of 0, heterozygous genotype carriers a value of 1, and homozygous carriers a value of 2 (10). The Kaplan–Meier curve was used to visualize genetic effects on cardiac mortality and recurrent AMI.

Quantitative trait loci (QTL) mapping

QTL analysis was performed using an in-house Python script (ver. 3.7.7). Significant variants from the GWAS were queried for their dose-dependent genetic influence on various molecular phenotypes previously reported in the publicly available QTLbase database (ver. 2.0; http://www.mulinlab.org/qtlbase) (11). QTLbase delivers 22 phenotypes ranging from apaQTL (alternative polyadenylation QTL), eQTL (expression QTL), and hQTL (histone QTL) to stQTL (mRNA stability QTL).

Results

Replication of genetic variants associated with acute myocardial infarction

We found that six variants out of the 85 suggestive early-onset markers were significantly replicated in the AMI group using GWAS over a statistically significant false discovery rate (FDR) threshold (FDR < 0.05; $P < 5.88 \times 10^{-4}$) (**Figure 1**, **Table 2**, **Supplementary Table S1**, and **Supplementary Figure S1**). Two intergenic variants (rs12639023 and rs12639020), located near *LINC02005* and *CNTN3* genes, were significantly associated with AMI (OR = 1.432, $P = 2.17 \times 10^{-8}$ for rs12639023 and OR = 1.267, $P = 4.05 \times 10^{-4}$ for rs12639020). Another variant, rs12921822 (OR = 1.388, $P = 2.77 \times 10^{-4}$), located in an intron of RNA binding fox-1 homolog 1 (*RBFOX1*), was also replicated. *RBFOX1* is known to be involved in cardiomyopathy (12). Furthermore, rs1560389462, which is an in-frame deletion in Mucin 4 (*MUC4*), was significantly associated with AMI (OR = 0.093, $P = 7.60 \times 10^{-5}$). *MUC4* was reported to contribute to cancer progression by suppressing apoptosis and prompting tumor cell proliferation (13). Other two significant variants were located in intergenic regions of *FRG1CP-FRG1DP* and *MIR1263-LINC01324* (OR = 5.126, $P = 4.66 \times 10^{-23}$ and OR = 0.400, $P = 1.13 \times 10^{-9}$) exerting risk and protective effect on the occurrence of AMI, respectively.

In addition, a variant related to fibrinolysis, rs78631167, located upstream of plasminogen activator urokinase receptor (*PLAUR*) was moderately significant in this study (OR = 0.691, $P = 1.58 \times 10^{-3}$). Although rs78631167 did not show a strong association in the new cohort, rs8109584 showed a significant association with AMI ($P = 1.43 \times 10^{-5}$), which is 13 bp away

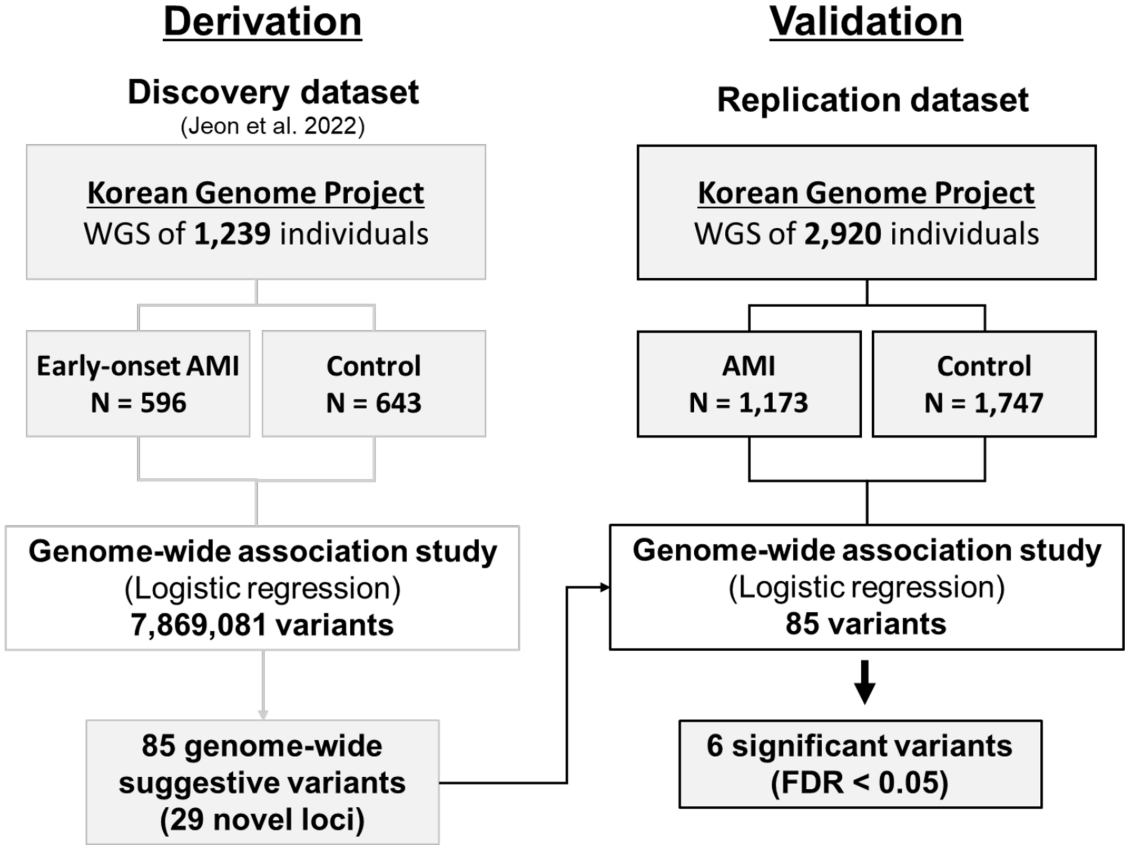

FIGURE 1
Validation process workflow for genetic variants associated with acute myocardial infarction (AMI).

from rs78631167, indicating that the genetic block where these variants lie may have a relationship with AMI. *PLAUR* encodes CD87, which converts plasminogen to plasmin, resulting in clot lysis and plaque healing (3, 14).

Quantitative trait locus associated with acute myocardial infarction

Four significantly replicated variants for AMI and two additional variants upstream of *PLAUR* were found to have at least one quantitative trait locus (QTL), such as eQTL (expression QTL), mQTL (methylation QTL), and tuQTL (transcript usage QTL), from the QTLbase (ver. 2.0), which accumulates information about molecular phenotypes and their QTLs to improve the biological interpretability of genetic markers (**Table 3** and **Supplementary Table S2**). Notably, we found evidence that rs12639020 and rs12639023, which are intergenic variants residing between *LINC02005* and *CNTN3*, may alter the expression and transcript usage of the *CNTN3* gene itself ($P = 1.54 \times 10^{-4}$ in rs12639020 and $P = 2.93 \times 10^{-3}$ in rs12639023; **Supplementary Table S2**) and its neighboring gene, *PDZRN3* ($P = 1.12 \times 10^{-4}$ in rs12639020 and rs12639023; **Table 3**). Both *CNTN3* and *PDZRN3* are involved in the regulation of vascular morphology and permeability (15–19). Moreover, the variant at rs12921822 was shown to affect the expression of a novel gene with an unknown function referred to as *AC009135.1* ($P = 9.08 \times 10^{-3}$; **Supplementary Table S2**), while also influencing the methylation status of the *RBFOX1* itself ($P = 2.43 \times 10^{-18}$; **Table 3**). *RBFOX1* has recurrently proven its relationship with cardiomyopathy (12).

Genetic effects on cardiac mortality and recurrent acute myocardial infarction

Of the six significantly replicated variants for AMI and two additional variants upstream of *PLAUR*, seven variants had greater allele frequency differences between AMI patients with cardiac death and controls than between living patients and controls (**Figures 2A,B**, and **Supplementary Table S3**). Rs12639023, located near the *LINC02005* and the *CNTN3*, showed the largest difference in allele frequency between the cardiac death and the living groups among the patients with AMI (**Figure 2A**; allele frequency in the cardiac death group = 0.3977, allele frequency in the living group = 0.2958, and allele frequency in the control group = 0.2171).

Furthermore, the two variants were found to have enhancing effects [Hazard Ratio (HR) > 1] on longitudinal cardiac mortality and recurrent AMI when the survival associations between the

10.3389/fcvm.2023.1226971

TABLE 2 Results of the genome-wide association studies (GWAS) for the replication of genetic variants associated with early-onset AMI.

Gene	Chromosome	Position	rsID	REF	ALT	Effect allele	Discovery (Early-onset AMI)		Replication (AMI)		Survival analysis		
							Odds ratio	*P*	Odds ratio	*P*	HR	95% CI	*P*
FRG1CP-FRG1DP	20	28,772,995	rs1277393322	G	A	A	5.713	3.36×10^{-18}	5.126	4.66×10^{-23}	0.633	0.271–1.48	0.291
MIR1263-LINC01324	3	164,704,630	rs1351282285	TTAAATG	T	T	0.239	5.67×10^{-10}	0.400	1.13×10^{-09}	NA	NA	NA
LINC02005-CNTN3	3	73,919,636	rs12639023	C	T	C	1.722	2.19×10^{-06}	1.432	2.17×10^{-08}	1.371	1.001–1.877	0.049
MUC4	3	195,788,126	rs1560389462	GGGTGGTGTGACC TGTGGATACTGAGG AAGTGTCGGTGACA GGAAGAGAGGTGG CGTGACCTGTGGAT GCTGAGGAAGTGTC GGTGACAGGAAGAG GGGTGGTGTGACCT GTGGATACTGAGGA AGTGTCGGTGACAG GAAGAGA	G	G	0.256	1.31×10^{-08}	0.093	7.60×10^{-05}	NA	NA	NA
RBFOX1	16	7,002,773	rs12921822	C	T	C	1.601	9.05×10^{-06}	1.388	2.77×10^{-04}	0.982	0.645–1.495	0.931
LINC02005-CNTN3	3	73,919,588	rs12639020	C	T	C	1.722	2.19×10^{-06}	1.267	4.05×10^{-04}	1.302	0.939–1.805	0.114
PLAUR-IRGC	19	43,676,115	rs78631167	T	C	C	0.473	2.93×10^{-06}	0.691	1.58×10^{-03}	1.063	0.525–2.152	0.865
PLAUR-IRGC	19	43,676,102	rs8109584	G	A	A	0.981	0.907	0.3531	1.43×10^{-05}	1.136	0.55–2.347	0.731

TABLE 3 Representative quantitative trait locus (QTL) results of the replicated variants for AMI by QTLbase.

QTL type	rsID	Gene	Tissue	Affected gene	*P*-value
eQTL	rs12639023	*LINC02005-CNTN3*	Blood-macrophage	*PDZRN3*	1.12×10^{-04}
eQTL	rs12639020	*LINC02005-CNTN3*	Blood-macrophage	*PDZRN3*	1.12×10^{-04}
eQTL	rs1560389462	*MUC4*	Artery-tibial	*SMBD1P*	4.18×10^{-06}
eQTL	rs78631167	*PLAUR-IRGC*	Blood-macrophage	*ZNF235*	6.64×10^{-05}
eQTL	rs8109584	*PLAUR-IRGC*	Blood	*PLAUR*	6.39×10^{-13}
eQTL	rs12921822	*RBFOX1*	Brain-prefrontal cortex	*AC009135.1*	9.08×10^{-03}
hQTL	rs8109584	*PLAUR-IRGC*	Blood-neutrophils CD16+	*PLAUR*	2.62×10^{-03}
m6AQTL	rs78631167	*PLAUR-IRGC*	Lymphocyte	*IRGQ*	4.06×10^{-02}
mQTL	rs12639023	*LINC02005-CNTN3*	Blood	*AKR1B1P2*	1.21×10^{-83}
mQTL	rs8109584	*PLAUR-IRGC*	Blood-monocytes CD14+	*PLAUR*	7.99×10^{-11}
mQTL	rs12921822	*RBFOX1*	Blood	*RBFOX1*	2.43×10^{-18}
tuQTL	rs12639023	*LINC02005-CNTN3*	Stem cell-iPSC	*PDZRN3*	7.78×10^{-03}
tuQTL	rs12639020	*LINC02005-CNTN3*	Stem cell-iPSC	*PDZRN3*	7.78×10^{-03}
tuQTL	rs8109584	*PLAUR-IRGC*	Stem cell-iPSC	*PLAUR*	1.98×10^{-03}

Representative QTL results show the QTL with the lowest *P*-value per genetic variant and QTL type.

variants and cardiac mortality were analyzed using longitudinal follow-up data after PCI in individuals with AMI (**Table 2**, **Figures 2C,D**, and **Supplementary Figure S2**). Among these, rs12639023 was the only variant with a significant enhancing effect (HR = 1.371, $P = 0.049$) on longitudinal cardiac mortality and recurrent AMI (**Figure 2C**).

Discussion

This study aimed to identify replicated genetic variants of AMI from 85 previously reported variants associated with early-onset AMI using a new set of 2,920 Koreans. The new independent replication dataset consisted mainly of patients with late-onset AMI. We hypothesized that there are markers that are applicable to both stages or types of AMI. Nonetheless, our sample size including 1,747 healthy controls is still relatively small.

Among the variants related to the four major mechanisms previously mentioned for early-onset AMI (3), a fibrinolysis-related variant was moderately replicated in this study, whereas variants related to thrombosis, inflammation, and lipid metabolism were not significantly replicated. This may be because the replication dataset was mainly composed of patients with late-onset AMI, who were probably more affected by environmental risk factors than by genetic factors. We anticipate that the variants related to the remaining major mechanisms may be significantly replicated if the dataset includes a larger number of patients with early-onset AMI with a high genetic predisposition in the replication dataset. Nevertheless, a variant related to fibrinolysis, rs78631167, located upstream of *PLAUR*, had a modest effect ($P = 1.58 \times 10^{-3}$). Moreover, rs8109584, located 13 bp downstream of rs78631167, was significantly associated with AMI ($P = 1.43 \times 10^{-5}$), suggesting that the genetic block located upstream of *PLAUR* is significantly associated with AMI.

The results of the present study propose that vascular permeability could serve as a crucial mechanism for predicting the occurrence and prognosis of AMI. Of the significantly replicated variants, rs12639023, located near *LINC02005* and *CNTN3*, showed the highest enhancing effect on longitudinal cardiac mortality and recurrent AMI expression. It is also a cis-eQTL that increases the expression of *CNTN3* encoding contactin 3 (**Supplementary Table S2**). Notably, contactin 3 is an activator of Arf6 that has been reported to affect inflammation-induced vascular permeability (15, 16). Elevated vascular permeability causes trackable macromolecules to extravasate, thereby threatening endothelial integrity and dysfunction in cardiovascular disease (19). However, the role of vascular permeability in AMI has not been sufficiently focused on. Phinikaridou et al. demonstrated that vascular permeability is elevated in atherosclerotic vessels compared to stable vessels, and it is higher in rupture-prone than in stable atherosclerotic lesions in a rabbit model (20, 21). Nonetheless, there was a paucity of human studies investigating the association between vascular permeability and AMI in patients, who experience atherosclerotic plaque rupture as a major cause of AMI. The present study suggests that increased vascular permeability could be a potential target as a major pathogenic mechanism contributing to plaque development and rupture, which represent primary steps in the development of AMI. Furthermore, our longitudinal result implies that patients with increased vascular permeability, even after PCI, may face a higher risk of plaque development and rupture, indicating a poor prognosis.

The two key strengths of our study include clearly defined sample collection and replication of genetic markers using thousands of samples in an independent cohort. While most studies have used patients with AMI with heterogeneous phenotypes (22, 23), the present study was designed to include only those patients with AMI who underwent PCI for atherothrombotic occlusive lesions to prevent misclassification of the AMI phenotype. Therefore, AMI samples with non-obstructive and non-atherothrombotic causes, such as spontaneous coronary artery dissection, spasm, and thromboembolism, were excluded. Strict sample filtering allowed us to identify and validate genetic factors related to

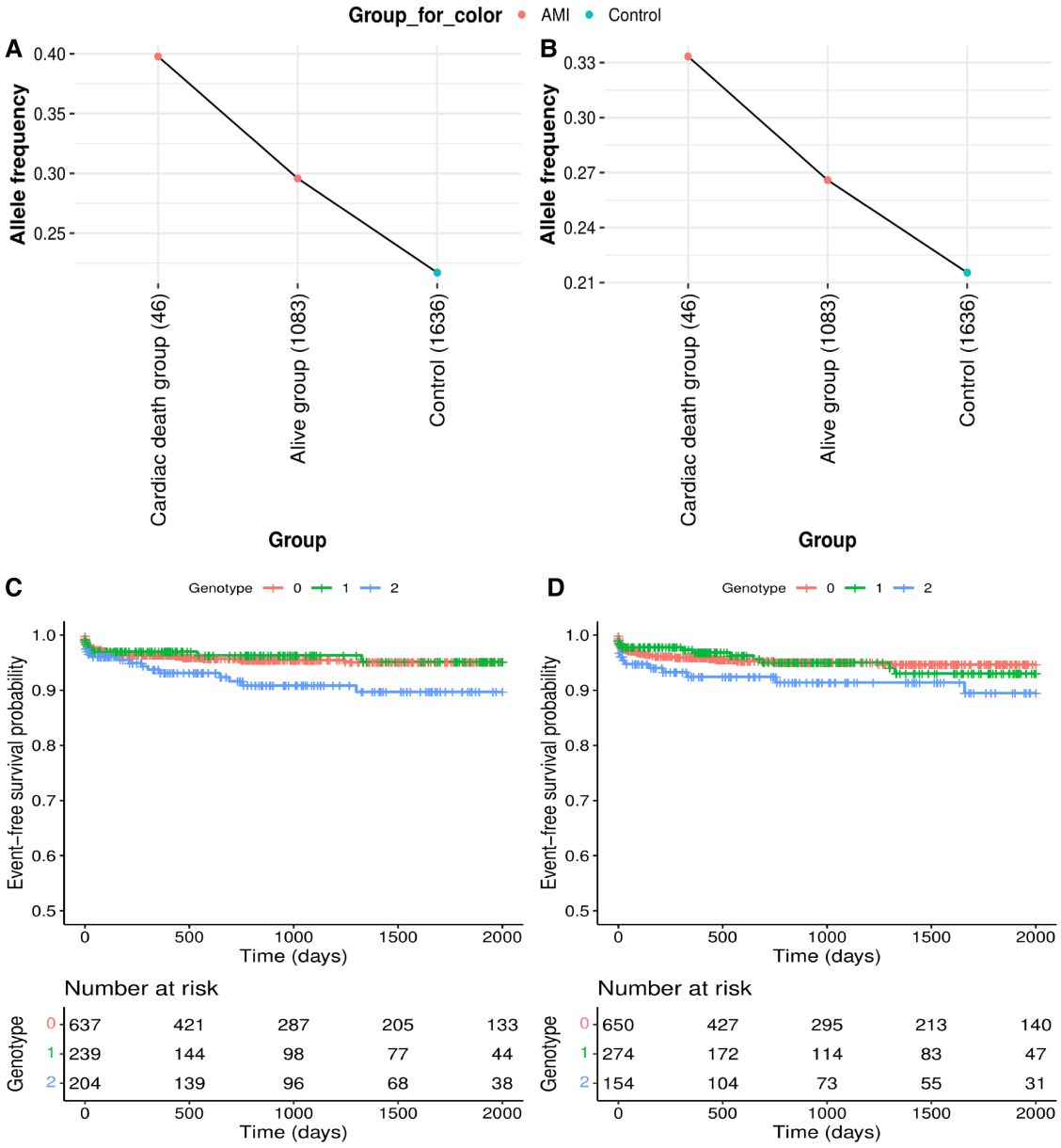

FIGURE 2
Genetic effects on cardiac mortality and recurrent acute myocardial infarction (AMI). (**A**,**B**) Comparison of allele frequencies among cardiac death, alive and control groups in (**A**) rs12639023, *LINC02005-CNTN3* and (**B**) rs12639020, *LINC02005-CNTN3*. (**C**,**D**) Kaplan–Meier curves for two variants with a positive genetic effect for cardiac mortality and recurrent AMI. (**C**) Survival curve by rs12639023 genotype. (**D**) Survival curve by rs12639020 genotype. *X*-axis denotes days from enrollment to death or last follow-up. *Y*-axis denotes event-free survival probability. Event means cardiac mortality and recurrent AMI.

atherothrombosis in AMI, which correspond to most AMI phenotypes. In addition, this study confirmed the replication of potential genetic markers associated with AMI using 2,920 individuals in an independent cohort. This provides evidence that these markers can be used to predict and diagnose AMI.

Our study has two limitations. First, this study was conducted in patients with AMI of Korean ancestry. These results should be validated in populations of multiple races. Second, this study confirmed the replication of AMI-associated variants in a small sample size of 2,920 individuals. While significant variants were observed not in the replication but in the discovery phase, rs8109584, which is 13 bp away from rs78631167, was significantly found in the replication rather than the discovery phase. It is necessary to increase the sample size to ensure validation.

In conclusion, this study confirmed the replication of six genetic variants associated with AMI by using GWAS, QTL mapping, and survival analyses. Our findings highlight the potential of rs12639023 as a prognostic marker for cardiac mortality in AMI. These results provide insights into the latent etiology of AMI. The replicated genetic variants are potential biomarkers for the prediction, prevention, prognosis, and

personalized treatment of AMI in individuals who carry the variant. They could be clinically utilized in routine health check-ups to assess the risk of AMI by a genetic risk score derived from these variants, enabling the early prediction of individuals with a higher genetic predisposition for AMI.

Data availability statement

Full summary statistics relating to the GWAS analysis generated during the current study is available on the Korean Genome Project website (http://koreangenome.org/Cardiomics). All other relevant data are available upon request from the authors.

Ethics statement

The studies involving human participants were reviewed and approved by Ulsan National Institute of Science and Technology. The patients/participants provided their written informed consent to participate in this study.

Author contributions

All authors contributed to the study concept and design. YJ, SJ, KA, JB, and E-SS wrote the manuscript. WK, SL, J-WB, J-YH, MK, and E-SS provided samples and insights into clinical study. YJ and KA conducted the data analysis and visualization. YeK, YoK, and SA performed wet-lab experiments. YJ, SJ, KA, YK, B-CK, HR, W-HC, HC, BK, JB, and E-SS revised the manuscript. JB and E-SS jointly supervised the study. All authors contributed to the article and approved the submitted version.

Funding

This work was supported by the Promotion of Innovative Business for Regulation-Free Special Zones funded by the Ministry of SMEs and Startups (MSS, Korea) (grant number [P0016195, P0016193] (1425156792, 1425157301) (2.220035.01, 2.220036.01)). This work was also supported by the Establishment of Demonstration Infrastructure for Regulation-Free Special Zones fund (MSS, Korea) (grant number [P0016191] (2.220037.01) (1425157253)) by the Ministry of SMEs and Startups. This work was also supported by the Research Project Funded by Ulsan City Research Fund [1.200047.01] of UNIST (Ulsan National Institute of Science and Technology).

Acknowledgments

We thank all the genome donating participants. The biospecimens for this replication study were provided by the Biobanks of Chungbuk National University Hospital (21-3). The biospecimens for the discovery study were provided by the Biobanks of Chungbuk National University Hospital (18-27, 20-04), Ulsan Medical Center, the Biobanks of Gyeongsang National University Hospital, and Kyung Hee University Hospital (2018-4, 2019-4, 2019-6). We thank the Korea Institute of Science and Technology Information (KISTI) which provided us with the Korean Research Environment Open NETwork (KREONET). We also appreciate the Ulsan ICT Promotion Agency (UIPA) which provided us with the BioDataFarm system which supports the storage, analysis, and management of the BioBigData. We thank Subio Bhak and Editage (www.editage.co.kr) for English language editing.

Conflict of interest

YJ, SJ, B-CK, HR, YeK, YoK, BK, and YK were employed by Clinomics Inc. JB is a CEO of Clinomics Inc.

The remaining authors declare that the research was conducted in the absence of any commercial or financial relationships that could be constructed as a potential conflict of interest.

Publisher's note

All claims expressed in this article are solely those of the authors and do not necessarily represent those of their affiliated organizations, or those of the publisher, the editors and the reviewers. Any product that may be evaluated in this article, or claim that may be made by its manufacturer, is not guaranteed or endorsed by the publisher.

Supplementary material

The Supplementary Material for this article can be found online at: https://www.frontiersin.org/articles/10.3389/fcvm.2023.1226971/full#supplementary-material

References

1. Mechanic OJ, Gavin M, Grossman SA. *Acute myocardial infarction*. Treasure Island, FL: StatPearls Publishing (2017).

2. Bhatnagar A. Environmental determinants of cardiovascular disease. *Circ Res*. (2017) 121(2):162–80. doi: 10.1161/CIRCRESAHA.117.306458

3. Jeon Y, Jeon S, Choi W-H, An K, Choi H, Kim B-C, et al. Genome-wide analyses of early-onset acute myocardial infarction identify 29 novel loci by whole genome sequencing. *Hum Genet*. (2022) 142:1–13. doi: 10.1007/s00439-022-02495-0

4. Marenberg ME, Risch N, Berkman LF, Floderus B, de Faire U. Genetic susceptibility to death from coronary heart disease in a study of twins. *N Engl J Med*. (1994) 330(15):1041–6. doi: 10.1056/NEJM199404143301503

5. Jeon S, Bhak Y, Choi Y, Jeon Y, Kim S, Jang J, et al. Korean genome project: 1094 Korean personal genomes with clinical information. *Sci Adv*. (2020) 6(22):eaaz7835. doi: 10.1126/sciadv.aaz7835

6. Jeon Y, Jeon S, Blazyte A, Kim YJ, Lee JJ, Bhak Y, et al. Welfare genome project: a participatory Korean personal genome project with free health check-up and genetic

report followed by counseling. *Front Genet*. (2021) 12:633731. doi: 10.3389/fgene.2021.633731

7. Bhak Y, Jeon Y, Jeon S, Yoon C, Kim M, Blazyte A, et al. Polygenic risk score validation using Korean genomes of 265 early-onset acute myocardial infarction patients and 636 healthy controls. *PLoS One*. (2021) 16(2):e0246538. doi: 10.1371/journal.pone.0246538

8. Purcell S, Neale B, Todd-Brown K, Thomas L, Ferreira MA, Bender D, et al. PLINK: a tool set for whole-genome association and population-based linkage analyses. *Am J Hum Genet*. (2007) 81(3):559–75. doi: 10.1086/519795

9. Therneau T, Lumley T, Elizabeth A. *A package for survival analysis in R*. R package version 3.4-0. (2022).

10. Dungan JR, Qin X, Hurdle M, Haynes CS, Hauser ER, Kraus WE. Genome-wide variants associated with longitudinal survival outcomes among individuals with coronary artery disease. *Front Genet*. (2021) 12:661497. doi: 10.3389/fgene.2021.661497

11. Zheng Z, Huang D, Wang J, Zhao K, Zhou Y, Guo Z, et al. QTLbase: an integrative resource for quantitative trait loci across multiple human molecular phenotypes. *Nucleic Acids Res*. (2020) 48(D1):D983–91. doi: 10.1093/nar/gkz888

12. Gao C, Hsiao Y-H, Wang M, Xiong Z, Ren S, Rau CD, et al. Cytosolic RBFox1 in cardiac pathological remodeling. *Circ Res*. (2018) 123(Suppl 1):A263. doi: 10.1161/res.123.suppl_1.263

13. Carraway KL, Theodoropoulos G, Kozloski GA, Carothers Carraway CA. Muc4/MUC4 functions and regulation in cancer. *Future Oncol*. (2009) 5(10):1631–40. doi: 10.2217/fon.09.125

14. Hill A, Kelly RJ, Hillmen P. Thrombosis in paroxysmal nocturnal hemoglobinuria. *Blood*. (2013) 121(25):4985–96. doi: 10.1182/blood-2012-09-311381

15. Raza A, Xie Z, Chan EC, Chen W-S, Scott LM, Robin Eisch A, et al. A natural mouse model reveals genetic determinants of systemic capillary leak syndrome (clarkson disease). *Commun Biol*. (2019) 2(1):398. doi: 10.1038/s42003-019-0647-4

16. Dickinson ME, Flenniken AM, Ji X, Teboul L, Wong MD, White JK, et al. High-throughput discovery of novel developmental phenotypes. *Nature*. (2016) 537(7621):508–14. doi: 10.1038/nature19356

17. Zhu W, London NR, Gibson CC, Davis CT, Tong Z, Sorensen LK, et al. Interleukin receptor activates a MYD88–ARNO–ARF6 cascade to disrupt vascular stability. *Nature*. (2012) 492(7428):252–5. doi: 10.1038/nature11603

18. Wongsurawat T, Woo CC, Giannakakis A, Lin XY, Cheow ESH, Lee CN, et al. Transcriptome alterations of vascular smooth muscle cells in aortic wall of myocardial infarction patients. *Data Brief*. (2018) 17:1112–35. doi: 10.1016/j.dib.2018.01.108

19. Tiwari A, Elgrably B, Saar G, Vandoorne K. Multi-scale imaging of vascular pathologies in cardiovascular disease. *Front Med (Lausanne)*. (2022) 8:754369. doi: 10.3389/fmed.2021.754369

20. Phinikaridou A, Andia ME, Lavin B, Smith A, Saha P, Botnar RM. Increased vascular permeability measured with an albumin-binding magnetic resonance contrast agent is a surrogate marker of rupture-prone atherosclerotic plaque. *Circ Cardiovasc Imaging*. (2016) 9(12):e004910. doi: 10.1161/CIRCIMAGING.116.004910

21. Phinikaridou A, Andia ME, Plaza BL, Saha P, Smith A, Botnar R. Increased vascular permeability is a surrogate marker of atherosclerotic plaque instability. *J Cardiovasc Magn Reson*. (2015) 17(1):1–2. doi: 10.1186/s12968-014-0101-1

22. Chapman AR, Adamson PD, Mills NL. Assessment and classification of patients with myocardial injury and infarction in clinical practice. *Heart*. (2017) 103(1):10–8. doi: 10.1136/heartjnl-2016-309530

23. McCarthy C, Murphy S, Cohen JA, Rehman S, Jones-O'Connor M, Olshan DS, et al. Misclassification of myocardial injury as myocardial infarction: implications for assessing outcomes in value-based programs. *JAMA Cardiol*. (2019) 4(5):460–4. doi: 10.1001/jamacardio.2019.0716

frontiers | Frontiers in Genetics

TYPE Original Research
PUBLISHED 04 September 2023
DOI 10.3389/fgene.2023.1222368

OPEN ACCESS

EDITED BY
Hongsong Zhang,
Nanjing Medical University, China

REVIEWED BY
Jun Tao,
The First Affiliated Hospital of Sun Yat-sen University, China
Donghai Lin,
Xiamen University, China
Wenhao Xia,
The First Affiliated Hospital of Sun Yat-sen University, China

*CORRESPONDENCE
Li Luo,
hluoli@126.com
Liangdi Xie,
ldxield@163.com

RECEIVED 14 May 2023
ACCEPTED 18 August 2023
PUBLISHED 04 September 2023

CITATION
Gao G, Chen A, Gong J, Lin W, Wu W, Mohammad Ismail Hajary S, Lian G, Luo L and Xie L (2023), Comprehensive analyses of m6A RNA methylation patterns and related immune microenvironment in idiopathic pulmonary arterial hypertension. *Front. Genet.* 14:1222368. doi: 10.3389/fgene.2023.1222368

Comprehensive analyses of m6A RNA methylation patterns and related immune microenvironment in idiopathic pulmonary arterial hypertension

Gufeng Gao [1,2,3,4,5], Ai Chen [1,2,3,4,5], Jin Gong [1,2,3,4,5], Weijun Lin [1,2,3,4,5], Weibin Wu [1,2,3,4,5], Sagor Mohammad Ismail Hajary [1,2,3,4,5], Guili Lian [1,2,3,4,5], Li Luo [1,2,3,4,5]* and Liangdi Xie [1,2,3,4,5]*

[1]Department of Geriatrics, The First Affiliated Hospital of Fujian Medical University, Fujian, Fuzhou, China, [2]Fujian Hypertension Research Institute, The First Affiliated Hospital of Fujian Medical University, Fujian, Fuzhou, China, [3]Clinical Research Center for Geriatric Hypertension Disease of Fujian Province, The First Affiliated Hospital of Fujian Medical University, Fujian, Fuzhou, China, [4]Branch of National Clinical Research Center for Aging and Medicine, The First Affiliated Hospital of Fujian Medical University, Fuzhou, Fujian, China, [5]Department of Geriatrics, National Regional Medical Center, Binhai Campus of the First Affiliated Hospital, Fujian Medical University, Fujian, Fuzhou, China

Idiopathic pulmonary arterial hypertension (IPAH) is a life-threatening disease with a poor prognosis and high heritability, characterized by elevated pulmonary vascular resistance (PVR) and pulmonary artery pressure. N6-methyladenosine (m6A) RNA modification influences many RNA metabolism pathways. However, the position of m6A methylation regulators in IPAH remains unknown. Therefore, the study aims to disclose the function m6A regulators exert in the pathological mechanisms of IPAH and the immune microenvironment involved. The GSE117261 dataset was downloaded from the Gene Expression Omnibus (GEO) to screen the differentially expressed genes (DEGs) between normal and IPAH samples. Functional and pathway enrichment analyses of DEGs were then conducted by Gene ontology (GO) analysis and Kyoto Encyclopedia of Genes and Genomes (KEGG). We also identified the differentially-expressed m6A (DEm6A) regulators between normal and IPAH samples. Key m6A regulators related to the prediction of IPAH were selected using the random forest model. The results showed that FMR1, RBM15, HNRNPA2B1 and IGFBP3 were upregulated in IPAH. In contrast, LRPPRC was downregulated. The single sample gene set enrichment analysis (ssGSEA) method was then adopted to estimate the immune microenvironment in distinct m6A clusters and m6A phenotype-related genes (PRGs) clusters, respectively. Furthermore, we calculated the m6A score via principal component analysis (PCA), and the Sankey diagram was selected to present the correlation among the m6A clusters, m6A PRGs clusters and m6A score. Finally, quantitative RT-PCR and Western blotting were used to validate the key genes in human pulmonary artery smooth muscle cells (HPASMCs) treated by human platelet-derived growth factor-BB (PDGF-BB). The relative mRNA and protein expression levels of FMR1 were significantly elevated, however, the relative mRNA and protein expression levels of LRPPRC were downregulated. Besides, the relative mRNA level of HNRNPA2B1 was increased. Generally, this bioinformatics analysis might provoke more insights into diagnosing and treating IPAH.

KEYWORDS

idiopathic pulmonary arterial hypertension, m6A methylation regulators, immune microenvironment, human pulmonary artery smooth muscle cells, platelet-derived growth factor-BB

1 Introduction

Pulmonary arterial hypertension (PAH) is a rare progressive disease characterized by the occlusion of small pulmonary arteries due to endothelial dysfunction and excessive proliferation of pulmonary arterial smooth muscle cells (PASMCs) and fibroblasts. Treated ineffectively, patients with PAH will die of right heart failure (Aulak et al., 2021). However, almost 30%–40% of PAH patients could not be detected with definite risk factors or causes, so-called idiopathic pulmonary arterial hypertension (IPAH) (Kennedy and Rodgers, 2019). Meanwhile, IPAH is a life-threatening disease with a poor prognosis and high heritability, characterized by elevated pulmonary vascular resistance (PVR) and pulmonary artery pressure (Miyamoto et al., 2021). Despite numerous research on the occurrence and development of IPAH, prevention and treatment remain unsolved problems. Thus, exploring promising biomarkers and prognostic indicators is of obvious necessity for suppressing IPAH.

N6-methyladenosine (m6A) RNA modification, as the major type of RNA modification pattern in eukaryotes, influences many RNA metabolism pathways (Sun et al., 2019). In recent years, new forms of RNA methylations (m5C, m6A, m7G, m1A) have been revealed to occupy an important position in cardiovascular diseases, including pulmonary hypertension (PH), heart failure, hypertension, etc. (Zhou et al., 2021). Zeng et al., (2021). Proved that m6A levels and the expression of methylation-related enzymes were altered in PAH rats, playing crucial roles in PAH development (Zeng et al., 2021). In addition, one of m6A regulators, YTHDF1, has been confirmed to facilitate hypoxic PASMCs proliferation in mice. While silencing of YTHDF1 attenuated pulmonary vascular changes, pulmonary fibrosis and decreased right ventricular systolic pressure compared with PAH mice (Kang et al., 2023). However, the function of m6A regulators in the occurrence of IPAH remains unknown. Therefore, there is of great essential to identify m6A regulators in the development of IPAH and discover new predicted biomarkers and therapeutic targets for IPAH.

In this study, we performed functional and pathway enrichment analysis of differentially expressed genes (DEGs) between normal and IPAH lung tissues on the basis of Gene Expression Omnibus (GEO) databases. A total of 22 m6A regulators in IPAH were then analyzed, and the samples were collected to illustrate m6A modification patterns. Correlation analysis was applied between the m6A modification patterns and the immune microenvironment. Besides, m6A phenotype-related genes (PRGs) between distinct m6A modification patterns were used to generate the m6A PRGs signature. Finally, we validated the relative mRNA and protein expression levels of key genes in platelet-derived growth factor-BB (PDGF-BB) treated human pulmonary artery smooth muscle cells (HPASMCs). Our research established the first integrated bioinformatics analysis of the function of m6A regulators in IPAH, providing some valuable insights into the molecular mechanisms of IPAH at the biological level.

2 Materials and methods

2.1 Data collection and process

GEO is a public database providing high-throughput gene expression and genomics data sets (Barrett et al., 2013). The gene expression dataset GSE117261 (GPL6244, human lung tissues) (Stearman et al., 2019; Romanoski et al., 2020) was accessed from the GEO database and processed by R software (version 4.2.1) and Perl language. The GSE117261 dataset was based on the GPL6244 platform, and the sample species was *homo sapiens*. GSE117261 included 32 IPAH and 25 normal lung tissues. Genes with different expression levels between normal and IPAH lung tissues were collected via the "limma" package with the criterion of adjusted p-value <0.05 and |logFC| >1. A total of 22 m6A regulators were obtained from previous research to observe their expressions between IPAH and normal samples in GSE117261. The regulators include eight writers (METTL3, METTL14, METTL16, WTAP, ZC3H13, RBM15, RBM15B and CBLL1), twelve readers (YTHDC1, YTHDC2, YTHDF1, YTHDF2, YTHDF3, FMR1, LRPPRC, HNRNPA2B1, IGFBP3, IGFBP2, IGFBP3, and ELAVL1) and two erasers (FTO and ALKBH5).

2.2 Functional and enrichment analyses

Gene ontology (GO) analysis and Kyoto Encyclopedia of Genes and Genomes (KEGG) were then performed as functional and enrichment analyses based on the DEGs (adjusted p-value <0.05 and |logFC| >1). GO analysis, including biological processes (BPs), molecular functions (MFs) and cellular components (CCs), is a bioinformatics tool providing annotated genes and analysis of the gene products (Ashburner et al., 2000). Meanwhile, KEGG is a database resource with higher-order functional information for understanding comprehensive analysis of gene functions and genomic information (Kanehisa and Goto, 2000).

2.3 Construction of random forest

With $p < 0.05$, differentially-expressed m6A (DEm6A) methylation regulators between normal and IPAH tissues were selected through the "limma" package. The random forest (RF) and support vector machine (SVM) were both conducted to predict the occurrence of IPAH as training models. A receiver operating characteristic (ROC) curve, reverse cumulative distribution of residual and boxplots of residual were adapted to estimate effective models. Predicting the occurrence of IPAH based on the DEm6A methylation regulators was performed by RF with the "randomForest" package in R software.

2.4 Nomogram model

We established a nomogram model to screen candidate genes using the "rms" package. Calibration curves were constructed to compare the heterogenicity between the observed and the predicted values. Then, we used decision curve analysis (DCA) (Fu J. et al., 2022) and a clinical impact curve to validate the clinical effectiveness of nomograms.

2.5 Discover different m6A clusters and immune microenvironment involved

The "ConsensusClusterPlus" package was operated to differentiate the m6A clusters on the basis of DEm6A methylation regulators. The number of clusters was determined following the cumulative distribution function (CDF) curve and specific k values (Wilkerson and Hayes, 2010). Then, the m6A modification patterns were further validated using principal component analysis (PCA) (Fu et al., 2022). The single sample gene set enrichment analysis (ssGSEA), as a method to evaluate the number of distinct infiltrating immunocytes and their specific immune reactions, was then adapted to estimate the abundance of 23 immune cells between distinct m6A clusters to explore the correlation (Zhang et al., 2021).

2.6 Exploring m6A PRGs signature and immune microenvironment

Genes with different expression levels between distinct m6A clusters (as known as m6A PRGs genes) were picked out through the "limma" package. The selection criteria were formulated as $|\log FC| > 0.5$ and the adjusted p-value < 0.05. Then, m6A PRGs were used to build the m6A Gene signature using the "ConsensusClusterPlus" package. Samples were then classified as distinct m6A PRGs clusters according to the m6A gene signature. The number of m6A PRGs clusters should align with the number of m6A clusters. Similarly, ssGSEA was then performed to observe the link between distinct immune cells and m6A gene signature.

2.7 m6A score calculation

PCA method was applied to calculate the m6A score of each sample based on DEm6A methylation regulators between the normal and IPAH groups. The formula

$$m6A\ score = \Sigma\ (PC1i + PC2i)$$

was used to calculate m6A score, where PC1 stands for principal component 1, PC2 stands for principal component 2, and i stands for the m6A-related genes. Moreover, box plots were performed to understand the m6A score in the two clustering types. Finally, the Sankey diagram was selected to present the correlation among the m6A clusters, m6A PRGs clusters and m6A score.

2.8 Isolation and treatment of HPASMCs

Human pulmonary arteriole samples were obtained based on the protocol approved by the Medical Research and Clinical Technology Application Branch of the Ethics Committee of the First Affiliated Hospital of Fujian Medical University [Approval No. MRCTA, FMU (2001) 483 ECFAH]. These samples were collected from 10 male patients, aged 60 ± 11 years, who had part of their lung lobes removed due to emphysema or lung abscess in the Department of Thoracic Surgery of the First Affiliated Hospital of Fujian Medical University. All participants have understood and signed the written informed consent. Meanwhile, we determined where to take the pulmonary arteries based on the lung lobe to be resected during surgery. Sterile ophthalmic scissors were used to cut the pulmonary arteries of patients into small pieces. Then, small pieces of pulmonary arteries were cultured in DMEM/F12 containing 20% FBS in a humidified environment of 5% CO_2 at 37°C (Wu et al., 2022). The medium was replaced by DMEM with 0.02% FBS and starved for 24 h when the cells were 70%–80% confluent. Treated with human PDGF-BB (Pepro Tech) (20 ng/mL) for 48 h, HPAMSCs were collected for the following testing.

2.9 RNA extraction and real-time quantitative RT-PCR

The Fast-Pure Cell/Tissue Total RNA Isolation KIT V2 (Vazyme, Nanjing, China) was used to extract the total RNA from HPASMCs. HiScript II Q RT SuperMix for qPCR (+gDNA wiper) (Vazyme, Nanjing, China) was selected to obtain cDNA. Finally, Quantitative RT-PCR was performed with ChamQ SYBR qPCR Master Mix in the LightCycler® 96 System (Roche Diagnostics, Mannheim, Germany). The relative expression level of mRNA was calculated based on the $2^{-\Delta\Delta CT}$ method. The primer pairs used in Quantitative RT-PCR were as follows: FMR1 F: 5′-ACT TACGGCAAATGTGTGCCA-3′; R: 5′-GCAGACTCCGAAAGT GCATGT-3′; LRPPRC F: 5′-GATTGCCTGCCGATTGAACC-3′; R: 5′- TGAAGCCCTTGATGTGGGTC-3′; RBM15 F: 5′-GCA GTCCAGAATTGAGCAGTAG-3′; R: 5′-TACCTCGTCTGTCTC TGATTGG-3′; HNRNPA2B1 F: 5′-TGGTGGTAGCAGGAACAT GG-3′; R: 5′-TCAGTATCGGCTCCTCCCAC-3′; IGFBP3 F: 5′-GAATCACCTGAAGTTCCTCAATGT-3′; R: 5′-CTTATCCAC ACACCAGCAGAAG-3′; GAPDH F: 5′-GGTGTGAACCATGAG AAGTATGA-3′; R: 5′-GAGTCCTTCCACGATACCAAAG-3′.

2.10 Protein extraction and Western blotting

Western blotting was performed as previously described (Chen et al., 2010). After PDGF-BB administration, proteins from HPASMCs were extracted by lysis buffer. Lysates were collected to detect the protein concentrations using a BCA protein assay kit (Beyotime, China). Equal volumes of protein lysates were separated by 8% or 10% sodium dodecyl sulfate-polyacrylamide gel electrophoresis and electroblotted onto PVDF membranes before blocking with 5% nonfat milk for 1 h. Subsequently, blots were incubated in primary anti-FMR1 (1:500; Abcam), anti-LRPPRC (1:

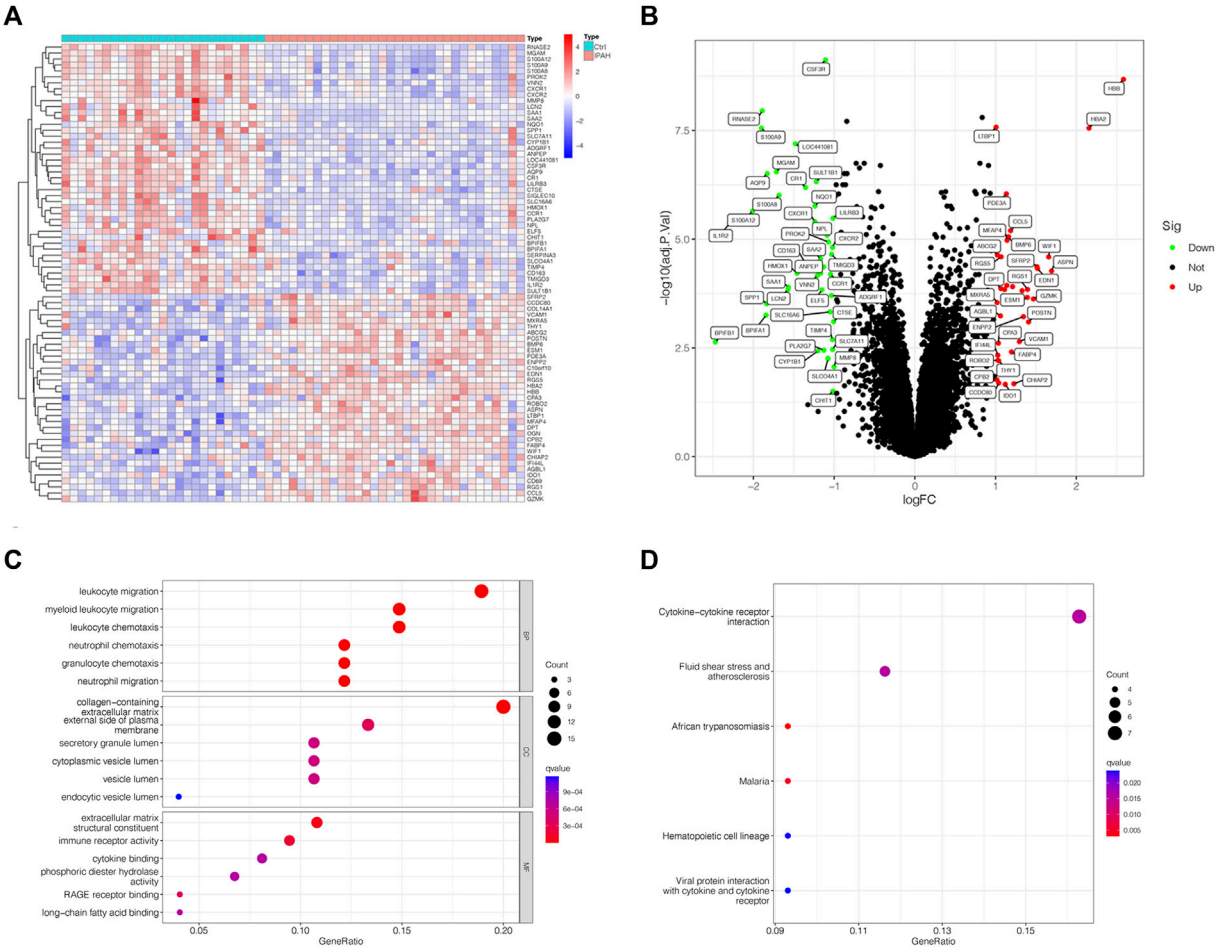

FIGURE 1
Functional and pathway enrichment analysis. **(A)** Heatmap of identified DEGs in lung tissues of normal and IPAH patients based on GSE117261 datasets. **(B)** A volcano map of the DEGs in 25 normal and 32 IPAH samples. **(C)** The BP, CC and MF of DEGs. **(D)** KEGG analysis illustrating pathway enrichment of DEG. DEG, differentially-expressed genes.

500; Proteintech), anti-RBM15 (1:500; Proteintech), antibodies at 4°C overnight. Then, the corresponding secondary antibody was diluted with the PVDF membrane for 1 h at room temperature after washing with TBST three times for 10 min each. Next, the blots were visualized using an ECL detection system (Beyotime, China). Further analysis of the blots was performed using ImageJ software (National Institutes of Health, Bethesda, MD, United States) (Zhong et al., 2018).

2.11 Statistical analysis

Perl, R for mac 4.2.1 software and R studio 2022.07.1 + 554 were conducted in our research. Student's *t*-test or non-parametric one-way analysis of variance (ANOVA) was applied in a two-group comparison or three or more group comparisons, respectively. *p*-value of less than 0.05 with 2-sided defined statistically significant. **** means *p*-value <0.0001; *** means *p*-value <0.001; ** means *p*-value <0.01; * means *p*-value <0.05 and ns means no significance.

3 Results

3.1 Functional and pathway enrichment analysis

DEGs between normal and IPAH samples were collected with the criteria of adjusted *p*-value <0.05 and |logFC| >1. A heatmap was conducted to show the DEGs expression in each sample (Figure 1A). Meanwhile, a volcano map was displayed for an in-depth understanding of the DEGs (Figure 1B). Functional and pathway enrichment analyses were subsequently applied to understand 77 DEGs between normal and IPAH samples comprehensively. The top 6 BP, CC and MF results according to the *p*-value were listed in Figure 1C. Meanwhile, the results of KEGG enrichment analysis suggested that DEGs were statistically concentrated in Pathways of Fluid shear stress and atherosclerosis, Cytokine-cytokine receptor interaction, African trypanosomiasis, cytokine receptor, Malaria and Viral protein interaction with cytokine and Hematopoietic cell lineage (Figure 1D). Notably, MF results showed

10.3389/fgene.2023.1222368

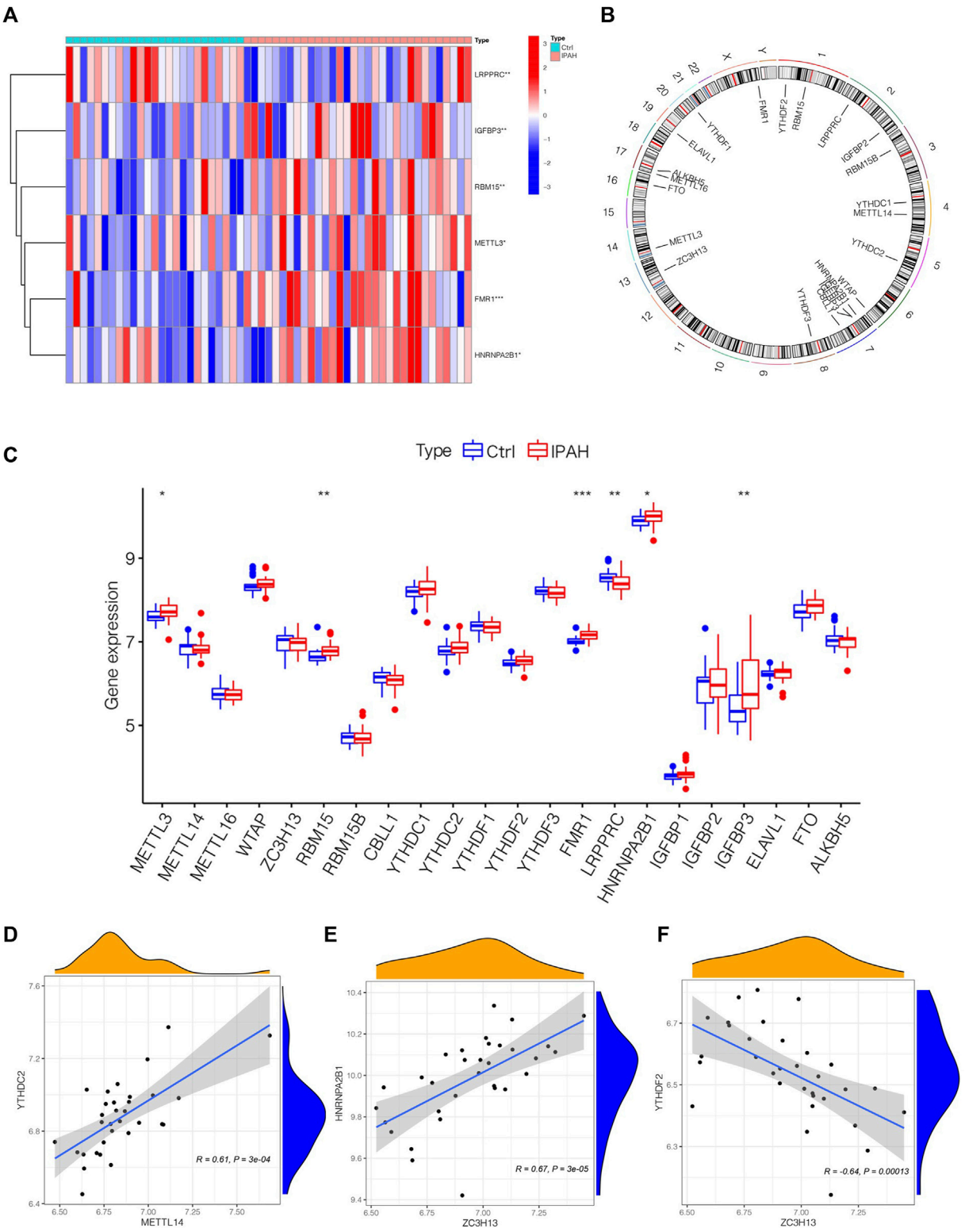

FIGURE 2
The outlook of m6A regulators in the lung tissues of normal and IPAH samples. **(A)** Heatmap of significantly differential-expressed 6 m6A regulators in samples of GSE117261 datasets. **(B)** The location of different m6A regulators on chromosomes. **(C)** Boxplot displaying m6A regulators of different expression levels between Ctrl and IPAH samples. *$p < 0.05$, **$p < 0.01$, ***$p < 0.001$. **(D)** The association between the expression level of METTL14 and YTHDC2. **(E)** The associations between the expression level of ZC3H13 and HNRNPA2B1. **(F)** The associations between the expression level of ZC3H13 and YTHDF2. Ctrl, normal group; IPAH, idiopathic pulmonary arterial hypertension.

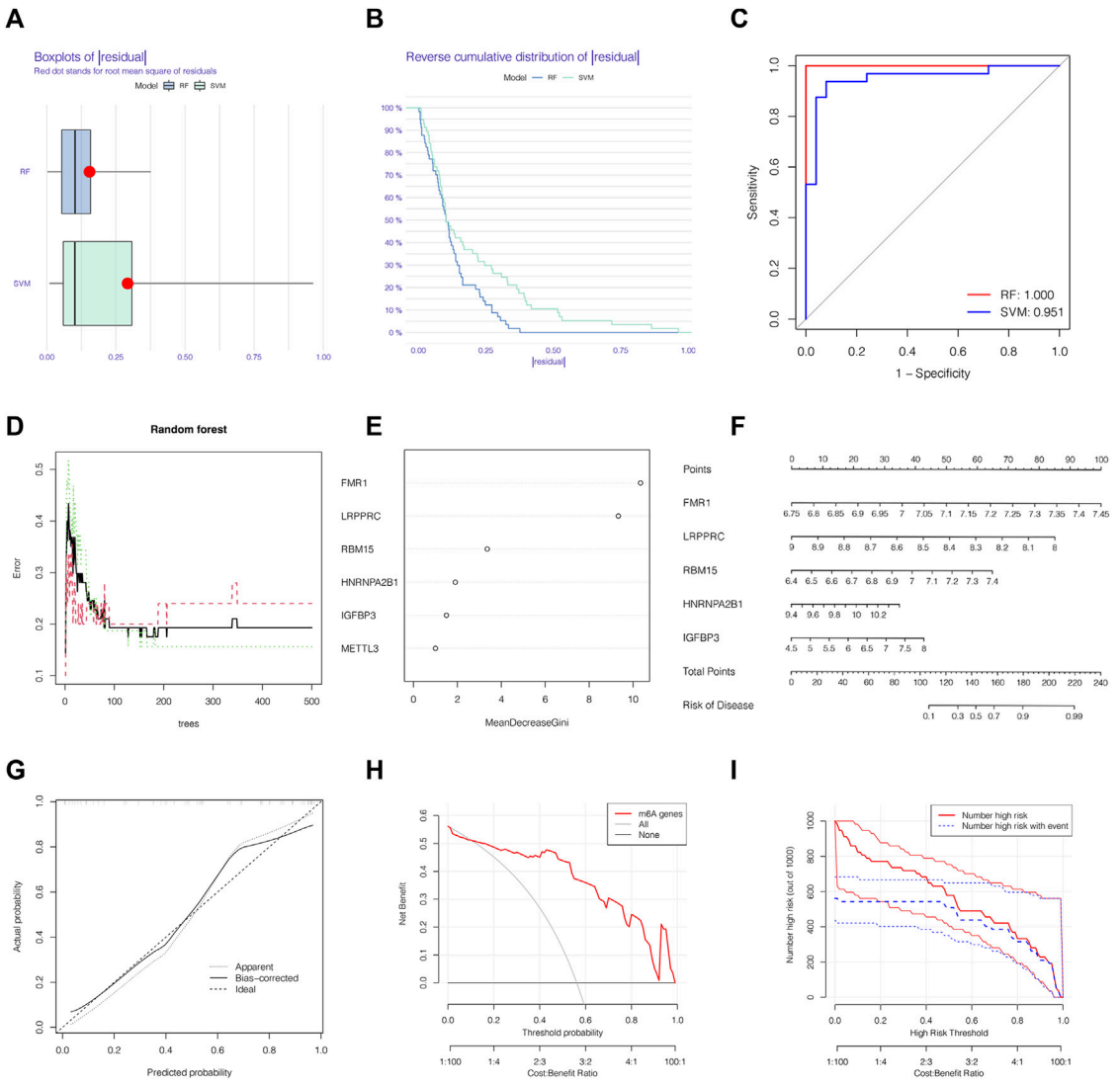

FIGURE 3
The RF was selected to build the IPAH predictive models. **(A)** Residual distribution of RF and SVM displayed by a boxplot. **(B)** The reverse cumulative distribution of residual curve of RF and SVM model. **(C)** The prediction ability of SVM and RF models shown by ROC curves. **(D)** The prediction error curves in the RF model. **(E)** Ranking of differential-expressed m6A regulators by their importance according to RF. **(F)** Nomogram model based on five m6A regulator genes to detect the predictive ability. **(G)** The production efficiency nomogram model illustrated by the calibration curves. **(H,I)** Determination of clinical prediction validity of nomogram model based on decision curve analysis and clinical impact plot. RF, random forest; Ctrl, normal group; IPAH, idiopathic pulmonary arterial hypertension.

that immune receptor activity changed significantly, indicating the disordered immune activity involved in the IPAH development.

3.2 The outlook of m6A regulators in the lung tissues of normal and IPAH samples

To depict the landscape of m6A methylation regulators, we analyzed the differential m6A methylation regulators between normal and IPAH lung tissues. The GSE117261 dataset was used to perform the subsequent analysis. After exploring DEm6A methylation regulators in control (n = 25) and IPAH (n = 32), the expression of m6A methylation regulators was shown by a heatmap (Figure 2A). We also analyzed the location of 22 m6A regulators on chromosomes (Figure 2B). Precisely, the expression of FMR1, RBM15, HNRNPA2B1, IGFBP3 and METTL3 were elevated in IPAH (the criterion of adjusted p-value <0.05 and |logFC| >1); however, LRPPRC was downregulated (the criterion of adjusted p-value <0.05 and |logFC| >1) in IPAH compared with the normal samples (Figure 2C). Furthermore, a co-expression analysis was performed to indicate the positive correlation between METTL14 and YTHDC2, ZC3H13 and HNRNPA2B1, respectively (Figures 2D, E), and the negative correlation between ZC3H13 and YTHDF2 (Figure 2F). In short, 6 differential m6A methylation regulators (FMR1, RBM15, HNRNPA2B1, IGFBP3, METTL3 and LRPPRC) were screened for subsequent studies with the criterion of adjusted p-value <0.05 and |logFC| >1.

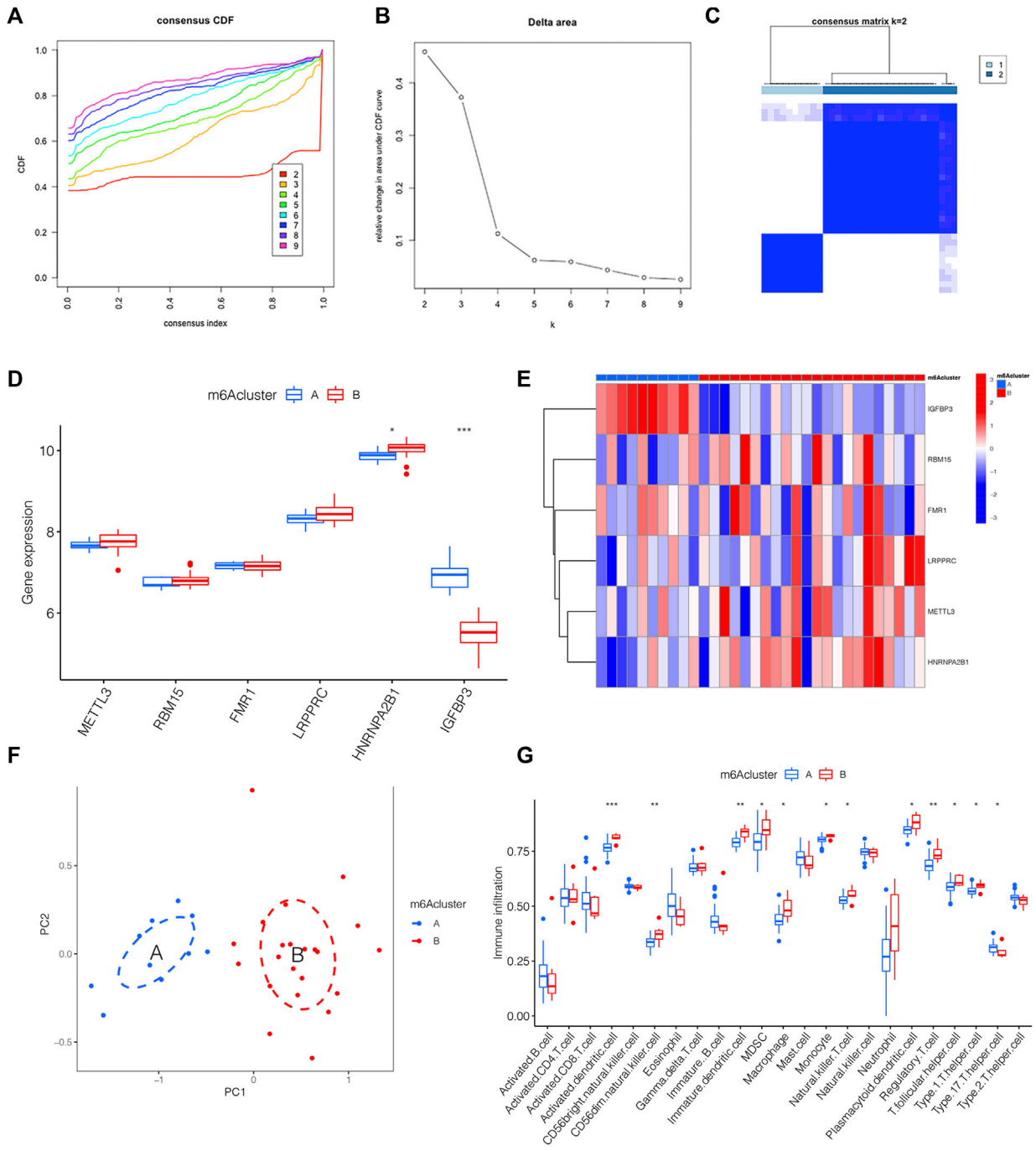

FIGURE 4
The link between distinct m6A clusters and immune microenvironment. **(A)** The consensus CDF curve based on various k (k = 2–9). **(B)** Relative change in area under distinct CDF curve (k = 2–9). **(C)** Consensus clustering matrix of 32 IPAH patients for k = 2. **(D)** The expression level of 6 m6A methylation regulator genes between distinct m6A clusters shown by the boxplot. **(E)** Heatmap displaying the transcriptional profile of 6 m6A methylation regulator genes of distinct m6A clusters. **(F)** PCA illustrating a significant difference between m6A clusters A and B. **(G)** Boxplot presenting the immune microenvironment in m6A clusters A and B. *$p < 0.05$, **$p < 0.01$, ***$p < 0.001$.

3.3 The RF was selected to build the IPAH predictive models

We chose boxplots of residual, reverse cumulative distribution of residual, and a ROC curve (Figures 3A–C) to appraise the prediction accuracy of the RF and SVM methods. Obviously, the RF method is of higher prediction accuracy, so RF method was chosen for ranking the importance of the DEm6A regulators. The optimal ntree was confirmed in Figure 3D. Then, the top 5 genes were defined as the 5 most significant m6A methylation regulators after ranking their importance (Figure 3E). Then, a nomogram model was applied to estimate the susceptibility to IPAH according to the 5 m6A

10.3389/fgene.2023.1222368

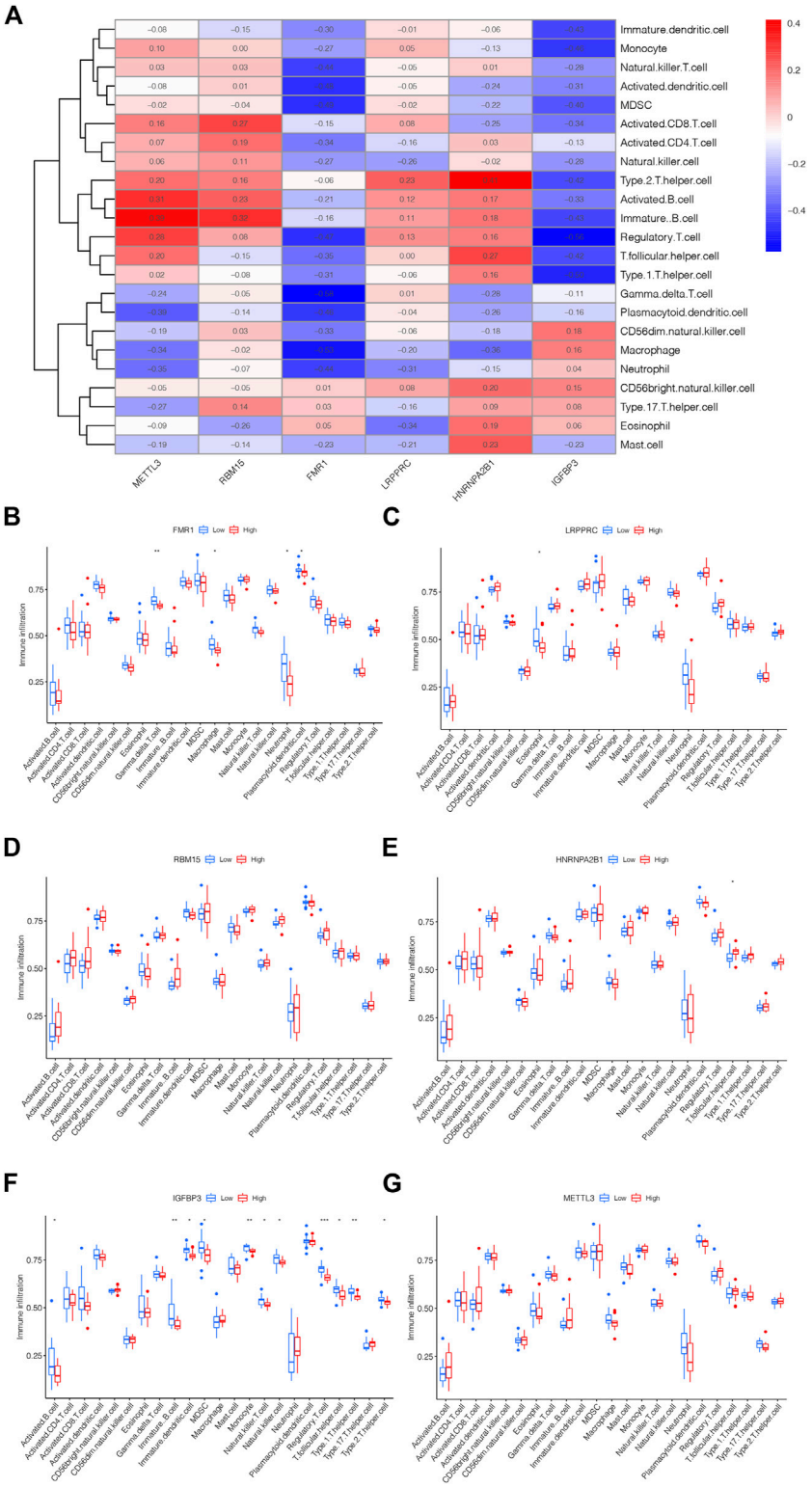

FIGURE 5
The link between m6A methylation regulators and immune microenvironment. **(A)** Heatmap showing the correlation between m5C methylation regulator genes and immune microenvironment. **(B)** The correlation between FMR1 and immune microenvironment. **(C)** The correlation between LRPPRC and immune microenvironment. **(D)** The correlation between RBM15 and immune microenvironment. **(E)** The correlation between HNRNPA2B1 and immune microenvironment. **(F)** The correlation between IGFBP3 and immune microenvironment. **(G)** The correlation between METTL3 and immune microenvironment. $*p < 0.05$, $**p < 0.01$, $***p < 0.001$.

methylation regulators (Figure 3F). The calibration curves revealed that the nomogram method has high predictive power for IPAH (Figure 3G). Finally, decision curve analysis (DCA) and clinical impact curves manifested that the nomogram model was a reliable predictive model for IPAH (Figures 3H, I). It is noteworthy that FMR1, LRPPRC, RBM15, HNRNPA2B1and IGFBP3 were selected as 5 most crucial m6A methylation regulators based on RF method to construct the nomogram model for IPAH.

3.4 The link between distinct m6A clusters and immune microenvironment

We classified distinct m6A clusters according to the seven m6A methylation regulators by conducting the "ConsensusClusterPlus" package in R. Taken 2 as the optimal k value, 32 IPAH samples were grouped into m6A clusters A and B (Figures 4A–C). Compared with m6A cluster A, the expression level of HNRNPA2B1 was higher in m6A cluster B, whereas IGFBP3 declined (Figure 4D). The heat map was also used to illustrate the distinct expression profiles of genes in two m6A clusters (Figure 4E). Then, PCA was used to validate the accuracy of our m6A cluster classification (Figure 4F). Considering the link between IPAH and the immune microenvironment, a deeper analysis of immune cell infiltration was applied. A total of 12 types of immune cells were determined to be statistically different between m6A clusters A and B in Figure 4G, implying that the immune response differs between the two clusters.

3.5 The link between m6A methylation regulators and immune microenvironment

The link between immune cell infiltration and the six m6A methylation regulators' expression profile was demonstrated via a heatmap based on ssGSEA (Figure 5A). Furthermore, we explored the relationship between the immune cell infiltration and six m6A methylation regulators via ssGSEA. As shown in Figure 5B, FMR1 was negatively correlated with Macrophage, Gamma delta T cell, Plasmacytoid dendritic cell and Neutrophil; LRPPRC was negatively correlated with Eosinophil as displayed in Figure 5C; The levels of RBM15 and METTL3 were not significantly linked with immune cell infiltration (Figures 5D, G); HNRNPA2B1 was positively linked with T follicular helper cell could be drawn from Figure 5E; while the IGFBP3 was negatively correlated with Activated B cell, Immature B cell, MDSC, Immature dendritic cell, Natural killer T cell, Natural killer cell, Monocyte, Regulatory T cell, T follicular helper cell, Type 1T helper cell and Type 2T helper cell, displayed in Figure 5F. The above findings confirmed the potential association of these DEm6A methylation regulators with the immune microenvironment in IPAH.

3.6 Generation of the m6A PRGs signature and immune microenvironment

m6A PRGs signature was constructed on the basis of m6A PRGs through the "ConsensusClusterPlus" package in R. In order to be consistent with the number of m6A clusters, the optimal k value of m6A PRG clusters was set as 2 (Figures 6A–C). A heatmap displaying the different expression profiles of m6A PRGs between two m6A PRGs clusters was adopted (Figure 6D). Compared with m6A PRGs cluster A, the expression level of LRPPRC, HNRNPA2B1 and METTL3 were increased in m6A PRGs cluster B; however, IGFBP3 showed the opposite trend (Figure 6E). Finally, we found that nine types of immune cells were statistically differentially expressed between m6A PRGs clusters A and B (Figure 6F), indicating the distinguished characteristics of immune microenvironment infiltration.

3.7 m6A score determination

For the sake of observing the different m6A score in m6A clusters and m6A PRGs clusters, boxplots were then applied, respectively. The m6A score of m6A cluster B was higher than that in m6A cluster A as shown in Figure 7A. Compared to m6A PRGs cluster A, m6A score was higher in m6A PRGs cluster B (Figure 7B). Thus, the m6A score in diverse m6A clusters and m6A PRGs clusters were both statistically different. To better understand the corresponding relations among m6A score, m6A clusters and m6A PRGs clusters, we used the "ggalluvial" R package to produce the Sankey diagram (Figure 7C).

3.8 The mRNA and protein expression levels of the key genes

In order to estimate the expression levels of the selected key genes in HPASMCs with PDGF-BB administration, the quantitative RT-qPCR experiment and Western blotting were conducted. After being treated with PDGF-BB for 48 h, the mRNA and protein expression levels of FMR1 were upregulated (Figures 8A, B); however, the mRNA and protein expression levels of LRPPRC were downregulated in comparison with the control groups (Figures 8C, D), both were in line with the bioinformatics analysis. While the mRNA and protein expression levels of RBM15 remained unchanged (Figures 8E, F), which were not consistent with the results of bioinformatics analysis. Besides, the relative mRNA level of HNRNPA2B1 was increased; the relative mRNA level of IGFBP3 was not changed (Supplementary Figure S1).

4 Discussion

The IPAH, characterized by elevated PVR due to lung remodeling and/or vasoconstriction, is a serious disease leading to cardiopulmonary dysfunction and premature death (Barnes et al., 2019). Recently, new RNA methylations (m5C, m6A, m7G, m1A) have been demonstrated to be a promising target for improving CVDs, including PH (Zhou et al., 2021). As the most common RNA modification in eukaryotes, m6A levels and the expression of m6A methylation regulators have been reported to be altered in monocrotaline (MCT)-induced PAH rats by an integrated analysis (Zeng et al., 2021). Meanwhile, METTL3 and YTHDF2 were proven to be involved in the PASMCs proliferation induced by hypoxia, providing a novel insight for

10.3389/fgene.2023.1222368

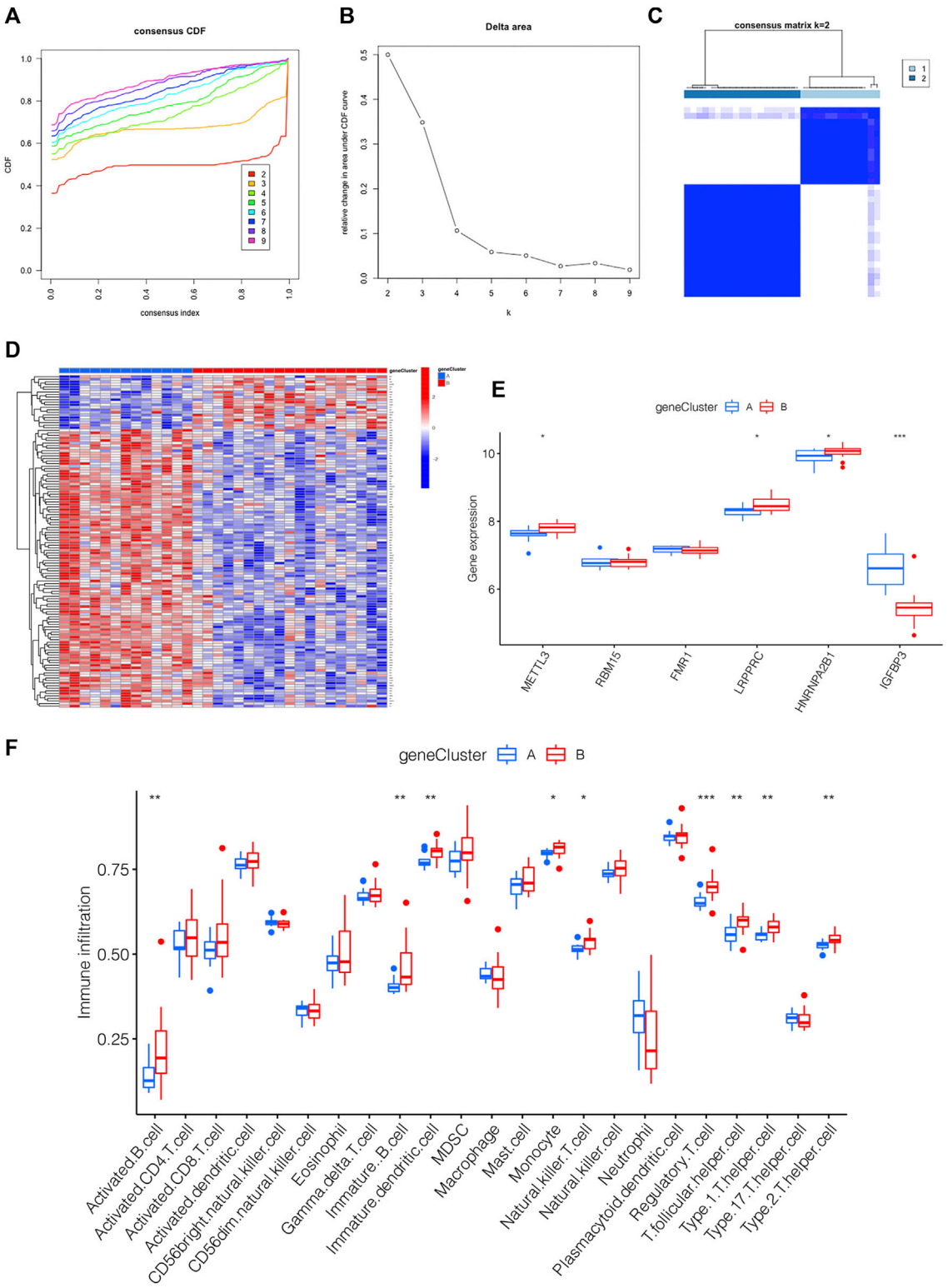

FIGURE 6
Generation of the m6A PRGs signature and immune microenvironment. **(A–C)** The consensus clustering of 130 m6A PRGs. **(D)** Heatmap showing the differential expression of m6A PRGs in distinct gene clusters. **(E)** Expression outlook of 6 m6A methylation regulators in distinct m6A PRGs clusters shown by a boxplot. **(F)** The immune microenvironment in the two m6A PRGs clusters. *$p < 0.05$, **$p < 0.01$, ***$p < 0.001$. Gene cluster, m6A PRGs clusters.

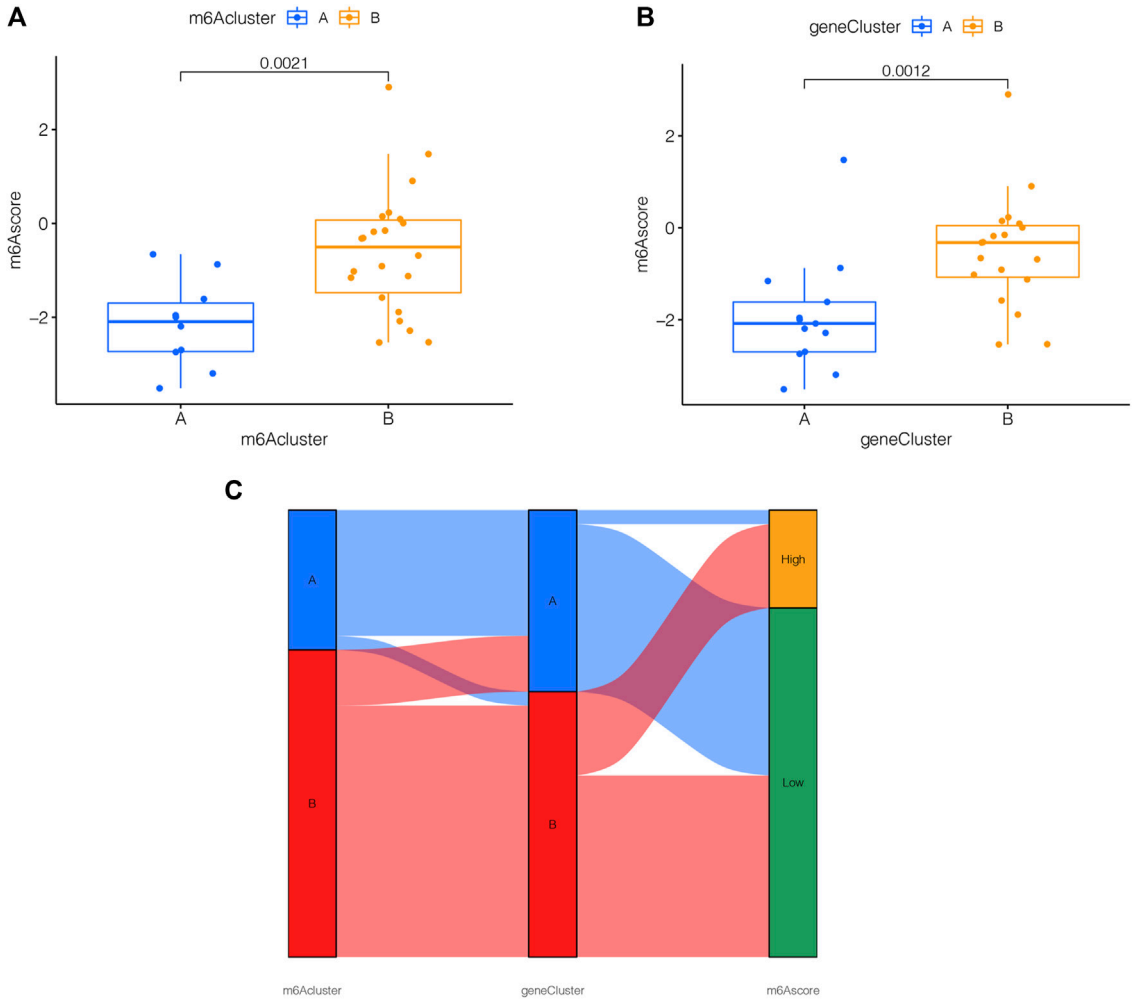

FIGURE 7
m6A score determination. m6A score calculated between **(A)** distinct m6A clusters and **(B)** m6A PRGs clusters. **(C)** Sankey diagram demonstrating the corresponding relations among m6A cluster, m6A PRGs clusters and m6A score. Gene cluster: m6A PRGs clusters.

treating hypoxic PH (HPH) (Qin et al., 2021). However, the function of m6A methylation regulators in IPAH has not been discussed yet.

Therefore, in this research, bioinformatics analysis was adopted on the basis of the GSE117261 database. GO and KEGG were performed to analyze the functional and pathway enrichment based on the DEGs between 25 normal samples and 32 IPAH samples. The results of MF suggested that the pathology of IPAH may be related to abnormal immune activity. Previous reports have also shown that compromised immune homeostasis might lead to IPAH progression (Heukels et al., 2021).

Besides, 6 differential-expressed m6A methylation regulators were screened, including 5 upregulated regulators and 1 downregulated regulator. Compared with SVM, the RF showed higher accuracy in predicting disease occurrence. Thence, FMR1, LRPPRC, RBM15, HNRNPA2B1, and IGFBP3 were identified as the 5 most important genes after ranking their importance via the RF model. Among them, the expression level of FMR1, RBM15, HNRNPA2B1 and IGFBP3 were upregulated in IPAH; however, LRPPRC was downregulated. Meanwhile, FMR1 ranked as the most crucial one.

Studies in recent years have revealed similarities in the pathological mechanisms of PAH and cancer, including increased cell proliferation, resistance to apoptosis, and enhanced Warburg effect, suggesting PAH is a pseudo-malignant disease (Rehman and Archer, 2010; Boucherat et al., 2017; Liu et al., 2017). Besides, elevated expression of FMR1 was regarded as a pathogenic target in promoting cell proliferation in esophageal squamous cell carcinoma (ESCC) (Men et al., 2022); the positive feedback loop HNF4α-BC200-FMR1 is also necessary in promoting invasive mucinous lung adenocarcinoma (IMA) progression and metastasis. Based on the above research, we assumed that the increased FMR1 might be associated with the hyperproliferation of PASMCs.

LRPPRC, as a mitochondrion-associated protein, has been demonstrated as an autophagy inhibitor in many pieces of research. LRPPRC has been reported to decline under constant mitophagy stress, then initiating the autophagy level in cells by impairing the stability of Bcl-2 (Zou et al., 2013; Zou et al., 2014; Zou et al., 2015). In addition, increased autophagy level have been reported to play a significant role in many lung diseases,

10.3389/fgene.2023.1222368

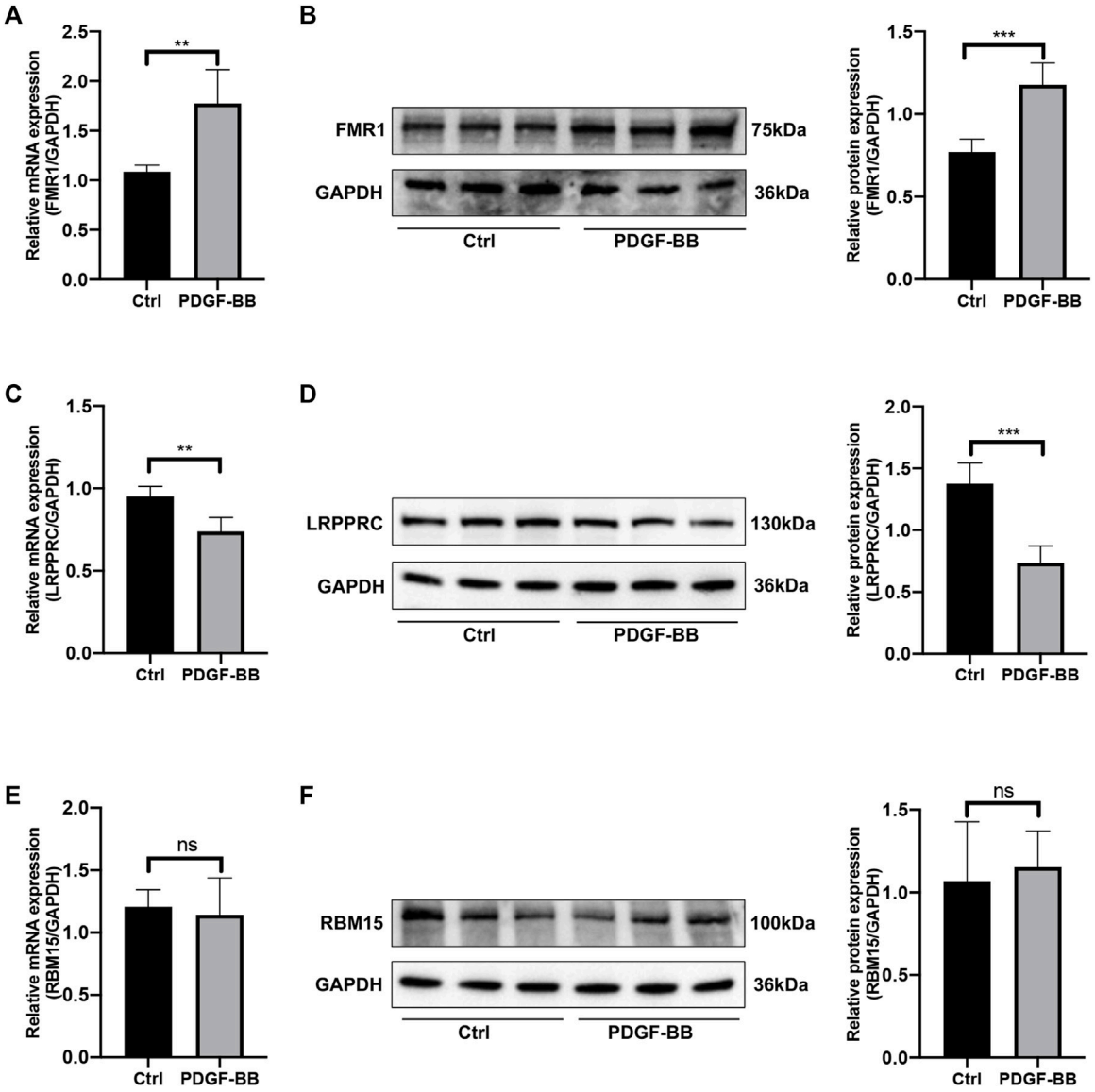

FIGURE 8
The mRNA and protein expression levels of key genes. **(A)** Relative mRNA level of FMR1 in control vs. PDGF-BB treated group. **(B)** Relative protein expression level of FMR1 in control vs. PDGF-BB treated group. **(C)** Relative mRNA level of LRPPRC in control vs. PDGF-BB treated group. **(D)** Relative protein expression level of LRPPRC in control vs. PDGF-BB treated group. **(E)** Relative mRNA level of RBM15 in control vs. PDGF-BB treated group. **(F)** Relative protein expression level of RBM15 in control vs. PDGF-BB treated group. *$p < 0.05$, **$p < 0.01$, ***$p < 0.001$, ns, no significance. Data are presented as mean ± standard deviation (mean ± SD), $n = 5$.

including PAH (Ornatowski et al., 2020). Thus, we supposed the decreased LRPPRC in our results might lead to enhanced autophagy levels in IPAH, which has not yet been illustrated in previous studies.

In our results, RBM15 is elevated. Consistent with previous research, increased RBM15 is also related to the development of tumors, such as colorectal cancer, laryngeal squamous cell cancer (LSCC) and pancreatic adenocarcinoma. It was reported that knocking down RBM15 inhibits colorectal cancer cell proliferation and metastasis as reported (Zhang Z. et al., 2021). Meanwhile, as a "writer" of methyltransferase, RBM15 was increased in LSCC, indicating an unfavorable prognosis; the decline of RBM15 reduced the proliferation, migration and invasion of LSCC cells (Wang et al., 2021). Besides, suppression RBM15 could significantly reduce pancreatic cancer cell proliferation in pancreatic adenocarcinoma (Zhao et al., 2022). Due to the similarity of PAH and tumors, we supposed RBM15 was a risk factor in the development of IPAH, which has not been proposed previously.

Similarly, increased HNRNPA2B1 was found in human PAH-PASMC and MCT-PAH rats, and inhibition of HNRNPA2B1 applied *in vivo* rescued PH in rats (Ruffenach et al., 2022); IGFBP-3 was revealed to promote the proliferation of HPASMCs under persistent hypoxia (Ismail et al., 2009); METTL3/YTHDF2/PTEN axis also plays a crucial role in hypoxia-induced PASMCs proliferation (Qin et al., 2021). In general, our analysis identified FMR1, LRPPRC and RBM15 as novel factors involved in PAH as well as IPAH for the first time, which is one of the most crucial scientific significances for our research. Therefore,

FMR1, LRPPRC and RBM15 were selected for quantitative RT-PCR and Western blotting validation. While for HNRNPA2B1 and IGFBP3, only quantitative RT-PCR was performed.

Previous reports displayed that PASMCs from patients with IPAH showed a higher growth rate stimulated by PDGF-BB than that of control cells (Ogawa et al., 2005; Fujio et al., 2006; Ikeda et al., 2010); besides, the PDGF-receptor inhibitor such as imatinib (STI571) is attracting more and more attention as a promising therapy for PH (Ghofrani et al., 2005; Schermuly et al., 2005; Perros et al., 2008; Hatano et al., 2010). Therefore, we observed the relative mRNA and protein expression levels of key genes in HPASMCs treated by PDGF-BB for 48 h.

Besides, the results of MF indicated that abnormal immune receptor activity was involved in IPAH. Furthermore, we found that the immune cells infiltration in two m6A clusters and two m6A PRGs clusters were identified, suggesting the distinguished immune responses in the different m6A clusters. We also used ssGSEA to estimate the relationship between the immune cell infiltration and six DEm6A methylation regulators. The results incarnate a tight correlation between the immune microenvironment in IPAH and these six methylation regulators. Besides, several past reports confirmed our fundings. Qu et al., (2022) demonstrated that PAH might be associated with dysregulation of the immune microenvironment as well as an abnormal immune response (Qu et al., 2022). In addition, modulation of the immune microenvironment may help to slow the progression of PH (Guo et al., 2021). The previous research also explored the potential association of m6A RNA methylation regulators with the tumor immune microenvironment in Esophageal squamous cell carcinoma (ESCC), indicating that these key m6A methylation regulators may be crucial mediators of immune cell infiltration (Guo et al., 2021). Similarly, it was shown that m6A-regulated genes are linked to immune status in hepatocellular carcinoma (HCC) (Li et al., 2022). In our result, the m6A score of m6A clusters and m6A PRGs clusters were also calculated to have a better understanding of samples in different clusters based on DEm6A methylation regulators.

Whereas, there are still some flaws in our research. First, the mechanisms underlying IPAH were still unclear; thus, deeper bioinformatics analyses and experimental verifications are needed. Second, multiple microarray analyses have higher detection accuracy than single microarray analyses, so integrated microarray analyses should be performed in a future study. Third, to improve the prediction accuracy of the screened genes related to IPAH, it is necessary to enlarge the sample size for further proof. Fourth, because of clinical data lacking and heterogeneity of IPAH patients, risk indicators related to the degree of patients under the severity of IPAH are hard to summarize. Fifth, samples of IPAH with different severity are essential to distinguish the mechanisms underlying the occurrence and development of IPAH.

In conclusion, our study provided an integrated analysis by processing GSE117261 to discover the DEm6A regulator genes connected to the development of IPAH. 77 DEGs between normal and IPAH samples were collected for functional and pathway enrichment analysis, indicating the abnormal immune activity involved with IPAH. 5 key m6A modification regulators were screened out. 2 m6A clusters and 2 m6A PRGs clusters were distinguished. Besides, the immune microenvironment correlated to different m6A modification patterns was also checked. Furthermore, quantitative RT-PCR and Western blotting were performed to determine the key genes in HPASMCs stimulated by PDGF-BB. The relative mRNA and protein expression levels of FMR1 were increased, while the relative mRNA and protein expression levels of LRPPRC were decreased. Besides, the relative mRNA level of HNRNPA2B1 was significantly increased.

Data availability statement

Publicly available datasets were analyzed in this study. This data can be found here: https://www.ncbi.nlm.nih.gov/geo/query/acc.cgi?acc=GSE117261.

Ethics statement

The studies involving humans were approved by the Medical Research and Clinical Technology Application Branch of the Ethics Committee of the First Affiliated Hospital of Fujian Medical University [Approval No. MRCTA, FMU (2001) 483 ECFAH]. The studies were conducted in accordance with the local legislation and institutional requirements. The participants provided their written informed consent to participate in this study.

Author contributions

GG organized and wrote the manuscript. AC, JG, and WL produced the figures and visualized the data. WW, SM, and GL validated the project. LL and LX revised the manuscript. All authors contributed to the article and approved the submitted version.

Funding

This work was supported by the National Natural Science Foundation of China (82170355), Joint Funds for the Innovation of Science and Technology, Fujian province (2019Y9124), Fujian Clinical Medical Research Center for Geriatric Hypertensive Disease (SLN-YJZX) and 2020 Joint Fund of the Provincial Science and Technology Department for the “Creation of Double Highs” (2020Y9108).

Acknowledgments

The authors would like to thank the editors and reviewers for their valuable comments and participants and participating physicians from the First Affiliated Hospital of Fujian Medical University, China. Meanwhile, the authors acknowledge GEO database for providing their platform and contributors for uploading their meaningful datasets.

Conflict of interest

The authors declare that the research was conducted in the absence of any commercial or financial relationships that could be construed as a potential conflict of interest.

Publisher's note

All claims expressed in this article are solely those of the authors and do not necessarily represent those of their affiliated organizations, or those of the publisher, the editors and the reviewers. Any product that may be evaluated in this article, or claim that may be made by its manufacturer, is not guaranteed or endorsed by the publisher.

Supplementary material

The Supplementary Material for this article can be found online at: https://www.frontiersin.org/articles/10.3389/fgene.2023.1222368/full#supplementary-material

References

Ashburner, M., Ball, C. A., Blake, J. A., Botstein, D., Butler, H., Cherry, J. M., et al. (2000). Gene ontology: tool for the unification of biology. The gene ontology Consortium. *Nat. Genet.* 25 (1), 25–29. doi:10.1038/75556

Aulak, K. S., Al Abdi, S., Li, L., Crabb, J. S., Ghosh, A., Willard, B., et al. (2021). Disease-specific platelet signaling defects in idiopathic pulmonary arterial hypertension. *Am. J. Physiology-Lung Cell. Mol. Physiology* 320 (5), L739–L749. doi:10.1152/ajplung.00500.2020

Barnes, J. W., Tian, L., Krick, S., Helton, E. S., Denson, R. S., Comhair, S. A., et al. (2019). O-GlcNAc transferase regulates angiogenesis in idiopathic pulmonary arterial hypertension. *Int. J. Mol. Sci.* 20 (24), 6299. doi:10.3390/ijms20246299

Barrett, T., Wilhite, S., Ledoux, P., Evangelista, C., Kim, I., Tomashevsky, M., et al. (2013). NCBI GEO: archive for functional genomics data sets--update. *Nucleic Acids Res.* 41, D991–D995. doi:10.1093/nar/gks1193

Boucherat, O., Vitry, G., Trinh, I., Paulin, R., Provencher, S., and Bonnet, S. (2017). The cancer theory of pulmonary arterial hypertension. *Pulm. Circ.* 7 (2), 285–299. doi:10.1177/2045893217701438

Chen, H.-F., Xie, L.-D., and Xu, C.-S. (2010). The signal transduction pathways of heat shock protein 27 phosphorylation in vascular smooth muscle cells. *Mol. Cell. Biochem.* 333, 49–56. doi:10.1007/s11010-009-0203-5

Fu, C., Feng, L., Zhang, J., and Sun, D. (2022a). Bioinformatic analyses of the role of m6A RNA methylation regulators in abdominal aortic aneurysm. *Ann. Transl. Med.* 10 (10), 547. doi:10.21037/atm-22-1891

Fu, J., Tu, M., Zhang, Y., Zhang, Y., Wang, J., Zeng, Z., et al. (2022b). A model of multiple tumor marker for lymph node metastasis assessment in colorectal cancer: A retrospective study. *PeerJ* 10, e13196. doi:10.7717/peerj.13196

Fujio, H., Nakamura, K., Matsubara, H., Kusano, K. F., Miyaji, K., Nagase, S., et al. (2006). Carvedilol inhibits proliferation of cultured pulmonary artery smooth muscle cells of patients with idiopathic pulmonary arterial hypertension. *J. Cardiovasc. Pharmacol.* 47 (2), 250–255. doi:10.1097/01.fjc.0000201359.58174.c8

Ghofrani, H. A., Seeger, W., and Grimminger, F. (2005). Imatinib for the treatment of pulmonary arterial hypertension. *N. Engl. J. Med.* 353 (13), 1412–1413. doi:10.1056/NEJMc051946

Guo, L., Qin, G., Cao, Y., Yang, Y., Dai, S., Wang, L., et al. (2021a). Regulation of the immune microenvironment by an NLRP3 inhibitor contributes to attenuation of acute right ventricular failure in rats with pulmonary arterial hypertension. *J. Inflamm. Res.* 14, 5699–5711. doi:10.2147/JIR.S336964

Guo, W., Tan, F., Huai, Q., Wang, Z., Shao, F., Zhang, G., et al. (2021b). Comprehensive analysis of PD-L1 expression, immune infiltrates, and m6A RNA methylation regulators in esophageal squamous cell carcinoma. *Front. Immunol.* 12, 669750. doi:10.3389/fimmu.2021.669750

Hatano, M., Yao, A., Shiga, T., Kinugawa, K., Hirata, Y., and Nagai, R. (2010). Imatinib mesylate has the potential to exert its efficacy by down-regulating the plasma concentration of platelet-derived growth factor in patients with pulmonary arterial hypertension. *Int. Heart J.* 51 (4), 272–276. doi:10.1536/ihj.51.272

Heukels, P., Corneth, O. B., van Uden, D., van Hulst, J. A., van den Toorn, L. M., van den Bosch, A. E., et al. (2021). Loss of immune homeostasis in patients with idiopathic pulmonary arterial hypertension. *Thorax* 76 (12), 1209–1218. doi:10.1136/thoraxjnl-2020-215460

Ikeda, T., Nakamura, K., Akagi, S., Kusano, K. F., Matsubara, H., Fujio, H., et al. (2010). Inhibitory effects of simvastatin on platelet-derived growth factor signaling in pulmonary artery smooth muscle cells from patients with idiopathic pulmonary arterial hypertension. *J. Cardiovasc. Pharmacol.* 55 (1), 39–48. doi:10.1097/FJC.0b013e3181c0419c

Ismail, S., Sturrock, A., Wu, P., Cahill, B., Norman, K., Huecksteadt, T., et al. (2009). NOX4 mediates hypoxia-induced proliferation of human pulmonary artery smooth muscle cells: the role of autocrine production of transforming growth factor-{beta}1 and insulin-like growth factor binding protein-3. *Am. J. Physiology-Lung Cell. Mol. Physiology* 296 (3), L489–L499. doi:10.1152/ajplung.90488.2008

Kanehisa, M., and Goto, S. (2000). Kegg: kyoto encyclopedia of genes and genomes. *Nucleic acids Res.* 28 (1), 27–30. doi:10.1093/nar/28.1.27

Kang, T., Liu, L., Tan, F., Zhang, D., Yu, L., Jiang, H., et al. (2023). Inhibition of YTHDF1 prevents hypoxia-induced pulmonary artery smooth muscle cell proliferation by regulating Foxm1 translation in an m6A-dependent manner. *Exp. Cell Res.* 424 (2), 113505. doi:10.1016/j.yexcr.2023.113505

Kennedy, P. G., and Rodgers, J. (2019). Clinical and neuropathogenetic aspects of human African trypanosomiasis. *Front. Immunol.* 10, 39. doi:10.3389/fimmu.2019.00039

Li, D., Li, K., Zhang, W., Yang, K.-W., Mu, D.-A., Jiang, G.-J., et al. (2022). The m6A/m5C/m1A regulated gene signature predicts the prognosis and correlates with the immune status of hepatocellular carcinoma. *Front. Immunol.* 13, 918140. doi:10.3389/fimmu.2022.918140

Liu, N., Parry, S., Xiao, Y., Zhou, S., and Liu, Q. (2017). Molecular targets of the Warburg effect and inflammatory cytokines in the pathogenesis of pulmonary artery hypertension. *Clin. Chim. Acta* 466, 98–104. doi:10.1016/j.cca.2017.01.015

Men, Y., Zhai, Y., Wu, L., Liu, L., Zhang, W., Jiang, W., et al. (2022). MiR-323a-3p acts as a tumor suppressor by suppressing FMR1 and predicts better esophageal squamous cell carcinoma outcome. *Cancer cell Int.* 22 (1), 140–212. doi:10.1186/s12935-022-02541-x

Miyamoto, K., Inai, K., Kobayashi, T., Maeda, J., Takatsuki, S., Nakayama, T., et al. (2021). Outcomes of idiopathic pulmonary arterial hypertension in Japanese children: A retrospective cohort study. *Heart vessels* 36 (9), 1392–1399. doi:10.1007/s00380-021-01806-1

Ogawa, A., Nakamura, K., Matsubara, H., Fujio, H., Ikeda, T., Kobayashi, K., et al. (2005). Prednisolone inhibits proliferation of cultured pulmonary artery smooth muscle cells of patients with idiopathic pulmonary arterial hypertension. *Circulation* 112 (12), 1806–1812. doi:10.1161/CIRCULATIONAHA.105.536169

Ornatowski, W., Lu, Q., Yegambaram, M., Garcia, A. E., Zemskov, E. A., Maltepe, E., et al. (2020). Complex interplay between autophagy and oxidative stress in the development of pulmonary disease. *Redox Biol.* 36, 101679. doi:10.1016/j.redox.2020.101679

Perros, F., Montani, D., Dorfmüller, P., Durand-Gasselin, I., Tcherakian, C., Le Pavec, J., et al. (2008). Platelet-derived growth factor expression and function in idiopathic pulmonary arterial hypertension. *Am. J. Respir. Crit. care Med.* 178 (1), 81–88. doi:10.1164/rccm.200707-1037OC

Qin, Y., Qiao, Y., Li, L., Luo, E., Wang, D., Yao, Y., et al. (2021). The m6A methyltransferase METTL3 promotes hypoxic pulmonary arterial hypertension. *Life Sci.* 274, 119366. doi:10.1016/j.lfs.2021.119366

Qu, L.-H., Luo, W.-J., Yan, Z.-G., and Liu, W.-P. (2022). FAM171B as a novel biomarker mediates tissue immune microenvironment in pulmonary arterial hypertension. *Mediat. Inflamm.* 2022, 1878766. doi:10.1155/2022/1878766

Rehman, J., and Archer, S. L. (2010). A proposed mitochondrial–metabolic mechanism for initiation and maintenance of pulmonary arterial hypertension in fawn-hooded rats: the Warburg model of pulmonary arterial hypertension. *Membr. Recept. channels Transp. Pulm. circulation* 661, 171–185. doi:10.1007/978-1-60761-500-2_11

Romanoski, C. E., Qi, X., Sangam, S., Vanderpool, R. R., Stearman, R. S., Conklin, A., et al. (2020). Transcriptomic profiles in pulmonary arterial hypertension associate with disease severity and identify novel candidate genes. *Pulm. Circ.* 10 (4), 2045894020968531. doi:10.1177/2045894020968531

Ruffenach, G., Medzikovic, L., Aryan, L., Li, M., and Eghbali, M. (2022). HNRNPA2B1: RNA-Binding protein that Orchestrates smooth muscle cell

phenotype in pulmonary arterial hypertension. *Circulation* 146, 1243–1258. doi:10.1161/CIRCULATIONAHA.122.059591

Schermuly, R. T., Dony, E., Ghofrani, H. A., Pullamsetti, S., Savai, R., Roth, M., et al. (2005). Reversal of experimental pulmonary hypertension by PDGF inhibition. *J. Clin. investigation* 115 (10), 2811–2821. doi:10.1172/JCI24838

Stearman, R. S., Bui, Q. M., Speyer, G., Handen, A., Cornelius, A. R., Graham, B. B., et al. (2019). Systems analysis of the human pulmonary arterial hypertension lung transcriptome. *Am. J. Respir. cell Mol. Biol.* 60 (6), 637–649. doi:10.1165/rcmb.2018-0368OC

Sun, T., Wu, R., and Ming, L. (2019). The role of m6A RNA methylation in cancer. *Biomed. Pharmacother.* 112, 108613. doi:10.1016/j.biopha.2019.108613

Wang, X., Tian, L., Li, Y., Wang, J., Yan, B., Yang, L., et al. (2021). RBM15 facilitates laryngeal squamous cell carcinoma progression by regulating TMBIM6 stability through IGF2BP3 dependent. *J. Exp. Clin. Cancer Res.* 40 (1), 80–18. doi:10.1186/s13046-021-01871-4

Wilkerson, M. D., and Hayes, D. N. (2010). ConsensusClusterPlus: A class discovery tool with confidence assessments and item tracking. *Bioinformatics* 26 (12), 1572–1573. doi:10.1093/bioinformatics/btq170

Wu, W., Chen, A., Lin, S., Wang, Q., Lian, G., Luo, L., et al. (2022). The identification and verification of hub genes associated with pulmonary arterial hypertension using weighted gene co-expression network analysis. *BMC Pulm. Med.* 22 (1), 474–511. doi:10.1186/s12890-022-02275-6

Zeng, Y., Huang, T., Zuo, W., Wang, D., Xie, Y., Wang, X., et al. (2021). Integrated analysis of m6A mRNA methylation in rats with monocrotaline-induced pulmonary arterial hypertension. *Aging (Albany NY)* 13 (14), 18238–18256. doi:10.18632/aging.203230

Zhang, X., Zhang, S., Yan, X., Shan, Y., Liu, L., Zhou, J., et al. (2021a). m6A regulator-mediated RNA methylation modification patterns are involved in immune microenvironment regulation of periodontitis. *J. Cell. Mol. Med.* 25 (7), 3634–3645. doi:10.1111/jcmm.16469

Zhang, Z., Mei, Y., and Hou, M. (2021b). Knockdown RBM15 inhibits colorectal cancer cell proliferation and metastasis via N6-methyladenosine (m6A) modification of MyD88 mRNA. *Cancer Biotherapy Radiopharm.* 37, 976–986. doi:10.1089/cbr.2021.0226

Zhao, Z., Ju, Q., Ji, J., Li, Y., and Zhao, Y. (2022). N6-Methyladenosine methylation regulator RBM15 is a potential prognostic biomarker and promotes cell proliferation in pancreatic adenocarcinoma. *Front. Mol. Biosci.* 9, 842833. doi:10.3389/fmolb.2022.842833

Zhong, H., Wang, T., Lian, G., Xu, C., Wang, H., and Xie, L. (2018). TRPM7 regulates angiotensin II-induced sinoatrial node fibrosis in sick sinus syndrome rats by mediating Smad signaling. *Heart vessels* 33, 1094–1105. doi:10.1007/s00380-018-1146-0

Zhou, W., Wang, C., Chang, J., Huang, Y., Xue, Q., Miao, C., et al. (2021). RNA methylations in cardiovascular diseases, molecular structure, biological functions and regulatory roles in cardiovascular diseases. *Front. Pharmacol.* 12, 722728. doi:10.3389/fphar.2021.722728

Zou, J., Li, W., Misra, A., Yue, F., Song, K., Chen, Q., et al. (2015). The viral restriction factor tetherin prevents leucine-rich pentatricopeptide repeat-containing protein (LRPPRC) from association with beclin 1 and B-cell CLL/lymphoma 2 (Bcl-2) and enhances autophagy and mitophagy. *J. Biol. Chem.* 290 (11), 7269–7279. doi:10.1074/jbc.M114.627679

Zou, J., Yue, F., Jiang, X., Li, W., Yi, J., and Liu, L. (2013). Mitochondrion-associated protein LRPPRC suppresses the initiation of basal levels of autophagy via enhancing Bcl-2 stability. *Biochem. J.* 454 (3), 447–457. doi:10.1042/BJ20130306

Zou, J., Yue, F., Li, W., Song, K., Jiang, X., Yi, J., et al. (2014). Autophagy inhibitor LRPPRC suppresses mitophagy through interaction with mitophagy initiator Parkin. *PloS one* 9 (4), e94903. doi:10.1371/journal.pone.0094903

frontiers | Frontiers in Cell and Developmental Biology

TYPE Review
PUBLISHED 12 September 2023
DOI 10.3389/fcell.2023.1268646

OPEN ACCESS

EDITED BY
Peng Zhang,
Institute of ENT and Shenzhen Key Laboratory of ENT, China

REVIEWED BY
Xiaodong Zhang,
Affiliated Hospital of Jiangnan University, China
Yunbin Xiao,
Hunan Children's Hospital, China

*CORRESPONDENCE
Xue-liang Zhou,
zhouxliang@ncu.edu.cn
Qi-cai Wu,
wuqicai13970012836@163.com

RECEIVED 28 July 2023
ACCEPTED 28 August 2023
PUBLISHED 12 September 2023

CITATION
Zhao S-s, Liu J, Wu Q-c and Zhou X-l (2023), Role of histone lactylation interference RNA m^{6}A modification and immune microenvironment homeostasis in pulmonary arterial hypertension. *Front. Cell Dev. Biol.* 11:1268646. doi: 10.3389/fcell.2023.1268646

Role of histone lactylation interference RNA m^{6}A modification and immune microenvironment homeostasis in pulmonary arterial hypertension

Shuai-shuai Zhao[1], Jinlong Liu[2], Qi-cai Wu[1]* and Xue-liang Zhou[1]*

[1]Department of Cardiac Surgery, The First Affiliated Hospital, Nanchang University, Nanchang, China, [2]Institute of Translational Medicine, Shanghai University, Shanghai, China

Pulmonary arterial hypertension (PAH) is a severe disease resulting from progressive increases in pulmonary vascular resistance and pulmonary vascular remodeling, ultimately leading to right ventricular failure and even death. Hypoxia, inflammation, immune reactions, and epigenetic modifications all play significant contributory roles in the mechanism of PAH. Increasingly, epigenetic changes and their modifying factors involved in reprogramming through regulation of methylation or the immune microenvironment have been identified. Among them, histone lactylation is a new post-translational modification (PTM), which provides a novel visual angle on the functional mechanism of lactate and provides a promising diagnosis and treatment method for PAH. This review detailed introduces the function of lactate as an important molecule in PAH, and the effects of lactylation on N6-methyladenosine (m^{6}A) and immune cells. It provides a new perspective to further explore the development of lactate regulation of pulmonary hypertension through histone lactylation modification.

KEYWORDS

pulmonary arterial hypertension, histone lactylation, epigenetic modifications, post-translational modification, m^{6}A, immune microenvironment

1 Introduction

PAH is a serious disease that involves pulmonary vasoconstriction, pulmonary vascular multiplication, and the development of plexiform lesions. At first, the right ventricle (RV) improves circulation by increasing contractility and ventricular wall thickness. With the progress of the disease, the RV gradually expands, eventually leading to right heart failure and even death (Harbaum et al., 2022). At the same time, PAH is also an important global health problem that can affect any age group. The prevalence of PAH is approximately 25 cases per population of 1 million (Maron et al., 2021). In the UK, the prevalence of PAH was 97 per million, with a female: male ratio of 1.8:1 (Galie et al., 2016), and in the United States, there are approximately 10.6 cases per 1 million adults (Badesch et al., 2010), with different epidemiological data of different types of PAH. With the development of medicine and the continuous efforts of doctors, the 5-year survival rate has increased from 34% to more than 60% through targeted treatment of PAH (Boucly et al., 2021). Even though currently available therapies focus on improving PAH symptoms and reducing pulmonary

vasoconstriction, the mortality rate remains unacceptably high. Therefore, the identification of new pathways responsible for pulmonary vascular remodeling as well as identifying novel therapeutic targets are crucial.

Epigenetics emerging research has brought about many novel discoveries in PAH. Previous research has already demonstrated that m^{6}A is a ubiquitous and abundant transcriptional modification. Mechanically, m^{6}A modification affects multiple functions of mRNA, including transport, degradation, and translation, thus participating in various pathophysiological processes. The imbalance of m^{6}A will lead to the occurrence and development of tumors, inflammation, cardiovascular disease, and immune disease (Efremova et al., 2020). The dynamic regulation of m^{6}A affects the expression level of specific genes involved in PAH. In addition, inflammation and immune disorders are also involved in pulmonary vascular remodeling, especially through the secretion of cytokines and metabolic reprogramming (Xu et al., 2021). The pathological specimens of PAH patients showed the accumulation of perivascular inflammatory cells, such as macrophages, lymphocytes, and mast cells (Jia et al., 2020).

The crosstalk between epigenetics and metabolism plays a key role in gene expression, cell differentiation, and proliferation (Vasconcelos et al., 2020). Lactate has been found to be a signaling molecule and a metabolism regulator, participate in intercellular signal transduction and immune reaction (Shime et al., 2008), and play a key role in epigenomic reprogramming (Bhagat et al., 2019). Under hypoxia, cells stimulate intracellular lactate production by inhibiting oxidative phosphorylation and enhancing glycolysis, thereby increasing histone lactylation and promoting metabolic reprogramming (Zhang et al., 2019). The increase or decrease of lactate concentration has been shown to affect cell differentiation and function through multiple pathways. The increasing understanding of lactate has promoted the development of new targets. However, it just begin research histone lactylation in PAH. This review describes the regulation of m^{6}A and the immune microenvironment by histone lactylation, affecting the occurrence and development of PAH.

2 Pulmonary arterial hypertension

In 1975, WHO published the first standardized hemodynamic criterion for pulmonary hypertension (PH) (Maron et al., 2018). In the resting state at sea level, check through the right heart catheterisation (RHC) technique, measure the mean pulmonary arterial pressure greater than 25 mmHg (mPAP ≥ 25 mmHg) (Al-Omary et al., 2020), and this definition has been followed ever since then. Until to 2018, the 6th World Symposium on Pulmonary Hypertension (WSPH) suggest that the diagnostic criteria for PH be modified to mPAP >20 mmHg, a pulmonary artery wedge pressure of 15 mmHg or lower, and a pulmonary vascular resistance of 3 Wood units or greater (Simonneau et al., 2019).

As shown in Table 1, PH is clinically divided into five major categories (Simonneau et al., 2019). The pathogenesis of PAH is complex and involves various factors, including vasoactive molecules (ET-1, Ang, PG, NO, etc.), ion channels (K^+ channel, Ca^{2+} channel, and new cation channels), signaling pathways (MAPK pathway, PI3K/AKT pathway, Notch pathway, etc.) (Shafiq et al., 2021; Zhang et al., 2022), apoptosis resistance, oxidative stress, inflammation, and immune dysregulation (Norton et al., 2020). The pathological changes of PH include proliferation of pulmonary arterial endothelial cells (PAECs) along with the inflammatory response, proliferation of pulmonary arterial smooth muscle cells (PASMCs) and sustained contraction, and fibrosis of the external membrane and matrix remodeling (Rhodes et al., 2019). The main pathological feature of PH is pulmonary vascular remodeling caused by phenotypic changes in endothelial cells and muscularization of the vessel wall (Hautefort et al., 2019). This review focuses on elucidating the molecular mechanisms underlying the first type of epigenetic modifications of PH.

TABLE 1 Updated clinical classification of pulmonary hypertension (PH).

1. PAH	2. PH due to left heart disease	4. PH due to pulmonary artery obstructions
1. 1 Idiopathic PAH	2. 1 PH due to HF with preserved LVEF	4. 1 Chronic thromboembolic PH
1.2 Heritable PAH	2.2 PH due to HF with reduced LVEF	4.2 Other pulmonary artery obstruction
1.3 Drug- and toxin-induced PAH	2.3 Valvular heart disease	
1.4 PAH associated with:connective tissue disease, HIV infection, portal hypertension, congenital heart disease,schistosomiasis	2.4 Congenital/ acquired cardiovascular conditions leading to post-capillary PH	
1.5 PAH long-term responders to calcium channel blockers	3. PH due to lung diseases and/or hypoxia	5. PH with unclear and/or multifactorial mechanisms
1.6 PAH with overt features ofvenous/ capillaries (PVOD/PCH) involvement	3. 1 Obstructive lung disease	5. 1 Haematological disorders
1.7 Persistent PH of the newborn syndrome	3.2 Restrictive lung disease	5.2 Systemic and metabolic disorders
	3.3 Other lung disease with mixed restrictive/ obstructive pattern	5.3 Others
	3.4 Hypoxia without lung disease	5.4 Complex congenital heart disease
	3.5 Developmental lung disorders	

PAH, pulmonary arterial hypertension; HF, heart failure; PVOD, pulmonary veno-occlusive disease; PCH, pulmonary capillary haemangiomatosis; LVEF, left ventricular ejection fraction.

Early symptoms of PAH are not specific and usually include fatigue and chest tightness. As the disease progresses, symptoms gradually become more severe, including dyspnea, syncope, chest pain and right heart failure. Experts believe that early diagnosis and treatment can improve survival (Simonneau et al., 2019). The treatment of PAH includes general treatment, special drug treatment, surgical treatment, and targeted drug therapy. General treatment includes: activity and rehabilitation, anticoagulant therapy, diuretic and cardiovascular active drug therapy, oxygen therapy, anemia improvement and iron supplementation therapy, and psychosocial support. The specific drug treatments include: calcium channel blockers (CCB); endothelin receptor antagonists (ERA) consisting of bosentan, ambrisentan, and macitentan; 5-phosphodiesterase inhibitor (sildenafil, tadalafil); guanylate cyclase agonist (sGC) include Adempas; prostacyclin analog (epoprostenol, treprostinil, iloprost) and prostacyclin receptor agonist (selexipag) (Humbert et al., 2022).

Additionally, combination therapy is considered a standard treatment method in PAH. In spite of the fact that these treatments can improve the life quality and survival of patients, they do not cure the disease, the long-term prognosis is poor and the mortality rate is high. Therefore, the development of new drugs and the search for new treatments are the key to the treatment of PAH.

3 Mechanism of m^{6}A methylation-modified mRNA affecting the development of PAH

3.1 The structure and function of m^{6}A

A large number of research have shown that epigenetic modifications play an important role in regulating cell proliferation, protein synthesis, and gene transcription, including methylation, histone lactylation modification, and microRNA dysregulation. It is worth noting that m^{6}A is a key regulator of mRNA stability, protein expression, and other cellular processes (Ries et al., 2019). The m^{6}A peaks are mainly found in the open reading frame (ORF) (Li et al., 2018), the 3′-untranslated regions (UTRs), and near the stop codons of the mRNA (Ke et al., 2015). Mechanistically, m^{6}A affects all stages of RNA metabolism, including translation, stabilization, and degradation, and plays a key role in the pathological and physiological processes of cells (H. Huang et al., 2019).

The mRNA methylation modifications are dynamically regulated by methyltransferases, demethylases, and methylation-binding proteins to maintain normal gene expression. Among them, the regulators involved are: methyltransferase including METTL3 (methyltransferase-like3) (Vu et al., 2017), METTL14 (methyltransferase-like14) (Chen et al., 2020), METTL16 (methyltransferase-like16) (Pendleton et al., 2017), WTAP (Wilms tumor 1associated protein) (Zhu et al., 2020), RBM15 (RNA binding motif protein15) and zinc finger CCCH-type containing 13 (ZC3H13) (Wen et al., 2018). The demethylases FTO (FAT mass and obesity-associated protein) (Mathiyalagan et al., 2019) and ALKBH5 (ALKB homologue5 protein) (Zhang et al., 2017) both are the ALKB protein family, and belong to the ferric hydride/ketoglutarate-dependent dioxygenase. The m^{6}A reader protein recognizes mRNA and binds to it to achieve corresponding functions. One class of direct and robust m^{6}A readers are proteins containing the YT521-B homology (YTH) domain, the YTH domain of the m^{6}A reader protein is composed of 134 amino acids (Zaccara, and Jaffrey, 2020), including YTH domain family 1–3 (YTHDF1-3) (Gao et al., 2019; Li et al., 2020) and YTH domain containing 1–2 (YTHDC1-2) (Roundtree et al., 2017; Jain et al., 2018) in humans, were confirmed to regulate the mRNA processing, translation, and degradation processes (Table 2). How to maintain the above molecular expression level in homeostasis is the key to preventing vascular dysplasia and elevated pulmonary arterial blood pressure.

Immunofluorescence showed that METTL3 is located on the nuclear spots rich in mRNA splicing factors and has a potential regulatory role in mRNA metabolism (Vu et al., 2017). Previous research showed that METTL3 might promote the development of thyroid cancer through the methylation modification of TCF1 (Wang et al., 2020). In mammals, both METTL3 and METTL14 are highly conserved, and both form stable heterodimers. Among them, METTL4 is an snRNA m^{6}Am methyltransferase involved in the regulation of pre-mRNA splicing (Chen et al., 2020). Li et al. found that METTL14 may contribute to hepatocellular carcinoma progression through modulation of m^{6}A methylation of cysteine sulfinic acid decarboxylase, glutamic-oxaloacetic transaminase 2, and cytokine signaling suppressor 2 (Li et al., 2020). The methyltransferase WTAP interacts with METTL3 and METTL14 to jointly regulate the m^{6}A levels of mRNA transcription (Ping et al., 2014). METTL16, a homolog of METTL3, regulates the expression of human MAT2A, controls cellular SAM levels, and is also a methyltransferase of U6 snRNA (Pendleton et al., 2017). In addition, a study has shown that at least 78 m^{6}A residues of XIST are highly methylated in human cells. Among them, RBM15 and RBM15B mediate the methylation of adenosine nucleotides in the common motif of m^{6}A in XIST and mRNA (Patil et al., 2016). The above methyltransferases achieve different functions by modifying different stages of mRNA.

The demethylases FTO and ALKBH5 play powerful functions in RNA translation, processing, and splicing (Tang et al., 2018). In terms of modified bases, the m^{6}Am is one of the most common near the first coding nucleotide of the 7-methylguanosine cap of mRNA. FTO preferentially demethylates m^{6}Am and reduces the stability of mRNA (Mauer et al., 2017). The regulation of mRNA function by FTO leads to FTO-dependent changes in m^{6}A demethylated protein levels (Su et al., 2018). A study found that FTO plays a key role in cardiac remodeling. Compared with healthy heart tissue, m^{6}A modification was increased and FTO expression was significantly decreased in heart failure and myocardial infarction regions (Mathiyalagan et al., 2019). ALKBH5 is the second discovered m^{6}A demethylase, which is similar to the m^{6}A demethylation activity of FTO (Zhang et al., 2017). A study showed that ALKBH5 overexpression can inhibit the proliferation of pancreatic cancer cells *in vitro*, whereas ALKBH5 knockdown promoted the progression of pancreatic cancer (Guo et al., 2020) (Table 2). This suggests that m^{6}A demethylase achieves distinct cellular functions by interfering with mRNA stability.

The m^{6}A binding protein YTHDF1 is translocated from the cytoplasm to the nucleus, where it initiates and enhances translation in a manner that is dependent on the eIF3 initiation factor

TABLE 2 The structure and function of m^{6}A.

Type	Regulator	Function	References
m^{6}A writer	METTL3	catalyzes m^{6}A modification	(Vu et al., 2017; Wang et al., 2020)
	METTL14	helps METTL3 to recognize the subtract	(Chen et al., 2020; Li et al., 2020)
	METTL16	catalyzes m^{6}A modification	(Pendleton et al., 2017)
	WTAP	contributes to the localization of METTL3-METTL14 heterodimer to the nuclear speckle	(Ping et al., 2014; Zhu et al., 2020)
	RBM15	binds the m^{6}A complex and recruit it to special RNA site	(Patil et al., 2016)
	ZC3H13	bridges WTAP to the mRNA-binding factor Nito	(Wen et al., 2018)
m^{6}A eraser	FTO	removes m^{6}A modification	(Mathiyalagan et al., 2019; Mauer et al., 2017; Su et al., 2018)
	ALKBH5	removes m^{6}A modification	(Guo et al., 2020; Tang et al., 2018; Zhang et al., 2017)
m^{6}A reader	YTHDF1	enhances mRNA translation	(Gao et al., 2019; Shi et al., 2018; Wang et al., 2015
	YTHDF2	promotes mRNA degradation	(Du et al., 2016; Li et al., 2020)
	YTHDF3	enhances translation and degradation by interacting with YTHDF1 and YTHDF2	(Gao et al., 2019; Shi et al., 2017)
	YTHDC1	contributes to RNA splicing and export	(Roundtree et al., 2017; Zhu et al., 2021b)
	YTHDC2	enhances the translation of target RNA and reduces the abundance of target RNA	(Jain et al., 2018)
	HNRNPC	mediates mRNA splicing	(Wu et al., 2018)

(Wang et al., 2015). YTHDF1 gene deletion leads to decreased memory and learning, while YTHDF1 expression enhances memory and learning (Shi et al., 2018). Transporting mRNA targets to cytoplasmic processing bodies and promoting their degradation are the functions of YTHDF2. The CCR4-NOT deadenylase complex partially promotes the degradation of target transcripts by cytoplasmic YTHDF2 (Du et al., 2016). The YTHDF3 protein interacts with the YTHDF1 and YTHDF2 proteins to enhance translation and degradation (Shi et al., 2017). A structural and binding study indicates that the YTH domain of YTHDC1, one of the core members of the YTH family proteins, preferentially recognizes the GG (m^{6}A)C sequence (Roundtree et al., 2017). It has been shown that YTHDC1 promotes the proliferation of cancer cells, the formation of tumors and the migration of cells (Zhu et al., 2021). In addition, YTHDC2 binds to the consensus motif of m^{6}A more preferentially than other members of the YTH family, improving translation efficiency and reducing mRNA bundling (Jain et al., 2018). Heterogeneous nuclear ribonucleoproteins (HNRNPs) regulate alternative splicing or processing of target transcripts, including HNRNPC, HNRNPG, and HNRNPA2B1 (Wu et al., 2018) (Table 2).

3.2 m^{6}A methylation-modified mRNA affects the occurrence and development of PAH

The physiological function of m^6 A in the cell is mediated by different mechanisms, m^6 A regulates the stem cell fate by modifying mRNA (Li et al., 2018). In the past 2 years, many studies have reported that the occurrence and development of PAH is closely associated with epigenetic modification of mRNA, particularly m^{6}A methylation modification (Zhu et al., 2021). Zeng et al. had confirmed that increased m^{6}A methylation in PAH (Zeng et al., 2021). In addition, some studies have demonstrated that METTL3 (Qin et al., 2021), METTL14 (Zhou et al., 2021), YTHDF1 (Hu et al., 2021), and YTHDF2 (Qin et al., 2021) are involved in PASMC proliferation and pulmonary vascular remodeling.

METTL3 plays an important role in the pathogenesis of hypoxia-induced PAH. Qin et al. pointed out that METTL3 is abnormally overexpressed in PASMCs of PAH. However, downregulation of METTL3 inhibited hypoxia-induced proliferation and migration of PASMCs (Qin et al., 2021). Meanwhile, study revealed that YTHDF2 regulates RNA metabolism by localizing bound mRNAs to degradation sites (Fei et al., 2020). There was a significant upregulation of YTHDF2 in PASMCs under hypoxia. Since YTHDF2 recognizes m^{6}A on PTEN mRNA, METTL3 decreases the stability of PTEN mRNA and accelerates its degradation via YTHDF2. The PI3K/Akt signaling pathway is activated in response to the reduced PTEN level, further promoting the proliferation of PASMCs (Qin et al., 2021). In addition, research also shows that SETD2 catalyzes H3K36me3 and plays a key role in hypoxic PAH formation (Yao et al., 2020). Hypoxia-induced PAH mice showed increased expression of SETD2 and m^{6}A transcript METTL14 in PASMCs, and SETD2-specific knockout in SMC ameliorated PAH and also decreased METTL14. This suggests that hypoxia-induced PAH is caused by METTL14-mediated m^{6}A modification and SETD2-mediated H3K36me3 modification (Zhou et al., 2021) (Table 3). Thus, the occurrence and development of PAH are commonly promoted by multiple m6A methylation modifications.

Recently, YTHDF1 has been shown to be overexpressed in human and rodent PAH samples and hypoxic PASMCs. The researchers found that MAGED1 regulates PAH pathogenesis by directly targeting m^{6}A. YTHDF1 promoted PASMC proliferation

TABLE 3 Role of m^{6}A methylation modification in PAH.

Type	Regulator	Expression	Mechanisms	References
m^{6}A writer	METTL3	Increase	METTL3/YTHDF2/PTEN axis promotes the hypoxia induced PAH.	(Qin et al., 2021; Zeng et al., 2021)
	METTL14	Increase	SEDT2/METTL14-mediated m^{6}A methylation contributes to the hypoxia induced PAH in mice	(Zhou et al., 2021)
m^{6}A reader	YTHDF1	Increase	YTHDF1 regulates the PAH through translational control of MAGED1	(Hu et al., 2021; Zeng et al., 2021)
	YTHDF2	Increase	METTL3/YTHDF2/PTEN axis promotes the hypoxia induced PAH.	(Qin et al., 2021)
	YTHDC1	Increase	FENDRR with YTHDC1 regulates PAH by mediating DRP1 DNA methylation	(Wang et al., 2022)
	HNRNPA2B1	Increase	Interfered with RNA splicing, transport, and maturation which mediate the phenotype translational of PASMCs	(Zheng et al., 2022)
m^{6}A eraser	FTO	Decreased	—	(Zeng et al., 2021)
	ALKBH5	Decreased	—	(Zeng et al., 2021)

and the development of PAH by increasing MAGED1 translation, and MAGED1 knockdown reduced hypoxia-induced proliferation of PASMCs by downregulating proliferating cell nuclear antigen (PCNA) (Hu et al., 2021). Meanwhile, Wang et al. showed that the expression of YTHDC1 was enriched in PAECs under hypoxic conditions and mediated FENDRR involved in the hypoxia-induced proliferation of PAECs (Wang et al., 2022). In addition, DEGs and HNRNPA2B1 target genes overlapped in PASMCs, indicating that HNRNPA2B1 was upregulated in PASMCs. HNRNPA2B1 regulates the Wnt signaling pathway, cAMP signaling pathway, P53 signaling pathway, and cell cycle of muscle cell differentiation, and participates in the signaling pathway by modifying m^{6}A modification (Zheng et al., 2022) (Table 3).

4 The immune microenvironment dysequilibrium promotes the development of PAH

Recent studies have found that the occurrence and development of PAH is the result of a variety of cell interactions, which is not only related to PAECs dysfunction, PASMCs phenotypic switching and fibroblast activation, moreover, it is also closely related to the immune microenvironment imbalance. Accumulating evidence suggests that inflammation is a major contributor to vascular remodeling in PAH (Xu et al., 2021). The disorder of the immune microenvironment plays an important role in the development of PAH, and the immune system regulates PAH via multiple mechanisms.

Mechanistically, immune cells induce an inflammatory response by releasing various types of inflammatory mediators and cytokines to bind to cytokines receptors on vascular endothelial cells, smooth muscle cells, and fibroblasts (Guihaire et al., 2021; Tang et al., 2021). Pulmonary vascular and perivascular inflammation is one of the major factors leading to vasoconstriction and vascular remodeling. PAEC dysfunction leads to the release of vasoconstrictive and inflammatory factors that promote excessive proliferation of PASMCs and pulmonary artery constriction (Florentin et al., 2018). Extensive research has shown that different subsets of T lymphocytes play distinct roles in PAH, including helper T lymphocytes (Th cells), cytotoxic T lymphocytes, and regulatory T lymphocytes (Tregs). Among them, Th1 and Th17 cells are involved in the autoimmune and inflammatory response of PAH by producing IL-2, IL-6, IL-21, IFN-c and TNF-α (Steiner et al., 2009). Meanwhile, Maston et al. found that Th17 cells promote the progression of hypoxia-induced PAH in rats by releasing IL-17A (Maston et al., 2017) (Figure 1).

Elevated levels of cytokines and chemokines have been found in patients with idiopathic PAH (Perros et al., 2013). Meanwhile, The expression of CRTH2 (chemoattractant receptor homologous molecule expressed on Th2 cells) was increased in both circulating $CD3^+CD4^+$ T cells in idiopathic PAH patients and rodent models of PAH. Chen et al. have shown that CRTH2 promotes PASMC proliferation by activating STAT6 (Chen et al., 2018; Harbaum et al., 2016). In addition to regulating collagen synthesis and proliferation of PASMCs, $CD44^+$ T cells play a key role in pulmonary vascular remodeling, immune regulation, and phenotypic transformation (Isobe et al., 2019). The above studies suggest that the release of inflammatory factors promotes the progression of PAH.

In humans and mice, studies have shown that Tregs make up approximately 5%–10% of peripheral blood lymphocytes (Elkord, 2009). They inhibit autoimmunity and maintain immune homeostasis. Previous studies have shown that abnormal Tregs may impair the anti-inflammatory function of PAECs and play a key role in the pathogenesis of PAH. A decreased number of Tregs was observed in the pulmonary vessels of PAH patients, while an increase was observed in the peripheral circulation, indicating the decreased suppressive function of Tregs (Huertas et al., 2016). In addition, Tregs are involved in the regulation of adaptive and innate immunity. In PAH, Treg deficiency promotes the emergence of destructive macrophage-based immunity that damages the endothelium and leads to vascular remodeling (Tian et al., 2013). In conclusion, normal function of Tregs may limit pulmonary vascular damage and prevent the development of PAH.

Bone morphogenetic protein receptor type 2 (BMPR2) is also involved in the pathogenesis of PAH, which is mainly secreted by PAECs and feeds back to them, then inhibits their proliferation and differentiation (Diebold et al., 2015). Research has shown that Tregs function by upregulating BMPR2 expression to decrease endothelial

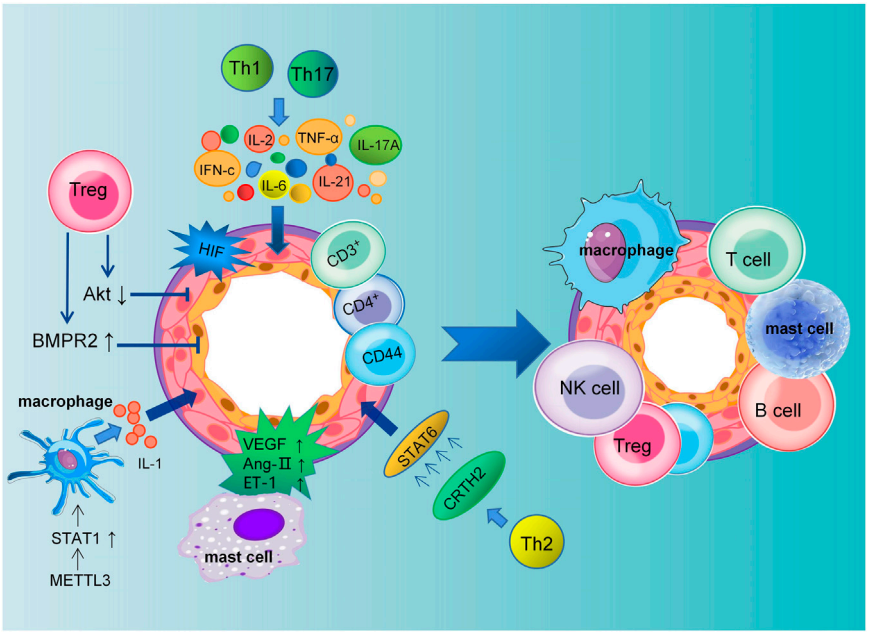

FIGURE 1
Schematic representation of pulmonary artery remodeling promoted by immune microenvironment dysregulation. The dysfunction of macrophages, mast cells, T cells, B cells, NK cells and Tregs together lead to pulmonary vascular remodeling in PAH. Th1 and Th17 cells mediate the inflammatory response in PAH by producing IL-2, IL-6, IL-21, IL-17A, IFN-c, and TNF-α. Meanwhile, PASMCs proliferation is promoted by CRTH2 from Th2 lymphocytes through the activation of STAT6. Tregs inhibit the proliferation of PASMCs by decreasing Akt activity and regulating the kinase of an extracellular signal. Tregs can reduce perivascular inflammation and PAECs apoptosis through upregulation of BMPR2. In addition, VEGF, Ang II, and ET-1 secreted by mast cells are all involved in the remodeling of the pulmonary vasculature.

cell apoptosis and perivascular inflammation. However, as a consequence of decreased BMPR2 secretion in injured PAECs, they are much more susceptible to PAH (Hong et al., 2008). In the meantime, the study by Chu et al. found that Tregs inhibit PASMC proliferation and PAH development by inhibiting Akt and extracellular signal-regulated kinase (Chu et al., 2015). According to several studies, macrophages are involved in the progression of PAH through their inflammatory response (Zhang et al., 2020). In addition, accumulation of B cells and macrophages after 1 week in Treg-deficient rats exposed to SU5416 (Tamosiuniene et al., 2011). Jia et al. have shown that by reducing vascular remodeling through stimulation of H-PGDS-dependent PGD2 release from macrophages, niacin blocks the progression of HySu-induced PAH in rodents (Jia et al., 2020).

The immune microenvironment was significantly altered when PAH rats were exposed to lipopolysaccharide (LPS) and M1 macrophage polarization was increased. By increasing the proportion of M1 macrophages, IL-1 and other inflammatory factors are released, further impairing pulmonary arterial and cardiac function (Guo et al., 2021). The key transcription factor STAT1 can activate signaling cascades leading to macrophage activation and inflammation. METTL3 can upregulate STAT1 expression and promote macrophage M1 polarization by directly methylating STAT1 mRNA (Liu et al., 2019). However, inhibition of METTL3 can inhibit the NF-κB pathway to reduce the macrophage inflammatory response induced by LPS, reducing the progression of PAH (Wang et al., 2019). This shows that inhibition of macrophage inflammatory response can reduce PAH in vascular remodeling. In addition, dysregulation of m^{6}A regulators was similarly observed in NK cells, B cells, T cells and Tregs in the stroma (Zheng et al., 2022). However, the mechanism of action between m^{6}A and numerous immune cells needs to be further investigated.

In addition, the vascular endothelial growth factor (VEGF) secreted by mast cells in PAH may cause angiogenesis to malfunction, and mast cells around blood vessels produce chymase. It is known that chymase could stimulate vasoconstriction and vascular remodeling by promoting the activation of Ang II, endothelin, and matrix metalloproteases (Qu et al., 2022) (Figure 1). Therefore, inhibiting the secretion of growth factors and cytokines by mast cells may slow the progression of PAH.

In summary, inhibiting the release of inflammatory factors is one of the most important ways to suppress the progression of PAH. In PAH, PASMCs, PAECs, fibroblasts and immune cells are dysfunctional, resulting in pulmonary vascular remodeling. Inflammation could activate the function of immune cells and promote the proliferation of PASMCs and PAECs, leading to pulmonary artery remodeling. Anti-inflammatory therapy may be a viable option for the treatment of severe PAH, which is associated with inflammation and dysregulated immunity.

5 Glycolysis and glucose oxidation in PAH

The interaction between metabolism and epigenetics plays a key role in gene expression, cell proliferation, and differentiation.

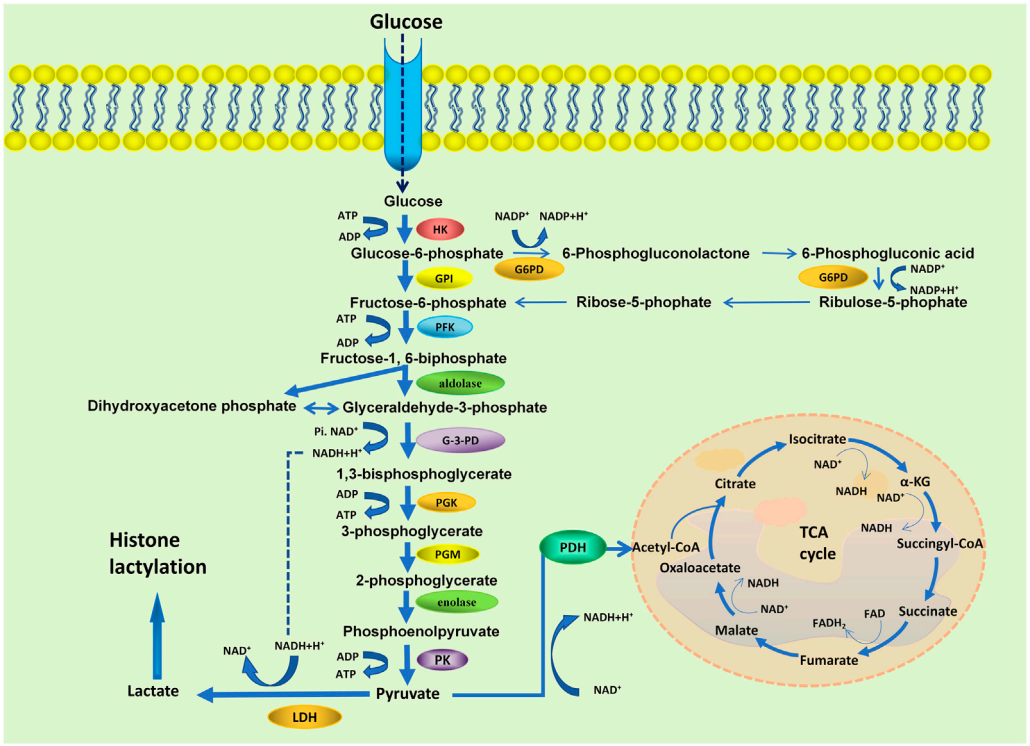

FIGURE 2
Schematic representation of the glycolysis and the TCA cycle. HK, hexokinase; GPI, phosphoglucose isomerase; G6PD, glycolysis/glucose-6-phosphate dehydrogenase; PFK, 6-phosphfructokinase-1; G-3-PD, glyceraldehyde-3-phosphate dehydrogenase; PGK, phosphoglycerate kinase; PGM, phosphoglycerate mutase; PK, pyruvate kinase; LDH, lactate dehydrogenase; PDH, pyruvate dehydrogenase.

During cellular metabolism, nutrients are absorbed, released, and converted into energy and complex biomolecules. Depending on the availability of nutrients, metabolic products modulate cell signaling and gene expression (Liberti, and Locasale, 2020). A large amount of lactate is produced by anaerobic glycolysis (Zhang et al., 2021), which is originally thought that it was a Warburg effect end product and a metabolic waste product by glycolysis. Nevertheless, lactate is now recognized as an energy source, a signaling molecule, and an immunoregulatory molecule (Bhagat et al., 2019).

Cellular metabolic reprogramming due to an imbalance between the glycolysis and the citric acid (TCA) cycle, leading to increased histone lactylation (Liberti, and Locasale, 2020). Glucose is first metabolized by glycolysis in tissues to pyruvate, which is then converted to circulating lactate. At the same time, pyruvate can also be oxidized to acetyl-CoA, which participates in the TCA cycle and ATP production (Gustafsson et al., 2007) (Figure 2). During hypoxia, cells reorganize metabolism by suppressing oxidative phosphorylation and increasing glycolysis, which accelerates lactate production (Zhang et al., 2019). Rather than entering the TCA cycle, pyruvate is converted into lactate by cytosolic lactate dehydrogenases (LDHs) in highly glycolytic cells. Finally, as a result of enhanced glycolysis, microenvironments become acidification with increased lactate production.

In PAECs (Cao et al., 2019) and PASMCs (Hernandez-Saavedra et al., 2020) from PAH patients and animal models of PAH, glucose metabolism gradually shifts from mitochondrial oxidative phosphorylation to glycolysis, ultimately leading to elevated lactate levels (Saygin et al., 2017). Meanwhile, evidence suggests that a glycolytic shift increases the proliferation and extracellular matrix (ECM) production of PASMCs, thereby promoting pulmonary vascular remodeling (Kovacs et al., 2019). In addition, glycolysis-related enzymes were increased in PAH lungs, including glycolytic regulator PFKFB2 (6-phosphofructo-2-kinase/fructose-2, 6-biphosphatase) (Zhao et al., 2014) and PFKFB3 (6-phosphofructo-2-kinase/fructose-2,6-bisphosphatase 3). With the increase of glycolysis and lactate level, the expression of PFKFB3 in PASMCs is upregulated, resulting in the proliferation and extracellular collagen synthesis of PASMCs. Studies have shown that PFKFB3 can induce calpain-2 activation and ERK1/2 phosphorylation in pulmonary artery smooth muscle cells, which promote vascular remodeling in PAH. In Sugen/Hypoxia PAH rat model, inhibition of calpain-2 can prevent ERK1/2 activity, and reduces lactate-induced increases of PAH and pulmonary vascular remodeling (Kovacs et al., 2019). Research has also shown that PFKFB3 promotes the production of proinflammatory cytokines and growth factors in PAECs through enhancing endothelial glycolysis. In PAH models, these factors promote inflammation in endothelial cells and the proliferation of PASMCs through autocrine and paracrine pathways (Hernandez-Saavedra et al., 2020).

The proliferation of PASMCs is influenced by endothelial dysfunction, hypoxia, inflammation, or mechanical stress, which are augmented by vasoconstrictors, growth factors, and chemokines. Enhanced anaerobic glycolysis can activate HIF, and the

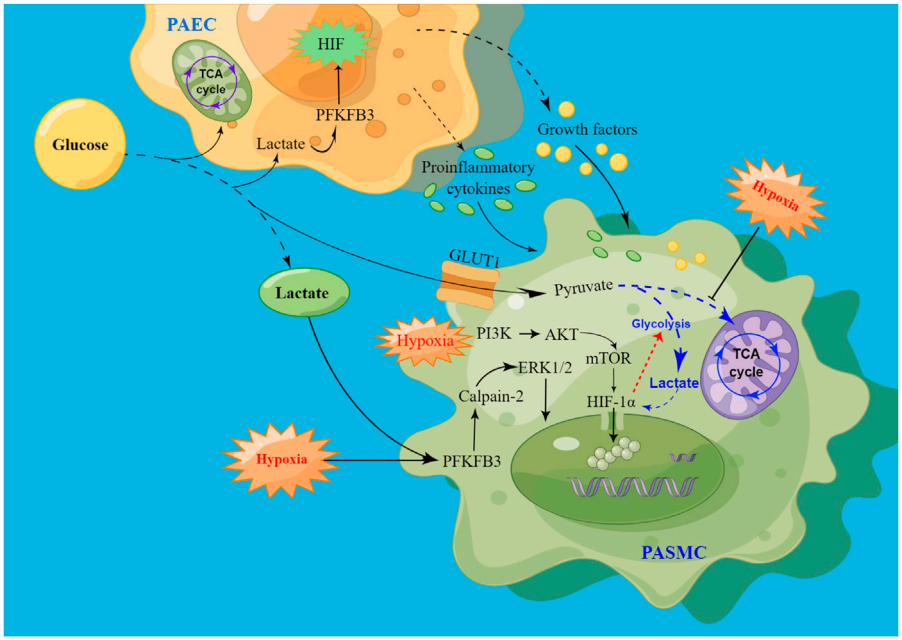

FIGURE 3
Schematic of signaling pathways driving PASMC proliferation via hypoxia-induced glycolysis. High levels of lactate promote HIF production by increasing PFKFB3 expression, leading to PAECs dysfunction. After injury, PAECs secrete growth factors and proinflammatory cytokines through the paracrine pathway to promote PASMC proliferation. At the same time, PFKFB3 promoted PASMCs proliferation by activating calpain-2 and phosphorylating ERK1/2. In addition, hypoxia promotes HIF release, promotes glycolysis, and inhibits the tricarboxylic acid cycle, thereby increasing lactate levels, and the increase in lactate can also enhance HIF expression. Hypoxia may also promote the onset and development of PAH by activating the PI3K/AKT/mTOR/HIF-1α signaling pathway.

overexpression of PFKFB3 also promotes the release of HIF, thus leading to the dysfunction of PAECs (Cao et al., 2019). Hypoxia-induced vasoconstriction is a unique response, and mechanistically, the cellular response to hypoxic conditions is primarily mediated by HIF activation (Yang et al., 2021). Induced vasoconstriction by acute hypoxia results in a reversible increase in pulmonary vascular resistance, whereas prolonged hypoxia promotes PASMCs proliferation and migration, thereby facilitating vascular remodeling and sustained vasoconstriction (Han et al., 2021) (Figure 3).

Under hypoxic conditions, HIF-1 enters the nucleus and associates with hypoxic regulatory genes, thereby enhancing anaerobic glycolysis and further contributing to the hypoxic response (Depping et al., 2008). Several downstream effects activated by HIF-1α are associated with immune escape, and HIF-1α is also an important regulator of macrophage glycolysis metabolism (Mouton et al., 2018). During hypoxia, HIF-1α is increased as a result of oxygen-independent protein synthesis and oxygen-dependent degradation (Kurosawa et al., 2019). During PAH progression, HIF-1α plays an important role in modulating downstream gene transcription (Kurosawa et al., 2019). Studies have shown that HIF-1α expression is upregulated in the pulmonary artery, leading to long-term sustained pulmonary artery constriction and promoting pulmonary artery remodeling (Mouton et al., 2018). Chen et al. have shown that mROS (mitochondrial reactive oxygen species)-dependent HIF-1α accumulation promotes the PASMCs proliferative phenotype (Chen et al., 2022). In addition, high levels of lactate also promote HIF-2α accumulation, leading to PAEC damage (Tang et al., 2018). This suggests that HIF homeostasis is regulated by multiple PTMs that control multiple pathophysiological processes by targeting transcription and translation.

Several signaling pathways may be activated during chronic hypoxia. The mTORC pathway has been shown to be activated in both PASMCs and distal pulmonary arteries from patients with idiopathic PAH (Goncharov et al., 2014). Mechanistically, the mTORC1 pathway activates certain glycolytic enzymes and accelerates glucose metabolism by increasing GLUT1 expression (Liang et al., 2022). With activation of the mTOR-HIF1α axis, the rate of glycolysis is accelerated, resulting in an increase in the production of pyruvate and lactate (Bekkering et al., 2018). In addition, HIF-1α is activated by PI3K/AKT and MAPK/ERK1 pathways in hypoxia conditions (Xu et al., 2016). A classic downstream signaling pathway in PAH, PI3K/AKT activation can promote smooth muscle proliferation in the pulmonary arteries. Previous studies confirmed PAH development by activating the PI3K/AKT/mTOR/HIF-1α signaling pathway (Xiao et al., 2017) (Figure 3). However, the cAMP/PKA signal pathway could suppress mTOR activity (He et al., 2020). Consequently, inhibition of the high expression of HIF and mTOR signaling pathway could suppress pulmonary artery remodeling and the development of PAH.

6 Histone lactylation regulates m^{6}A affects the development of PAH

Cellular metabolic reactions require glucose and oxygen as substrates. During glycolysis, large amounts of lactate are

produced as an energy source to maintain cellular metabolism. Histone lysine lactylation has been shown to be caused by lactate accumulation and regulated by lactate levels. The regulation of gene expression by lactate through histone lactylation modification is a newly discovered epigenetic modification, and a novel PTM has been identified in human and mouse core histones (Bhagat et al., 2019). Histone lactylation is involved in many cellular processes, including translation, metabolism, recombination, and repair (Zhang et al., 2021). Mechanically, lactate is used as a substrate to generate lactyl-CoA for lysine lactylation on histones, a process that regulates gene expression in a variety of pathophysiological conditions (Zhang et al., 2019). Meanwhile, in terms of transcription and antigenic variation, chromatin repression or induction is determined by the PTM status of core histones (Stillman, 2018).

In addition to their critical function in signal transduction and cellular metabolism, PTMs also play a key role in regulating protein conformation, stability and function (Zhang et al., 2021). Several factors were associated with PASMCs and PAECs proliferation, including lactate metabolism, oxidative stress response, HIF-1 pathway and PTMs. A number of studies have shown that glycolysis plays a critical role in PASMC proliferation, and inhibition of glycolysis can inhibit PASMC proliferation and migration and also reverse PAH in animal models (Xiao et al., 2017). Chen et al. found that mROS-mediated HIF-1α-driven glycolysis promotes pulmonary artery remodeling. Mechanistically, lactate accumulation increases histone lactylation at HIF-1α targets linked to proliferative phenotype (Chen et al., 2022).

Lactate in the intracellular environment can promote the lactylation of histone H3 on the promoters of homeostatic genes, which activates their expression (Zhang et al., 2019). A study found that METTL3 expression was upregulated in tumor-infiltrating myeloid cells (TIMs) and associated with poor prognosis. Meanwhile, study confirmed that lactylation was indeed present in METTL3, and H3K18la was enriched in the promoter regions of METTL3. In a mechanical manner, lactate promotes METTL3 transcription by modifying H3K18la. Lactate accumulated in the tumor microenvironment potently promoted METTL3 upregulation in TIMs through H3K18la, and lactylation of METTL3 in TIMs promoted m^{6}A-mediated immunosuppression (Xiong et al., 2022). In addition, the "CCCH" zinc finger domains (ZFDs) of the METTL3 protein can be directly lactylated, which via the METTL3-JAK1-STAT3 signaling pathway. METTL3 was bound and enhances m^{6}A modification of target RNA and promotes the expression of downstream immunosuppressive effector molecules like iNOS, IL-6, and IL-10 (Kumagai et al., 2022). This suggests that lactate could promote METTL3 expression through H3K18la modification, thereby affecting downstream signaling and gene expression.

METTL3 expression is upregulated in hypoxia-induced PASMCs, which promotes pulmonary artery remodeling through the METTL3/YTHDF2/PTEN axis (Qin et al., 2021). Meanwhile, studies have shown that lactate promotes PASMC proliferation through histone lactylation modification. H3K18laChIP-seq analysis of PDH kinase 1 (PDK1) and PDK2 silenced hypoxic PASMCs revealed that the density of H3K18la around the HIF-1α peak was also reduced (Chen et al., 2022). This suggests that both histone lactylation and METTL3 play important roles in PAH. However, the specific role of H3K18la and METTL3 in PAH is still unclear and needs to be further explored, which will also provide an important basis for the treatment of PAH.

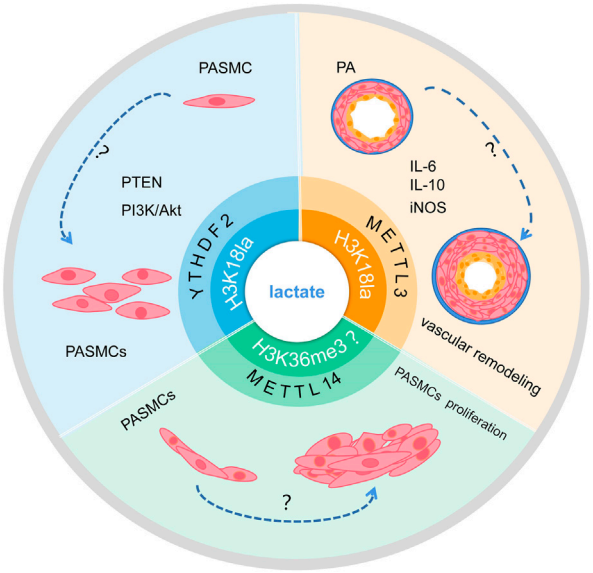

FIGURE 4
Schematic of the hypothesis that lactate regulates m^{6}A to affect PAH development via histone lactylation modification. Lactate may promote transcription of RNA METTL3 and YTHDF2 through H3K18la modification, and whether it may further influence PAH progression remains to be studied. In addition, whether lactate can affect the transcription of METTL14 and interfere with PASMC proliferation through H3K36me3 modification remains to be investigated.

The metabolic dynamics of glucose and lactate levels change to regulate histone lactylation (Varner et al., 2020). Previous studies have shown that histone lactylation may contribute to tumor growth by increasing YTHDF2 transcription. One study confirmed that H3K18la enrichment is present at the promoter of YTHDF2, transcription of YTHDF2 is regulated by H3K18la, and glycolysis inhibitors reduced this enrichment (Yu et al., 2021). Meanwhile, another study showed that the translation and expression of LDHB are decreased by YTHDF2, which inhibits aerobic glycolysis and cell proliferation by promoting mRNA degradation (Huang et al., 2020; Qing et al., 2021). YTHDF2 is upregulated and expressed in PAH and inhibited YTHDF2 can prevent hypoxia-induced PASMC proliferation. However, the specific role of histone lactylation and YTHDF2 in PAH needs to be further explored (Figure 4).

In addition, modifications of m^{6}A are enriched around H3K36me3 peaks, and are reduced globally when H3K36me3 is depleted in the cell, this indicated that loss of H3K36me3 reduces m^{6}A methylation. H3K36me3 and m^{6}A modifications overlapped well with METTL14 binding sites on RNA, according to distance analysis. In terms of mechanism, METTL14 recognizes and binds H3K36me3 directly, m^{6}A co-transcriptionally deposited by delivering the m^{6}A methyltransferase complex (MTC) on actively transcribed nascent RNAs (Huang et al., 2019). Evidence shown that METTL14 is upregulated expressed in PAH and inhibited METTL14 can prevent hypoxia-induced PASMCs proliferation (Zhou et al., 2021). However, The mechanism of action between lactate and H3K36me3 remains unclear. The target mechanism of histone lactylation involved in the methylation modification of

METTL14 to regulate the occurrence and development of PAH requires further study.

7 The immune microenvironment disrupted by histone lactylation and promotes the development of PAH

Histone lysine lactylation is involved in the regulation of gene expression by affecting mRNA splicing, translation, processing, and degradation. A growing body of evidence suggests that lactate regulates both innate and adaptive immune cells and affects significant changes in gene expression in a unique way (Zhang et al., 2019). According to lactate homeostasis, lactate is vital in fine-tuning cellular metabolism by regulating extracellular metabolism, and the function of lactate metabolism is further emphasized by energy homeostasis (Lagarde et al., 2021). In addition to playing a role in metabolism, lactate or signal molecules are involved in a variety of physiological and pathological processes. Lactate shuttles between and within cells to accomplish its effects and affects cell function. This shows that connect histone lactylation metabolism and the importance of epigenetic process.

Lactate is an active signal that regulates immune cells, metabolically reprogramming them to regulate their function (Lee et al., 2018). Histone lactylation has been shown to modulate immune responses and play important biological roles in the immune system. Lactate promotes the release of pro-inflammatory cytokines by regulating a variety of immune cell functions. Lactate can accumulate in response to inflammation or hypoperfusion. Studies have shown that lactate is a powerful amplifier of inflammation in arthritis (Souto-Carneiro et al., 2020). In PAH, an altered immune system contributes significantly to pulmonary vascular remodelling by promoting inflammatory cell recruitment and autoimmune dysfunction (Xu et al., 2021).

Most immunometabolic studies have focused on tumour-associated macrophages in cancer or abnormal B and T lymphocyte function in autoimmune diseases. Several studies have shown that lactate suppresses the proliferation, migration and function of T cells (Brand et al., 2016). Extracellular lactate levels are sensed by T cells, causing intracellular signalling and altering cell function and homeostasis. Excessive lactate inhibits T-cell mediated immune responses (Watson et al., 2021). By aerobic oxidative metabolism, glucose is mainly metabolised to carbon dioxide by resting T cells, whereas activated cytotoxic T cells utilise glycolysis and produce lactate for energy and biosynthesis (Fischer et al., 2007).

Lactate signalling in $CD4^+$ T cells promotes Th17 cell differentiation and suppresses T cell migration and trafficking (Pucino et al., 2019). Lactate enters $CD4^+$ T cells via MCT1, through LDHB into pyruvate, promote TCA cycle, decrease T-cell glycolysis, inhibits $CD4^+$ T cell proliferation, induces effector T cell dysfunction (Kaushik et al., 2019), favors Treg expansion, and maintains their suppressive function (Watson et al., 2021). A link has been established between aerobic glycolysis and cytokine production. Several studies have shown that glycolytic enzymes are involved in the production of cytokines. *Ex vivo* T-cell activation assays have shown that lactate stimulates the secretion of cytokines such as IFN-γ, IL-2 and TNF-α (Wen et al., 2021). In addition, other studies found that the high lactate microenvironment decreased IFN-g production and inhibited NKT cell proliferation, survival and effector function (Kumar et al., 2019) (Figure 5).

An important mechanism for the induction of macrophage plasticity is the modulation of phenotypic stability and epigenetic dynamics in the context of inflammation, autoimmune responses and cancer. Under physiological or pathological conditions, epigenetic modification may form an integrated pathway during lactate-induced cell polarisation (Bekkering et al., 2018). Previous studies have shown that glycolysis and oxidative phosphorylation (OXPHOS) are closely linked to macrophage polarisation. There are two types of activated macrophages: pro-inflammatory M1 macrophages rely primarily on glycolysis, whereas reparative and immunoregulatory M2 macrophages rely on OXPHOS (Watanabe et al., 2018) (Figure 5). Thus, these factors that affect macrophage metabolism may disrupt M1/M2 homeostasis and exacerbate inflammation.

PAH is the result of a variety of factors and one of the most important is the imbalance of the immune microenvironment. Lactate can increase the expression of pro-inflammatory cytokines and regulate macrophage polarisation both *in vivo* and *in vitro*. Boutens et al. found that in human cell lines, hypoxia and glucose supplementation increased intracellular lactate levels and upregulated the expression of histone lactylation, and in particular promoted histone H3K18 lactylation (Sun et al., 2021), thereby promoting the polarisation of M1-type macrophages (Boutens et al., 2018) (Figure 5). The research showed that lactate production is required for proper histone lactylation, which induces gene expression and maintains homeostasis by promoting an M2-like phenotype in the late stages of M1 macrophage polarisation. In the M1 macrophage polarisation model, ChIP-seq showed that H3K18la was enriched at specific genes. When M1 macrophages are polarised by infection, this is characterised by increased histone lactylation in promoter regions and leads to the expression of homeostatic genes (Zhang et al., 2019). One line of clinical evidence suggests that the expression of H3K18 in peripheral blood monocytes is strongly correlated with the severity of critically ill patients. Therefore, H3K18 is a very promising biomarker (Chu et al., 2021).

Endothelial dysfunction accompanied by glycolysis increase metabolic changes in the pathophysiology, PAH is of great importance. Recent studies have shown that lactate increases the acetylation and lactylation of high mobility group protein B1 (HMGB1), and enhances its release from macrophages through exosomes. In addition, lactate inhibits the steady state and promotes vascular permeability, which induces vascular endothelial cell injury (Yang et al., 2022). Meanwhile, from *in vitro* cultured PASMC, HMGB1 by increasing the endoplasmic reticulum stress-related protein PERK and ATF4 reduce HIPK2 expression, increase SIAH2 expression, thus promoting PASMC proliferation and migration. Through glycyrrhizic acid interference, HMGB1 can reduce the development of PAH (Zhang et al., 2023). Glucose enters the cytoplasm through the glucose transporter 1 (GLUT1) and is metabolized through the pathways of glycolysis and the tricarboxylic acid cycle. Overexpression of the primary macrophage GLUT1 enhances glycolysis and pro-inflammatory cytokine release. Similarly, lacking GLUT1 of macrophages

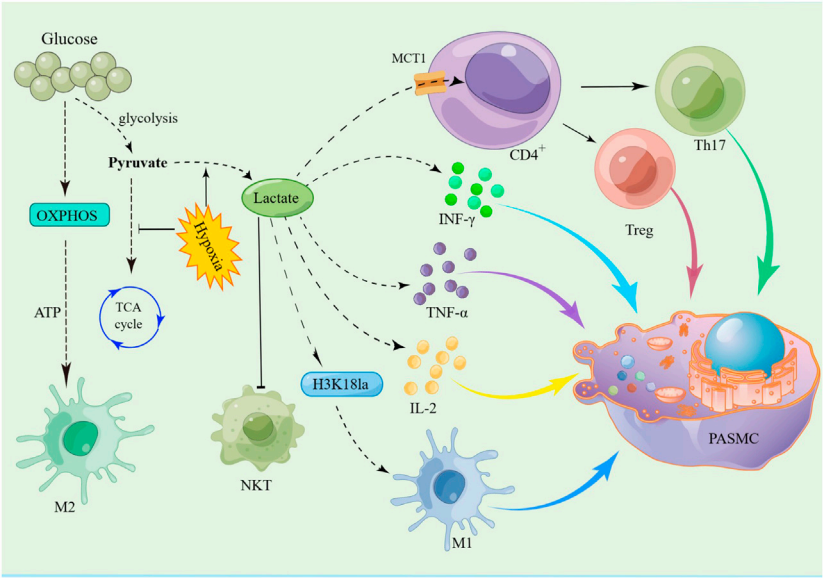

FIGURE 5
Schematic of the hypothesis that lactate promotes PASMC proliferation by disrupting the immune microenvironment via histone lactylation modification. Glycolysis and the TCA cycle are the major metabolic processes of glucose in the body. When oxygen is adequate, cells produce energy primarily through the TCA cycle. However, in hypoxia, glucose is metabolized by glycolysis to produce large amounts of lactate. Lactate is transported via MCT1 to $CD4^+$ T cells, which then promote the differentiation of Th17 cells and the expansion of Treg cells. At the same time, the increase in lactate promotes the secretion of IFN-γ, IL-2 and TNF-α by immune cells, which promotes PASMC proliferation by activating downstream signalling pathways. In addition, lactate promotes the release of IL-1 through histone lactylation modification of M1 macrophages, thereby promoting the proliferation of PASMC.

promoted M2 polarization (Freemerman et al., 2019). It has been shown that GLUT-1 is over-expressed in PAs and PASMCs in an animal model of MCT-induced PAH (Li et al., 2019). In addition, studies have shown that the increase of pyruvate kinase M2 (PKM2) protein expression in PAH can promote the phosphorylation of ERK1/2 and further upregulate the expression of key glycolytic enzymes LDHA and GLUT1, thereby participating in vascular remodeling in PAH. However, increasing shikonin decreased the protein level of PKM2, decreased the phosphorylation level of ERK1/2 and the expression level of GLUT1 protein, and inhibited the progression of PAH (Li et al., 2023).

A hypoxia-induced adaptive response is initiated by HIF-1, which increases or represses the expression of genes regulating vascular tone, autophagic response, cell metabolism, and proliferation. HIF-1 could enhance the transcription of a glycolysis and pro-inflammatory M1 gene profile (Boutens et al., 2018). Lactate, as a promoter of angiogenesis, increases angiogenesis through HIF-1α stabilization to promote the expression of VEGF (Depping et al., 2008) Furthermore, studies have shown that the progression of PAH is due to VEGF (Wang et al., 2022) and Arginase (Arg) (Ji et al., 2022) overexpression. Hypoxia induces changes in the subcellular distribution of nuclear proteins and significantly promotes the activation of EGFR signaling. The phosphorylation modification of EGFR increases the sensitivity of vascular cells to Ca^{2+}, leading to enhanced vasoconstriction and the development of pulmonary vascular remodeling, whereas injection of EGFR inhibitors can improve pulmonary artery remodeling in MCT-induced PH rats (Wang et al., 2022). EGFR can activate downstream ERK, and ERK phosphorylation can activate HIF-1. In addition, lactate induced M2 macrophage polarization can be attributed to the activator ERK of the STAT3 signaling pathway as well as increased VEGF and Arg-1 expression (Mu et al., 2018).

In conclusion, lactate accumulation and histone lactylation contribute to the development of immunotherapy (Cascone et al., 2018). Several studies have shown that there is some correlation between immune cells and glucose metabolites. Therapies targeting immune metabolism are in the early stages of development. However, the mechanism of their interaction, whether through direct or indirect signaling pathways, remains unclear and needs to be further explored. In this review, we bridge the gap between histone lactylation and the immune microenvironment for the first time, providing new insights into PAH research.

8 Conclusion

PAH is a serious cardiovascular disease that results from a complex mechanism involving many cellular and molecular interactions, and recent studies have shown that lactate plays an important role in PAH. While impressive progress has been made, there are still many questions that remain unanswered. Specifically, lactate can affect m^6A through histone lactylation modification, thereby altering transcription and translation of mRNA, which in turn affects cell growth and metabolism. In addition, lactate may also affect the immune microenvironment by regulating the number and function of immune cells, thereby affecting the disease course of patients with PAH.

Existing literature shows that in almost all proteins involved in at least one regulatory PTM. Lactylated proteins are widely involved

in PTMs and protein turnover, and are involved in chaperones, ribosomal structure, and biogenesis (Zhang et al., 2021). Lactate regulates cellular metabolism through histone lactylation-mediated gene expression. In addition, lactate has been shown to play an important role in angiogenesis, energy supply, immunosuppression, and epigenetic regulation (Jiang et al., 2021). The lysine lactylation in core histones is a novel type of histone mark. So far, 28 lactylation sites have been identified, H3, H4, H2A, and H2B are among the sites for lactylation on core histones (Zhang et al., 2019). The discovery of novel signaling pathways, transcription factors, biomarkers and metabolic mediators of PAH, as well as intersections that may aid in the development of effective targeted therapies, is essential.

Investigating the biological mechanisms behind the onset and progression of PAH is critical to more effectively treating the disease, improving its prognosis and developing effective strategies to reverse it. With the discovery of lactylation, the historical role of lactate has been re-examined from a biological and functional perspective. Therapeutic strategies targeting lactate metabolism are becoming increasingly useful and promising. Because lactate stimulates histone lactylation modifications and contributes to gene expression, advancing our knowledge of the physiopathology of PAH with histone lactylation modification is likely to fill an important knowledge gap.

Author contributions

S-sZ: Data curation, Project administration, Writing–original draft, Writing–review and editing. JL: Writing–review and editing, Methodology, Resources, Supervision. Q-cW: Methodology, Resources, Supervision, Writing–review and editing, Project administration. X-lZ: Methodology, Project administration, Resources, Supervision, Writing–review and editing.

Funding

The authors declare financial support was received for the research, authorship, and/or publication of this article. This work was supported by grants from the National Natural Science Foundation of China (Nos 81970199, 82160082, and 82360060), the Natural Science Foundation of Jiangxi Province (Nos 20232ACB206003 and 20202BAB206006).

Conflict of interest

The authors declare that the research was conducted in the absence of any commercial or financial relationships that could be construed as a potential conflict of interest.

Publisher's note

All claims expressed in this article are solely those of the authors and do not necessarily represent those of their affiliated organizations, or those of the publisher, the editors and the reviewers. Any product that may be evaluated in this article, or claim that may be made by its manufacturer, is not guaranteed or endorsed by the publisher.

References

Al-Omary, M. S., Sugito, S., Boyle, A. J., Sverdlov, A. L., and Collins, N. J. (2020). Pulmonary hypertension due to left heart disease: diagnosis, pathophysiology, and therapy. *Hypertension* 75 (6), 1397–1408. doi:10.1161/HYPERTENSIONAHA.119.14330

Badesch, D. B., Raskob, G. E., Elliott, C. G., Krichman, A. M., Farber, H. W., Frost, A. E., et al. (2010). Pulmonary arterial hypertension: baseline characteristics from the REVEAL registry. *Chest* 137 (2), 376–387. doi:10.1378/chest.09-1140

Bekkering, S., Arts, R. J. W., Novakovic, B., Kourtzelis, I., van der Heijden, C., Li, Y., et al. (2018). Metabolic induction of trained immunity through the mevalonate pathway. *Cell* 172 (1-2), 135–146. doi:10.1016/j.cell.2017.11.025

Bhagat, T. D., Von Ahrens, D., Dawlaty, M., Zou, Y., Baddour, J., Achreja, A., et al. (2019). Lactate-mediated epigenetic reprogramming regulates formation of human pancreatic cancer-associated fibroblasts. *Elife* 8, e50663. doi:10.7554/eLife.50663

Boucly, A., Savale, L., Jais, X., Bauer, F., Bergot, E., Bertoletti, L., et al. (2021). Association between initial treatment strategy and long-term survival in pulmonary arterial hypertension. *Am. J. Respir. Crit. Care Med.* 204 (7), 842–854. doi:10.1164/rccm.202009-3698OC

Boutens, L., Hooiveld, G. J., Dhingra, S., Cramer, R. A., Netea, M. G., and Stienstra, R. (2018). Unique metabolic activation of adipose tissue macrophages in obesity promotes inflammatory responses. *Diabetologia* 61 (4), 942–953. doi:10.1007/s00125-017-4526-6

Brand, A., Singer, K., Koehl, G. E., Kolitzus, M., Schoenhammer, G., Thiel, A., et al. (2016). LDHA-associated lactic acid production blunts tumor immunosurveillance by T and NK cells. *Cell Metab.* 24 (5), 657–671. doi:10.1016/j.cmet.2016.08.011

Cao, Y., Zhang, X., Wang, L., Yang, Q., Ma, Q., Xu, J., et al. (2019). PFKFB3-mediated endothelial glycolysis promotes pulmonary hypertension. *Proc. Natl. Acad. Sci. U. S. A.* 116 (27), 13394–13403. doi:10.1073/pnas.1821401116

Cascone, T., McKenzie, J. A., Mbofung, R. M., Punt, S., Wang, Z., Xu, C., et al. (2018). Increased tumor glycolysis characterizes immune resistance to adoptive T cell therapy. *Cell Metab.* 27 (5), 977–987. doi:10.1016/j.cmet.2018.02.024

Chu, Y., Xiangli, X., and Xiao, W. (2015). Regulatory T cells protect against hypoxia-induced pulmonary arterial hypertension in mice. *Mol. Med. Rep.* 11 (4), 3181–3187. doi:10.3892/mmr.2014.3106

Chen, G., Zuo, S., Tang, J., Zuo, C., Jia, D., Liu, Q., et al. (2018). Inhibition of CRTH2-mediated Th2 activation attenuates pulmonary hypertension in mice. *J. Exp. Med.* 215 (8), 2175–2195. doi:10.1084/jem.20171767

Chen, H., Gu, L., Orellana, E. A., Wang, Y., Guo, J., Liu, Q., et al. (2020). METTL4 is an snRNA m(6)Am methyltransferase that regulates RNA splicing. *Cell Res.* 30 (6), 544–547. doi:10.1038/s41422-019-0270-4

Chen, J., Zhang, M., Liu, Y., Zhao, S., Wang, Y., Wang, M., et al. (2022). Histone lactylation driven by mROS-mediated glycolytic shift promotes hypoxic pulmonary hypertension. *J. Mol. Cell Biol.* 14 (12), mjac073. doi:10.1093/jmcb/mjac073

Chu, X., Di, C., Chang, P., Li, L., Feng, Z., Xiao, S., et al. (2021). Lactylated histone H3K18 as a potential biomarker for the diagnosis and predicting the severity of septic shock. *Front. Immunol.* 12, 786666. doi:10.3389/fimmu.2021.786666

Depping, R., Steinhoff, A., Schindler, S. G., Friedrich, B., Fagerlund, R., Metzen, E., et al. (2008). Nuclear translocation of hypoxia-inducible factors (HIFs): involvement of the classical importin alpha/beta pathway. *Biochim. Biophys. Acta* 1783 (3), 394–404. doi:10.1016/j.bbamcr.2007.12.006

Diebold, I., Hennigs, J. K., Miyagawa, K., Li, C. G., Nickel, N. P., Kaschwich, M., et al. (2015). BMPR2 preserves mitochondrial function and DNA during reoxygenation to promote endothelial cell survival and reverse pulmonary hypertension. *Cell Metab.* 21 (4), 596–608. doi:10.1016/j.cmet.2015.03.010

Du, H., Zhao, Y., He, J., Zhang, Y., Xi, H., Liu, M., et al. (2016). YTHDF2 destabilizes m(6)A-containing RNA through direct recruitment of the CCR4-NOT deadenylase complex. *Nat. Commun.* 7, 12626. doi:10.1038/ncomms12626

Efremova, M., Vento-Tormo, M., Teichmann, S. A., and Vento-Tormo, R. (2020). CellPhoneDB: inferring cell-cell communication from combined expression of multi-subunit ligand-receptor complexes. *Nat. Protoc.* 15 (4), 1484–1506. doi:10.1038/s41596-020-0292-x

Elkord, E. (2009). Frequency of human T regulatory cells in peripheral blood is significantly reduced by cryopreservation. *J. Immunol. Methods* 347 (1-2), 87–90. doi:10.1016/j.jim.2009.06.001

Fei, Q., Zou, Z., Roundtree, I. A., Sun, H. L., and He, C. (2020). YTHDF2 promotes mitotic entry and is regulated by cell cycle mediators. *PLoS Biol.* 18 (4), e3000664. doi:10.1371/journal.pbio.3000664

Fischer, K., Hoffmann, P., Voelkl, S., Meidenbauer, N., Ammer, J., Edinger, M., et al. (2007). Inhibitory effect of tumor cell-derived lactic acid on human T cells. *Blood* 109 (9), 3812–3819. doi:10.1182/blood-2006-07-035972

Florentin, J., Coppin, E., Vasamsetti, S. B., Zhao, J., Tai, Y. Y., Tang, Y., et al. (2018). Inflammatory macrophage expansion in pulmonary hypertension depends upon mobilization of blood-borne monocytes. *J. Immunol.* 200 (10), 3612–3625. doi:10.4049/jimmunol.1701287

Freemerman, A. J., Zhao, L., Pingili, A. K., Teng, B., Cozzo, A. J., Fuller, A. M., et al. (2019). Myeloid slc2a1-deficient murine model revealed macrophage activation and metabolic phenotype are fueled by GLUT1. *J. Immunol.* 202 (4), 1265–1286. doi:10.4049/jimmunol.1800002

Galie, N., Humbert, M., Vachiery, J. L., Gibbs, S., Lang, I., Torbicki, A., et al. (2016). 2015 ESC/ERS guidelines for the diagnosis and treatment of pulmonary hypertension. *Rev. Esp. Cardiol. Engl. Ed.* 69 (2), 177. doi:10.1016/j.rec.2016.01.002

Gao, Y., Pei, G., Li, D., Li, R., Shao, Y., Zhang, Q. C., et al. (2019). Multivalent m(6)A motifs promote phase separation of YTHDF proteins. *Cell Res.* 29 (9), 767–769. doi:10.1038/s41422-019-0210-3

Goncharov, D. A., Kudryashova, T. V., Ziai, H., Ihida-Stansbury, K., DeLisser, H., Krymskaya, V. P., et al. (2014). Mammalian target of rapamycin complex 2 (mTORC2) coordinates pulmonary artery smooth muscle cell metabolism, proliferation, and survival in pulmonary arterial hypertension. *Circulation* 129 (8), 864–874. doi:10.1161/CIRCULATIONAHA.113.004581

Guihaire, J., Deuse, T., Wang, D., Spin, J. M., Blankenberg, F. G., Fadel, E., et al. (2021). Immunomodulation therapy using tolerogenic macrophages in a rodent model of pulmonary hypertension. *Stem Cells Dev.* 30 (10), 515–525. doi:10.1089/scd.2021.0007

Guo, L., Qin, G., Cao, Y., Yang, Y., Dai, S., Wang, L., et al. (2021). Regulation of the immune microenvironment by an NLRP3 inhibitor contributes to attenuation of acute right ventricular failure in rats with pulmonary arterial hypertension. *J. Inflamm. Res.* 14, 5699–5711. doi:10.2147/JIR.S336964

Guo, X., Li, K., Jiang, W., Hu, Y., Xiao, W., Huang, Y., et al. (2020). RNA demethylase ALKBH5 prevents pancreatic cancer progression by posttranscriptional activation of PER1 in an m6A-YTHDF2-dependent manner. *Mol. Cancer* 19 (1), 91. doi:10.1186/s12943-020-01158-w

Gustafsson, J., Eriksson, J., and Marcus, C. (2007). Glucose metabolism in human adipose tissue studied by 13C-glucose and microdialysis. *Scand. J. Clin. Lab. Invest.* 67 (2), 155–164. doi:10.1080/00365510600995259

Han, X. J., Zhang, W. F., Wang, Q., Li, M., Zhang, C. B., Yang, Z. J., et al. (2021). HIF-1α promotes the proliferation and migration of pulmonary arterial smooth muscle cells via activation of Cx43. *J. Cell Mol. Med.* 25 (22), 10663–10673. doi:10.1111/jcmm.17003

Harbaum, L., Renk, E., Yousef, S., Glatzel, A., Luneburg, N., Hennigs, J. K., et al. (2016). Acute effects of exercise on the inflammatory state in patients with idiopathic pulmonary arterial hypertension. *BMC Pulm. Med.* 16 (1), 145. doi:10.1186/s12890-016-0301-6

Harbaum, L., Rhodes, C. J., Wharton, J., Lawrie, A., Karnes, J. H., Desai, A. A., et al. (2022). Mining the plasma proteome for insights into the molecular pathology of pulmonary arterial hypertension. *Am. J. Respir. Crit. Care Med.* 205 (12), 1449–1460. doi:10.1164/rccm.202109-2106OC

Hautefort, A., Mendes-Ferreira, P., Sabourin, J., Manaud, G., Bertero, T., Rucker-Martin, C., et al. (2019). Bmpr2 mutant rats develop pulmonary and cardiac characteristics of pulmonary arterial hypertension. *Circulation* 139 (7), 932–948. doi:10.1161/CIRCULATIONAHA.118.033744

He, Y., Zuo, C., Jia, D., Bai, P., Kong, D., Chen, D., et al. (2020). Loss of DP1 aggravates vascular remodeling in pulmonary arterial hypertension via mTORC1 signaling. *Am. J. Respir. Crit. Care Med.* 201 (10), 1263–1276. doi:10.1164/rccm.201911-2137OC

Hernandez-Saavedra, D., Sanders, L., Freeman, S., Reisz, J. A., Lee, M. H., Mickael, C., et al. (2020). Stable isotope metabolomics of pulmonary artery smooth muscle and endothelial cells in pulmonary hypertension and with TGF-beta treatment. *Sci. Rep.* 10 (1), 413. doi:10.1038/s41598-019-57200-5

Hong, K. H., Lee, Y. J., Lee, E., Park, S. O., Han, C., Beppu, H., et al. (2008). Genetic ablation of the BMPR2 gene in pulmonary endothelium is sufficient to predispose to pulmonary arterial hypertension. *Circulation* 118 (7), 722–730. doi:10.1161/CIRCULATIONAHA.107.736801

Hu, L., Wang, J., Huang, H., Yu, Y., Ding, J., Yu, Y., et al. (2021). YTHDF1 regulates pulmonary hypertension through translational control of MAGED1. *Am. J. Respir. Crit. Care Med.* 203 (9), 1158–1172. doi:10.1164/rccm.202009-3419OC

Huang, H., Weng, H., Zhou, K., Wu, T., Zhao, B. S., Sun, M., et al. (2019). Histone H3 trimethylation at lysine 36 guides m(6)A RNA modification co-transcriptionally. *Nature* 567 (7748), 414–419. doi:10.1038/s41586-019-1016-7

Huang, T., Liu, Z., Zheng, Y., Feng, T., Gao, Q., and Zeng, W. (2020). YTHDF2 promotes spermagonial adhesion through modulating MMPs decay via m(6)A/mRNA pathway. *Cell Death Dis.* 11 (1), 37. doi:10.1038/s41419-020-2235-4

Huertas, A., Phan, C., Bordenave, J., Tu, L., Thuillet, R., Le Hiress, M., et al. (2016). Regulatory T cell dysfunction in idiopathic, heritable and connective tissue-associated pulmonary arterial hypertension. *Chest* 149 (6), 1482–1493. doi:10.1016/j.chest.2016.01.004

Humbert, M., Kovacs, G., Hoeper, M. M., Badagliacca, R., Berger, R. M. F., Brida, M., et al. (2022). 2022 ESC/ERS Guidelines for the diagnosis and treatment of pulmonary hypertension. *Eur. Heart J.* 43 (38), 3618–3731. doi:10.1093/eurheartj/ehac237

Isobe, S., Kataoka, M., Endo, J., Moriyama, H., Okazaki, S., Tsuchihashi, K., et al. (2019). Endothelial-Mesenchymal transition drives expression of CD44 variant and xCT in pulmonary hypertension. *Am. J. Respir. Cell Mol. Biol.* 61 (3), 367–379. doi:10.1165/rcmb.2018-0231OC

Jain, D., Puno, M. R., Meydan, C., Lailler, N., Mason, C. E., Lima, C. D., et al. (2018). Ketu mutant mice uncover an essential meiotic function for the ancient RNA helicase YTHDC2. *Elife* 7, e30919. doi:10.7554/eLife.30919

Ji, L., Su, S., Xin, M., Zhang, Z., Nan, X., Li, Z., et al. (2022). Luteolin ameliorates hypoxia-induced pulmonary hypertension via regulating HIF-2α-Arg-NO axis and PI3K-AKT-eNOS-NO signaling pathway. *Phytomedicine* 104, 154329. doi:10.1016/j.phymed.2022.154329

Jia, D., Bai, P., Wan, N., Liu, J., Zhu, Q., He, Y., et al. (2020). Niacin attenuates pulmonary hypertension through H-pgds in macrophages. *Circ. Res.* 127 (10), 1323–1336. doi:10.1161/CIRCRESAHA.120.316784

Jiang, J., Huang, D., Jiang, Y., Hou, J., Tian, M., Li, J., et al. (2021). Lactate modulates cellular metabolism through histone lactylation-mediated gene expression in non-small cell lung cancer. *Front. Oncol.* 11, 647559. doi:10.3389/fonc.2021.647559

Kaushik, D. K., Bhattacharya, A., Mirzaei, R., Rawji, K. S., Ahn, Y., Rho, J. M., et al. (2019). Enhanced glycolytic metabolism supports transmigration of brain-infiltrating macrophages in multiple sclerosis. *J. Clin. Invest.* 129 (8), 3277–3292. doi:10.1172/JCI124012

Ke, S., Alemu, E. A., Mertens, C., Gantman, E. C., Fak, J. J., Mele, A., et al. (2015). A majority of m6A residues are in the last exons, allowing the potential for 3' UTR regulation. *Genes Dev.* 29 (19), 2037–2053. doi:10.1101/gad.269415.115

Kovacs, L., Cao, Y., Han, W., Meadows, L., Kovacs-Kasa, A., Kondrikov, D., et al. (2019). PFKFB3 in smooth muscle promotes vascular remodeling in pulmonary arterial hypertension. *Am. J. Respir. Crit. Care Med.* 200 (5), 617–627. doi:10.1164/rccm.201812-2290OC

Kumagai, S., Koyama, S., Itahashi, K., Tanegashima, T., Lin, Y. T., Togashi, Y., et al. (2022). Lactic acid promotes PD-1 expression in regulatory T cells in highly glycolytic tumor microenvironments. *Cancer Cell* 40 (2), 201–218.e9. doi:10.1016/j.ccell.2022.01.001

Kumar, A., Pyaram, K., Yarosz, E. L., Hong, H., Lyssiotis, C. A., Giri, S., et al. (2019). Enhanced oxidative phosphorylation in NKT cells is essential for their survival and function. *Proc. Natl. Acad. Sci. U. S. A.* 116 (15), 7439–7448. doi:10.1073/pnas.1901376116

Kurosawa, R., Satoh, K., Kikuchi, N., Kikuchi, H., Saigusa, D., Al-Mamun, M. E., et al. (2019). Identification of celastramycin as a novel therapeutic agent for pulmonary arterial hypertension. *Circ. Res.* 125 (3), 309–327. doi:10.1161/CIRCRESAHA.119.315229

Lagarde, D., Jeanson, Y., Barreau, C., Moro, C., Peyriga, L., Cahoreau, E., et al. (2021). Lactate fluxes mediated by the monocarboxylate transporter-1 are key determinants of the metabolic activity of beige adipocytes. *J. Biol. Chem.* 296, 100137. doi:10.1074/jbc.RA120.016303

Lee, Y. S., Kim, T. Y., Kim, Y., Lee, S. H., Kim, S., Kang, S. W., et al. (2018). Microbiota-Derived lactate accelerates intestinal stem-cell-mediated epithelial development. *Cell Host Microbe* 24 (6), 833–846. doi:10.1016/j.chom.2018.11.002

Li, B., He, W., Ye, L., Zhu, Y., Tian, Y., Chen, L., et al. (2019). Targeted delivery of sildenafil for inhibiting pulmonary vascular remodeling. *Hypertension* 73 (3), 703–711. doi:10.1161/HYPERTENSIONAHA.118.11932

Li, J., Xie, H., Ying, Y., Chen, H., Yan, H., He, L., et al. (2020a). YTHDF2 mediates the mRNA degradation of the tumor suppressors to induce AKT phosphorylation in N6-methyladenosine-dependent way in prostate cancer. *Mol. Cancer* 19 (1), 152. doi:10.1186/s12943-020-01267-6

Li, W., Chen, W., Peng, H., Xiao, Z., Liu, J., Zeng, Y., et al. (2023). Shikonin improves pulmonary vascular remodeling in monocrotaline-induced pulmonary arterial hypertension via regulation of PKM2. *Mol. Med. Rep.* 27 (3), 60. Epub 2023 Feb 3. doi:10.3892/mmr.2023.12947

Li, Z., Li, F., Peng, Y., Fang, J., and Zhou, J. (2020b). Identification of three m6A-related mRNAs signature and risk score for the prognostication of hepatocellular carcinoma. *Cancer Med.* 9 (5), 1877–1889. doi:10.1002/cam4.2833

Li, Z., Qian, P., Shao, W., Shi, H., He, X. C., Gogol, M., et al. (2018). Suppression of m(6)A reader Ythdf2 promotes hematopoietic stem cell expansion. *Cell Res.* 28 (9), 904–917. doi:10.1038/s41422-018-0072-0

Liang, Y., Wang, X., Wang, H., Yang, W., Yi, P., Soong, L., et al. (2022). IL-33 activates mTORC1 and modulates glycolytic metabolism in CD8(+) T cells. *Immunology* 165 (1), 61–73. doi:10.1111/imm.13404

Liberti, M. V., and Locasale, J. W. (2020). Histone lactylation: A new role for glucose metabolism. *Trends Biochem. Sci.* 45 (3), 179–182. doi:10.1016/j.tibs.2019.12.004

Liu, Y., Liu, Z., Tang, H., Shen, Y., Gong, Z., Xie, N., et al. (2019). The N(6)-methyladenosine (m(6)A)-forming enzyme METTL3 facilitates M1 macrophage polarization through the methylation of STAT1 mRNA. *Am. J. Physiol. Cell Physiol.* 317 (4), C762-C775–C775. doi:10.1152/ajpcell.00212.2019

Maron, B. A., Abman, S. H., Elliott, C. G., Frantz, R. P., Hopper, R. K., Horn, E. M., et al. (2021). Pulmonary arterial hypertension: diagnosis, treatment, and novel advances. *Am. J. Respir. Crit. Care Med.* 203 (12), 1472–1487. doi:10.1164/rccm.202012-4317SO

Maron, B. A., Brittain, E. L., Choudhary, G., and Gladwin, M. T. (2018). Redefining pulmonary hypertension. *Lancet Respir. Med.* 6 (3), 168–170. doi:10.1016/S2213-2600(17)30498-8

Maston, L. D., Jones, D. T., Giermakowska, W., Howard, T. A., Cannon, J. L., Wang, W., et al. (2017). Central role of T helper 17 cells in chronic hypoxia-induced pulmonary hypertension. *Am. J. Physiol. Lung Cell Mol. Physiol.* 312 (5), L609-L624–L624. doi:10.1152/ajplung.00531.2016

Mathiyalagan, P., Adamiak, M., Mayourian, J., Sassi, Y., Liang, Y., Agarwal, N., et al. (2019). FTO-dependent N(6)-methyladenosine regulates cardiac function during remodeling and repair. *Circulation* 139 (4), 518–532. doi:10.1161/CIRCULATIONAHA.118.033794

Mauer, J., Luo, X., Blanjoie, A., Jiao, X., Grozhik, A. V., Patil, D. P., et al. (2017). Reversible methylation of m(6)A(m) in the 5' cap controls mRNA stability. *Nature* 541 (7637), 371–375. doi:10.1038/nature21022

Mouton, A. J., DeLeon-Pennell, K. Y., Rivera Gonzalez, O. J., Flynn, E. R., Freeman, T. C., Saucerman, J. J., et al. (2018). Mapping macrophage polarization over the myocardial infarction time continuum. *Basic Res. Cardiol.* 113 (4), 26. doi:10.1007/s00395-018-0686-x

Mu, X., Shi, W., Xu, Y., Xu, C., Zhao, T., Geng, B., et al. (2018). Tumor-derived lactate induces M2 macrophage polarization via the activation of the ERK/STAT3 signaling pathway in breast cancer. *Cell Cycle* 17 (4), 428–438. doi:10.1080/15384101.2018.1444305

Norton, C. E., Sheak, J. R., Yan, S., Weise-Cross, L., Jernigan, N. L., Walker, B. R., et al. (2020). Augmented pulmonary vasoconstrictor reactivity after chronic hypoxia requires src kinase and epidermal growth factor receptor signaling. *Am. J. Respir. Cell Mol. Biol.* 62 (1), 61–73. doi:10.1165/rcmb.2018-0106OC

Patil, D. P., Chen, C. K., Pickering, B. F., Chow, A., Jackson, C., Guttman, M., et al. (2016). m(6)A RNA methylation promotes XIST-mediated transcriptional repression. *Nature* 537 (7620), 369–373. doi:10.1038/nature19342

Pendleton, K. E., Chen, B., Liu, K., Hunter, O. V., Xie, Y., Tu, B. P., et al. (2017). The U6 snRNA m(6)A methyltransferase METTL16 regulates SAM synthetase intron retention. *Cell* 169 (5), 824–835. doi:10.1016/j.cell.2017.05.003

Perros, F., Cohen-Kaminsky, S., Gambaryan, N., Girerd, B., Raymond, N., Klingelschmitt, I., et al. (2013). Cytotoxic cells and granulysin in pulmonary arterial hypertension and pulmonary veno-occlusive disease. *Am. J. Respir. Crit. Care Med.* 187 (2), 189–196. doi:10.1164/rccm.201208-1364OC

Ping, X. L., Sun, B. F., Wang, L., Xiao, W., Yang, X., Wang, W. J., et al. (2014). Mammalian WTAP is a regulatory subunit of the RNA N6-methyladenosine methyltransferase. *Cell Res.* 24 (2), 177–189. doi:10.1038/cr.2014.3

Pucino, V., Certo, M., Bulusu, V., Cucchi, D., Goldmann, K., Pontarini, E., et al. (2019). Lactate buildup at the site of chronic inflammation promotes disease by inducing CD4(+) T cell metabolic rewiring. *Cell Metab.* 30 (6), 1055–1074. doi:10.1016/j.cmet.2019.10.004

Qin, Y., Qiao, Y., Li, L., Luo, E., Wang, D., Yao, Y., et al. (2021). The m(6)A methyltransferase METTL3 promotes hypoxic pulmonary arterial hypertension. *Life Sci.* 274, 119366. doi:10.1016/j.lfs.2021.119366

Qing, Y., Dong, L., Gao, L., Li, C., Li, Y., Han, L., et al. (2021). R-2-hydroxyglutarate attenuates aerobic glycolysis in leukemia by targeting the FTO/m(6)A/PFKP/LDHB axis. *Mol. Cell* 81 (5), 922–939.e9. doi:10.1016/j.molcel.2020.12.026

Qu, L. H., Luo, W. J., Yan, Z. G., and Liu, W. P. (2022). FAM171B as a novel biomarker mediates tissue immune microenvironment in pulmonary arterial hypertension. *Mediat. Inflamm.* 2022, 1878766. doi:10.1155/2022/1878766

Rhodes, C. J., Batai, K., Bleda, M., Haimel, M., Southgate, L., Germain, M., et al. (2019). Genetic determinants of risk in pulmonary arterial hypertension: international genome-wide association studies and meta-analysis. *Lancet Respir. Med.* 7 (3), 227–238. doi:10.1016/S2213-2600(18)30409-0

Ries, R. J., Zaccara, S., Klein, P., Olarerin-George, A., Namkoong, S., Pickering, B. F., et al. (2019). m(6)A enhances the phase separation potential of mRNA. *Nature* 571 (7765), 424–428. doi:10.1038/s41586-019-1374-1

Roundtree, I. A., Luo, G. Z., Zhang, Z., Wang, X., Zhou, T., Cui, Y., et al. (2017). YTHDC1 mediates nuclear export of N(6)-methyladenosine methylated mRNAs. *Elife* 6, e31311. doi:10.7554/eLife.31311

Saygin, D., Highland, K. B., Farha, S., Park, M., Sharp, J., Roach, E. C., et al. (2017). Metabolic and functional evaluation of the heart and lungs in pulmonary hypertension by gated 2-[18F]-Fluoro-2-deoxy-D-glucose positron emission tomography. *Pulm. Circ.* 7 (2), 428–438. doi:10.1177/2045893217701917

Shafiq, M., Jagavelu, K., Iqbal, H., Yadav, P., Chanda, D., Verma, N. K., et al. (2021). Inhibition of mitogen-activated protein kinase (MAPK)-Activated protein kinase 2 (MK2) is protective in pulmonary hypertension. *Hypertension* 77 (4), 1248–1259. doi:10.1161/HYPERTENSIONAHA.120.15229

Shi, H., Wang, X., Lu, Z., Zhao, B. S., Ma, H., Hsu, P. J., et al. (2017). YTHDF3 facilitates translation and decay of N(6)-methyladenosine-modified RNA. *Cell Res.* 27 (3), 315–328. doi:10.1038/cr.2017.15

Shi, H., Zhang, X., Weng, Y. L., Lu, Z., Liu, Y., Lu, Z., et al. (2018). m(6)A facilitates hippocampus-dependent learning and memory through YTHDF1. *Nature* 563 (7730), 249–253. doi:10.1038/s41586-018-0666-1

Shime, H., Yabu, M., Akazawa, T., Kodama, K., Matsumoto, M., Seya, T., et al. (2008). Tumor-secreted lactic acid promotes IL-23/IL-17 proinflammatory pathway. *J. Immunol.* 180 (11), 7175–7183. doi:10.4049/jimmunol.180.11.7175

Simonneau, G., Montani, D., Celermajer, D. S., Denton, C. P., Gatzoulis, M. A., Krowka, M., et al. (2019). Haemodynamic definitions and updated clinical classification of pulmonary hypertension. *Eur. Respir. J.* 53 (1), 1801913. doi:10.1183/13993003.01913-2018

Souto-Carneiro, M. M., Klika, K. D., Abreu, M. T., Meyer, A. P., Saffrich, R., Sandhoff, R., et al. (2020). Effect of increased lactate dehydrogenase A activity and aerobic glycolysis on the proinflammatory profile of autoimmune CD8+ T cells in rheumatoid arthritis. *Arthritis Rheumatol.* 72 (12), 2050–2064. doi:10.1002/art.41420

Steiner, M. K., Syrkina, O. L., Kolliputi, N., Mark, E. J., Hales, C. A., and Waxman, A. B. (2009). Interleukin-6 overexpression induces pulmonary hypertension. *Circ. Res.* 104 (2), 236–244. doi:10.1161/CIRCRESAHA.108.182014

Stillman, B. (2018). Histone modifications: insights into their influence on gene expression. *Cell* 175 (1), 6–9. doi:10.1016/j.cell.2018.08.032

Su, R., Dong, L., Li, C., Nachtergaele, S., Wunderlich, M., Qing, Y., et al. (2018). R-2HG exhibits anti-tumor activity by targeting FTO/m(6)A/MYC/CEBPA signaling. *Cell* 172 (1-2), 90–105. doi:10.1016/j.cell.2017.11.031

Sun, S., Xu, X., Liang, L., Wang, X., Bai, X., Zhu, L., et al. (2021). Lactic acid-producing probiotic *Saccharomyces cerevisiae* attenuates ulcerative colitis via suppressing macrophage pyroptosis and modulating gut microbiota. *Front. Immunol.* 12, 777665. doi:10.3389/fimmu.2021.777665

Tamosiuniene, R., Tian, W., Dhillon, G., Wang, L., Sung, Y. K., Gera, L., et al. (2011). Regulatory T cells limit vascular endothelial injury and prevent pulmonary hypertension. *Circ. Res.* 109 (8), 867–879. doi:10.1161/CIRCRESAHA.110.236927

Tang, C., Klukovich, R., Peng, H., Wang, Z., Yu, T., Zhang, Y., et al. (2018a). ALKBH5-dependent m6A demethylation controls splicing and stability of long 3'-UTR mRNAs in male germ cells. *Proc. Natl. Acad. Sci. U. S. A.* 115 (2), E325-E333–E333. doi:10.1073/pnas.1717794115

Tang, C., Luo, Y., Li, S., Huang, B., Xu, S., and Li, L. (2021). Characteristics of inflammation process in monocrotaline-induced pulmonary arterial hypertension in rats. *Biomed. Pharmacother.* 133, 111081. doi:10.1016/j.biopha.2020.111081

Tang, H., Babicheva, A., McDermott, K. M., Gu, Y., Ayon, R. J., Song, S., et al. (2018b). Endothelial HIF-2α contributes to severe pulmonary hypertension due to endothelial-to-mesenchymal transition. *Am. J. Physiol. Lung Cell Mol. Physiol.* 314 (2), L256-L275–L275. doi:10.1152/ajplung.00096.2017

Tian, W., Jiang, X., Tamosiuniene, R., Sung, Y. K., Qian, J., Dhillon, G., et al. (2013). Blocking macrophage leukotriene b4 prevents endothelial injury and reverses pulmonary hypertension. *Sci. Transl. Med.* 5 (200), 200ra117. doi:10.1126/scitranslmed.3006674

Varner, E. L., Trefely, S., Bartee, D., von Krusenstiern, E., Izzo, L., Bekeova, C., et al. (2020). Quantification of lactoyl-CoA (lactyl-CoA) by liquid chromatography mass spectrometry in mammalian cells and tissues. *Open Biol.* 10 (9), 200187. doi:10.1098/rsob.200187

Vasconcelos, E. S. J., Simao, D., Terrasso, A. P., Silva, M. M., Brito, C., Isidro, I. A., et al. (2020). Unveiling dynamic metabolic signatures in human induced pluripotent and neural stem cells. *PLoS Comput. Biol.* 16 (4), e1007780. doi:10.1371/journal.pcbi.1007780

Vu, L. P., Pickering, B. F., Cheng, Y., Zaccara, S., Nguyen, D., Minuesa, G., et al. (2017). The N(6)-methyladenosine (m(6)A)-forming enzyme METTL3 controls myeloid differentiation of normal hematopoietic and leukemia cells. *Nat. Med.* 23 (11), 1369–1376. doi:10.1038/nm.4416

Wang, J., Yan, S., Lu, H., Wang, S., and Xu, D. (2019). METTL3 attenuates LPS-induced inflammatory response in macrophages via NF-κB signaling pathway. *Mediat. Inflamm.* 2019, 3120391. doi:10.1155/2019/3120391

Wang, K., Jiang, L., Zhang, Y., and Chen, C. (2020). Progression of thyroid carcinoma is promoted by the m6A methyltransferase METTL3 through regulating m(6)A methylation on TCF1. *Onco Targets Ther.* 13, 1605–1612. doi:10.2147/OTT.S234751

Wang, R. R., Yuan, T. Y., Chen, D., Chen, Y. C., Sun, S. C., Wang, S. B., et al. (2022a). Dan-shen-yin granules prevent hypoxia-induced pulmonary hypertension *via* STAT3/

HIF-1α/VEGF and FAK/AKT signaling pathways. *Front. Pharmacol.* 13, 844400. doi:10.3389/fphar.2022.844400

Wang, X., Li, Q., He, S., Bai, J., Ma, C., Zhang, L., et al. (2022b). LncRNA FENDRR with m6A RNA methylation regulates hypoxia-induced pulmonary artery endothelial cell pyroptosis by mediating DRP1 DNA methylation. *Mol. Med.* 28 (1), 126. doi:10.1186/s10020-022-00551-z

Wang, X., Zhao, B. S., Roundtree, I. A., Lu, Z., Han, D., Ma, H., et al. (2015). N(6)-methyladenosine modulates messenger RNA translation efficiency. *Cell* 161 (6), 1388–1399. doi:10.1016/j.cell.2015.05.014

Watanabe, R., Hilhorst, M., Zhang, H., Zeisbrich, M., Berry, G. J., Wallis, B. B., et al. (2018). Glucose metabolism controls disease-specific signatures of macrophage effector functions. *JCI Insight* 3 (20), e123047. doi:10.1172/jci.insight.123047

Watson, M. J., Vignali, P. D. A., Mullett, S. J., Overacre-Delgoffe, A. E., Peralta, R. M., Grebinoski, S., et al. (2021). Metabolic support of tumour-infiltrating regulatory T cells by lactic acid. *Nature* 591 (7851), 645–651. doi:10.1038/s41586-020-03045-2

Wen, J., Cheng, S., Zhang, Y., Wang, R., Xu, J., Ling, Z., et al. (2021). Lactate anions participate in T cell cytokine production and function. *Sci. China Life Sci.* 64 (11), 1895–1905. doi:10.1007/s11427-020-1887-7

Wen, J., Lv, R., Ma, H., Shen, H., He, C., Wang, J., et al. (2018). Zc3h13 regulates nuclear RNA m(6)A methylation and mouse embryonic stem cell self-renewal. *Mol. Cell* 69 (6), 1028–1038. doi:10.1016/j.molcel.2018.02.015

Wu, B., Su, S., Patil, D. P., Liu, H., Gan, J., Jaffrey, S. R., et al. (2018). Molecular basis for the specific and multivariant recognitions of RNA substrates by human hnRNP A2/B1. *Nat. Commun.* 9 (1), 420. doi:10.1038/s41467-017-02770-z

Xiao, Y., Peng, H., Hong, C., Chen, Z., Deng, X., Wang, A., et al. (2017). PDGF promotes the Warburg effect in pulmonary arterial smooth muscle cells via activation of the PI3K/AKT/mTOR/HIF-1α signaling pathway. *Cell Physiol. Biochem.* 42 (4), 1603–1613. doi:10.1159/000479401

Xiong, J., He, J., Zhu, J., Pan, J., Liao, W., Ye, H., et al. (2022). Lactylation-driven METTL3-mediated RNA m(6)A modification promotes immunosuppression of tumor-infiltrating myeloid cells. *Mol. Cell* 82 (9), 1660–1677.e10. doi:10.1016/j.molcel.2022.02.033

Xu, D., Li, Y., Zhang, B., Wang, Y., Liu, Y., Luo, Y., et al. (2016). Resveratrol alleviate hypoxic pulmonary hypertension via anti-inflammation and anti-oxidant pathways in rats. *Int. J. Med. Sci.* 13 (12), 942–954. doi:10.7150/ijms.16810

Xu, S., Xu, X., Zhang, Z., Yan, L., Zhang, L., and Du, L. (2021a). The role of RNA m(6)A methylation in the regulation of postnatal hypoxia-induced pulmonary hypertension. *Respir. Res.* 22 (1), 121. doi:10.1186/s12931-021-01728-6

Xu, Z., Ruan, J., Pan, L., and Chen, C. (2021b). Candidate genes identified in systemic sclerosis-related pulmonary arterial hypertension were associated with immunity, inflammation, and cytokines. *Cardiovasc Ther.* 2021, 6651009. doi:10.1155/2021/6651009

Yang, K., Fan, M., Wang, X., Xu, J., Wang, Y., Tu, F., et al. (2022). Lactate promotes macrophage HMGB1 lactylation, acetylation, and exosomal release in polymicrobial sepsis. *Cell Death Differ.* 29 (1), 133–146. doi:10.1038/s41418-021-00841-9

Yang, W., Wang, P., Cao, P., Wang, S., Yang, Y., Su, H., et al. (2021). Hypoxic *in vitro* culture reduces histone lactylation and impairs pre-implantation embryonic development in mice. *Epigenetics Chromatin* 14 (1), 57. doi:10.1186/s13072-021-00431-6

Yao, M. Z., Ge, X. Y., Liu, T., Huang, N., Liu, H., Chen, Y., et al. (2020). MEIS1 regulated proliferation and migration of pulmonary artery smooth muscle cells in hypoxia-induced pulmonary hypertension. *Life Sci.* 255, 117822. doi:10.1016/j.lfs.2020.117822

Yu, J., Chai, P., Xie, M., Ge, S., Ruan, J., Fan, X., et al. (2021). Histone lactylation drives oncogenesis by facilitating m(6)A reader protein YTHDF2 expression in ocular melanoma. *Genome Biol.* 22 (1), 85. doi:10.1186/s13059-021-02308-z

Zaccara, S., and Jaffrey, S. R. (2020). A unified model for the function of YTHDF proteins in regulating m(6)a-modified mRNA. *Cell* 181 (7), 1582–1595. doi:10.1016/j.cell.2020.05.012

Zeng, Y., Huang, T., Zuo, W., Wang, D., Xie, Y., Wang, X., et al. (2021). Integrated analysis of m(6)A mRNA methylation in rats with monocrotaline-induced pulmonary arterial hypertension. *Aging (Albany NY)* 13 (14), 18238–18256. doi:10.18632/aging.203230

Zhang, D., Tang, Z., Huang, H., Zhou, G., Cui, C., Weng, Y., et al. (2019). Metabolic regulation of gene expression by histone lactylation. *Nature* 574 (7779), 575–580. doi:10.1038/s41586-019-1678-1

Zhang, N., Jiang, N., Yu, L., Guan, T., Sang, X., Feng, Y., et al. (2021). Protein lactylation critically regulates energy metabolism in the Protozoan parasite trypanosoma brucei. *Front. Cell Dev. Biol.* 9, 719720. doi:10.3389/fcell.2021.719720

Zhang, Q., Chen, Y., Wang, Q., Wang, Y., Feng, W., Chai, L., et al. (2023). HMGB1-induced activation of ER stress contributes to pulmonary artery hypertension *in vitro* and *in vivo*. *Respir. Res.* 24 (1), 149. doi:10.1186/s12931-023-02454-x

Zhang, S., Liu, X., Ge, L. L., Li, K., Sun, Y., Wang, F., et al. (2020). Mesenchymal stromal cell-derived exosomes improve pulmonary hypertension through inhibition of pulmonary vascular remodeling. *Respir. Res.* 21 (1), 71. doi:10.1186/s12931-020-1331-4

Zhang, S., Zhao, B. S., Zhou, A., Lin, K., Zheng, S., Lu, Z., et al. (2017). m(6)A demethylase ALKBH5 maintains tumorigenicity of glioblastoma stem-like cells by sustaining FOXM1 expression and cell proliferation program. *Cancer Cell* 31 (4), 591–606. doi:10.1016/j.ccell.2017.02.013

Zhang, Y., Hernandez, M., Gower, J., Winicki, N., Morataya, X., Alvarez, S., et al. (2022). JAGGED-NOTCH3 signaling in vascular remodeling in pulmonary arterial hypertension. *Sci. Transl. Med.* 14 (643), eabl5471. doi:10.1126/scitranslmed.abl5471

Zhao, Y., Peng, J., Lu, C., Hsin, M., Mura, M., Wu, L., et al. (2014). Metabolomic heterogeneity of pulmonary arterial hypertension. *PLoS One* 9 (2), e88727. doi:10.1371/journal.pone.0088727

Zheng, H., Hua, J., Li, H., He, W., Chen, X., Ji, Y., et al. (2022). Comprehensive analysis of the expression of N6-methyladenosine RNA methylation regulators in pulmonary artery hypertension. *Front. Genet.* 13, 974740. doi:10.3389/fgene.2022.974740

Zhou, X. L., Huang, F. J., Li, Y., Huang, H., and Wu, Q. C. (2021). SEDT2/METTL14-mediated m6A methylation awakening contributes to hypoxia-induced pulmonary arterial hypertension in mice. *Aging (Albany NY)* 13 (5), 7538–7548. doi:10.18632/aging.202616

Zhu, B., Gong, Y., Shen, L., Li, J., Han, J., Song, B., et al. (2020). Total Panax notoginseng saponin inhibits vascular smooth muscle cell proliferation and migration and intimal hyperplasia by regulating WTAP/p16 signals via m(6)A modulation. *Biomed. Pharmacother.* 124, 109935. doi:10.1016/j.biopha.2020.109935

Zhu, F., Yang, T., Yao, M., Shen, T., and Fang, C. (2021a). HNRNPA2B1, as a m(6)A reader, promotes tumorigenesis and metastasis of oral squamous cell carcinoma. *Front. Oncol.* 11, 716921. doi:10.3389/fonc.2021.716921

Zhu, X., Yang, H., Zhang, M., Wu, X., Jiang, L., Liu, X., et al. (2021b). YTHDC1-mediated VPS25 regulates cell cycle by targeting JAK-STAT signaling in human glioma cells. *Cancer Cell Int.* 21 (1), 645. doi:10.1186/s12935-021-02304-0

frontiers | Frontiers in Cardiovascular Medicine

TYPE Case Report
PUBLISHED 01 December 2023
DOI 10.3389/fcvm.2023.1294197

OPEN ACCESS

EDITED BY
Lingshan Gou,
Xuzhou Medical University, China

REVIEWED BY
Emanuele Micaglio,
IRCCS San Donato Polyclinic, Italy
Matteo Elia Mangoni,
Centre National de la Recherche Scientifique (CNRS), France

*CORRESPONDENCE
Suxin Luo
✉ luosuxin_0204@163.com
Bi Huang
✉ huangbi120@163.com

RECEIVED 14 September 2023
ACCEPTED 17 November 2023
PUBLISHED 01 December 2023

CITATION
Liang J, Luo S and Huang B (2023) Case Report: *SCN5A* mutations in three young patients with sick sinus syndrome.
Front. Cardiovasc. Med. 10:1294197.
doi: 10.3389/fcvm.2023.1294197

Case Report: *SCN5A* mutations in three young patients with sick sinus syndrome

Jiayu Liang, Suxin Luo* and Bi Huang*

Department of Cardiology, The First Affiliated Hospital of Chongqing Medical University, Chongqing, China

Background: Sick Sinus Syndrome (SSS) is generally regarded as a degenerative disease with aging; however, genetic mutations have been confirmed to be associated with SSS. Among them, mutations in *SCN5A* are common in patients with SSS. We report three young SSS patients with *SCN5A* mutations at different sites that have not been previously reported in Asian patients.
Case presentation: The three patients were all young females who presented with symptoms of severe bradycardia and paroxysmal atrial flutter, for which two patients received ablation therapy. However, after ablation, Holter monitoring indicated a significant long cardiac arrest; therefore, the patients received pacemaker implantation. The three patients had familial SSS, and genetic testing was performed. Mutations were found in *SCN5A* at different sites in the three families. All three patients received pacemaker implantation, resulting in the symptoms of severe bradycardia disappearing.
Conclusion: *SCN5A* heterozygous mutations are common among patients clinically affected by SSS. Their causative role is confirmed by our data and by the co-occurrence of genetic arrhythmias among our patients. Genetic testing for SSS cannot be performed as a single gene panel because of feasible literature results, but in presence of familial and personal history of SSS in association with arrhythmias can provide clinically useful information.

KEYWORDS
sick sinus syndrome, gene mutation, *SCN5A* gene, gene testing, pacemaker implantation

Introduction

Sick Sinus Syndrome (SSS) is caused by impaired electrical automaticity of the sinus node or impaired conduction of electrical impulses generated by the sinus node to the surrounding atrial muscles, leading to sinus bradycardia, sinus block, or sinus arrest on the electrocardiogram (ECG) (1). Although SSS is usually regarded as a degenerative disease with aging, gene mutations have been confirmed to be associated with SSS in previous studies (2). Such genetic mutations include genes involved in sodium channels (3) and potassium channels (4), as well as *ANK2* (5), *HCN4* (6), and myosin heavy chain genes and their regulator genes (7), among which *SCN5A* (a sodium channel gene) is a common cause of familial SSS. Although SSS is prevalent in the elderly, patients with hereditary SSS can present with symptoms at a young age.

We report the cases of three unrelated young patients with familial SSS with missense mutations in *SCN5A*.

Case presentation

Case 1

A 19-year-old Chinese woman was admitted to hospital due to left limb weakness. She has no history of cardiovascular disease but has occasional episodes of dizziness for 3 months. Her mother was diagnosed with SSS and received pacemaker implantation in her 30's. After admission, neurological examinations showed acute cerebral infarction in the right centrum semiovale and basal ganglia. At admission, ECG was obtained and it showed atrial flutter with 2:1 conduction (**Figure 1A**). The patient did not receive any pharmacological control for atrial flutter. One day later, the atrial flutter terminated spontaneously and it showed no obvious P wave and significant bradycardia with junctional rhythm (**Figure 1B**). A subsequent Holter examination indicated paroxysmal atrial fibrillation accompanied by a severe sinus arrest with a minimum ventricular rate of 21 beats per minute and the maximum R–R interval of 7.96 s (**Figure 1C**). Echocardiography revealed no structural and functional changes. In addition, cardiac magnetic resonance imaging did not display obvious fibrosis and other biochemical tests were all normal. Taken together, this young patient was diagnosed with SSS; her stroke was thought to be related to the atrial standstill and thrombosis. Subsequently, genetic testing (whole exome sequencing, Illumina NovaSeq 6,000, Illumina, US) indicated a heterozygous mutation from cytosine C to guanine G (C.664C > G) at nucleotide 664 of *SCN5A*, causing amino acid no. 222 to change from arginine to glycine (p.R222G) (**Figure 1D**). This mutation is consistent with her mother's genetic test results. Therefore, familial SSS was finally diagnosed, and this young patient received dual-chamber pacemaker implantation and prophylactic anticoagulation with edoxaban for stroke treatment. After pacemaker implantation, the sinus rate was around 55 beats per minute with 2.5% of atrial pacing by Holter monitoring. During a follow-up of 2 years, the patient had no symptoms of bradycardia and did not undergo stroke or other systemic embolisms.

Case 2

A woman aged 33 years was admitted to hospital due to paroxysmal palpitation lasting 5 years. She denied a history of cardiovascular disease and the physical examination was

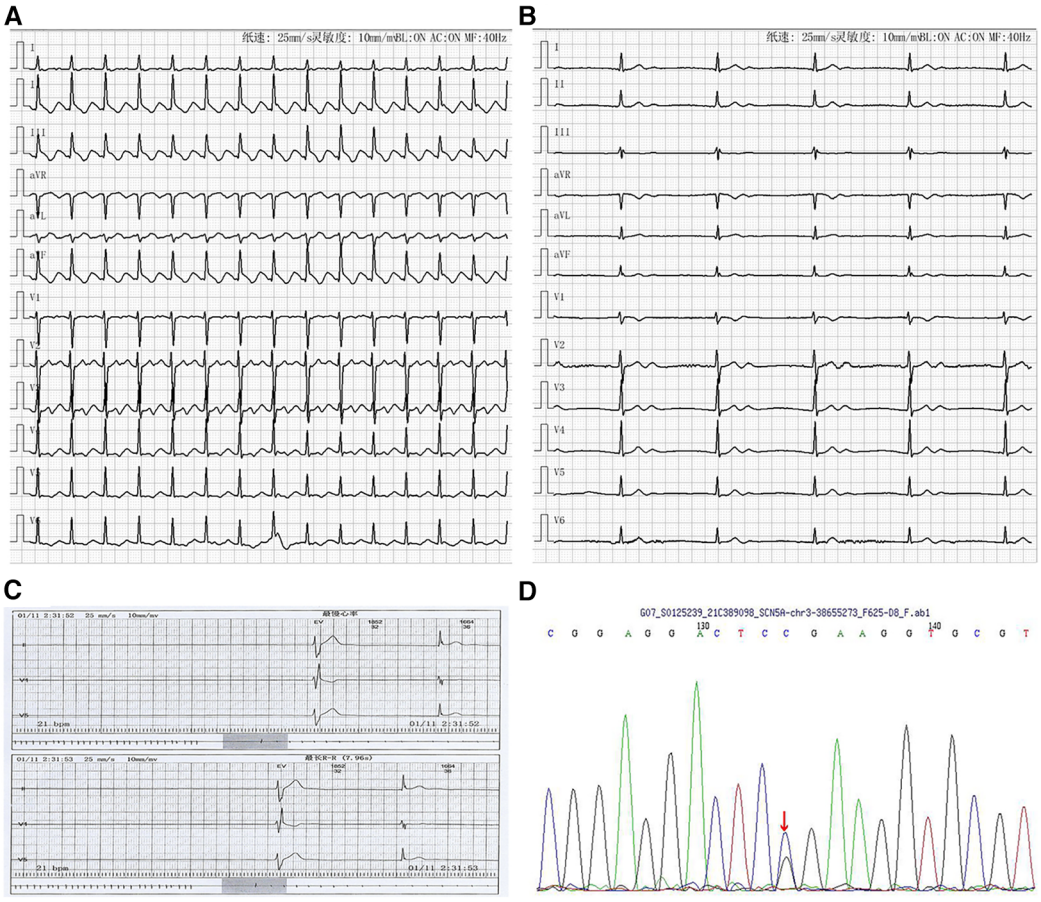

FIGURE 1
Arrhythmia in case 1. (**A**) Atrial flutter with 2:1 conduction; (**B**) Junctional escape rhythm with atrial standstill; (**C**) Holter indicated maximum R-R interval of 7.96 s; (**D**) Gene testing revealed SGN5A gene mutation (C.664C > G).

unremarkable. Her mother received pacemaker implantation in her 30's due to SSS. ECG upon admission showed atrial flutter (Figure 2A). Echocardiography and blood testing were normal. The patient was diagnosed lone atrial flutter and received radiofrequency ablation. However, after the procedure, Holter examination revealed that the minimum ventricular rate was 15 beats per minute and the maximum R–R interval was 6.73 s (Figure 2B). The severe bradyarrhythmia was sinus arrest and origined from atrial site or atrioventricular node. Therefore, SSS was diagnosed. Genetic testing (whole exome sequencing, Illumina NovaSeq 6,000, Illumina, US) revealed a heterozygous mutation in *SCN5A* located at nucleotide 3,823 from guanine G to adenine A (c.3823G > A), resulting in amino acid no. 1,275 changing from aspartic acid to asparagine (D1275N) (Figure 2C), consistent with her mother's genetic test results. The patient received dual-chamber pacemaker implantation and the sinus rate was around 60 beats per minute with 7.8% atrial pacing by Holter monitoring. Following pacemaker implantation, this patient no longer experienced palpitation.

Case 3

A woman in her 30s presented with recurrent dizziness and palpitation. She reported that she had experienced atrial flutter (Figure 3A) for 5 years without symptoms. Recently, she felt episodes of dizziness and palpitation and was admitted to hospital. Her mother also had atrial flutter in her 30's and received radiofrequency ablation; however, after the procedure, she presented with severe bradycardia and received pacemaker implantation. Due to the obvious symptom of atrial flutter, she requested radiofrequency ablation. However, severe bradycardia occurred after the procedure with a minimum ventricular rate of 32 beats per minute and a maximum R-R interval of 4.11 s by Holter monitoring (Figure 3B). She was also diagnosed with SSS and was recommended to receive pacemaker implantation; however, the patient refused. Genetic testing (whole exome sequencing, Illumina NovaSeq 6,000, Illumina, US) also demonstrated that she and her mother had the same heterozygous mutation in *SCN5A* located at position 4,895 from guanine G to adenine A (c.4895G > A), causing amino acid no.1,632 to be altered from arginine to histidine (p.R1632H) (Figure 3C). During the follow-up period, the patient was found to suffer from breast cancer and the maximum R-R interval by Holter monitoring was extended to 5.01 s. Finally, she received leadless pacemaker implantation and the sinus rate was around 50 beats per minute with 2.5% atrial pacing by Holter monitoring. During follow up, no symptoms of bradycardia occurred again.

The timelines of the diagnosis and treatment in the three patients are shown in Figure 4. In Case 1 and Case 2, after diagnosed with SSS, they received pacemaker implantation immediately. In Case 3, the patient refused to receive

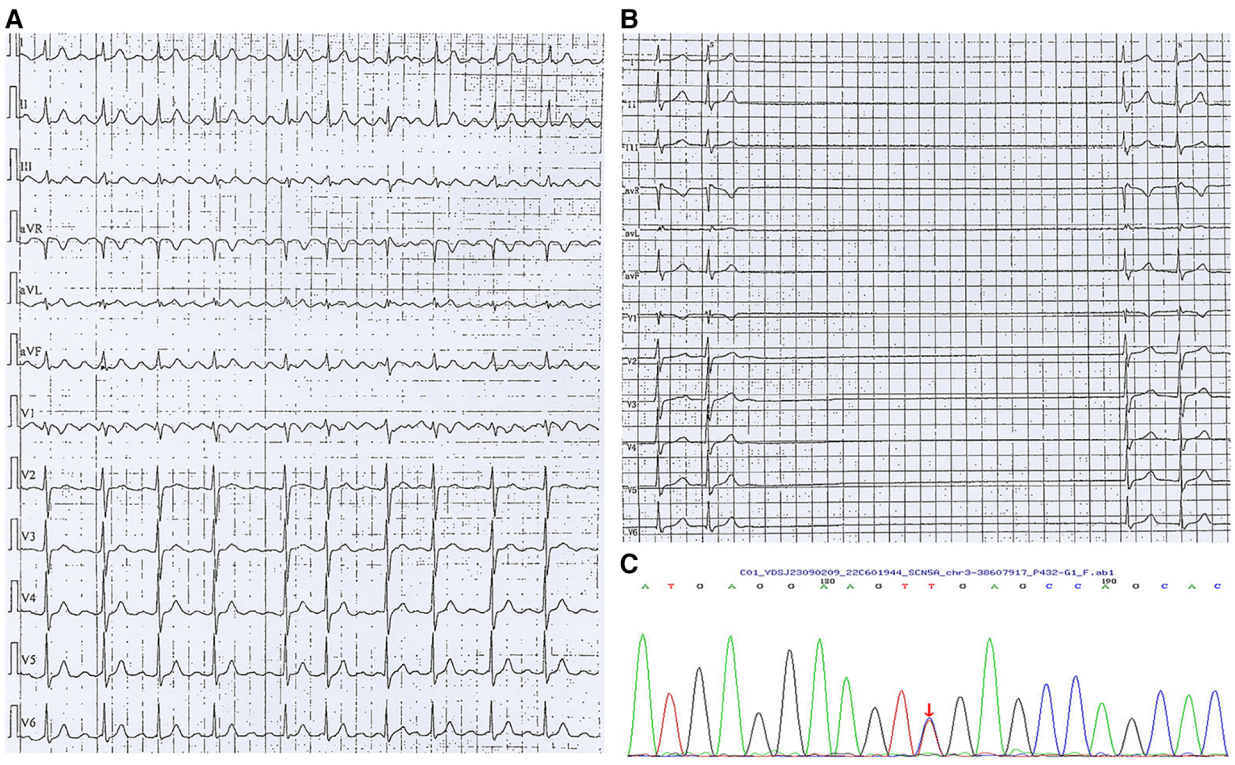

FIGURE 2
Arrhythmia in case 2. (**A**) Atrial flutter with 2:1 conduction; (**B**) Holter indicated maximum R-R interval of 6.73 s; (**C**) Gene testing revealed SGN5A gene mutation (c.3823G > A).

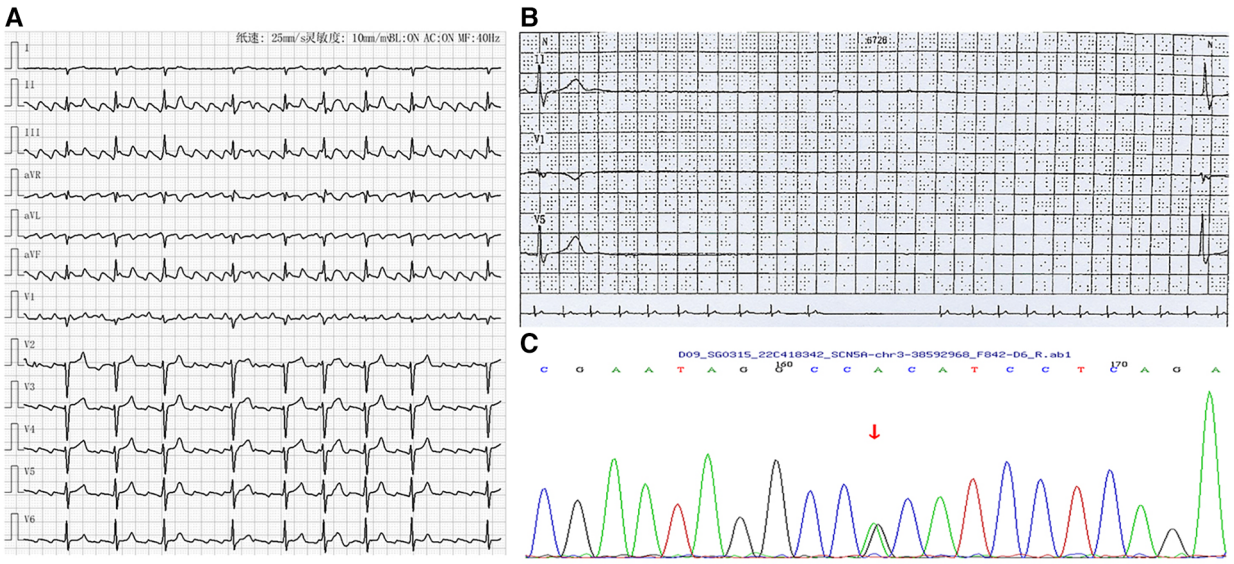

FIGURE 3
Arrhythmia in case 3. (A) Atrial flutter with 2-4:1 conduction; (B) Holter indicated maximum R-R interval of 4.11 s; (C) Gene testing revealed SGN5A gene mutation (c.4895G > A).

pacemaker implantation when she was diagnosed with SSS; however, the symptoms worsened during follow up and finally she received pacemaker implantation. None of the three patients received any antiarrhythmic drug and neither underwent symptoms of bradycardia after pacemaker implantation.

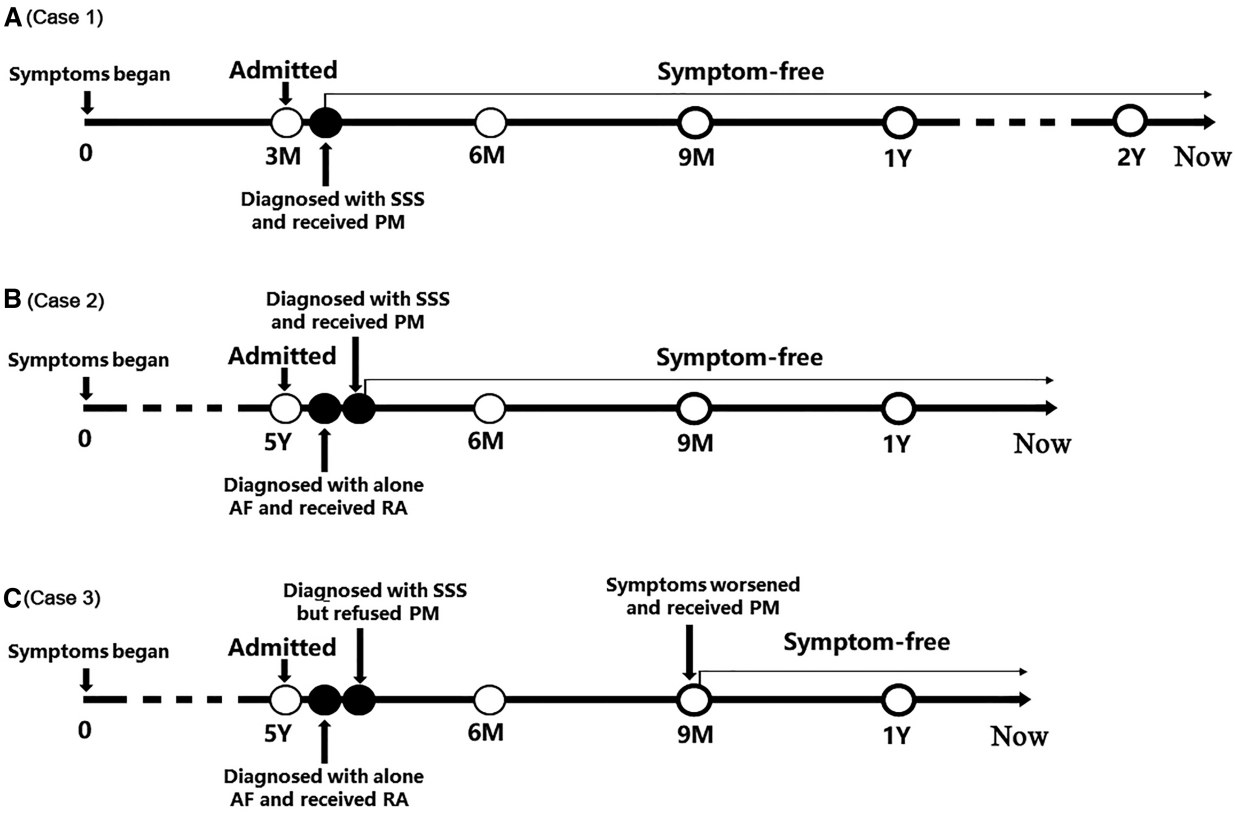

FIGURE 4
The timelines of the diagnosis and treatment in the three patients. (A) Timeline of case 1; (B) Timeline of case 2; (C) Timeline of case 3. AF, atrial flutter; PM, pacemaker; RA, radiofrequency ablation; SSS, sick sinus syndrome.

Discussion

In the present study, we report three unrelated young patients suffering from SSS, all of whom had a mutation in *SCN5A* at different sites. All patients received pacemaker implantation and no symptoms occurred again. Although SSS often develops in the elderly, it has been reported to occur at any age, including childhood. Therefore, SSS should be considered to be congenital due to the presence of gene mutations.

SCN5A is located in the first band of region 2 on the short arm of chromosome 3 (3p21) and encodes sodium channels in the cardiomyocytes, which plays a critical role in the excitation process underlying cardiac contraction (8). Previous studies have shown that mutations in *SCN5A* are related to a variety of hereditary arrhythmias, such as Brugada syndrome, long QT syndrome, familial progressive cardiac conduction disease (Lenegre disease), familial atrial fibrillation, and familial atrial standstill, etc. (9–13), among which Brugada syndrome is one of the most common phenotypes associated with single-copy *SCN5A* mutation (14–16). In fact, *SCN5A* mutation was the first genetic variant shown to be associated with Brugada syndrome (17) and has been shown to be responsible for 20%–25% of the disease in Caucasian populations (18). Mechanically, *SCN5A* mutations are associated with Nav1.5 loss-of-function either by decreased expression of Nav1.5 in the sarcolemma, expression of nonfunctional channels, or altered gating properties, resulting loss of action potential dome and consequently phase-2 re-entry upon arrival of a subendocardial action potential wavefront (19). Arrhythmias caused by *SCN5A* mutations can be divided into two categories according to the changes in sodium channel function; first is functionally enhanced mutations, such as long QT syndrome type 3, and the second is reduced function mutations, including Brugada syndrome, heart conduction system diseases, and SSS (20). Several reports have revealed the *SCN5A* mutant sites from the myocardium in humans (10, 21, 22); however, there appears to be no simple correspondence between mutated genes and phenotypes. One the one hand, patients who have the same mutation sites do not definitely present with the same clinical phenotypes; and on the other hand, mutations at the different sites may present the same arrhythmia. Therefore, there is a complex relationship between *SCN5A* mutations and the clinical phenotype.

Arrhythmias associated with *SCN5A* mutations have been previously reported to involve multiple mutant sites. The mutant sites in the three patients in the present study have also been reported previously. The first patient presented with C.664C > G (R222G) in *SCN5A* gene. Mutation in this site was reported to mainly relate with Purkinje ventricular arrhythmia and bigeminal arrhythmia possibly due to the missense amino acid substitution located in the S4 voltage sensor in domain I (23). However, Lehmann et al. (21) also reported a German family who suffered from atrial standstill and were found to have this site mutation in *SCN5A*. Further studies demonstrated that *SCN5A* mutation at this site reduced the current density with alteration of biophysical tissue properties, leading to SSS in an animal model (24). Although most studies reported this site mutation related with ventricular arrhythmia, bradyarrhythmia such as the atrial standstill is also a clinical phenotype, indicating a complex relationship between genotype and phenotype. Moreover, the patient's mother also diagnosed with SSS and received pacemaker implantation, and also had the same mutation site in *SCN5A* as in her daughter; however, the ECG of the patient's mother is unavailable and whether the clinical phenotypes were consistent between the patient and her mother deserves further study.

A previous study has shown that the mutation *SCN5A* (D1275N) is pathological (25); it was first reported by Groenewegen et al. (26) who found that co-inheritance of the mutation in *SCN5A* (D1275N) led to atrial standstill in a Dutch family, and it was associated with a range of cardiac diseases including dilated cardiomyopathy, sinus node dysfunction, atrial and ventricular tachyarrhythmias, conduction disease, etc. Subsequently the clinical phenotype associated with this mutation was extensively confirmed (22, 27–30). However, the clinical phenotype varies significantly, even if the mutation occurs at the same site, ranging from atrial to ventricular arrhythmia, from bradycardia to tachycardia, and from presenting in childhood to older age. Therefore, the mechanisms associated with the different clinical phenotypes are quite different. C.3823G > A makes negative charge of aspartic acid replaced by the neutral electric behavior of asparagine and therefore alters the electric properties of Nav1.5 (29). Furthermore, the clinical phenotypes are not completely isolated and have some overlap among the different clinical profiles. For example, case 2 in our study presented with familial atrial flutter and sinus pause, indicating the complexity in the pathogenesis of *SCN5A* (D1275N).

The *SCN5A* (R1632H) variant was reported in 2003; scholars from the United States recruited ten pediatric patients with an explicit diagnosis of congenital SSS from seven families. Probands of these patients exhibited six mutations in *SCN5A* identified by polymerase chain reaction, including the R1632H mutant (10). The *SCN5A* (R1632H) mutation was also found in the family of a 14-year-old girl, who described fast palpitations during exercise lasting a couple of minutes resulting in pre-syncope, heavy transpiration and retrosternal pain. After a series of examinations, she was diagnosed with atrial flutter and then received ablation (31). Studies have shown R1632H is related with various arrhythmias, including bradyarrhythmia, such as SSS, atrioventricular block, and tachyarrhythmia, such as Brugada syndrome. The clinical phenotype the present case 3 is similar to that reported in previous studies. Case 3 also received ablation, but presented with severe bradycardia after ablation, indicating that bradycardia–tachycardia syndrome is a common phenomenon in patients with *SCN5A* mutation. It also suggested that ablation should be carefully administered in young patients with bradycardia–tachycardia syndrome.

Notably, in addition to *SCN5A*, some genetic mutations such as in *MYH6* (32), *HCN4* (6), *PITX2*, *ZFHX3*, *TTN/CCDC141*, *SCN10A* and *KRT8* have been reported to associated with SSS (33); however, these genes above mentioned are included in the panel used in our present sequencing and did not detect any mutation, suggesting the mutation of *SCN5A* gene is responsible for the clinical phenotype in the three patients.

Our present study has some clinical implications. First, previous studies have shown familial SSS with *SCN5A* mutation has strong male predominance (34); however, in our present study, all three familial SSS patients were female, suggesting that both males and females are susceptible to *SCN5A* mutation. Second, although the three mutations have been reported previously, there is lack of Asian patients reported to suffer from these mutations. Our present study extends previous findings, indicating the clinical phenotypes associated with *SCN5A* mutation are similar among different races. Third, the frequency of these mutations in *SCN5A* such as C.3823G > A is unknown among population of Asian descent (35) and our present study provided some potential available data. In addition, although SSS is regarded as a degenerative disease and usually occurs in the elderly, taking our findings and previous studies together, patients with SSS associated with *SCN5A* mutation tend to have an earlier age of onset. When young patients present with SSS, there is a definite family history; thus, familial SSS should be considered and genetic testing is warranted.

There are some limitations in our present study. First, intracardiac maps during radiofrequency ablation could provide important information regarding the origin of atrial flutter and sinus rhythm as well as the electrophysiological characteristics of the conduction system. However, the intracardiac maps were unavailable in our present study. Second, some simple methods, such as current cardioversion can be used to evaluate the sinus function in patients with paroxysmal atrial arrhythmia. A severe bradyarrhythmia after cardioversion is an indication of sinus dysfunction and further radiofrequency ablation for such patients should be cautious. In our present study, none of the three patients undergo current cardioversion. However, if the patients received current cardioversion, it would probably present severe bradyarrhythmia due to the sinus node dysfunction and overdrive suppression by atrial flutter which was demonstrated in case 1. Third, the severe sinus node dysfunction in the three patients may be related with multigene variation in addition to *SCN5A* mutation, such as HCN and/or calcium channels. Silent variant in one of these channels combined with *SCN5A* mutation together could cause the severe sinus node dysfunction because previous studies have shown silent variation was involved in the pathogenicity of arrhythmia such as in long Q-T syndrome (36). Although we used whole exome sequencing to identify the potential gene variations and did not find mutated sites in HCN or calcium channels, the whole exome sequencing also has some limitations such as only identifying the common variations and may omit some rare or novel variations. Therefore, whole genome sequencing may provide more variation information and more studies are warranted. Last but not least, we only provided the clinical presentation and the genetic results, but did not provide evidence of mechanisms associated the mutation of *SCN5A* gene in our cases and the precise mechanisms needed to be clarified.

Conclusion

SCN5A heterozygous mutations are common among patients clinically affected by SSS. Their causative role is confirmed by our data and by the co-occurrence of genetic arrhythmias among our patients. Genetic testing for SSS cannot be performed as a single gene panel because of feasible literature results, but in presence of familial and personal history of SSS in association with arrhythmias can provide clinically useful information.

Data availability statement

The original contributions presented in the study are included in the article/Supplementary Material, further inquiries can be directed to the corresponding authors.

Ethics statement

The studies involving humans were approved by The Ethics Committee of The First Affiliated Hospital of Chongqing medical university. The studies were conducted in accordance with the local legislation and institutional requirements. The participants provided their written informed consent to participate in this study. Written informed consent was obtained from the individual(s) for the publication of any potentially identifiable images or data included in this article.

Author contributions

JL: Data curation, Writing – original draft. SL: Conceptualization, Supervision, Writing – review & editing. BH: Writing – review & editing.

Funding

The author(s) declare financial support was received for the research, authorship, and/or publication of this article.

This research was supported by Project of Chongqing Talent Plan (cstc2022ycjh-bgzxm0231) and CQMU Program for Youth Innovation in Future Medicine (0184).

Acknowledgments

We would like to thank all of the patients for their participation in this study.

Conflict of interest

The authors declare that the research was conducted in the absence of any commercial or financial relationships that could be construed as a potential conflict of interest.

Publisher's note

References

1. De Ponti R, Marazzato J, Bagliani G, Leonelli FM, Padeletti L. Sick sinus syndrome. *Card Electrophysiol Clin*. (2018) 10:183–95. doi: 10.1016/j.ccep.2018.02.002

2. Manoj P, Kim JA, Kim S, Li T, Sewani M, Chelu MG, et al. Sinus node dysfunction: current understanding and future directions. *Am J Physiol Heart Circ Physiol*. (2023) 324:H259–78. doi: 10.1152/ajpheart.00618.2022

3. Ruan Y, Liu N, Priori SG. Sodium channel mutations and arrhythmias. *Nat Rev Cardiol*. (2009) 6:337–48. doi: 10.1038/nrcardio.2009.44

4. Sun C, Li N, Wang QQ, Yan LY, Ba SK, Zhang SS, et al. Whole genome sequencing identifies a deletion mutation in the unknown-functional KCNG2 from familial sick sinus syndrome. *Physiol Genomics*. (2022) 54:141–52. doi: 10.1152/physiolgenomics.00132.2021

5. Robaei D, Ford T, Ooi SY. Ankyrin-b syndrome: a case of sinus node dysfunction, atrial fibrillation and prolonged QT in a young adult. *Heart Lung Circ*. (2015) 24:e31–4. doi: 10.1016/j.hlc.2014.09.013

6. Milanesi R, Baruscotti M, Gnecchi-Ruscone T, DiFrancesco D. Familial sinus bradycardia associated with a mutation in the cardiac pacemaker channel. *N Engl J Med*. (2006) 354:151–7. doi: 10.1056/NEJMoa052475

7. Ishikawa T, Jou CJ, Nogami A, Kowase S, Arrington CB, Barnett SM, et al. Novel mutation in the alpha-myosin heavy chain gene is associated with sick sinus syndrome. *Circ Arrhythm Electrophysiol*. (2015) 8:400–8. doi: 10.1161/CIRCEP.114.002534

8. George AJ, Varkony TA, Drabkin HA, Han J, Knops JF, Finley WH, et al. Assignment of the human heart tetrodotoxin-resistant voltage-gated na+ channel alpha-subunit gene (SCN5A) to band 3p21. *Cytogenet Cell Genet*. (1995) 68:67–70. doi: 10.1159/000133892

9. Wilde A, Amin AS. Clinical spectrum of SCN5A mutations: long qt syndrome, brugada syndrome, and cardiomyopathy. *JACC Clin Electrophysiol*. (2018) 4:569–79. doi: 10.1016/j.jacep.2018.03.006

10. Benson DW, Wang DW, Dyment M, Knilans TK, Fish FA, Strieper MJ, et al. Congenital sick sinus syndrome caused by recessive mutations in the cardiac sodium channel gene (SCN5A). *J Clin Invest*. (2003) 112:1019–28. doi: 10.1172/JCI18062

11. Bezzina CR, Rook MB, Groenewegen WA, Herfst LJ, van der Wal AC, Lam J, et al. Compound heterozygosity for mutations (w156x and r225w) in SCN5A associated with severe cardiac conduction disturbances and degenerative changes in the conduction system. *Circ Res*. (2003) 92:159–68. doi: 10.1161/01.res.0000052672.97759.36

12. Makiyama T, Akao M, Shizuta S, Doi T, Nishiyama K, Oka Y, et al. A novel SCN5A gain-of-function mutation M1875T associated with familial atrial fibrillation. *J Am Coll Cardiol*. (2008) 52:1326–34. doi: 10.1016/j.jacc.2008.07.013

13. Makita N, Sasaki K, Groenewegen WA, Yokota T, Yokoshiki H, Murakami T, et al. Congenital atrial standstill associated with coinheritance of a novel SCN5A mutation and connexin 40 polymorphisms. *Heart Rhythm*. (2005) 2:1128–34. doi: 10.1016/j.hrthm.2005.06.032

14. Pearman CM, Denham NC, Mills RW, Ding WY, Modi SS, Hall M, et al. Relationship between sodium channel function and clinical phenotype in SCN5A variants associated with brugada syndrome. *Hum Mutat*. (2020) 41:2195–204. doi: 10.1002/humu.24128

15. Hoshi M, Du XX, Shinlapawittayatorn K, Liu H, Chai S, Wan X, et al. Brugada syndrome disease phenotype explained in apparently benign sodium channel mutations. *Circ Cardiovasc Genet*. (2014) 7:123–31. doi: 10.1161/CIRCGENETICS.113.000292

16. Kapplinger JD, Tester DJ, Alders M, Benito B, Berthet M, Brugada J, et al. An international compendium of mutations in the SCN5A-encoded cardiac sodium channel in patients referred for brugada syndrome genetic testing. *Heart Rhythm*. (2010) 7:33–46. doi: 10.1016/j.hrthm.2009.09.069

17. Chen Q, Kirsch GE, Zhang D, Brugada R, Brugada J, Brugada P, et al. Genetic basis and molecular mechanism for idiopathic ventricular fibrillation. *Nature*. (1998) 392:293–6. doi: 10.1038/32675

18. Alings M, Wilde A. "Brugada" syndrome: clinical data and suggested pathophysiological mechanism. *Circulation*. (1999) 99:666–73. doi: 10.1161/01.cir.99.5.666

19. Blok M, Boukens BJ. Mechanisms of arrhythmias in the brugada syndrome. *Int J Mol Sci*. (2020) 21:7051. doi: 10.3390/ijms21197051

20. Li W, Yin L, Shen C, Hu K, Ge J, Sun A. SCN5A variants: association with cardiac disorders. *Front Physiol*. (2018) 9:1372. doi: 10.3389/fphys.2018.01372

21. Lehmann HI, Meltendorf U, Klein HU. Long-term follow-up of permanent atrial standstill in a German family with mutation in the SCN5A gene. *Heart Rhythm Case Rep*. (2018) 4:356–8. doi: 10.1016/j.hrcr.2018.04.015

22. McNair WP, Ku L, Taylor MR, Fain PR, Dao D, Wolfel E, et al. SCN5A mutation associated with dilated cardiomyopathy, conduction disorder, and arrhythmia. *Circulation*. (2004) 110:2163–7. doi: 10.1161/01.CIR.0000144458.58660.BB

23. Nair K, Pekhletski R, Harris L, Care M, Morel C, Farid T, et al. Escape capture bigeminy: phenotypic marker of cardiac sodium channel voltage sensor mutation R222Q. *Heart Rhythm*. (2012) 9:1681–8. doi: 10.1016/j.hrthm.2012.06.029

24. Butters TD, Aslanidi OV, Inada S, Boyett MR, Hancox JC, Lei M, et al. Mechanistic links between na+ channel (SCN5A) mutations and impaired cardiac pacemaking in sick sinus syndrome. *Circ Res*. (2010) 107:126–37. doi: 10.1161/CIRCRESAHA.110.219949

25. Watanabe H, Yang T, Stroud DM, Lowe JS, Harris L, Atack TC, et al. Striking in vivo phenotype of a disease-associated human SCN5A mutation producing minimal changes in vitro. *Circulation*. (2011) 124:1001–11. doi: 10.1161/CIRCULATIONAHA.110.987248

26. Groenewegen WA, Firouzi M, Bezzina CR, Vliex S, van Langen IM, Sandkuijl L, et al. A cardiac sodium channel mutation cosegregates with a rare connexin40 genotype in familial atrial standstill. *Circ Res*. (2003) 92:14–22. doi: 10.1161/01.res.0000050585.07097.d7

27. Olson TM, Michels VV, Ballew JD, Reyna SP, Karst ML, Herron KJ, et al. Sodium channel mutations and susceptibility to heart failure and atrial fibrillation. *JAMA*. (2005) 293:447–54. doi: 10.1001/jama.293.4.447

28. Laitinen-Forsblom PJ, Makynen P, Makynen H, Yli-Mayry S, Virtanen V, Kontula K, et al. SCN5A mutation associated with cardiac conduction defect and atrial arrhythmias. *J Cardiovasc Electrophysiol*. (2006) 17:480–5. doi: 10.1111/j.1540-8167.2006.00411.x

29. Moreau A, Janin A, Millat G, Chevalier P. Cardiac voltage-gated sodium channel mutations associated with left atrial dysfunction and stroke in children. *Europace*. (2018) 20:1692–8. doi: 10.1093/europace/euy041

30. Lei M, Zhang H, Grace AA, Huang CL. SCN5A and sinoatrial node pacemaker function. *Cardiovasc Res*. (2007) 74:356–65. doi: 10.1016/j.cardiores.2007.01.009

31. Robyns T, Nuyens D, Van Casteren L, Corveleyn A, De Ravel T, Heidbuchel H, et al. Reduced penetrance and variable expression of SCN5A mutations and the importance of co-inherited genetic variants: case report and review of the literature. *Indian Pacing Electrophysiol J*. (2014) 14:133–49. doi: 10.1016/s0972-6292(16)30754-9

32. Holm H, Gudbjartsson DF, Sulem P, Masson G, Helgadottir HT, Zanon C, et al. A rare variant in MYH6 is associated with high risk of sick sinus syndrome. *Nat Genet*. (2011) 43:316–20. doi: 10.1038/ng.781

33. Thorolfsdottir RB, Sveinbjornsson G, Aegisdottir HM, Benonisdottir S, Stefansdottir L, Ivarsdottir EV, et al. Genetic insight into sick sinus syndrome. *Eur Heart J*. (2021) 42:1959–71. doi: 10.1093/eurheartj/ehaa1108

34. Abe K, Machida T, Sumitomo N, Yamamoto H, Ohkubo K, Watanabe I, et al. Sodium channelopathy underlying familial sick sinus syndrome with early onset and predominantly male characteristics. *Circ Arrhythm Electrophysiol*. (2014) 7:511–7. doi: 10.1161/CIRCEP.113.001340

35. Available at: https://varsome.com/variant/hg38/SCN5A(NM_198056.3)%3Ac.3823G%3EA?annotation-mode=germline

36. O'Hara T, Rudy Y. Arrhythmia formation in subclinical ("silent") long QT syndrome requires multiple insults: quantitative mechanistic study using the KCNQ1 mutation Q357R as example. *Heart Rhythm*. (2012) 9:275–82. doi: 10.1016/j.hrthm.2011.09.066

frontiers | Frontiers in Genetics

TYPE Original Research
PUBLISHED 07 December 2023
DOI 10.3389/fgene.2023.1293393

OPEN ACCESS

EDITED BY
Peng Zhang,
Institute of ENT and Shenzhen Key Laboratory of ENT, China

REVIEWED BY
Xiaodong Zhang,
Affiliated Hospital of Jiangnan University, China
Jian Xu,
Shenzhen Longgang Institute of Stomatology, China
Guosheng Wu,
Jiangnan University, China

*CORRESPONDENCE
Zheng Zhang,
zhangzhengccu@yeah.net

†These authors have contributed equally to this work and share first authorship

RECEIVED 13 September 2023
ACCEPTED 15 November 2023
PUBLISHED 07 December 2023

CITATION
Tang Y, Wang Y, Wang S, Wang R, Xu J, Peng Y, Ding L, Zhao J, Zhou G, Sun S and Zhang Z (2023), Methylation and transcriptomic expression profiles of HUVEC in the oxygen and glucose deprivation model and its clinical implications in AMI patients.
Front. Genet. 14:1293393.
doi: 10.3389/fgene.2023.1293393

Methylation and transcriptomic expression profiles of HUVEC in the oxygen and glucose deprivation model and its clinical implications in AMI patients

Yuning Tang[1,2,3,4†], Yongxiang Wang[2,4,5†], Shengxiang Wang[6†], Runqing Wang[1,2,4], Jin Xu[1,2,4], Yu Peng[2,4,5], Liqiong Ding[2,4,5], Jing Zhao[1,2,4,5], Gang Zhou[1], Shougang Sun[3] and Zheng Zhang[1,2,4,5*]

[1]The First School of Clinical Medicine, Lanzhou University, Lanzhou, China, [2]Gansu Key Laboratory of Cardiovascular Diseases, The First Hospital of Lanzhou University, Lanzhou, China, [3]Department of Cardiology, Lanzhou University Second Hospital, Lanzhou, China, [4]Cardiovascular Clinical Research Center of Gansu Province, Lanzhou, China, [5]Heart Center, The First Hospital of Lanzhou University, Lanzhou, China, [6]School of Life and Environmental Sciences, Minzu University of China, Beijing, China

The obstructed coronary artery undergoes a series of pathological changes due to ischemic-hypoxic shocks during acute myocardial infarction (AMI). However, the altered DNA methylation levels in endothelial cells under these conditions and their implication for the etiopathology of AMI have not been investigated in detail. This study aimed to explore the relationship between DNA methylation and pathologically altered gene expression profile in human umbilical vein endothelial cells (HUVECs) subjected to oxygen-glucose deprivation (OGD), and its clinical implications in AMI patients. The Illumina Infinium MethylationEPIC BeadChip assay was used to explore the genome-wide DNA methylation profile using the Novaseq6000 platform for mRNA sequencing in 3 pairs of HUVEC-OGD and control samples. GO and KEGG pathway enrichment analyses, as well as correlation, causal inference test (CIT), and protein-protein interaction (PPI) analyses identified 22 hub genes that were validated by MethylTarget sequencing as well as qRT-PCR. ELISA was used to detect four target molecules associated with the progression of AMI. A total of 2,524 differentially expressed genes (DEGs) and 22,148 differentially methylated positions (DMPs) corresponding to 6,642 differentially methylated genes (DMGs) were screened ($|\Delta\beta|>0.1$ and detection $p < 0.05$). After GO, KEGG, correlation, CIT, and PPI analyses, 441 genes were filtered. qRT-PCR confirmed the overexpression of VEGFA, CCL2, TSP-1, SQSTM1, BCL2L11, and TIMP3 genes, and downregulation of MYC, CD44, BDNF, GNAQ, RUNX1, ETS1, NGFR, MME, SEMA6A, GNAI1, IFIT1, and MEIS1. DNA fragments BDNF_1_ ($r = 0.931$, $p < 0.0001$) and SQSTM1_2_NEW

Abbreviations: GO, gene ontology; KEGG, Kyoto Encyclopedia of Genes and Genomes; DO, disease ontology; MSP, methylation-specific polymerase chain reaction; TSS, transcription start site; UTR, untranslated region; AMI, acute myocardial infarction; HUVECs, human umbilical vein endothelial cells; OGD, Oxygen-Glucose Deprivation; DEGs, differentially expressed gens; DMPs, differentially methylated positions; DMGs, differentially methylated genes; DMRs, differentially methylated regions; CpG, 5′-C-phosphate-G-3′; CIT, Causal Inference Test; PPI, protein-protein interaction network; BDNF, Brain-derived neurotrophic factor; TNFSF10, Tumor necrosis factor superfamily member 10.

(r = 0.758, p = 0.0043) were positively correlated with the expressions of corresponding genes, and MYC_1_ (r = −0.8245, p = 0.001) was negatively correlated. Furthermore, ELISA confirmed TNFSF10 and BDNF were elevated in the peripheral blood of AMI patients (p = 0.0284 and p = 0.0142, respectively). Combined sequencing from *in vitro* cellular assays with clinical samples, aiming to establish the potential causal chain of the causal factor (DNA methylation) - mediator (mRNA)—cell outcome (endothelial cell ischemic-hypoxic injury)-clinical outcome (AMI), our study identified promising OGD-specific genes, which provided a solid basis for screening fundamental diagnostic and prognostic biomarkers of coronary endothelial cell injury of AMI. Moreover, it furnished the first evidence that during ischemia and hypoxia, the expression of BNDF was regulated by DNA methylation in endothelial cells and elevated in peripheral blood.

KEYWORDS

DNA methylation, oxygen-glucose deprivation, acute myocardial infarction, mRNA sequence, brain-derived neurotrophic factor, tumor necrosis factor superfamily member 10

1 Introduction

Acute myocardial infarction (AMI) is a common but critical disease with high mortality and morbidity rates. Once the plaque in the coronary artery ruptures and the blood flow is interrupted, it not only leads to injury in cardiomyocytes due to reduced oxygen and glucose supply, but also triggers a series of pathophysiological changes in endothelial cells. Recently, studies have illustrated that endothelial cells release an enormous number of extracellular vesicles following an AMI event, including exosomes and microvesicles, which facilitate myocardial repair and angiogenesis (Loyer et al., 2018; Liu et al., 2020). Moreover, endothelial cells play an essential role in cardiac ischemia/reperfusion (I/R) injury (Cochain et al., 2013) and the revascularization of the surrounding vessels in the infarcted area (Li et al., 2019). Although early reperfusion after AMI could be beneficial to limit the infarct size, delayed diagnosis of patients with massive myocardial injuries often leads to poor outcomes, suggesting that new treatment modalities are urgently required to promote myocardial perfusion, cardiac repair, and regeneration for this subset of high-risk AMI patients. Through revascularization and the promotion of angiogenesis, the apoptosis and necrosis of cardiomyocytes can be effectively reduced, which is the key treatment for myocardial infarction to save cardiomyocytes (Virani et al., 2020). Therefore, clarifying the underlying pathomechanisms of endothelial cell injury during AMI is necessary, as it enables early diagnosis and improved treatments (Wu et al., 2015).

DNA hypermethylation-mediated suppression of gene expression is the primary type of epigenetic regulation in living organisms, including humans. DNA methylation occurs at the C5 position of cytosine by conjugation of methyl groups, most commonly known as 5′-C-phosphate-G-3’ (CpG) dinucleotides (Razin et al., 1984). Hypermethylation of specific promoter regions of acute coronary syndrome (ACS)-associated genes can inhibit their transcriptional activation and alter their biological functions, leading to an increased risk in these patients (Lu et al., 2013). Besides, genome-wide and site-specific DNA methylation alterations have been found in cardiovascular disease (Afzali et al., 2013) and ACS (Li et al., 2010; Kim et al., 2015) patients and disease models. Previous studies suggest that modulation of DNA methylation might be a promising tool for early ACS prediction and diagnosis (Li et al., 2017; Soares et al., 2020; Long et al., 2021; Park et al., 2021; Schiano et al., 2022). However, there are no disease-oriented datasets of systematic analyses of AMI-linked changes in genomic DNA methylation status in endothelial cells. Oxygen-glucose deprivation (OGD)-induced hypoxia and metabolic stress in cultured endothelial cells is used to mimic the conditions experienced by coronary arteries during AMI (Zhang et al., 2021). Hence, in this study, we used the human umbilical vein endothelial cells (HUVEC) stressed with the OGD model to explore the DNA methylation patterns in endothelial cells and delineate their significance in acute ischemic-hypoxic conditions. In addition, we analyzed peripheral blood samples from AMI patients to investigate potential biomarkers released into the circulation during the onset of AMI and to evaluate their clinical significance.

2 Materials and methods

The pramiry materials and methods used in the experiments were listed below, and the flow chart of the whole study was shown in Figure 1.

2.1 Study subjects

The present study recruited 71 AMI patients and 17 age-matched control subjects who were negatively diagnosed with coronary angiography (CAG) from the Heart Center of the First Hospital of Lanzhou University (Lanzhou, China) between June 2021 and January 2022. The patients with non-ST-elevation myocardial infarction (NSTEMI) were those with no characteristic ST-segment elevation on ECG but with chest pain symptoms and elevated levels of myocardial enzymes (TNI>0.023 ng/mL) for more than 4h, as well as confirmed vascular occlusion in the coronary angiography. In contrast the control subjects had no coronary stenosis confirmed by coronary

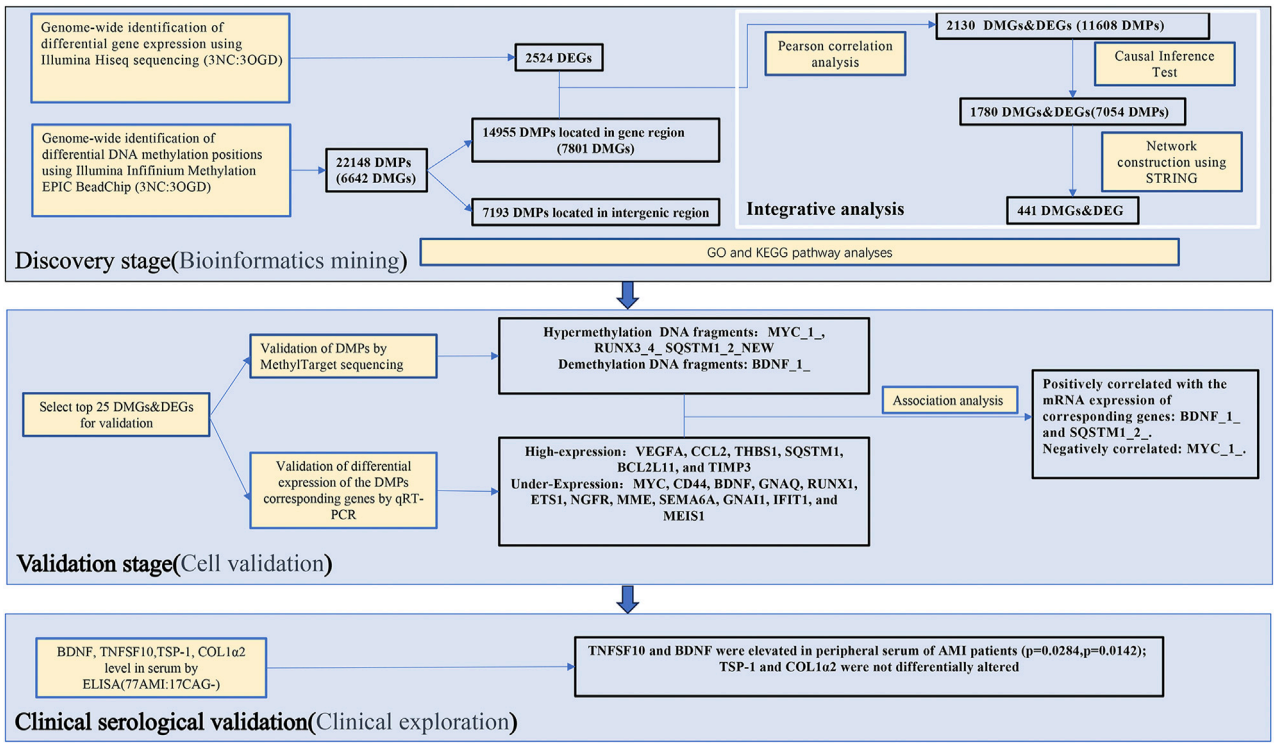

FIGURE 1
A flow chart illustration of the study design and experimental strategies.

angiography and had normal physical examinations and ECG findings. The patients with tumours, severe hepatic or renal abnormalities, severe infections, and any other conditions that the investigators deemed inappropriate for participation were excluded from this study. This study was approved by the Ethics Committee of the First Hospital of Lanzhou University (Approval No. LDYYLL-2023-42).

2.2 Blood sampling

Peripheral venous blood samples from the elbow vein were collected from the patients in EDTA-coated tubes before the coronary angiography. Tubes were turned upside down 8-10 times to mix the blood with EDTA and centrifuged at 3500 rpm for 10 min. The uppermost layer was aspirated as plasma and stored at −80°C for downstream analysis.

2.3 Cell culture and OGD treatments

The HUVEC line was purchased from ATCC (Manassas, VA, United States) and cultured in the endothelial cell medium (ECM, ScienalysisnCell, CA, United States) containing 5% fetal bovine serum, endothelial cell growth supplement, and 1X penicillin/streptomycin solution. Cells were passaged into a 1:3 ratio when the density reached 80%-90%. Cells between the third and eighth passages were taken for experiments. OGD is used as an *in vitro* model to mimic *in vivo* hypoxia-ischemia injury. Cells were plated, walled for 12h, and washed three times with PBS. Then the culture medium was replaced with glucose-free DMEM (Meilunbio, Dalian, China) followed by incubation in a chamber containing a mixture of 94%N_2, 5% CO_2 and 1% O_2 (Thermo Fisher Scientific, MA, United States) for certain hours (Baldea et al., 2018). The normal control group was maintained all the time in a complete medium. Cells were collected immediately after the treatment and stored at −80°C for future use. All studies were performed using 3 biologically independent sets of experiments.

2.4 MTT assay

The HUVEC cells were incubated overnight to adhere to the wall. After treatment with OGD for 0h, 2h, 4h, 6h, and 8h, 10 μL of MTT solution (concentration of 5 mg/mL) (solarbio, Beijing, China) was added and incubated for 4 h. The culture solution was carefully aspirated. 150μL of dimethyl sulfoxide (solarbio, Beijing, China) was added to each well, and the wells were shaken horizontally for 10 min at low speed on a shaker. The absorbance of each well was measured at 490 nm on an enzyme marker (Tecan).

2.5 RNA isolation

According to the manufacturer's instructions, the total RNA was isolated from HUVECs using the M5 universal RNA Mini Kit (Mei5 Biotechnology, Beijing, China). In brief, the culture medium was thoroughly aspirated from the treated HUVECs,

and 350 μL of RLT lysis buffer was added. The cells were lysed by repeatedly blowing. An equal volume of 70% ethanol was added to the mixture and immediately mixed by blowing. The mixture was then transferred to an adsorption column (RA) placed in a collection tube, and centrifuged at 13,000 rpm for 30 s, with the flow-through being discarded. Next, 700 μL of proteinase-free buffer (RW1) was added, incubated at room temperature for 30 s, and centrifuged at 13,000 rpm for 30 s, followed by discarding the flow-through. Subsequently, 500 μL of wash buffer (RW) was added, centrifuged at 13,000 rpm for 30 s, and the flow-through was discarded. The wash step was repeated. The adsorption column (RA) was placed back into an empty collection tube, and centrifuged at 13,000 rpm for 2 min to remove excess wash buffer. The adsorption column (RA) was then transferred to a 1.5 mL centrifuge tube, and 30-50 μL of RNase-Free H2O was added to the middle portion of the adsorption membrane, depending on the expected RNA yield. The mixture was incubated at room temperature for 1 min, followed by centrifugation at 13,000 rpm for 1 min to obtain the RNA solution. The purity of RNA was assessed by a Nanodrop 2000 spectrophotometer (Thermo Fisher Scientific, Waltham, United States) and the concentration was measured on an Invitrogen Qubit 3.0 spectrophotometer (Thermo Fisher Scientific, Waltham, United States). RNA quality was evaluated on a Bioanalyzer 2,100 (Agilent Technologies, Santa Clara, United States), and DNA integrity was analyzed by agarose gel electrophoresis.

2.6 DNA methylation and expression profiling

The cells prepared in step 1.3 were collected into 1.5 mL centrifuge tubes, added 500 μL of proteinase K solution (10 mg/mL) to each tube. Extracted DNA according to the instructions from the nucleic acid purification kit (Concert, Xiamen, China) and performed quality assessment. Treated DNA with bisulfite, followed by whole genome amplification (WGA) and fragmentation to generate fragmented DNA. Precipitated and resuspended the obtained DNA then hybridized it with the beads on the chip, where specific bases were attached. Washed away the unhybridized and non-specifically hybridized DNA, and performed single-base extension reactions on the chip, incorporating detectable label moieties. Placed the processed chip into a scanner and used laser excitation to stimulate the fluorescence emitted by the single-base extension products on the chip. The scanner captured the fluorescence signals emitted by the fluorescent moieties. The DNA methylation level was measured using the Illumina Infinium Methylation EPIC v2.0 BeadChip and processed with ChAMP package in R (https://bioconductor.org/packages/release/bioc/html/ChAMP.html). The cDNA samples prepared in step 1.5 were sequenced for RNA expression profiling using the Illumina Novaseq 6,000 system (von Kanel and Huber, 2013; Bibikova and Fan, 2010). The raw reads were filtered using TrimGalore (http://www.bioinformatics.babraham.ac.uk/projects/trim_galore/), and the filtered data were analyzed using FastQC software. The methylation level at an individual locus was reported as b a value, which varied from 0 (unmethylated) to 1 (fully methylated).

Based on the defined differentially methylated positions (DMPs), hierarchical clustering was conducted using Cluster 3.0 and Java TreeView software. DMPs located in the gene region were assigned to the corresponding genes, which were defined as DMGs (Zhu et al., 2019).

The differentially expressed genes (DEGs) between the OGD and control groups were identified using Deseq2 software. The DEGs were selected by $p < 0.05$ and |log2 (fold change, FC)|>1, where log2(FC) > 1 and log2(FC)<-1 respectively indicated upregulated and downregulated genes. The combined datasets, including 3 OGDs and 3 negative controls (NCs), were normalized by the BMIQ algorithm.

The gene ontology (GO), Kyoto Encyclopedia of Genes and Genomes (KEGG), and disease ontology (DO) enrichment analyses were performed using the clusterProfiler. STRINGdb (Szklarczyk et al., 2017; Szklarczyk et al., 2019) was used to analyze DEGs' protein-protein interaction (PPI) network.

2.7 Integrative analysis of DNA methylation and gene expression data

To determine whether the methylation level was associated with the expression profile of the concerned gene, a correlation analysis was performed by R as well as Causal Inference Test (CIT) Analysis by the R package CausalImpact (https://google.github.io/CausalImpact/). Correlation analysis screened out CpG loci whose methylation levels were negatively correlated with the unique DEGs expression (r > 0.8). The CpG locus is within 1,000 kb of the gene it regulates and therefore has a cis-regulatory effect on the gene. Subsequently, the screened CpGs and DEGs were analyzed by CIT to find out the differentially methylated CpG loci and DEGs that were statistically causally related. The STRING database was used for the PPI analysis of causally related DEGs and differentially methylated genes (DMGs). The fast greedy algorithm of the igraph package was used to cluster the constructed internetworks and partition it into different modules for plotting.

2.8 Quantitative real-time PCR (qRT-PCR) analysis

The extracted RNA was used to synthesize complementary DNA (cDNA) for the downstream qRT-PCR analysis using SYBR Green Master Mix (ABI/QuantStudioTM DX, United States). The primer sequences of each gene were listed in Table 1. The relative gene expression level was determined by the $2^{-\Delta\Delta CT}$ method, using GAPDH as an internal reference.

2.9 Targeted methylation sequencing

DNA extraction was performed after remodeling, and the samples were processed using the EZ DNA Methylation-Gold Kit (ZYMO, CA, United States) to convert unmethylated cytosine C) to uracil U). Multiplex PCR tests were conducted to target specific fragments of the samples, and specific label sequences were added.

TABLE 1 Primer sequence.

No.	Gene	Forward Sequence (5′-3′)	Reverse Sequence (5′-3′)
1	MYC	TCGGATTCTCTGCTCTCCTCG	TCTTCTTGTTCCTCCTCAGAGTCG
2	VEGFA	CTTCAAGCCATCCTGTGTGCC	GTTTGATCCGCATAATCTGCATGG
3	CD44	GTCGCTACAGCATCTCTCGG	CAGAGCTTTCTCCATCTGGGC
4	BDNF	TGGAGGTGGGGCATGGTATT	AAAGCACGAGGTCCAAGCAG
5	CCL2	TGAAAGTCTCTGCCGCCCTT	GGGGCATTGATTGCATCTGGC
6	TSP-1	AACACGGACCCCGGCTACAA	TACGGGGCTTGCACACCTGTT
7	TNFSF10	TGGCTATGATGGAGGTCCAGGG	GACTGCAGGAGCACTGTGAAGA
8	COL1A2	CCCAGAGTGGAGCAGTGGTTA	CCGGATACAGGTTTCGCCAG
9	GNAQ	AGAGTTCGAGTCCCCACCAC	CCCCCTACATCGACCATTCTGA
10	SQSTM1	GTAGCGTCTGCGAGGGAAAG	TGCGAGAAGCCCTCAGACA
11	RUNX1	CCCATCGCTTTCAAGGTGGT	TGGCTGCGGTAGCATTTCTC
12	ETS1	CAGATGCCGACGAGTGATGG	GAGTCCAACCAACACGGCTG
13	NGFR	CACCGACAACCTCATCCCTGT	CTTGCAGCTGTTCCACCTCTTG
14	BCL2L11	ACCAAATGGCAAAGCAACCTTC	GCTCTGTCTGTAGGGAGGTAGG
15	LUM	GCAGTGTCAAGACAGTAAGGATTC	ACCACCAATCAATGCCAGGA
16	MME	CTGGAGATCAGCCTCTCGGT	TCGTAGGTTGCATAGAGTGCG
17	SEMA6A	CGTTGCACTGTTTGCAGATGG	TGAATCGTGCTTGACGGTCC
18	TIMP3	ACCGAGGCTTCACCAAGATG	CCATCATAGACGCGACCTGT
19	GNAI1	GGTGCCCTTCTGGGAACTAC	GTCCAATGCTGGAGGACTCG
20	IFIT1	CGCTGGGTATGCGATCTCTG	CCTGCCTTAGGGGAAGCAAAG
21	LRP5	CAACGGCAGGACGTGTAAGG	CACGATGTCGGTGAAGTCCG
22	MEIS1	CTGCACTCGCATCAGTACCC	GGGAAGAGGGGGTGTCCATA

All samples' Index PCR amplification products were mixed in equal amounts, and the MethylTarget sequencing library was obtained by gel purification. After accurately quantifying the molar concentration of the library, high-throughput sequencing was performed on the Illumina Hiseq/Miseq platform using a 2 × 150 bp/2 × 250 bp paired-end sequencing mode, resulting in FastQ data. The analysis methods were as shown in step 1.6.

2.10 The enzyme-linked immunosorbent assay (ELISA)

The ELISA kit (Elabscience, Wuhan, China) was used to detect extracted plasma samples, according to the manufacturer's instructions.

2.11 Statistical analysis

Statistical analyses were performed using GraphPad Prism 7 (San Diego, CA, United States). D'Agostino-Pearson omnibus normality test was used to evaluate the normality of the distribution of the variables. Normally distributed values were expressed as the mean ± standard deviation (SD), and the differences between the groups were analyzed by unpaired *t*-test. Non-normally distributed data were expressed as median and quartile and analyzed by the Mann-Whitney test. A *p*-value of <0.05 was considered statistically significant.

3 Results

3.1 Identification of DEGs in the HUVEC-OGD group by mRNA sequencing

The MTT results showed a significant decrease in cellular activities of HUVECs at 4 h of OGD treatment (Figure 2A). Therefore, we used HUVECs sequencing at the 4 h time point of OGD induction to identify disease-associated deregulated gene expressions and the involved signaling pathways. About 2,524 DEGs were detected by examining mRNA expressions of 3 HUVEC-OGD and 3 HUVEC samples by the Illumina Novaseq 6,000 (Illumina, United States) after normalization. According to the screening criteria, 1,393 genes (including *HSPA6*, *ZFAND2A*, *CCL2*, *N4BP3*, and *F2RL3*) were significantly upregulated, and 1,466 genes (including *ID1*, *SMAD6*, *ZBTB16*, *SLC16A14*, and *TRIM8*) were

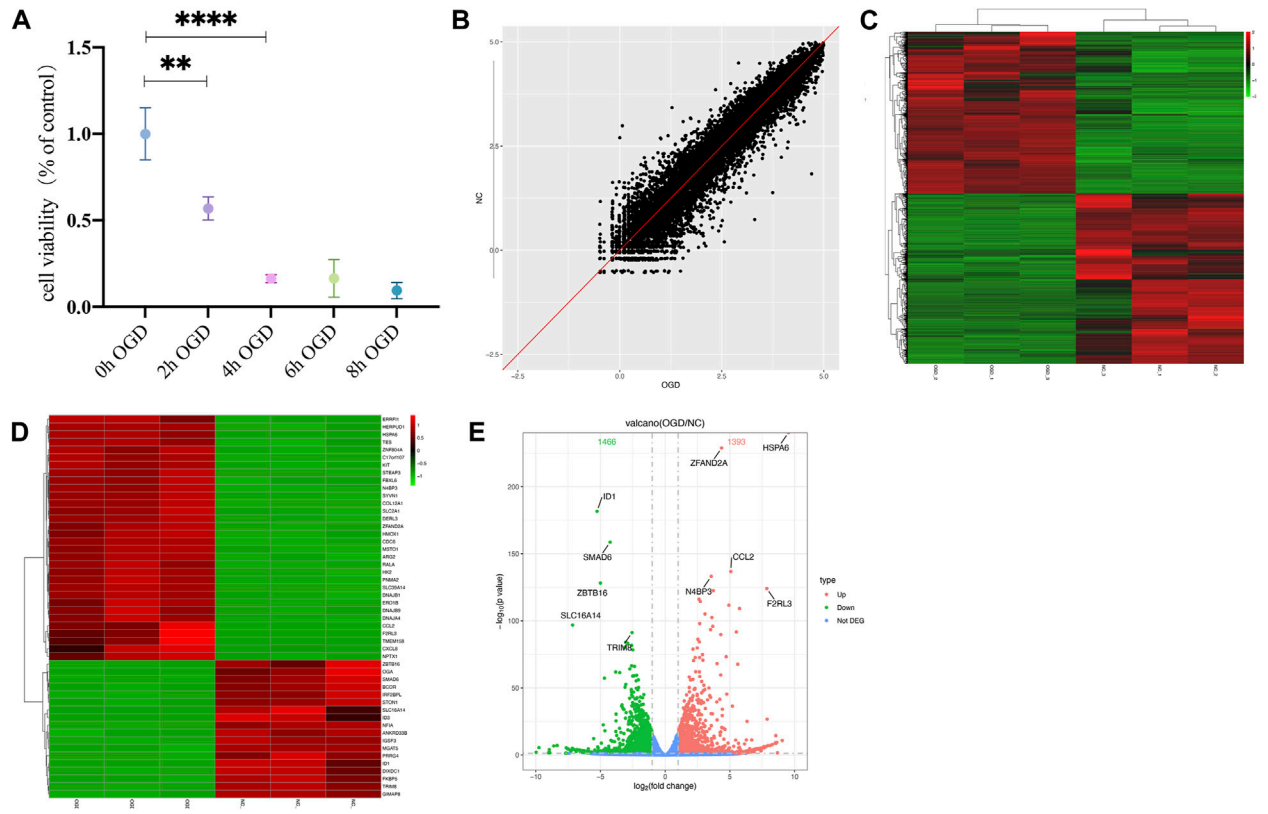

FIGURE 2
Differentially expressed genes (DEGs) were analyzed by a scatter plot. **(A)** MTT results of HUVECs at specific time points of OGD treatment. $^{**}p < 0.01$ and $^{****}p < 0.0001$vs control group; At 2h, the cell viability decreased almost 50% and 20% at 4 h. **(B)** Each point in this plot represents the logarithmic value of the mean expression of a gene after correction in two groups-the *X*-axis for the OGD group and the *Y*-axis for the NC group. The points of the diagonal surface represent relatively highly expressed genes in the corresponding group. **(C)** Heat map of clustering of DEGs. The *X*-axis indicates different samples and *Y*-axis for different genes; the red color represents highly expressed and green for genes with decreased expressions. **(D)** Heat map of top 50 significant DEGs. **(E)** Volcano plot of DEGs. Red dots indicate genes with upregulated expressions in the OGD group relative to the NC group, green dots for downregulated, and blue dots for genes with no significant differences.

downregulated in the HUVEC-OGD group (Figures 2B–E). To further explore these DEGs' related pathways and biological functions, we performed GO and KEGG analyses (Figures 3A,B). Biological process (BP) analysis demonstrated most of these DEGs were related to the regulation of cell-cell adhesion (93 genes), peptidyl-tyrosine phosphorylation (92 genes), response to endoplasmic reticulum (ER) stress (74 genes), as well as response to topologically incorrect (63 genes) and unfolded (61genes) proteins. Cellular components (CC) categorisation showed that 112 DEGs were distributed in the extracellular matrix (ECM) and 87 in the cytoplasm. The molecular function (MF) analysis detected 103 DEGs that were relevant to receptor-ligand activities and 64 DEGs specific to the cytokine receptor binding function. Enrichments were also found in the KEGG analysis. Possible underlying pathomechanistic pathways of ischemia-hypoxia injury involved cytokine receptor signaling (74 genes), PI3K-Akt signaling (74 genes), hyperlipidemia and atherosclerosis (52 genes), and others.

To elaborate on the interaction between DEGs, we performed PPI network analyses on significant DEGs. 151 DEGs of top 1,000 exhibited interactions, which were divided into 42 clusters with 136 edges (Figure 3C). The top 20 hub genes were also closely related (Figure 3D).

3.2 Identification of OGD-associated DNA methylation positions

We measured DNA methylation levels at 865,100 methylation sites in 3 HUVECs-OGD and 865,315 in 3 HUVEC controls using the Illumina Infinium MethylationEPIC BeadChip. After screening and QC check, 732,322 methylation positions were subjected to differential analysis. As shown in Figure 4A, the overall methylation levels of six samples were comparable. In total, 22,148 differentially methylated positions (DMPs; $|\Delta\beta|>0.1$ and $p = 0.0302$), including 8,764 hypermethylated and 13,384 hypomethylated ones, were identified, which correctly separated most OGDs and NCs in the clustering analysis, as shown in the volcano plot of DMPs in Figure 4D. Locations of genome-wide distribution of differentially methylated CpG islands are described in Table 2. In contrast, 505 differentially methylated regions (DMRs) were identified among the 2,134 methylation regions examined. Of these, 276 were hyper- and 229 were hypo-methylated in the OGD group (Figure 4G). The differential analysis of DMPs and DMRs and their distribution levels in chromosomes are shown in Figures 4E,H. The heat map of top 1,000 DMPs and 100 DMRs are illustrated in Figures Figure4B,G. According to the annotation,

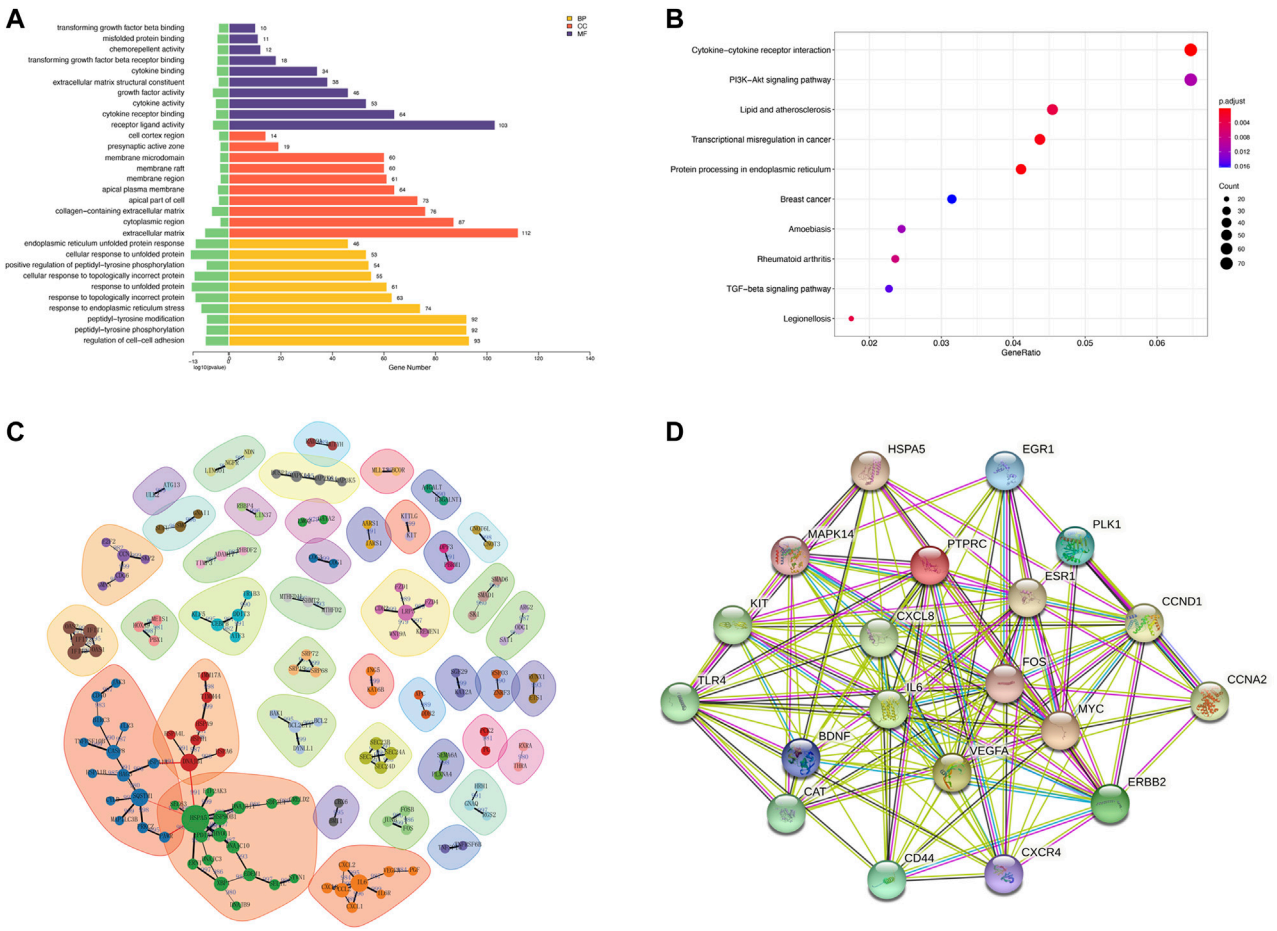

FIGURE 3
Functional enrichment and protein-protein interaction (PPI) analyses of DEGs. **(A)** Gene ontology (GO) enrichments in a bar graph. The log10 (*p* values) are shown in green at the left of the *X*-axis. The categories of BP, MF, and CC in GO analysis were illustrated in yellow, purple, and red, respectively. **(B)** The KEGG scatter plot. The horizontal coordinate represents the GeneRatio and the vertical coordinate is the -log10 (Q-value). **(C)** PPI analysis of top 1,000 DEGs. The nodes in the graph are proteins, and the edges are reciprocal relationships. Different clusters of modules are indicated by different base colors. **(D)** PPI analysis of the top 20 hub genes.

22,148 DMPs were physically located within 6,642 unique genes. Figure 4C indicates the top70 genes, including *SOX2OT*, *HOXC4*, *PTPRN2*, and *COL4A2*, are associated with numerous DMPs. Functional enrichment analyses showed that the 1844 genes were significantly enriched in some BP, most of which were related to OGD (Figure 4F). For example, 229 genes like *SQSTM1* and *NGFR* were enriched in GO:0007264/small GTPase-mediated signaling. Furthermore, the hub genes validated in the subsequent experiments also showed significant enrichment in pathways related to OGD, for instance, 167 DEGs were involved in GO:0050900/leukocyte migration, including COL1A2, TSP-1, VEGFA, CD44, and CCL2, and 194 DMGs were associated with GO:0198738/cell-cell Wnt signaling, including RUNX1, LRP5, and GNAQ. The enrichment was also found in KEGG pathways for OGD injury (e.g., hsa04151/PI3K–Akt signaling, hsa04010/MAPK signaling, hsa04510/focal adhesion, and hsa04020/calcium signaling) (Figure 4I). These results suggest that DNA methylation differences may play critical roles in the pathogenesis of ischemia and hypoxia in HUVECs.

3.3 Identified DMPs regulate mRNA expressions

Pearson correlation analysis showed that within 500 kb of upstream and downstream of differentially methylated CpG loci (Mendelson et al., 2018), there were 2,130 unique genes (covering 11,608 DMPs) with differentially expressed mRNA levels ($p < 0.05$; Pearson correlation coefficient>0.8). The distribution of DMPs associated with DEGs on the chromosome is shown in Figure 5A. Because correlation analysis alone does not establish causation, we conducted in-depth CIT analyses to investigate whether DNA methylation causes endothelial cell ischemic-hypoxic injury by regulating gene expression. In other words, we aimed to assess the potential causal chain of the causal factor (DNA methylation) - mediator (mRNA)—cell outcome (endothelial cell ischemic-hypoxic injury)-clinical outcome (AMI) (Zhu et al., 2019).which identified 1780 unique genes with 7,054 differentially methylated CpG loci. To investigate which pathophysiological processes were influenced by these 1780 DEGs, we conducted

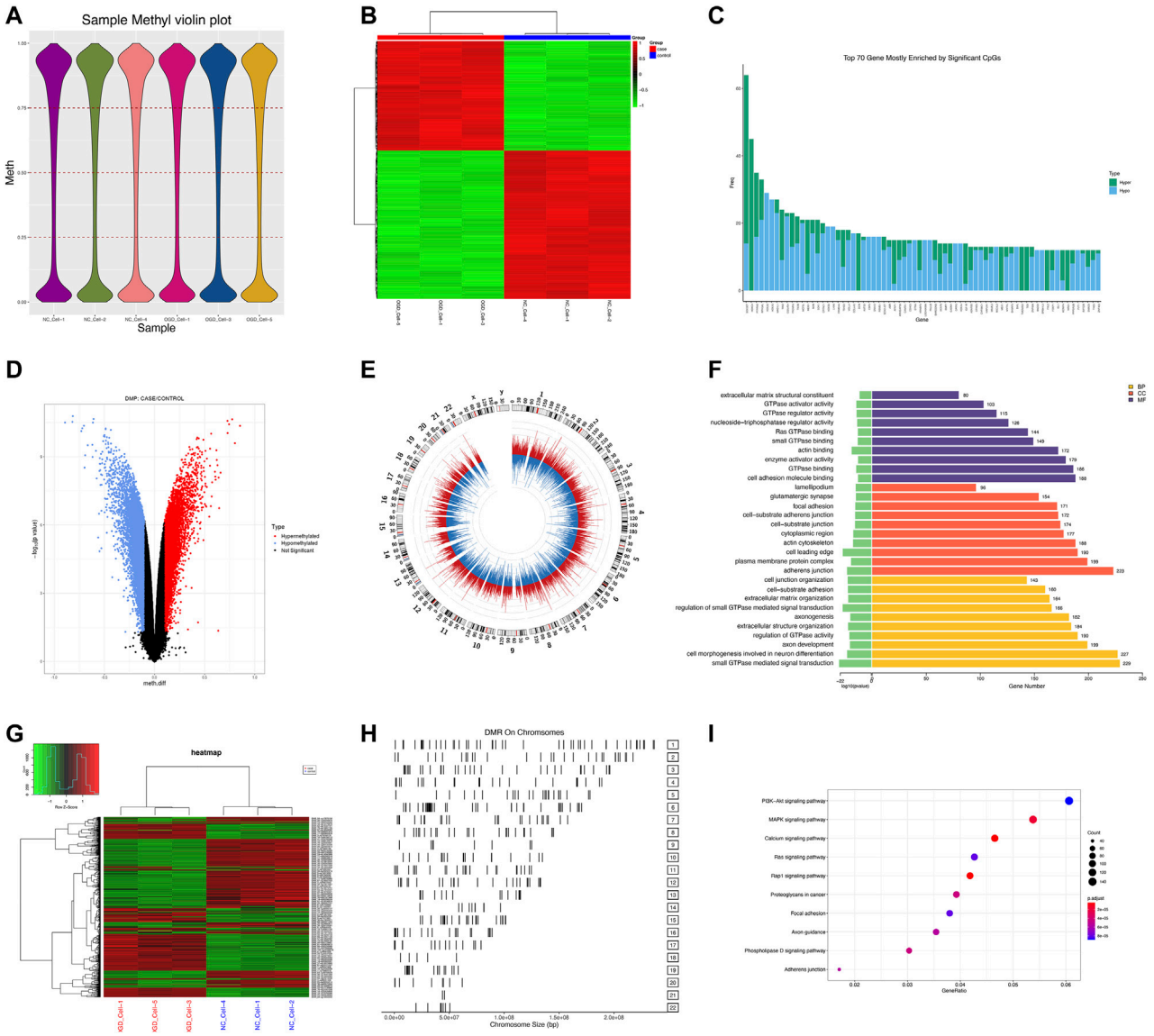

FIGURE 4
DMP and DMR analyses. **(A)** Violin plot for DNA methylation. The horizontal coordinate represents each sample and the vertical coordinate indicates the overall methylation level of that sample. **(B)** Heat map of top 1,000 DMPs. Each column represents a sample, and each row represents a gene where a DMP is located. **(C)** Bar plot of top 70 genes enriched for DMPs, where the horizontal coordinate indicates the single gene name, and the vertical coordinate shows the number of DMPs in that gene. **(D)** Volcano plot of DMPs. Red color for the hypermethylated OGD group relative to that of the control group, while blue color denotes hypomethylation. **(E)** Circle diagram of the chromosomal distribution of DMPs. The height of the bar inside the circle plot indicates |log2(FC)|, red color for the hypermethylated OGD group, and blue for the hypomethylated group. **(F)** Bar graph for GO enrichment of DMPs. **(G)** Heat map of top 100 DMRs. **(H)** Chromosomal distribution of DMRs. **(I)** KEGG scatter plot of DMPs.

DO, GO term, and KEGG pathway enrichment analyses. DO enrichment analysis, including 759 genes, showed that kidney and nervous system cancer involved many of these genes, but still, there were 32 genes enriched in the DO (ID:326) of ischemia (p = 0.0038). GO term suggested there were 1,551 genes enriched in 984 functional categories (adjusted $p < 0.05$). The most considerable portion of the functional terms comprised BP (n = 845), while the rests were CC (n = 56) and MF (n = 83). When BPs were used for categorization, the majority of enriched groups included responses to ER stress, topologically incorrect protein stress, and unfolded protein-ER-nucleus signaling pathway. Categorization by CC indicated that proteins encoded by the target genes were mainly associated with the localization in the ECM and cytoplasm. The MF analysis demonstrated a significant gene enrichment in transcription factor (TF) activity, RNA polymerase II proximal promoter sequence–specific DNA binding, and receptor-ligand interaction. Figure 5B presents the top 10 terms of the three GO categories ranked by their statistical significance and scatter plot of DO is illustrated in Figure 5C. In the KEGG pathway analysis (Figure 5D), 727 genes showed significant enrichment in pathways, including PI3K–Akt signaling, cytokine receptor signaling, and ER signaling for protein processing. Further

10.3389/fgene.2023.1293393

TABLE 2 Distribution of genomic regions of significant differentially methylated CpG sites.

	Genomic region of CpG sites	All CpG sites,n (%)	Hypermethylated CpG sites,n (%)	Hypomethylated CpG sites,n (%)
Region-level gene based	TSS1500	2087	960 (46.00%)	1,127 (54.00%)
	TSS200	715	287 (40.14%)	428 (59.86%)
	5′-UTR	1783	597 (33.48%)	1,186 (66.52%)
	1st Exon	251	100 (39.84%)	151 (60.16%)
	Body	8,825	3,369 (38.18%)	5,456 (61.82%)
	ExonBnd	100	41 (41.00%)	59 (59.00%)
	IGR	7,928	3,217 (40.58%)	4,711 (59.42%)
	3′-UTR	459	193 (42.05%)	266 (57.95%)
Region-level island based	island	1,404	523 (37.25%)	881 (62.75%)
	N-shore	2070	813 (39.28%)	1,257 (60.72%)
	S-shore	1715	687 (40.06%)	1,028 (59.94%)
	N-shelf	752	228 (30.32%)	524 (69.68%)
	S-shelf	681	231 (33.92%)	450 (66.08%)
	opensea	15,526	6,282 (40.46%)	9,244 (59.54%)
total		22,148	8,764 (39.57%)	13,384 (60.43%)

[a]CpG, 5′-C-phosphate-G-3′; UTR, untranslated region; TSS, transcription start site; N, north; S, south, and IGR, intergenic region.

PPI analysis suggested 441 nodes and 770 edges, with an average node degree of 0.34, an average local clustering coefficient of 0.34, and an expected number of edges of 542 (PPI enrichment, $p < 1.0e-16$). These 441 genes were enriched in 75 BPs. For instance, 224 genes were enriched in GO: 0050896 (response to stimulus), 159 genes in GO: 0007154 (cell communication), 115 genes in GO: 0030154 (cell differentiation), 42 genes in GO:0016477 (cell migration), 41 genes in GO: 0007155 (cell adhesion), and 40 genes in GO: 0035295 (tube development). Furthermore, among the 6 enriched CCs, 38 genes were in GO: 0070161 (anchoring junction) and 27 genes in GO: 0005911 (cell-cell junction). These results indicated that DEGs in ischemic-hypoxic HUVECs were closely related to intercellular interactions and angiogenesis, where DNA methylation regulation played an important role. Figure 5E demonstrated the STRING analysis of 3 clusters of 441 DMGs.

3.4 Validation of key DMPs and corresponding DEGs

To verify the reliability of the sequencing results, we validated the top 25 hub genes in PPI analysis and their CpG islands in a new sample of the same OGD model. PPI analysis of these 25 genes was revealed in Figure 5F. Among them, *RUNX3*, *TNFRSF9*, and *MAP3K5* were not tested by qRT-PCR as we failed to construct any efficient and reproducible primer pairs, and no CpG islands were detected for genes *CCL2*, *IFIT1*, *LUM*, and *TNFSF10*.

The results of qRT-PCR, the number of nodes in the PPI analysis, and the categories and examples involved in the functional clustering analysis of these 22 hub genes are listed in Table 3. The qRT-PCR analysis revealed that altered expressions of 12 DMGs were consistent with the sequenced samples, while 6 DMGs exhibited opposite expression patterns. Expressions of *COL1A2*, *LRP5*, *LUM*, and *TNFSF10* were not significantly changed ($p > 0.05$). As shown in Table 3 and Figure 6, expression levels of *VEGFA*, *CCL2*, *TSP-1*, *SQSTM1*, *BCL2L11*, and *TIMP3* were significantly elevated in the OGD group, while that of *MYC*, *CD44*, *BDNF*, *GNAQ*, *RUNX1*, *ETS1*, *NGFR*, *MME*, *SEMA6A*, *GNAI1*, *IFIT1*, and *MEIS1* decreased due to ischemia and hypoxic shocks.

We quantified the methylation levels of CpG islands and DNA fragments from 21 DMGs by MethylTarget sequencing. Notably, 42 of 1,179 CpG sites were differentially expressed, and 15 of 486 methylated haplotypes were significantly different in abundance (see Table 2; Table 3 in the supplement). Four of the 66 fragments were differentially expressed: BDNF_1_demethylated in the OGD group ($p = 0.02334636$), MYC_1_ ($p = 0.0443373$), RUNX3_4_ ($p = 0.03415566$) and SQSTM1_2_NEW ($p = 0.04771069$) had higher methylation levels than before (Figures 7A–D), where fragments BDNF_1_ ($r = 0.931$, $p < 0.0001$) and SQSTM1_2_NEW ($r = 0.758$, $p = 0.0043$) were positively correlated with the mRNA expressions of corresponding genes, and MYC_1_ ($r = -0.8245$, $p = 0.001$) was negatively correlated with the mRNA expression (Figures 7E–G).

3.5 BDNF and TNFSF10 overexpresses in AMI patients

Since the expressions of target genes were significantly altered in endothelial cells during ischemia and hypoxia, we hypothesized that

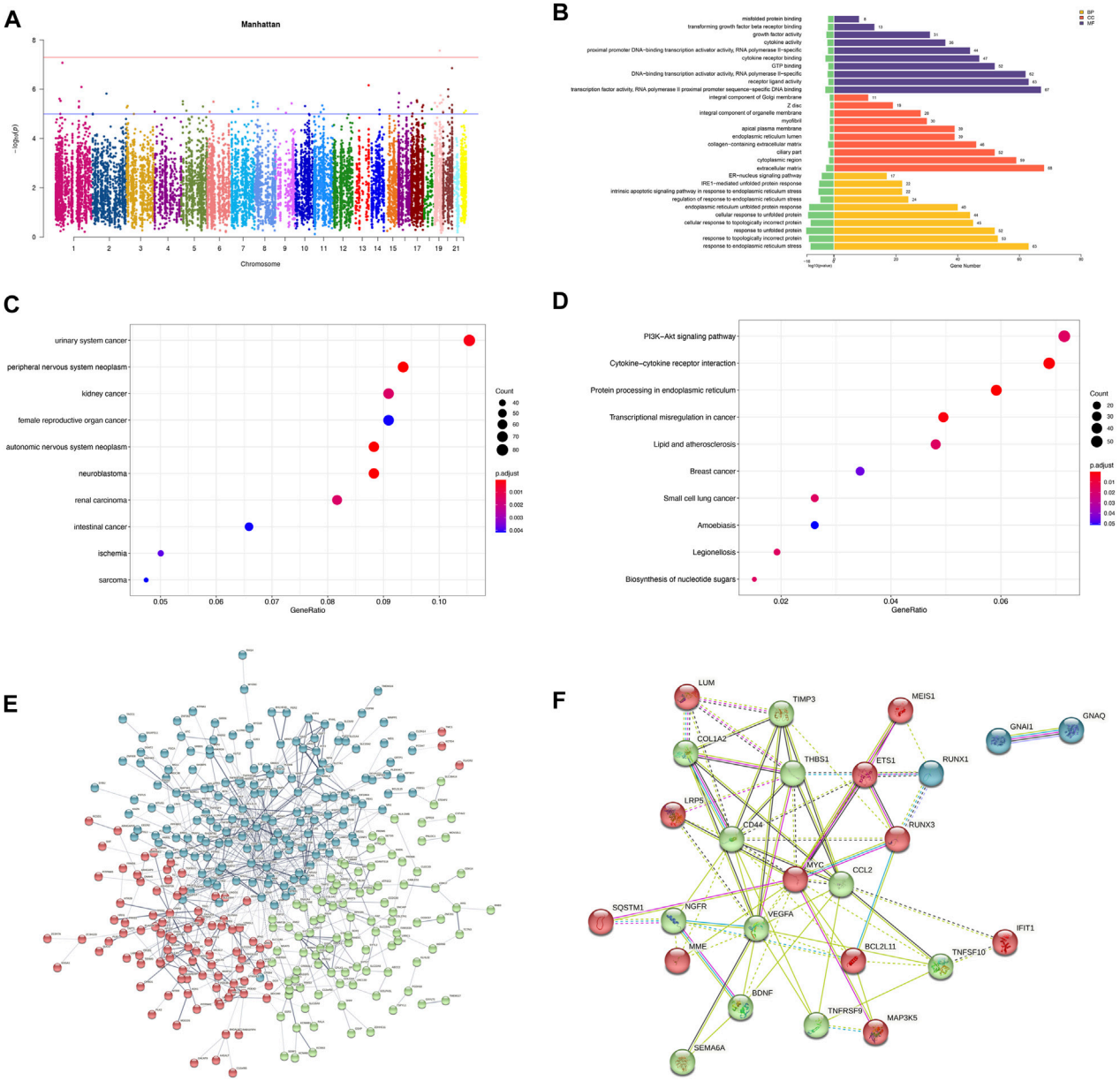

FIGURE 5
Analysis of DEGs associated with DMPs. **(A)** Manhattan plot of DEGs associated with DMPs. The horizontal coordinate indicates the chromosome and the vertical coordinate for the -log10 (*p*-value) of the DEGs associated with DMPs on the corresponding chromosome. **(B)** Bar graph of GO enrichment. **(C)** Scatter plot of DO. **(D)** Scatter plot of KEGG pathway enrichment. **(E)** PPI network constructed by the STRING using 441 DMGs and DEGs. The stronger associations are represented by thicker edges. The disconnected nodes are hided. Different colors represent different clusters. **(F)** PPI network constructed by the STRING using the top 25 hub genes (DMGs and DEGs).

there might have corresponding changes in coronary artery endothelial cells in the AMI patients and if disease-related factors released into the blood might be exploited as biomarkers. Based on previous findings and the differential expression analyses, we selected four indicators to be tested in downstream experiments. The basic clinical characteristics of the patients are described in Table 4. ELISA test results revealed that BDNF and TNFSF10 levels were indeed elevated in the peripheral blood of AMI patients (Table 5; Figure 8 C&E), and the BDNF expression was slightly lower in the group with complete occlusion under coronary angiography, compared with the group with non-complete occlusion [2,962 (2,362, 3,909) vs. 5,347 (2048, 9,181); p = 0.0204; Figure 8 D]. Correlation analysis showed that TNFSF10 was positively correlated with the expression of homocysteine, COL1α2 and BDNF, while negatively correlated with EF, suggesting that TNFSF10 might be associated with heart failure. BDNF, in turn, was positively correlated with TSP-1 level and platelet and leukocyte count. In contrast, although COL1α2 and TSP-1 expressions could not be detected among differentially expressed genes in the AMI group, correlation analysis revealed that the expression of COL1α2 was positively correlated with the length of time from the disease onset to a blood draw and negatively

TABLE 3 Expression and cluster analysis of 22 hub genes.

Gene	DEGs in sequencing			Validation by RT-qPCR				String node degrees	GO analysis		KEGG analysis	
	log2FoldChange	Type	p adjust value	Expression[a]		*p*-value	Type		Count	Example	Count	Example
				NC (%)	OGD (%)							
BDNF	1.251,956,305	Up	3.98264E-05	0.0023	0.0012	0.0015	Down	23	90	transport vesicle	9	MAPK signaling pathway
COL1A2	2.10,533,194	Up	5.0646E-12	0.0443	0.0457	0.4,461,868	Up	15	43	platelet activation	11	PI3K-Akt signaling pathway
TSP-1	1.272,757,804	Up	1.2377E-23	14.4803	20.0269	0.0006954	Up	19	323	response to decreased oxygen levels	12	p53 signaling pathway
MYC	1.025,573,653	Up	0.000118844	0.8137	0.4278	3.402E-06	Down	49	176	cellular response to hypoxia	33	Hippo signaling pathway
VEGFA	2.076,530,808	Up	5.89859E-14	0.0667	0.2030	1.77E-05	Up	39	359	regulation of transcription from RNA polymerase II promoter in response to hypoxia	23	HIF-1 signaling pathway
CD44	1.159,563,467	Up	0.001,341,815	0.5391	0.4210	3.694E-05	Down	34	113	leukocyte migration	6	ECM-receptor interaction
CCL2	5.069,944,423	Up	5.5462E-134	0.2544	0.7800	4.98E-07	Up	21	149	positive regulation of endothelial cell apoptotic process	17	NOD-like receptor signaling pathway
SQSTM1	1.548,462,125	Up	2.29785E-09	1.4727	1.7631	0.0004683	Up	15	85	autophagy of mitochondrion	9	Fluid shear stress and atherosclerosis
RUNX1	1.196,038,099	Up	3.15132E-12	0.1028	0.0477	1.66E-07	Down	14	125	positive regulation of angiogenesis	5	Tight junction
ETS1	1.606,366,428	Up	1.34887E-21	0.0904	0.0639	0.0165721	Down	13	87	response to hypoxia	4	Ras signaling pathway
BCL2L11	2.075,699,979	Up	3.44266E-28	0.0250	0.0469	3.648E-05	Up	11	163	tube formation	9	FoxO signaling pathway
MME	1.448,298,803	Up	9.58586E-06	0.0705	0.0430	0.0016804	Down	11	0		0	
TIMP3	1.64,760,662	Up	1.00799E-26	0.1460	0.3782	6.798E-07	Up	11	49	regulation of ERK1 and ERK2 cascade	2	MicroRNAs in cancer
GNAI1	−1.484,975,055	Down	1.19953E-14	0.0012	0.0004	0.0016735	Down	10	59	response to platelet aggregation inhibitor	40	Adrenergic signaling in cardiomyocytes
IFIT1	−2.936,485,257	Down	9.38353E-10	0.0057	0.0012	4.065E-06	Down	10	50	negative regulation of immune system process	1	Hepatitis C
LRP5	−1.469,642,161	Down	3.34967E-11	0.1383	0.1275	0.2,818,192	Down	10	113	tissue remodeling	8	Wnt signaling pathway
MEIS1	−1.76,793,772	Down	4.55049E-11	0.0180	0.0064	2.738E-05	Down	10	60	cardiac muscle tissue growth	2	Signaling pathways regulating pluripotency of stem cells
GNAQ	−1.068,236,204	Down	5.71031E-15	0.2201	0.1403	6.761E-05	Down	15	85	regulation of circadian rhythm	47	Rap1 signaling pathway
NGFR	−4.690,983,395	Down	1.67034E-55	0.0065	0.0008	4.48E-07	Down	13	87	regulation of blood vessel endothelial cell proliferation involved in sprouting angiogenesis	8	Apoptosis - multiple species

(Continued on following page)

10.3389/fgene.2023.1293393

TABLE 3 (*Continued*) Expression and cluster analysis of 22 hub genes.

Gene	DEGs in sequencing			Validation by RT-qPCR			String node degrees	GO analysis		KEGG analysis	
	log2FoldChange	Type	p adjust value	Expression[a]		*p*-value	Type		Count	Example	Count	Example
				NC (%)	OGD (%)							
LUM	−2.996,325,065	Down	0.013,749,732	0.0023	0.0016	0.2,637,541	Down	11	40	regulation of transforming growth factor beta production	1	Proteoglycans in cancer
SEMA6A	−1.924,779,711	Down	1.381E-15	0.0056	0.0022	0.000511	Down	11	84	negative regulation of cell adhesion	1	Axon guidance
TNFSF10	−1.268,836,896	Down	1.24894E-07	0.0143	0.0148	0.667154	Up	16	45	apoptotic mitochondrial changes	10	Cytokine-cytokine receptor interaction

[a]Expression relative to GAPDH.

correlated when patients took a double antiplatelet prior to phlebotomy. TSP-1, on the other hand, was positively correlated with NT-proBNP expression (Table 6).

4 Discussion

Acute myocardial infarction (AMI) is a complication of atherosclerosis that takes place in the coronary arteries (Xiao et al., 2020). It causes severe damage to the coronary microcirculation, resulting in vascular disintegration and capillary thinning in the infarct zone. Cardiac endothelial cells are estimated to be almost triple the number of cardiomyocytes (Pinto et al., 2016; Xiao et al., 2020). Endothelial dysfunction is involved from the initial stage of atherosclerosis to the late stage of cardiovascular complications (Gimbrone and Garcia-Cardena, 2016). Additionally, it serves as a marker of cardiovascular risk and a contributor to the progression of cardiovascular events. What is more, cardiac endothelial cells play a vital role in remodeling injured cardiac myocytes after cardiac tissue injury (Segers et al., 2018). Tissue repair following the myocardial infarction involves a drastic angiogenic response that begins in the infarction border zone and extends to the necrotic infarct core. Cell lineage tracing studies have revealed that new capillary structures are generated by angiogenesis only from pre-existing endothelial cells in the infarction border zone (Zhou et al., 2011; Dube et al., 2017; Tang et al., 2018). As a key factor in the function of blood vessels, the viability of endothelial cells is decisive in the reconstruction of blood flow for rescuing cardiomyocytes, reducing infarct size, and improving cardiac function (Guo et al., 2021). Furthermore, animal studies also support the notion that post-AMI endogenous angiogenic responses can be boosted to reduce scarring and adverse left ventricular remodeling (Wu et al., 2021).

The combination of LAD ligation and the OGD model is commonly used *in vivo* and *in vitro* studies of AMI (Xiao et al., 2020; Wang et al., 2021; Guo et al., 2021; Zhang et al., 2021; Wu et al., 2022). As early as 2000, researchers used the OGD model to simulate oxidative stress in myocardial cells under ischemic and hypoxic conditions (Persky et al., 2000). OGD/R-induced endothelial cytotoxicity alters the cellular pH balance, increases oxidative stress, and reduces endothelial nitric oxide production (Yang et al., 2016). These changes are inseparable from the regulation of DNA methylation. Therefore, to explore the gene expression profiles of endothelial cells under ischemic-hypoxic stress and reveal the regulatory roles of DNA methylation on the mRNA expression, facilitating further exploration of early diagnosis of AMI and therapeutic targets in post-AMI angiogenesis, we utilized the HUVEC OGD model to simulate *in vitro* ischemic-hypoxic conditions in endothelial cells.

Firstly, We performed sequencing and validation to identify a large number of DEG and differentially methylated loci. Among them, fragment BDNF_1_ was demethylated, and BDNF gene expression was decreased in response to ischemia and hypoxic shocks. SQSTM1_2_NEW methylation level and SQSTM1 gene expression were both elevated. Hypermethylation of MYC_1_ did cause a decrease in MYC gene expression. In addition, we found that TNFSF10 and BDNF proteins were differentially elevated in the peripheral serum of AMI patients. The inconsistent trends in the

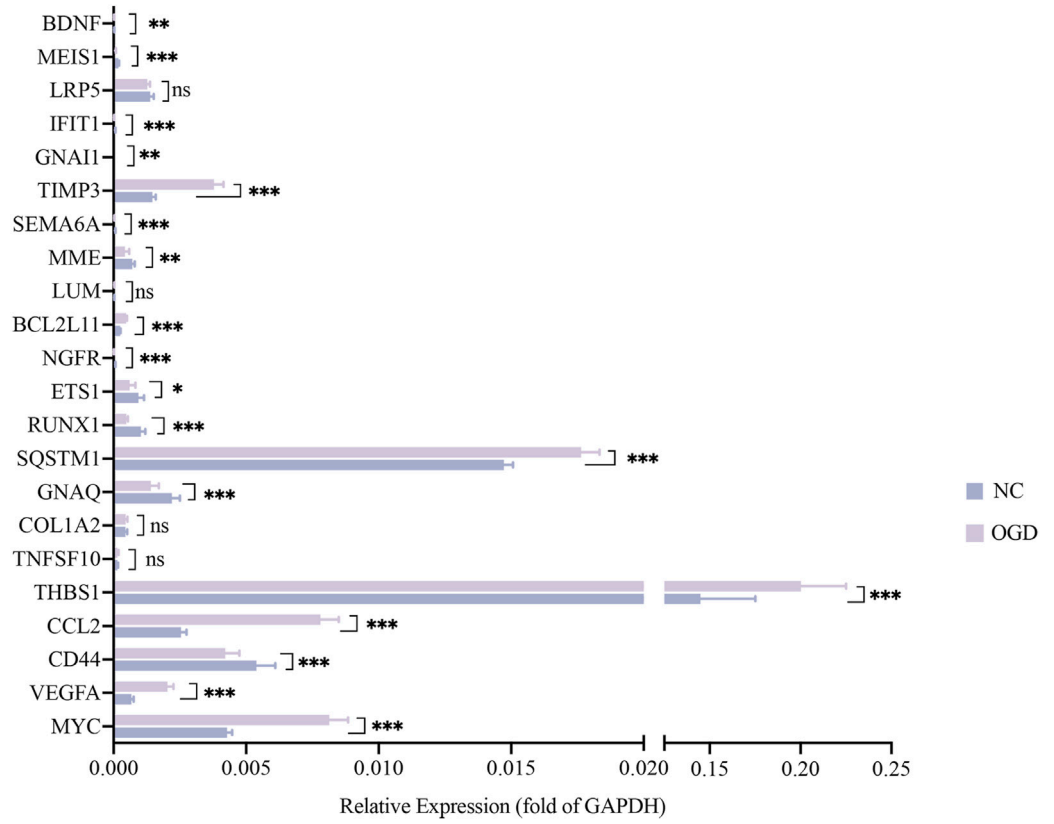

FIGURE 6
The mRNA expressions of 22 hub genes relative to GAPDH. The horizontal coordinates show each genes and the vertical coordinates for the expressions relative to GAPDH. Green color for the NC group and purple for the OGD group. *$p < 0.05$, **$p < 0.01$ and ***$p < 0.001$vs control group.

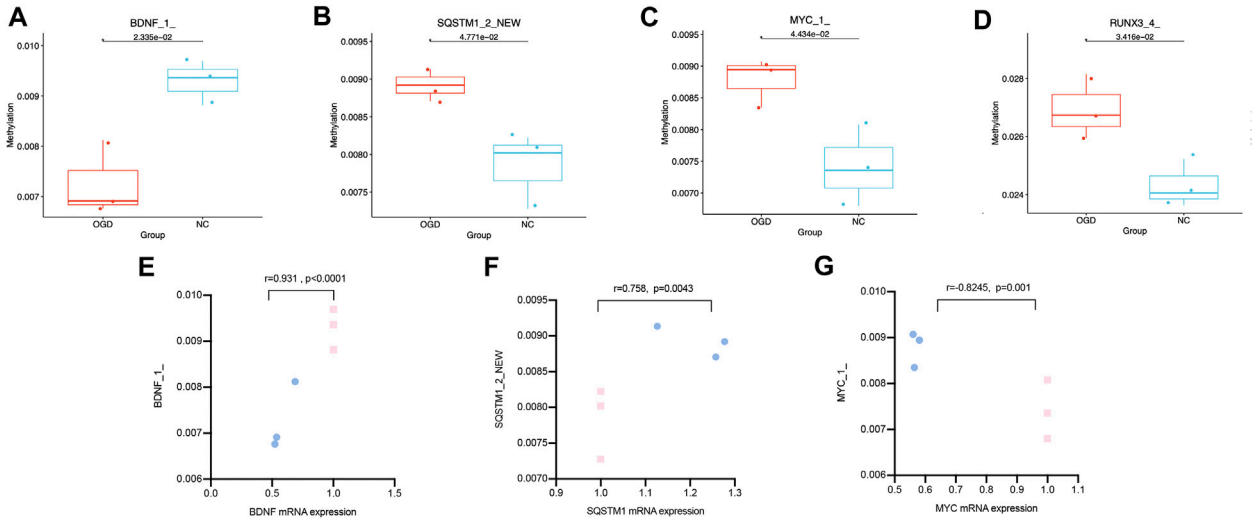

FIGURE7
Differentially expressed CpG fragments and correlation analysis. **(A–D)** The horizontal coordinates represent each groups and the vertical coordinates represent the methylation levels. Each point represents each sample, and the box plot illustrates the median and quartiles. **(E–G)** The horizontal coordinates represent the relative mRNA expression levels, and the vertical coordinates represent the methylation levels of methylated fragments. The pink squares represent the NC group, while the blue dots represent the OGD group.

TABLE 4 The clinicopathological features of candidates.

	Group		*p*-value
	CAG(−) (n = 17)	AMI (n = 71)	
Age, years (medium (25% Percentile, 75% Percentile))	56 (52, 68.5)	59 (54, 69)	>0.05
Male (%)	10 (62.5%)	65 (90.3%)	0.005
BMI (mean ± SD)	23.87 ± 2.509	25.66 ± 5.461	>0.05
Family history (%)	1 (5.9%)	17 (18.3%)	>0.05
History of hypertension (%)	5 (29.4%)	38 (53.5%)	>0.05
History of diabetes (%)	5 (29.4%)	10 (14.1%)	>0.05
History of hyperlipidemia (%)	0 (0.0%)	1 (1.4%)	>0.05
History of drinking (%)	1 (5.9%)	12 (16.9%)	>0.05
History of Smoking (%)	3 (17.6%)	36 (50.7%)	0.014
History of COPD(%)	1 (5.9%)	1 (1.4%)	>0.05
History of cardiovascular and cerebrovascular disease (%)	0 (0.0%)	6 (8.5%)	>0.05
Systolic pressure, mmHg	131.80 ± 19.95	133.30 ± 25.63	>0.05
Diastolic pressure, mmHg	77.88 ± 8.97	74.58 ± 13.66	>0.05
HR, bpm	79.06 ± 19.32	72.42 ± 13.97	>0.05
TNI, ng/mL	0.01 (0.01,0.01)	2.4 (0.94,16)	<0.0001
MYO, ng/mL	55.76 ± 28.01	335.7 ± 217.4	0.0005
CKMB, ng/mL	2 (2, 2.4)	45.46 (15.28, 177)	<0.0001
d-Dimer, ug/mL	0.25 (0.17, 0.6555)	0.339 (0.17, 2.07)	>0.05
NT-proBNP, pg/mL	64 (37, 598)	617.5 (234.3, 1,363)	0.0025
Leukocytes, 10–9/L	6.346 ± 1.829	10.41 ± 3.4	<0.0001
Hb, g/L	147 (141.5, 162)	161 (147, 168)	>0.05
NE%, %	70.7 (61.75, 73.8)	81.3 (74.5, 84.9)	<0.0001
Platelet, 10–9/L	175 (111, 204)	183 (161, 222)	>0.05
Creatinine, ummol/L	78.21 ± 25.2	71.75 ± 15.78	>0.05
Uric acid, ummol/L	343.9 ± 101.1	347.6 ± 86.74	>0.05
Total cholesterol, mmol/L	3.975 ± 0.8251	4.599 ± 1.011	0.0205
Triglycerides, mmol/L	1.55 (1.065, 3.185)	1.66 (1.12, 2.34)	>0.05
HDL-C, mmol/L	1.052 ± 0.364	1.018 ± 0.2294	>0.05
LDL-C, mmol/L	2.462 ± 0.5984	3.089 ± 0.7789	0.0026
APOAI, g/L	1.24 ± 0.3082	1.18 ± 0.2245	>0.05
APOB, g/L	0.8482 ± 0.3331	0.9909 ± 0.2654	>0.05
APOB/AI	0.68 (0.52, 0.79)	0.82 (0.655, 1.015)	0.0105
LP(a), mg/dL	7.53 (4.27, 31.27)	12.62 (5.615, 26.64)	>0.05
Hcy, umol/L	14.6 (10.6, 24.75)	16.5 (12.55, 22.5)	>0.05
Glycohemoglobin, %	5.7 (5.3, 7.1)	5.7 (5.225, 6.15)	>0.05
PT, s	11.4 (10.95, 12.75)	11.9 (11.5, 12.5)	>0.05
APTT, s	31.8 (29.5, 34.7)	33.4 (30.1, 44.3)	>0.05

(Continued on following page)

TABLE 4 (*Continued*) The clinicopathological features of candidates.

	Group		*p*-value
	CAG(−) (n = 17)	AMI (n = 71)	
FDP, ug/mL	0.9 (0.77, 1.53)	1.15 (0.69, 3.45)	>0.05
EF, %	62 (58.5, 64.5)	55 (50, 58)	0.0001
Infarct related artery			
LM		2 (2.8%)	
LAD		30 (42.3%)	
LCX		8 (11.3%)	
RCA		31 (43.7%)	
number of stenosed coronary vessel			
1		31 (43.7%)	
2		23 (32.4%)	
3		17 (23.9%)	
Onset-blood drawing time			
up to 6 h		28 (39.44%)	
7-12 h		24 (33.80%)	
over 12 h		19 (26.76%)	
coronary occlusion in angiography		38 (53.52%)	
Thrombolytic therapy		17 (23.94)	

TABLE 5 Expression of BDNF, TNFSF10,TSP-1 and COL1α2 in AMI and control patients.

Variable	Group		*p*-value
	Control (n = 17)	AMI (n = 71)	
BDNP (pg/mL)	2011 (1,597, 4,053)	3,609 (2,256, 6,082)	0.0284
TNFSF10 (pg/mL)	13.18 (6.875, 36.51)	48.46 (11.65, 117.7)	0.0309
TSP-1 (ng/mL)	71.17 (22.93, 85.38)	56.79 (25.79, 95.66)	>0.05
COL1α2 (ng/mL)	16.62 (6.912, 39.71)	15.09 (9.836, 30.04)	>0.05

expression of target molecules measured in cells and patient serum were also well understood. Levels of target molecules in the cellular assays only represented the local distribution in HUVECs. On the contrary, these factors represented their total amounts corresponding to overall tissues and organs In the serum.

Brain-derived neurotrophic factor (BDNF), a member of the neurotrophic factor family, is involved in stress and inflammation. As an essential component of ischemic tissue angiogenesis, BDNF can stimulate the migration and proliferation of ischemic local endothelial cells mediating cell survival (Pius-Sadowska and Machalinski, 2017). Recently, it has been discovered that vascular smooth muscle cells, endothelial cells, and atherosclerotic arteries express BDNF (Ejiri et al., 2005). A study (Donovan et al., 2000) using animal models showed that endothelial cell survival in intramyocardial arteries and capillaries during the early postnatal period could be compromised by low levels of BDNF expression. Insufficient BDNF can cause intraventricular wall bleeding, decreased heart contractility, and early postnatal mortality because of reduced endothelial cell-cell interactions and increased apoptosis. In clinical research, Luigi Manni et al. (Manni et al., 2005) found that serum BDNF levels decreased in acute coronary syndromes, but the number of cases in this study was very minimal (n = 31). On the contrary, Haibo Wu et al. (Wu et al., 2019) reported that serum BDNF expressions were higher in AMI patients combined with AHF than in AMI patients without AHF. Shinpei Kadowaki et al. (Kadowaki et al., 2016) demonstrated that serum BDNF levels in 134 chronic heart failure patients were significantly lower than that of 23 control subjects. In another study (Ejiri et al., 2005), the difference in BDNF levels between the coronary sinus and aorta was significantly greater in the unstable angina group compared with the stable angina and non-coronary artery disease groups. A review that included 35 studies showed that BDNF levels were lower in patients with chronic heart failure and stroke, but higher in patients with unstable angina and myocardial infarction. Our finding match those observed in earlier studies that BDNF expression was significantly higher in the AMI group, but we performed subgroup analysis and found no significant difference between the ST-segment elevation myocardial infarction (STEMI) and NSTEMI groups, while was significantly lower in the completely occluded group than in the non-occluded group at coronary angiography. Moreover, serum BDNF levels correlated with the number of platelets in peripheral blood since circulating BDNF

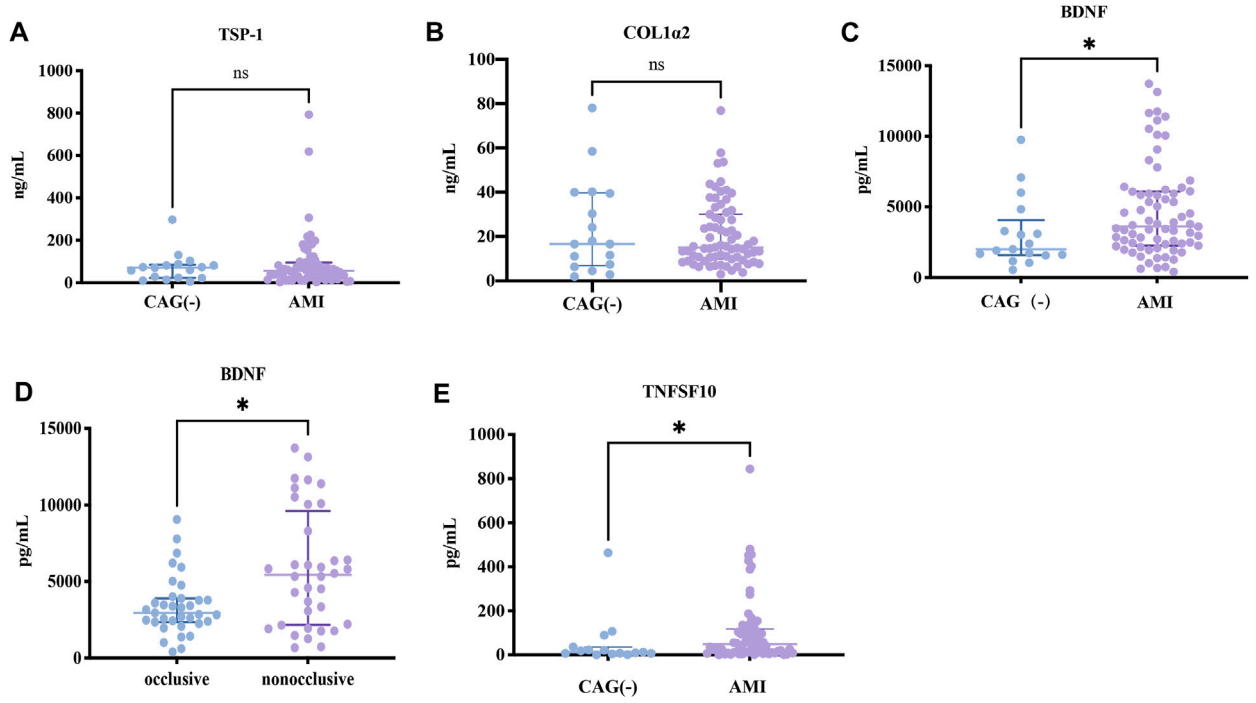

FIGURE 8
ELISA results about key candidates. **(A,B)** There were no differences in expressions of TSP-1 and COL1α2 between AMI and NC patients ($p > 0.05$). **(C,D)** BDNF and TNFSF10 were overexpressed in AMI patients ($p = 0.0284$ and $p = 0.0142$, respectively). **(E)** BDNF expression was lower in the occlusion group compared to the non-occlusion group ($p = 0.0118$).

TABLE 6 Correlation analysis of key indicators.

Variable	Variable	Pearson's correlation coefficient	*p*-value
TNFSF10	Hcy	0.294	0.006
TNFSF10	COL1α2	0.281	0.008
TNFSF10	BDNF	0.563	<0.001
TNFSF10	EF	−0.274	0.01
TSP-1	BDNF	0.293	0.006
COL1α2	Onset-blood drawing time	0.317	0.007
COL1α2	Dual antiplatelet before blood drawing	−0.256	0.03
BDNF	platelet	0.246	0.021
BDNF	WBC	0.223	0.037
TSP-1	NT-proBNP	0.264	0.018

was captured and sequestered by circulating platelets, consistent with previous studies (Yang et al., 2006; Farmer et al., 2021). Considering the relationship between BDNF expression and inflammation, it is reasonable to suggest that there could be a link between BDNF level and white blood cell count. Hence, we suspected the elevated BDNF expression in the AMI group might be related to rapid endothelial cell proliferation and revascularization after ischemia.

Tumor necrosis factor superfamily member 10 (TNFSF10), also known as tumor necrosis factor-related apoptosis inducing ligand (TRAIL), is a soluble marker of apoptosis. TNFSF10 is normally a membrane-bound ligand expressed by immunocytes. Soluble TNFSF10 can also act as a weaker inducer of apoptosis compared to membrane-bound TNFSF10 (Li et al., 2003). The significance of TNFSF10 in endothelial cells has been studied. Jie Hui Li et al. (Li et al., 2003) showed that incubation of endothelial cells with TNFSF10 induces inflammation and apoptosis. In surviving cells, TNFSF10 promotes the adhesion of leukocytes. Injection of TNFSF10 into human skin xenografts promotes focal EC injury accompanied by limited neutrophil infiltration. Also,

TNFSF10 protects endothelial cells from apoptosis and proliferation through the activation of Akt and extracellular signal-regulated kinase (ERK) pathways, partly due to nitric oxide generation (Wu et al., 2021; Wu et al., 2022). Several studies (Secchiero et al., 2009; Osmancik et al., 2013; Teringova et al., 2018) revealed that TNFSF10 level was lower after PCI in AMI patients compared to a pre-procedure or healthy population and gradually increased after that. A low TNFSF10 level is an indicator of heart failure and poor prognosis (Teringova et al., 2018). Nakajima et al. (Nakajima et al., 2003) indicated that the expression of TNFSF10 on peripheral lymphocytes in AMI patients increases compared with healthy controls. This study also reported that TNFSF10 protein expression was higher in human atherosclerotic plaques, especially the most vulnerable ones, and could be induced by the ox-LDL expression. Soluble active TNFSF10 negatively regulates calcium influx through store-operated calcium release-activated calcium channels, which is crucial to activating lymphocytes (Lunemann et al., 2002). Our sequencing results in endothelial cells showed that TNFSF10 was significantly downregulated during ischemia and hypoxia and slightly elevated upon re-modeling verification. Whereas analysis of blood samples of AMI patients before PCI demonstrated that the level of soluble TNFSF10 was elevated, and its expression was positively correlated with that of BNDF and COL1α2. This contradictory conclusion may be related to the involvement of different types of receptors. There are five types of TNFSF10 receptors: TRAIL-RI (DR4), TRAIL-R2 (DR5), TRAIL-R3 (DcRl), RAIL-R4 (DcR2), and osteoprotegerin (OPG) (Buchsbaum et al., 2006). The first two are death receptors, and the last three are decoy receptors, playing a role in promoting and inhibiting apoptosis, respectively. In this study, TNFSF10 was not found to correlate with LDL, ApoAI, APOB, and LPa, but we did not detect the ox-LDL level. This study further suggests that TNFSF10 correlates with EF and Hcy, and is needed to explore the mechanisms involved.

Collagen type 1 alpha 2 (COL1α2), a major component of fibrotic tissue and associated with excessive collagen production, is less studied in the heart, rather than that in the kidney. In diabetic nephropathy studies, excessive aggregation of COL1α2 has been associated with renal fibrosis (Das et al., 2022). In clinical investigations, increased levels of COL1α2 have also been associated with inflammatory fibrosis (Wang et al., 2021). Studies have shown that COL1α2 expression is directly regulated by HIF-1α binding to a functional hypoxia-responsive element in its promoter at −335bp relative to the transcription start site (TSS). Phosphorylated Smad3 also associates with the −335 hypoxia-responsive element of the COL1α2 promoter region independent of a Smad DNA binding sequence (Baumann et al., 2016). Hypoxia simultaneously stimulates ECM synthesis and suppresses its turnover due to increased production of COL1α2, decreased collagenase expression, and increased tissue inhibitor of metalloproteinase (TIMP)-1 (Norman et al., 2000). In terms of COL1α2 in heart research, a bioinformatics analysis revealed that COL1α2 underlies the comorbidity mechanisms of HF and depression (Huang et al., 2022). Single-cell sequencing results using an obese mouse model suggested that COL1α2 and COL1α1 might be important markers of obesity-induced cardiac fibrosis (Pan et al., 2022). Another investigation confirmed the association between COL1α2 and cardiac fibrosis (Xu et al., 2021). In our study, COL1α2 was overexpressed in the OGD group. Although any significant increase in expression was not observed in the peripheral blood of AMI patients, the analysis showed a positive correlation between the expressions of COL1α2 and TNFSF10, and the time from onset to blood sampling, and a negative correlation with the administration of dual antiplatelet agents, suggesting a gradual initiation of fibrosis with prolonged ischemia. Based on these findings, we measured the COL1α2 level in endothelial cells, indicating that endothelial cells could be involved in the post-ischemic myocardial fibrosis processes and that the administration of antiplatelet agents would attenuate the degree of fibrosis.

Thrombospondin-1 (TSP-1 or THBS-1) is a significant component of platelet granules and a thrombin-sensitive ECM glycoprotein (McLaughlin et al., 2005), that produces adaptive ER stress through interaction with activating transcription factor 6α (ATF6α). Increased expression of TSP-1 has been reported to be associated with thrombosis (Vallejo et al., 2000), which is significantly elevated in large vessels with atherosclerotic lesions (Smadja et al., 2011), peripheral arterial diseases (Huang et al., 2015), as well as AMI (Abdelmonem et al., 2017). The pathophysiological mechanisms may include upregulation of platelet aggregation, adhesion of endothelial cells and leukocytes (Narizhneva et al., 2004), chemotaxis and proliferation of VSMCs (McLaughlin et al., 2005; Krishna and Golledge, 2013), reduction of the physiological protective effects of nitric oxide (NO) (Rogers et al., 2014), impact on angiogenesis, and expression of cell adhesion factors that play crucial roles in inflammation and atherosclerosis (Krieglstein and Granger, 2001). Studies have shown that thrombin can not only induce platelet activation and regulate TSP-1 by releasing granules but also modulate the expression of TSP-1 in endothelial cells (McLaughlin et al., 2005). Yang Xiang et al. (Xiang et al., 2022) found that elevated levels of TSP-1 and BNP in patients with chronic heart failure and TSP-1 expression were significantly correlated with alterations in cardiac functions. Our study revealed that the TSP-1 mRNA level was significantly elevated in the OGD treatment. However, there was no overexpression of TSP-1 in the serum of AMI patients. Further expansion of sample size and refinement of blood sampling time may lead to more objective experimental results. Nevertheless, the expression of TSP-1 was positively correlated with the serum levels of BDNF and NT-proBNP. In summary, TSP-1 might not only be related to plaque formation but also play an essential role in heart failure and may also have a mechanistic connection with TSP-1 expression in promoting the release of tumor necrosis factor-alpha (TNF-α) from macrophages (Lopez-Dee et al., 2011; Li et al., 2013).

Furthermore, among the validated hub gene products, MYC binds to the VEGFA promoter region to activate VEGFA expression and subsequent sprouting of angiogenesis (Shi et al., 2014). Studies in tumor tissues have indicated that CD44 plays a role as a cell surface receptor in processes like cell-cell interaction, adhesion, and migration, thereby facilitating the sensing and immune response to pathological lesions in the tumor microenvironment (Yoshida et al., 2012). CCL2 may be involved in the recruitment of monocytes into the arterial wall during the progression of atherosclerosis (Li et al., 1993). GNAQ (a G-protein subunit alpha q) is required for platelet activation, and its mutation in endothelial cells leads to capillary malformations (Couto et al., 2016). ETS1, as a transcription factor,

can regulate angiogenesis by modulating the expression of genes controlling endothelial cell migration and invasion (Yordy et al., 2005). Semaphorin 6A (SEMA6A), as a cell surface receptor for PLXNA2, plays an important role in cell-cell signaling as well as promotes the reorganization of the actin cytoskeleton (Perez-Branguli et al., 2016). TIMP metallopeptidase inhibitor 3 (TIMP3) is an antagonist of the matrix metalloproteinases, a group of peptidases involved in the degradation of the ECM. TIMP3 was reduced in various cardiovascular diseases, and study had shown that TIMP3 replenishment ameliorates the disease, suggesting a therapeutic potential for TIMP3 in cardiovascular diseases (Fan and Kassiri, 2020). Nerve growth factor receptor (NGFR), also known as TNF receptor superfamily member 16 (TNFRSF16), binds to BDNF (Tapia-Arancibia et al., 2004). Lumican (LUM), membrane metalloendopeptidase (MME), G protein subunit alpha i1 (GNAI1), interferon-induced protein with tetratricopeptide repeats (1IFIT1), LDL receptor-related protein 5 (LRP5), and Meis homeobox 1 (MEIS1) was barely studied in the ischemic-hypoxic endothelial cells or AMI, even though qRT-PCR confirmed that the expressions of *NGFR*, *LUM*, *SEMA6A*, *GNAI1*, and *IFIT1* were relatively lower. Specific roles played by these factors and the regulatory pathways in the OGD-treated HUVECs can further be investigated *in vivo* models.

Our study focused on the importance of endothelial cells in AMI, aimed to establish the potential causal chain of the causal factor (DNA methylation) - mediator (mRNA)—cell outcome (endothelial cell ischemic-hypoxic injury)-clinical outcome (AMI), and the findings laid a solid foundation for screening essential diagnostic and prognostic biomarkers of coronary endothelial cell injury of AMI. Secondly, we combined the sequencing results from *in vitro* cell experiments with clinical samples to demonstrate the feasibility of cellular assay screening and *in vivo* validation. Furthermore, our study provided the first evidence that during ischemia and hypoxia, the expression of BNDF was regulated by DNA methylation in endothelial cells and elevated in peripheral blood. Our study also had some shortcomings that were worth improving. Firstly, Hi-C experiments should be employed to elucidate the genes associated with DNA methylation based on the physical interaction. Moreover, the lack of validation regarding the specific pivotal role of BDNF, is a question we need to address. Last but not least, the clinical significance of the screened target proteins could be further explored by drawing blood from the coronary circulation before and after the primary PCI in the future.

Data availability statement

The data generated in this study, including RNA-seq and DNA methylation chip are deposited at https://www.ncbi.nlm.nih.gov/bioproject/PRJNA1035287 and https://www.ncbi.nlm.nih.gov/bioproject/PRJNA934412.

Ethics statement

The studies involving humans were approved by the Ethics Committee of the First Hospital of Lanzhou University (Approval No. LDYYLL-2023-42). The studies were conducted in accordance with the local legislation and institutional requirements. The ethics committee/institutional review board waived the requirement of written informed consent for participation from the participants or the participants' legal guardians/next of kin because the peripheral blood used in this study was the remaining material from preoperative blood tests required for patients, and this study has no adverse or beneficial effects on the patients, it is an observational study.

Author contributions

YT: Methodology, Validation, Writing–original draft, Writing–review and editing. YT: Conceptualization, Project administration, Writing–original draft. SW: Data curation, Visualization, Writing–original draft. RW: Data curation, Investigation, Writing–original draft. JX: Investigation, Software, Writing–original draft. YP: Project administration, Resources, Writing–original draft. LD: Validation, Writing–original draft. JZ: Formal Analysis, Validation, Writing–original draft. GZ: Data curation, Validation, Writing–original draft. SS: Resources, Writing–original draft. ZZ: Conceptualization, Funding acquisition, Project administration, Resources, Supervision, Writing–review and editing.

Funding

The author(s) declare financial support was received for the research, authorship, and/or publication of this article. This work was supported by the Gansu Provincial Youth Science and Technology Fund Program (No.21JR7RA423), Gansu Provincial Clinical Research Center for Cardiovascular Diseases (No. 18JR2FA005), Gansu Provincial Higher Education Innovation Fund (2021B-059), Lanzhou Science and Technology Plan Project (2023-2-42) and Lanzhou Science and Technology Plan Project (2023-2-45).

Conflict of interest

The authors declare that the research was conducted in the absence of any commercial or financial relationships that could be construed as a potential conflict of interest.

Publisher's note

Supplementary material

The Supplementary Material for this article can be found online at: https://www.frontiersin.org/articles/10.3389/fgene.2023.1293393/full#supplementary-material

References

Abdelmonem, N. A., Turky, N. O., Hashad, I. M., Abdel Rahman, M. F., El-Etriby, A., and Gad, M. Z. (2017). Association of thrombospondin-1 (N700S) and thrombospondin-4 (A387P) gene polymorphisms with the incidence of acute myocardial infarction in Egyptians. *Curr. Pharm. Biotechnol.* 18 (13), 1078–1087. doi:10.2174/1389201019666180115144028

Afzali, M., Nakhaee, A., Tabatabaei, S. P., Tirgar-Fakheri, K., and Hashemi, M. (2013). Aberrant promoter methylation profile of Niemann-pick type C1 gene in cardiovascular disease. *Iran. Biomed. J.* 17 (2), 77–83. doi:10.6091/ibj.11432.2013

Baldea, I., Teacoe, I., Olteanu, D. E., Vaida-Voievod, C., Clichici, A., Sirbu, A., et al. (2018). Effects of different hypoxia degrees on endothelial cell cultures-Time course study. *Mech. Ageing Dev.* 172, 45–50. doi:10.1016/j.mad.2017.11.003

Baumann, B., Hayashida, T., Liang, X., and Schnaper, H. W. (2016). Hypoxia-inducible factor-1α promotes glomerulosclerosis and regulates COL1A2 expression through interactions with Smad3. *Kidney Int.* 90 (4), 797–808. doi:10.1016/j.kint.2016.05.026

Bibikova, M., and Fan, J. B. (2010). Genome-wide DNA methylation profiling. *Wiley Interdiscip. Rev. Syst. Biol. Med.* 2 (2), 210–223. doi:10.1002/wsbm.35

Buchsbaum, D. J., Zhou, T., and Lobuglio, A. F. (2006). TRAIL receptor-targeted therapy. *Future Oncol.* 2 (4), 493–508. doi:10.2217/14796694.2.4.493

Cochain, C., Channon, K. M., and Silvestre, J. S. (2013). Angiogenesis in the infarcted myocardium. *Antioxid. Redox Signal* 18 (9), 1100–1113. doi:10.1089/ars.2012.4849

Couto, J. A., Huang, L., Vivero, M. P., Kamitaki, N., Maclellan, R. A., Mulliken, J. B., et al. (2016). Endothelial cells from capillary malformations are enriched for somatic GNAQ mutations. *Plast. Reconstr. Surg.* 137 (1), 77e–82e. doi:10.1097/PRS.0000000000001868

Das, F., Ghosh-Choudhury, N., Maity, S., Kasinath, B. S., and Choudhury, G. G. (2022). Oncoprotein DJ-1 interacts with mTOR complexes to effect transcription factor Hif1α-dependent expression of collagen I (α2) during renal fibrosis. *J. Biol. Chem.* 298 (9), 102246. doi:10.1016/j.jbc.2022.102246

Donovan, M. J., Lin, M. I., Wiegn, P., Ringstedt, T., Kraemer, R., Hahn, R., et al. (2000). Brain derived neurotrophic factor is an endothelial cell survival factor required for intramyocardial vessel stabilization. *Development* 127 (21), 4531–4540. doi:10.1242/dev.127.21.4531

Dube, K. N., Thomas, T. M., Munshaw, S., Rohling, M., Riley, P. R., and Smart, N. (2017). Recapitulation of developmental mechanisms to revascularize the ischemic heart. *JCI Insight* 2 (22), e96800. doi:10.1172/jci.insight.96800

Ejiri, J., Inoue, N., Kobayashi, S., Shiraki, R., Otsui, K., Honjo, T., et al. (2005). Possible role of brain-derived neurotrophic factor in the pathogenesis of coronary artery disease. *Circulation* 112 (14), 2114–2120. doi:10.1161/CIRCULATIONAHA.104.476903

Fan, D., and Kassiri, Z. (2020). Biology of tissue inhibitor of metalloproteinase 3 (TIMP3), and its therapeutic implications in cardiovascular pathology. *Front. Physiol.* 11, 661. doi:10.3389/fphys.2020.00661

Farmer, C. A., Thurm, A. E., Honnekeri, B., Kim, P., Swedo, S. E., and Han, J. C. (2021). The contribution of platelets to peripheral BDNF elevation in children with autism spectrum disorder. *Sci. Rep.* 11 (1), 18158. doi:10.1038/s41598-021-97367-4

Gimbrone, M. A., Jr., and Garcia-Cardena, G. (2016). Endothelial cell dysfunction and the pathobiology of atherosclerosis. *Circ. Res.* 118 (4), 620–636. doi:10.1161/CIRCRESAHA.115.306301

Guo, W., Feng, W., Huang, J., Zhang, J., Fan, X., Ma, S., et al. (2021). Supramolecular self-assembled nanofibers efficiently activate the precursor of hepatocyte growth factor for angiogenesis in myocardial infarction therapy. *ACS Appl. Mater Interfaces* 13 (19), 22131–22141. doi:10.1021/acsami.0c23153

Huang, C. L., Jong, Y. S., Wu, Y. W., Wang, W. J., Hsieh, A. R., Chao, C. L., et al. (2015). Association of plasma thrombospondin-1 level with cardiovascular disease and mortality in hemodialysis patients. *Acta Cardiol. Sin.* 31 (2), 113–119. doi:10.6515/acs20140630d

Huang, K., Zhang, X., Duan, J., Wang, R., Wu, Z., Yang, C., et al. (2022). STAT4 and COL1A2 are potential diagnostic biomarkers and therapeutic targets for heart failure comorbided with depression. *Brain Res. Bull.* 184, 68–75. doi:10.1016/j.brainresbull.2022.03.014

Kadowaki, S., Shishido, T., Honda, Y., Narumi, T., Otaki, Y., Kinoshita, D., et al. (2016). Additive clinical value of serum brain-derived neurotrophic factor for prediction of chronic heart failure outcome. *Heart Vessels* 31 (4), 535–544. doi:10.1007/s00380-015-0628-6

Kim, J. M., Stewart, R., Kang, H. J., Bae, K. Y., Kim, S. W., Shin, I. S., et al. (2015). BDNF methylation and depressive disorder in acute coronary syndrome: the K-DEPACS and EsDEPACS studies. *Psychoneuroendocrinology* 62, 159–165. doi:10.1016/j.psyneuen.2015.08.013

Krieglstein, C. F., and Granger, D. N. (2001). Adhesion molecules and their role in vascular disease. *Am. J. Hypertens.* 14, 44S-54S. doi:10.1016/s0895-7061(01)02069-6

Krishna, S. M., and Golledge, J. (2013). The role of thrombospondin-1 in cardiovascular health and pathology. *Int. J. Cardiol.* 168 (2), 692–706. doi:10.1016/j.ijcard.2013.04.139

Li, J., Zhu, X., Yu, K., Jiang, H., Zhang, Y., Deng, S., et al. (2017). Genome-wide analysis of DNA methylation and acute coronary syndrome. *Circ. Res.* 120 (11), 1754–1767. doi:10.1161/CIRCRESAHA.116.310324

Li, J. H., Kirkiles-Smith, N. C., McNiff, J. M., and Pober, J. S. (2003). TRAIL induces apoptosis and inflammatory gene expression in human endothelial cells. *J. Immunol.* 171 (3), 1526–1533. doi:10.4049/jimmunol.171.3.1526

Li, Y., Liu, Y., Strickland, F. M., and Richardson, B. (2010). Age-dependent decreases in DNA methyltransferase levels and low transmethylation micronutrient levels synergize to promote overexpression of genes implicated in autoimmunity and acute coronary syndromes. *Exp. Gerontol.* 45 (4), 312–322. doi:10.1016/j.exger.2009.12.008

Li, Y., Qi, X., Tong, X., and Wang, S. (2013). Thrombospondin 1 activates the macrophage Toll-like receptor 4 pathway. *Cell. Mol. Immunol.* 10 (6), 506–512. doi:10.1038/cmi.2013.32

Li, Y. S., Shyy, Y. J., Wright, J. G., Valente, A. J., Cornhill, J. F., and Kolattukudy, P. E. (1993). The expression of monocyte chemotactic protein (MCP-1) in human vascular endothelium *in vitro* and *in vivo*. *Mol. Cell. Biochem.* 126 (1), 61–68. doi:10.1007/BF01772208

Li, Z., Solomonidis, E. G., Meloni, M., Taylor, R. S., Duffin, R., Dobie, R., et al. (2019). Single-cell transcriptome analyses reveal novel targets modulating cardiac neovascularization by resident endothelial cells following myocardial infarction. *Eur. Heart J.* 40 (30), 2507–2520. doi:10.1093/eurheartj/ehz305

Liu, S., Chen, J., Shi, J., Zhou, W., Wang, L., Fang, W., et al. (2020). M1-like macrophage-derived exosomes suppress angiogenesis and exacerbate cardiac dysfunction in a myocardial infarction microenvironment. *Basic Res. Cardiol.* 115 (2), 22. doi:10.1007/s00395-020-0781-7

Long, P., Wang, Q., Zhang, Y., Zhu, X., Yu, K., Jiang, H., et al. (2021). Profile of copper-associated DNA methylation and its association with incident acute coronary syndrome. *Clin. Epigenetics* 13 (1), 19. doi:10.1186/s13148-021-01004-w

Lopez-Dee, Z., Pidcock, K., and Gutierrez, L. S. (2011). Thrombospondin-1: multiple paths to inflammation. *Mediat. Inflamm.* 2011, 296069. doi:10.1155/2011/296069

Loyer, X., Zlatanova, I., Devue, C., Yin, M., Howangyin, K. Y., Klaihmon, P., et al. (2018). Intra-cardiac release of extracellular vesicles shapes inflammation following myocardial infarction. *Circ. Res.* 123 (1), 100–106. doi:10.1161/CIRCRESAHA.117.311326

Lu, C. X., Xu, R. D., Cao, M., Wang, G., Yan, F. Q., Shang, S. S., et al. (2013). FOXP3 demethylation as a means of identifying quantitative defects in regulatory T cells in acute coronary syndrome. *Atherosclerosis* 229 (1), 263–270. doi:10.1016/j.atherosclerosis.2013.05.007

Lunemann, J. D., Waiczies, S., Ehrlich, S., Wendling, U., Seeger, B., Kamradt, T., et al. (2002). Death ligand TRAIL induces no apoptosis but inhibits activation of human (auto)antigen-specific T cells. *J. Immunol.* 168 (10), 4881–4888. doi:10.4049/jimmunol.168.10.4881

Manni, L., Nikolova, V., Vyagova, D., Chaldakov, G. N., and Aloe, L. (2005). Reduced plasma levels of NGF and BDNF in patients with acute coronary syndromes. *Int. J. Cardiol.* 102 (1), 169–171. doi:10.1016/j.ijcard.2004.10.041

McLaughlin, J. N., Mazzoni, M. R., Cleator, J. H., Earls, L., Perdigoto, A. L., Brooks, J. D., et al. (2005). Thrombin modulates the expression of a set of genes including thrombospondin-1 in human microvascular endothelial cells. *J. Biol. Chem.* 280 (23), 22172–22180. doi:10.1074/jbc.M500721200

Mendelson, M. M., Johannes, R., Liu, C., Huan, T., Yao, C., Miao, X., et al. (2018). Epigenome-wide association study of soluble tumor necrosis factor receptor 2 levels in the framingham heart study. *Front. Pharmacol.* 9, 207. doi:10.3389/fphar.2018.00207

Nakajima, H., Yanase, N., Oshima, K., Sasame, A., Hara, T., Fukazawa, S., et al. (2003). Enhanced expression of the apoptosis inducing ligand TRAIL in mononuclear cells after myocardial infarction. *Jpn. Heart J.* 44 (6), 833–844. doi:10.1536/jhj.44.833

Narizhneva, N. V., Byers-Ward, V. J., Quinn, M. J., Zidar, F. J., Plow, E. F., Topol, E. J., et al. (2004). Molecular and functional differences induced in thrombospondin-1 by the single nucleotide polymorphism associated with the risk of premature, familial myocardial infarction. *J. Biol. Chem.* 279 (20), 21651–21657. doi:10.1074/jbc.M311090200

Norman, J. T., Clark, I. M., and Garcia, P. L. (2000). Hypoxia promotes fibrogenesis in human renal fibroblasts. *Kidney Int.* 58 (6), 2351–2366. doi:10.1046/j.1523-1755.2000.00419.x

Osmancik, P., Teringova, E., Tousek, P., Paulu, P., and Widimsky, P. (2013). Prognostic value of TNF-related apoptosis inducing ligand (TRAIL) in acute coronary syndrome patients. *PLoS One* 8 (2), e53860. doi:10.1371/journal.pone.0053860

Pan, X., Chen, X., Ren, Q., Yue, L., Niu, S., Li, Z., et al. (2022). Single-cell transcriptomics identifies Col1a1 and Col1a2 as hub genes in obesity-induced cardiac fibrosis. *Biochem. Biophys. Res. Commun.* 618, 30–37. doi:10.1016/j.bbrc.2022.06.018

Park, S. H., Lee, S. Y., and Kim, S. A. (2021). Mitochondrial DNA methylation is higher in acute coronary syndrome than in stable coronary artery disease. *Vivo* 35 (1), 181–189. doi:10.21873/invivo.12247

Perez-Branguli, F., Zagar, Y., Shanley, D. K., Graef, I. A., Chedotal, A., and Mitchell, K. J. (2016). Reverse signaling by semaphorin-6A regulates cellular aggregation and neuronal morphology. *PLoS One* 11 (7), e0158686. doi:10.1371/journal.pone.0158686

Persky, A. M., Green, P. S., Stubley, L., Howell, C. O., Zaulyanov, L., Brazeau, G. A., et al. (2000). Protective effect of estrogens against oxidative damage to heart and skeletal muscle *in vivo* and *in vitro*. *Proc. Soc. Exp. Biol. Med.* 223 (1), 59–66. doi:10.1046/j.1525-1373.2000.22308.x

Pinto, A. R., Ilinykh, A., Ivey, M. J., Kuwabara, J. T., D'Antoni, M. L., Debuque, R., et al. (2016). Revisiting cardiac cellular composition. *Circ. Res.* 118 (3), 400–409. doi:10.1161/CIRCRESAHA.115.307778

Pius-Sadowska, E., and Machalinski, B. (2017). BDNF - a key player in cardiovascular system. *J. Mol. Cell. Cardiol.* 110, 54–60. doi:10.1016/j.yjmcc.2017.07.007

Razin, A., Webb, C., Szyf, M., Yisraeli, J., Rosenthal, A., Naveh-Many, T., et al. (1984). Variations in DNA methylation during mouse cell differentiation *in vivo* and *in vitro*. *Proc. Natl. Acad. Sci. U. S. A.* 81 (8), 2275–2279. doi:10.1073/pnas.81.8.2275

Rogers, N. M., Sharifi-Sanjani, M., Csanyi, G., Pagano, P. J., and Isenberg, J. S. (2014). Thrombospondin-1 and CD47 regulation of cardiac, pulmonary and vascular responses in health and disease. *Matrix Biol.* 37, 92–101. doi:10.1016/j.matbio.2014.01.002

Schiano, C., Balbi, C., Burrello, J., Ruocco, A., Infante, T., Fiorito, C., et al. (2022). *De novo* DNA methylation induced by circulating extracellular vesicles from acute coronary syndrome patients. *Atherosclerosis* 354, 41–52. doi:10.1016/j.atherosclerosis.2022.06.1026

Secchiero, P., Corallini, F., Ceconi, C., Parrinello, G., Volpato, S., Ferrari, R., et al. (2009). Potential prognostic significance of decreased serum levels of TRAIL after acute myocardial infarction. *PLoS One* 4 (2), e4442. doi:10.1371/journal.pone.0004442

Segers, V. F. M., Brutsaert, D. L., and De Keulenaer, G. W. (2018). Cardiac remodeling: endothelial cells have more to say than just NO. *Front. Physiol.* 9, 382. doi:10.3389/fphys.2018.00382

Shi, Y., Xu, X., Zhang, Q., Fu, G., Mo, Z., Wang, G. S., et al. (2014). tRNA synthetase counteracts c-Myc to develop functional vasculature. *Elife* 3, e02349. doi:10.7554/eLife.02349

Smadja, D. M., d'Audigier, C., Bieche, I., Evrard, S., Mauge, L., Dias, J. V., et al. (2011). Thrombospondin-1 is a plasmatic marker of peripheral arterial disease that modulates endothelial progenitor cell angiogenic properties. *Arterioscler. Thromb. Vasc. Biol.* 31 (3), 551–559. doi:10.1161/ATVBAHA.110.220624

Soares, F. C. S., Amorim, E. A. S., Araujo, R. M., Werkhauser, R. P., Diniz, G. T. N., Carvalho, V., et al. (2020). Evaluation of the influence of global DNA methylation level in patients with acute coronary syndrome. *Clin. Chim. Acta* 511, 336–341. doi:10.1016/j.cca.2020.10.016

Szklarczyk, D., Gable, A. L., Lyon, D., Junge, A., Wyder, S., Huerta-Cepas, J., et al. (2019). STRING v11: protein-protein association networks with increased coverage, supporting functional discovery in genome-wide experimental datasets. *Nucleic Acids Res.* 47 (D1), D607–D613. doi:10.1093/nar/gky1131

Szklarczyk, D., Morris, J. H., Cook, H., Kuhn, M., Wyder, S., Simonovic, M., et al. (2017). The STRING database in 2017: quality-controlled protein-protein association networks, made broadly accessible. *Nucleic Acids Res.* 45 (D1), D362-D368–D368. doi:10.1093/nar/gkw937

Tang, J., Zhang, H., He, L., Huang, X., Li, Y., Pu, W., et al. (2018). Genetic fate mapping defines the vascular potential of endocardial cells in the adult heart. *Circ. Res.* 122 (7), 984–993. doi:10.1161/CIRCRESAHA.117.312354

Tapia-Arancibia, L., Rage, F., Givalois, L., and Arancibia, S. (2004). Physiology of BDNF: focus on hypothalamic function. *Front. Neuroendocrinol.* 25 (2), 77–107. doi:10.1016/j.yfrne.2004.04.001

Teringova, E., Kozel, M., Knot, J., Kocka, V., Benesova, K., and Tousek, P. (2018). Relationship between TRAIL and left ventricular ejection fraction in patients with ST-elevation myocardial infarction treated with primary percutaneous coronary intervention. *Biomed. Res. Int.* 2018, 3709084. doi:10.1155/2018/3709084

Vallejo, A. N., Mugge, L. O., Klimiuk, P. A., Weyand, C. M., and Goronzy, J. J. (2000). Central role of thrombospondin-1 in the activation and clonal expansion of inflammatory T cells. *J. Immunol.* 164 (6), 2947–2954. doi:10.4049/jimmunol.164.6.2947

Virani, S. S., Alonso, A., Benjamin, E. J., Bittencourt, M. S., Callaway, C. W., Carson, A. P., et al. (2020). Heart disease and stroke statistics-2020 update: a report from the American heart association. *Circulation* 141 (9), e139–e596. doi:10.1161/CIR.0000000000000757

von Kanel, T., and Huber, A. R. (2013). DNA methylation analysis. *Swiss Med. Wkly.* 143, w13799. doi:10.4414/smw.2013.13799

Wang, D., Lv, L., Xu, Y., Jiang, K., Chen, F., Qian, J., et al. (2021a). Cardioprotection of Panax Notoginseng saponins against acute myocardial infarction and heart failure through inducing autophagy. *Biomed. Pharmacother.* 136, 111287. doi:10.1016/j.biopha.2021.111287

Wang, S., Sun, K., Hu, H., Jin, X., Wang, Z., Zhang, H., et al. (2021b). MiR-1297 attenuates high glucose-induced injury in HK-2 cells via targeting COL1A2. *Nephrol. Carlt.* 26 (7), 623–631. doi:10.1111/nep.13881

Wu, H., Cao, G., Wang, Y., Tian, H., and Du, R. (2019). Increased serum CA125 and brain-derived neurotrophic factor (BDNF) levels on acute myocardial infarction: a predictor for acute heart failure. *Med. Sci. Monit.* 25, 913–919. doi:10.12659/MSM.912642

Wu, J. W., Hu, H., Hua, J. S., and Ma, L. K. (2022). ATPase inhibitory factor 1 protects the heart from acute myocardial ischemia/reperfusion injury through activating AMPK signaling pathway. *Int. J. Biol. Sci.* 18 (2), 731–741. doi:10.7150/ijbs.64956

Wu, S. S., Lin, X., Yuan, L. Q., and Liao, E. Y. (2015). The role of epigenetics in arterial calcification. *Biomed. Res. Int.* 2015, 320849. doi:10.1155/2015/320849

Wu, X., Reboll, M. R., Korf-Klingebiel, M., and Wollert, K. C. (2021). Angiogenesis after acute myocardial infarction. *Cardiovasc Res.* 117 (5), 1257–1273. doi:10.1093/cvr/cvaa287

Xiang, Y., Zhang, Z., Xie, C., Wang, L., Wu, Y., Zhan, Y., et al. (2022). Serum cat S, TSP-1, IL-11, BNP and sST2 diagnostic and prognostic value in chronic heart failure. *Altern. Ther. Health Med.* 28 (4), 55–59.

Xiao, M., Lu, D., Tian, J., Yu, Y., Zhang, Q., Zhang, L., et al. (2020). The protective effects of GLP-1 receptor agonist lixisenatide on oxygen-glucose deprivation/reperfusion (OGD/R)-induced deregulation of endothelial tube formation. *RSC Adv.* 10 (17), 10245–10253. doi:10.1039/c9ra09959j

Xu, H., Shen, Y., Liang, C., Wang, H., Huang, J., Xue, P., et al. (2021). Inhibition of the mevalonate pathway improves myocardial fibrosis. *Exp. Ther. Med.* 21 (3), 224. doi:10.3892/etm.2021.9655

Yang, Q., He, G. W., Underwood, M. J., and Yu, C. M. (2016). Cellular and molecular mechanisms of endothelial ischemia/reperfusion injury: perspectives and implications for postischemic myocardial protection. *Am. J. Transl. Res.* 8 (2), 765–777.

Yang, Z. F., Ho, D. W., Lau, C. K., Tam, K. H., Lam, C. T., Yu, W. C., et al. (2006). Significance of the serum brain-derived neurotrophic factor and platelets in hepatocellular carcinoma. *Oncol. Rep.* 16 (6), 1237–1243. doi:10.3892/or.16.6.1237

Yordy, J. S., Moussa, O., Pei, H., Chaussabel, D., Li, R., and Watson, D. K. (2005). SP100 inhibits ETS1 activity in primary endothelial cells. *Oncogene* 24 (5), 916–931. doi:10.1038/sj.onc.1208245

Yoshida, T., Matsuda, Y., Naito, Z., and Ishiwata, T. (2012). CD44 in human glioma correlates with histopathological grade and cell migration. *Pathol. Int.* 62 (7), 463–470. doi:10.1111/j.1440-1827.2012.02823.x

Zhang, Y., Li, C., Pei, Y., Zheng, L., Sun, X., Zhao, Z., et al. (2021). Trelagliptin ameliorates oxygen-glucose deprivation/reperfusion (OGD/R)-induced mitochondrial dysfunction and metabolic disturbance of endothelial cells. *Hum. Cell.* 34 (6), 1717–1726. doi:10.1007/s13577-021-00594-0

Zhou, B., Honor, L. B., He, H., Ma, Q., Oh, J. H., Butterfield, C., et al. (2011). Adult mouse epicardium modulates myocardial injury by secreting paracrine factors. *J. Clin. Invest.* 121 (5), 1894–1904. doi:10.1172/JCI45529

Zhu, H., Wu, L. F., Mo, X. B., Lu, X., Tang, H., Zhu, X. W., et al. (2019). Rheumatoid arthritis-associated DNA methylation sites in peripheral blood mononuclear cells. *Ann. Rheum. Dis.* 78 (1), 36–42. doi:10.1136/annrheumdis-2018-213970

frontiers | Frontiers in Cell and Developmental Biology

TYPE Original Research
PUBLISHED 16 January 2024
DOI 10.3389/fcell.2024.1276288

OPEN ACCESS

EDITED BY
Hongsong Zhang,
Nanjing Medical University, China

REVIEWED BY
Wieslawa Lesniak,
Polish Academy of Sciences, Poland
Peichang Wang,
Capital Medical University, China

*CORRESPONDENCE
Yi Zhang,
zhangyi@pzhu.edu.cn

RECEIVED 11 August 2023
ACCEPTED 05 January 2024
PUBLISHED 16 January 2024

CITATION
Zhang Y and Shen S (2024), Epigenome-wide DNA methylation analysis of late-stage mild cognitive impairment.
Front. Cell Dev. Biol. 12:1276288.
doi: 10.3389/fcell.2024.1276288

Epigenome-wide DNA methylation analysis of late-stage mild cognitive impairment

Yi Zhang* and Shasha Shen

Institute of Neuroscience, Panzhihua University, Panzhihua, China

Background: Patients with late-stage mild cognitive impairment (LMCI) have a higher risk of progression to Alzheimer's disease (AD) than those with early-stage mild cognitive impairment (EMCI). However, previous studies have often pooled EMCI and LMCI patients into a single MCI group, with limited independent investigation into the pathogenesis of LMCI.

Methods: In this study, we employed whole-genome methylation association analysis to determine the differences in peripheral blood methylation profiles between 663 cognitive aging (CN) and 554 LMCI patients.

Results: Our results revealed 2,333 differentially methylated probes (DMPs) and 85 differentially methylated regions (DMRs) specific to LMCI. The top hit methylation sites or regions were associated with genes such as SNED1, histone deacetylases coding gene HDACs, and HOX and ZNF gene family. The DNA methylations upregulated the expression of HDAC4, HDAC8, and HOX family genes HOXC5 and HOXC9, but they downregulated the expression of SNED1, ADCYAP1, and ZNF family genes ZNF415 and ZNF502. Gene Ontology (GO) and KEGG analysis showed that the genes associated with these methylation sites were predominantly related to the processes of addiction disorders, neurotransmission, and neurogenesis. Out of the 554 LMCI patients included in this study, 358 subjects (65%) had progressed to AD. Further association analysis between the LMCI subjects with a stable course (sLMCI) and those who progressed to AD (pLMCI) indicated that the methylation signal intensities of HDAC6, ZNF502, HOXC5, HOXC6, and HOXD8 were associated with increased susceptibility to AD. Protective effects against progression to AD were noticed when the methylation of SNED1 and ZNF727 appeared in LMCI patients.

Conclusion: Our findings highlight a substantial number of LMCI-specific methylated biomarkers that differ from those identified in previous MCI case–control studies. These biomarkers have the potential to contribute to a better understanding of the pathogenesis of LMCI.

KEYWORDS

EWAS, LMCI, methylation, blood, Alzheimer's disease

1 Introduction

Mild cognitive impairment (MCI) is a complex and heterogeneous condition between normal cognitive aging (CN) and dementia, specifically Alzheimer's disease (AD) (Petersen et al., 2001; McGirr et al., 2022). Patients with MCI have memory complaints and objective memory impairment that is abnormal for their age, while their general cognitive function

remains relatively preserved, enabling them to perform everyday activities independently (Petersen, 2004; Chen et al., 2022). MCI can be subcategorized into early-stage MCI (EMCI) and late-stage MCI (LMCI), where LMCI is accompanied by more severe memory decline in cognitive domains, such as language, executive function, and visuospatial skills (Aisen et al., 2010; Zhang et al., 2019). It has been reported that approximately 10%–15% of patients each year, MCI progresses to AD, and 75% of such individuals have LMCI (Petersen et al., 2001; Farias et al., 2009; Jessen et al., 2014; Tábuas-Pereira et al., 2016). Therefore, the early recognition of MCI, especially LMCI, is essential for preventing AD.

Epigenetic changes in the central nervous system (CNS) and peripheral blood have widely been used for the early diagnosis of MCI and AD (Lunnon et al., 2014; Madrid et al., 2018; Roubroeks et al., 2020; Vasanthakumar et al., 2020; Li et al., 2021). These changes reflect potential immune system disorders, altered proteostasis, neuronal decay, and changes in brain structure that are associated with the disease (Lunnon et al., 2014; Madrid et al., 2018; Roubroeks et al., 2020; Vasanthakumar et al., 2020; Li et al., 2021). However, most studies have pooled patients with EMCI and LMCI into a single MCI group, which may obscure the different disease progression risks between these two subgroups (Zhang et al., 2019; Vasanthakumar et al., 2020; Li et al., 2021). Given that the risk of conversion to AD is higher for LMCI than for EMCI (36% vs. 15%) (Jessen et al., 2014), identifying epigenetic biomarkers specific to LMCI can be more beneficial in reducing the incidence of AD and improving the effectiveness of rehabilitation exercises and medication. In this study, we compared the peripheral blood methylome of CN individuals and LMCI patients. We revealed a significant number of LMCI-specific methylated biomarkers, which differ from those identified in previous MCI case–control studies. These biomarkers may help to elucidate the pathogenesis of LMCI.

2 Materials and methods

2.1 Subjects

The data utilized in this study were sourced from the Alzheimer's Disease Neuroimaging Initiative (ADNI) database. The ADNI is a multicenter, longitudinal study encompassing approximately 50 sites across the United States and Canada, and it was initiated in 2003 with the primary aim of monitoring the progression of AD through the use of clinical and cognitive assessments, magnetic resonance imaging (MRI), fludeoxyglucose positron emission tomography (PET), amyloid PET, cerebrospinal fluid analysis, and blood biomarker analysis. For the purposes of ADNI research, a total of 1,720 samples from 653 individuals who participated in two phases of ADNI (ADNI2 and ADNIGO) were selected for DNA methylation analysis. These samples were randomized using a modified incomplete balanced block design, in which all of the samples from a single subject were placed on the same chip, while the remaining space on the chip was filled with age-matched samples from a subject of the opposite sex with a different diagnosis.

Amnestic MCI was defined in accordance with the diagnostic criteria established by ADNI as detailed in the ADNI protocol (http://adni.loni.usc.edu/methods/documents/). Specifically, the criteria were as follows: a) a score of 24–30 on the Mini-Mental State Examination (MMSE); b) a self-reported memory complaint, as well as objective evidence of memory loss as measured by education-adjusted scores on the Wechsler Memory Scale Logical Memory II; c) a Clinical Dementia Rating (CDR) score of 0.5; and d) the absence of significant impairment in other cognitive domains, as well as the preservation of activities of daily living and the absence of dementia (Jack Jr et al., 2008). MCI was further classified into two subtypes, namely, EMCI and LMCI based on the severity of memory impairment. The criteria for LMCI were the same as those for EMCI, with the exception that the memory impairment on the Logical Memory II subscale had to be more severe. Specifically, the cutoff scores for LMCI were ≤8 for individuals with 16 or more years of education, ≤4 for 8–15 years of education, and ≤2 for 0–7 years of education. The corresponding cutoff scores for EMCI were 9–11 for individuals with 16 or more years of education, 5–9 for 8–15 years of education, and 3–6 for 0–7 years of education (Jack Jr et al., 2008).

The datasets utilized in this study included clinical information and epigenetic data obtained from the ADNI database (http://adni.loni.usc.edu), accessed on 12 June 2021. The methylation profile pertained to 1,220 samples, including 665 individuals with CN status and 555 individuals with LMCI status. Data processing and quality control procedures were performed on the collected data, which resulted in the selection of 663 CN and 554 LMCI samples for downstream analysis.

2.2 Data quality control

The analysis was conducted in accordance with the previously outlined protocol (Fortin et al., 2017; Tian et al., 2017). Specifically, we employed a rigorous quality control and preprocessing approach utilizing the Minfi package from the R software. The detection *p* values (detP) were calculated through the "m + u" method, which compared the total DNA signal (methylated + unmethylated) for each probe to the background signal level. None of the samples had mean detP value higher than 0.05, but three samples were excluded due to a low ratio of unmethylated to methylated sites (uMeth/mMeth), i.e., less than 10.5 (as shown in Supplementary Figure S1). The call rate was determined as the proportion of probes present in each sample. The probes with a detection *p*-value of 0.05 or higher in at least 1% of the samples were filtered out. Finally, a total of 1,217 samples (663 CN and 554 LMCI) comprising 823605 probes were retained for downstream analysis.

2.3 Identification of differentially methylated probes (DMPs)

We performed a probe-wise analysis to identify DMPs using the Bioconductor package limma. To ensure statistical validity, beta values were converted to M-values, which are considered more statistically robust than beta values due to their higher detection rates and true positive rates for both highly methylated and unmethylated CpG sites. The experimental design was modeled as follows: ≈class (disease status) + age + gender + education + DNA source (buffy coat or whole blood) + B cells + CD4 T + CD8 T + Mono + Neu + NK, where the last six terms represent cell type

composition estimations obtained using estimateCellCounts from R Package FlowSorted.Blood.EPIC at default settings. The estimateCellCounts function combined the reference library from FlowSorted.Blood.450K with the target methylation dataset to build the model with cellular deconvolution algorithms for the relative quantification of the proportion of cell types (Houseman et al., 2012; Fortin et al., 2017; Tian et al., 2017). Because the study was prone to significant inflation and bias of test statistics, we applied a Bayesian method based on estimation of the empirical null distribution in the Bioconductor package limma to control for inflation of test statistics and for lambda inflation factors. A stringent threshold using Bonferroni correction was used to declare study-wide significance (adjusted p-value <0.05).

2.4 Identification and annotation of differentially methylated regions (DMRs)

We employed a DMR analysis in the R package DMRcate to identify a group of CpGs associated with LMCI. DMRcate models Gaussian kernel smoothing within a predefined distance (1 kbp in this study) and collapses contiguous significant CpGs ($p < 0.05$) after multiple testing correction. The default algorithm parameters were utilized, which included the following: a) regions with gaps ≥1,000 nucleotides between significant CpG sites were separated; b) regions containing at least two different CpGs within 1 kb with a minimum methylation difference of 10% were included in the analysis. The regions with an adjusted p-value lower than 0.05 from Stouffer's, Harmonic, and Fisher's tests were considered to be significant. Visualization and functional analysis of DMRs were performed by means of the R package coMET.

2.5 Functional analysis of DMPs

Using the missMethyl R package, we performed a generalized gene set enrichment analysis to assess pathway enrichment through a hypergeometric test, which took into account the number of CpG sites per gene on the EPIC array. The analysis included curated gene sets from the KEGG database and Gene Ontology (GO) gene sets related to biological processes, cellular components, and molecular functions. The pathways or terms with a Benjamini–Hochberg false discovery rate (FDR)–corrected p-value lower than 0.05 were considered significant. The ratio values of the number of significantly annotated genes in a particular pathway to the total number of genes in the pathway were calculated.

2.6 Gene expression profile

We utilized the microarray expression data of 318 samples (207 CN, 175 LMCI) in the ADNI cohort to investigate the effect of DNA methylation on the overlapping genes. A total of 28 protein-coding genes (PCGs) overlapping between DMPs or DMRs were included. We processed the raw data based on the standard quality control (QC) procedures described in ADNI (http://adni.loni.usc.edu/methods/documents/). The raw expression values were normalized for differential gene expression (DEG) analysis with the Bioconductor package limma. The model design was similar to the previously described DMP analysis. Specifically, we adjusted for the effect of age, gender, education, DNA source, and cell type compositions. The genes with a Benjamini–Hochberg FDR-corrected p-value lower than 0.05 were considered to be DEGs.

2.7 Serum proteomic profiling

We further employed the serum proteomic profile data of 20 samples (10 with CN, 10 with LMCI) in the ADNI cohort to validate the results of epigenome-wide association studies (EWAS). The data were obtained from the Gene Expression Omnibus (GEO) under accession number GSE74763. Due to the limitation of fluorescence probes for specific proteins, we could only filter out the proteomic data of HDAC4, HDAC6, HDAC8, HOXC5, HOXC6, HOXC9, ZNF415, and ZNF502. The raw data were processed and normalized in line with Invitrogen's standard instructions (www.invitrogen.com/protoarray). One-way ANOVA was used for statistical analysis. Proteins with a Benjamini–Hochberg FDR-corrected p-value lower than 0.05 were considered to be differentially expressed across the groups.

2.8 Association analysis between DMPs and conversion from LMCI to AD

A logistic regression model was built to evaluate the effects of 27 candidate methylation probes on the conversion from LMCI to AD. These DMPs were associated with SNED1, RP11-526P5.2, ADCYAP1, HDACs, and HOX and ZNF gene family (listed in Figure 6; Supplementary Table S12). A total of 554 LMCI subjects, including 196 subjects with a stable course (sLMCI) and 358 subjects who had progressed to AD (pLMCI), were involved in the analysis. The effects of age, gender, education, DNA source, and ApoEε4 alleles were adjusted for in the model. We calculated the odds ratio (OR) and confidence interval of each DMP to assess the effect of DNA methylation on the progression to AD. OR values with p-value lower than 0.05 were considered significant.

Furthermore, we filtered pLMCI subjects and evaluated the association of DMPs with the progression time and cognitive impairment levels. We checked the Pearson correlation coefficients between DMP signal intensity and indicators related with cognitive impairment, such as the scores at the baseline diagnosis with the mini-mental state examination (MMSE), the clinical dementia rating scale sum of boxes (CDRSB), the modified preclinical Alzheimer cognitive composite using digit symbol substitution test (mPACCdigit), and the modified preclinical Alzheimer cognitive composite using trail-making test part B (mPACCtrailsB). Higher MMSE, mPACCdigit, and mPACCtrailsB scores indicate better cognitive function. However, a higher CDRSB score represents more severe cognitive impairment. Correlation coefficients with a p-value lower than 0.05 were considered significant.

Besides, we measured the speed of cognitive decline based on MMSE (MMSE_speed), CDRSB (CDRSB_speed), mPACCdigit (mPACCdigit_speed), and mPACCtrailsB (mPACCtrailsB_speed). The speed scores were calculated as $|\text{Score}_{(\text{first diagnosis as AD})}-\text{Score}$

TABLE 1 Demographic data of the selected ADNI subjects separated by diagnosis group.

Variable	CN	LMCI	*p*-value
N	663	554	
Age	74.77 ± 5.46	73.07 ± 7.22	$3.35E^{-06}$
Education	16.45 ± 2.65	16.01 ± 2.87	$5.20E^{-03}$
Gender (proportion of males)	50.53%	61.55%	$9.99E^{-01}$
Gender (proportion of females)	49.47%	38.45%	
ApoEε4 (proportion of subjects with 0 alleles)	73.30%	45.13%	$9.12E^{-01}$
ApoEε4 (proportion of subjects with 1 alleles)	24.74%	43.68%	
ApoEε4 (proportion of subjects with 2 alleles)	1.96%	11.19%	

ApoEε4, the ε4 allele of the Apolipoprotein E gene; CN, cognitive normal; EMCI, early mild cognitive impairment; LMCI, early mild cognitive impairment; AD, Alzheimer's disease. Data were expressed as mean ± standard error of the mean (SEM). One-way ANOVA, was used for statistical analysis of age and education across groups. Chi-square test was used for statistical analysis of gender and ApoEε4 allele across groups.

$_{\text{(baseline diagnosis as LMCI)}}$|/progression time $_{\text{(months)}}$. Higher MMSE_speed, CDRSB_speed, mPACCdigit_speed, and mPACCtrailsB_speed scores represent greater speeds of cognitive decline. We also calculated the Pearson correlation coefficients between DMP signal intensity and scores of cognitive decline speed. Correlation coefficients with a *p*-value lower than 0.05 were considered significant.

3 Results

3.1 Study participants

The association of DNA methylation with LMCI was analyzed by using the Illumina EPIC array datasets from the ADNI. We filtered three samples that had been lost during processing or excluded during the QC procedure, and we finally kept 1,217 samples for peripheral blood DNA methylation analysis (Table 1; Supplementary Figure S1; Supplementary Table S1). The demographic characteristics and cognitive assessments of the samples used in the comparative analysis are presented in Table 1.

3.2 Alterations of blood cell composition in different groups

Altered blood cell composition has been observed in various neurodegenerative disorders, thus suggesting the possibility of systemic immune perturbations. DNA methylation signals offer a promising approach for estimating the relative abundance of different lymphocyte subpopulations. Compared with the CN cases, the patients with LMCI presented a smaller estimated proportion of B cells and CD8 T cells ($p = 2.75E^{-04}$ and $p = 6.3E^{-06}$, respectively, *t*-test with Wilcoxon *post hoc* test), a higher proportion of neutrophils ($p = 3.87E^{-04}$), and no significant changes in CD4 T cells, monocytes, and natural killer cells (NK) ($p > 0.05$) (Figure 1A). We also evaluated the changes in blood cell composition driven by sex distribution (Figure 1B) and DNA sources (buff coat or whole blood; Figure 1C). Except for CD8 T cells and NK cells, the overall blood composition varied between the male and female groups, where the female cases showed an increased proportion of B cells and CD4 T cells ($p = 1.35E^{-09}$ and $p = 2.78E^{-11}$, respectively, *t*-test with Wilcoxon *post hoc* test), but a reduced proportion of monocytes and neutrophils ($p = 2.76E^{-11}$ and $p = 8.1E^{-05}$, respectively). Previous studies have reported that differences in the storage of the sample used for DNA isolation (buff coat or whole blood) influence the cell composition. However, in our study, the whole-blood samples only demonstrated significant alterations in neutrophils and NK cells compared with the buff-coat samples (Figure 1C), showing increased neutrophils ($p = 9.84E^{-03}$) and reduced NK cells ($p = 2.54E^{-02}$). Moreover, we assessed the effect of APOE4 gene alleles on blood lymphocyte composition. There were significant differences in lymphocyte composition only between individuals with zero alleles and those with one allele ($p < 0.05$; Figure 1D).

3.3 DMPs in LMCI vs. CN

A cross-sectional analysis of blood methylation was performed in LMCI and CN cases. Linear regression models were employed, adjusting for age, gender, education, DNA source, and blood cell composition. We identified 2,333 DMPs in LMCI vs. CN (raw $p < 1.42\ E^{-06}$; adjusted $p < 0.05$), 709 of which reached genome-wide significance at adjusted $p < 0.01$ (raw $p < 8.56E^{-06}$; Table 2; Figure 2; Supplementary Table S2). The Quantile–Quantile plot showed that the genomic inflation factor (lambda) was less than 1.10 (lambda = 1.0115; Figure 2; Supplementary Figure S2). Overall changes in methylation were modest, with |log2 of fold-change| ≤ 0.8 (Table 2; Supplementary Table S2). Among these DMPs, 1,608 CpG sites showed increased methylation in the LMCI patients (625 of them without overlapping annotated genes, e.g., cg03709428 and cg07934746; Table 2; Supplementary Table S2), while the rest showed lower levels of methylation in the LMCI cases compared with the CN group (Supplementary Table S2).

We found 74 sex-linked DMPs, 2 DMPs with unknown chromosome location, and 2,257 DMPs uniformly distributed across the autosomal chromosomes. Six of the 10 most significant CpGs were associated with PCGs (Table 2; Supplementary Table S4), including DMPs annotated to SNED1

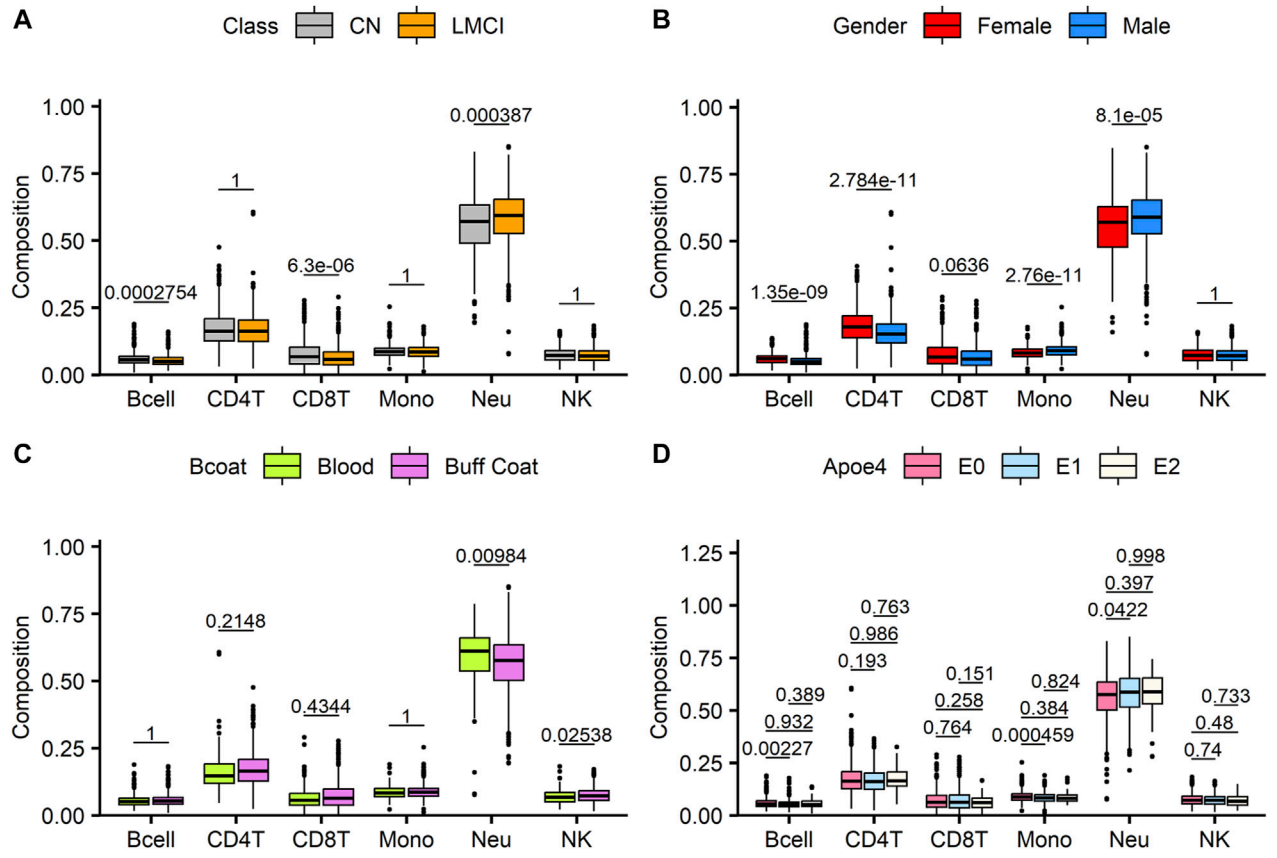

FIGURE 1
Analysis of estimated blood cell type composition in late-stage mild cognitive impairment (LMCI) versus normal cognitive aging individuals (CN). Abundance of specific blood cell types was estimated based on unique methylation markers for cell identity. Estimated proportions of B lymphocytes (Bcell), CD4T cells (CD4T), CD8T cells (CD8T), monocytes (mono), neutrophils (Neu) and natural killer cells (NK) were compared across disease groups **(A)**, genders **(B)**, sample sources **(C)** and Apoe4 alleles **(D)**. Significant differences across groups are estimated by using Wilcoxon test after correction for multiple observations **(A–C)** or one-way analysis of variance with Bonferroni correction for multiple observations **(D)**.

TABLE 2 List of differentially methylated probes (DMPs) with adjusted *p* less than Bonferroni correction threshold of 0.05.

Probes	Chr	Pos	Strand	GencodeCompV12	LogFC	Ave M-value	t	*p*-value	Adjusted *p*-value
cg15361291	Chr2	242,003,523	–	AC005237.4; SNED1	−0.28	−0.58	−7.48	$1.45E^{-13}$	$6.89E^{-08}$
cg09261703	Chr10	2,543,967	+	RP11-526P5.2	−0.41	1.10	−7.42	$2.16E^{-13}$	$6.89E^{-08}$
cg16288125	Chr18	904,243	+	ADCYAP1	−0.30	0.71	−7.40	$2.51E^{-13}$	$6.89E^{-08}$
cg21239079	Chr2	242,003,549	–	SNED1; AC005237.4	−0.32	−0.86	−7.36	$3.47E^{-13}$	$7.14E^{-08}$
cg17750572	Chr10	2,544,120	+	RP11-526P5.2	−0.29	1.29	−6.95	$5.86E^{-12}$	$9.63E^{-07}$
cg21228068	Chr16	50,827,518	+	CYLD; RP11-327F22.4	−0.48	2.89	−6.93	$7.02E^{-12}$	$9.63E^{-07}$
cg09173768	Chr2	176,989,349	–	HOXD9; HOXD-AS2	−0.19	−0.32	−6.83	$1.35E^{-11}$	$1.59E^{-06}$
cg03709428	Chr6	31,275,741	+		0.31	0.82	6.79	$1.72E^{-11}$	$1.68E^{-06}$
cg07934746	Chr19	15,774,266	+		0.21	−0.41	6.78	$1.84E^{-11}$	$1.68E^{-06}$
cg24082680	Chr1	63,249,199	+	ATG4C	0.26	−0.25	6.55	$8.44E^{-11}$	$6.95E^{-06}$

Chr, chromosome; Pos, DNA, base position; Strand, DNA, strand; GencodeCompV12, GENCODE, Comprehensive database version 12 containing all transcripts at protein-coding loci; LogFC, log2 of fold change of M-value across groups; Ave M-value, average M–value across all samples.

(cg15361291, chr2: 242,003,523, adjusted $p = 6.89E^{-08}$; cg21239079, chr2: 242,003,549, adjusted $p = 7.14E^{-08}$), ADCYAP1 (cg16288125, chr18: 904,243, adjusted $p = 6.89E^{-08}$), CYLD (cg21228068, chr16: 50,827,518, adjusted $p = 9.63E^{-07}$), HOXD9 (cg09173768, chr2: 176,989,349, adjusted $p = 1.59E^{-06}$), and ATG4C (cg24082680, chr1: 63,249,199, adjusted $p = 6.95E^{-06}$). Four non PCGs (NCGs;

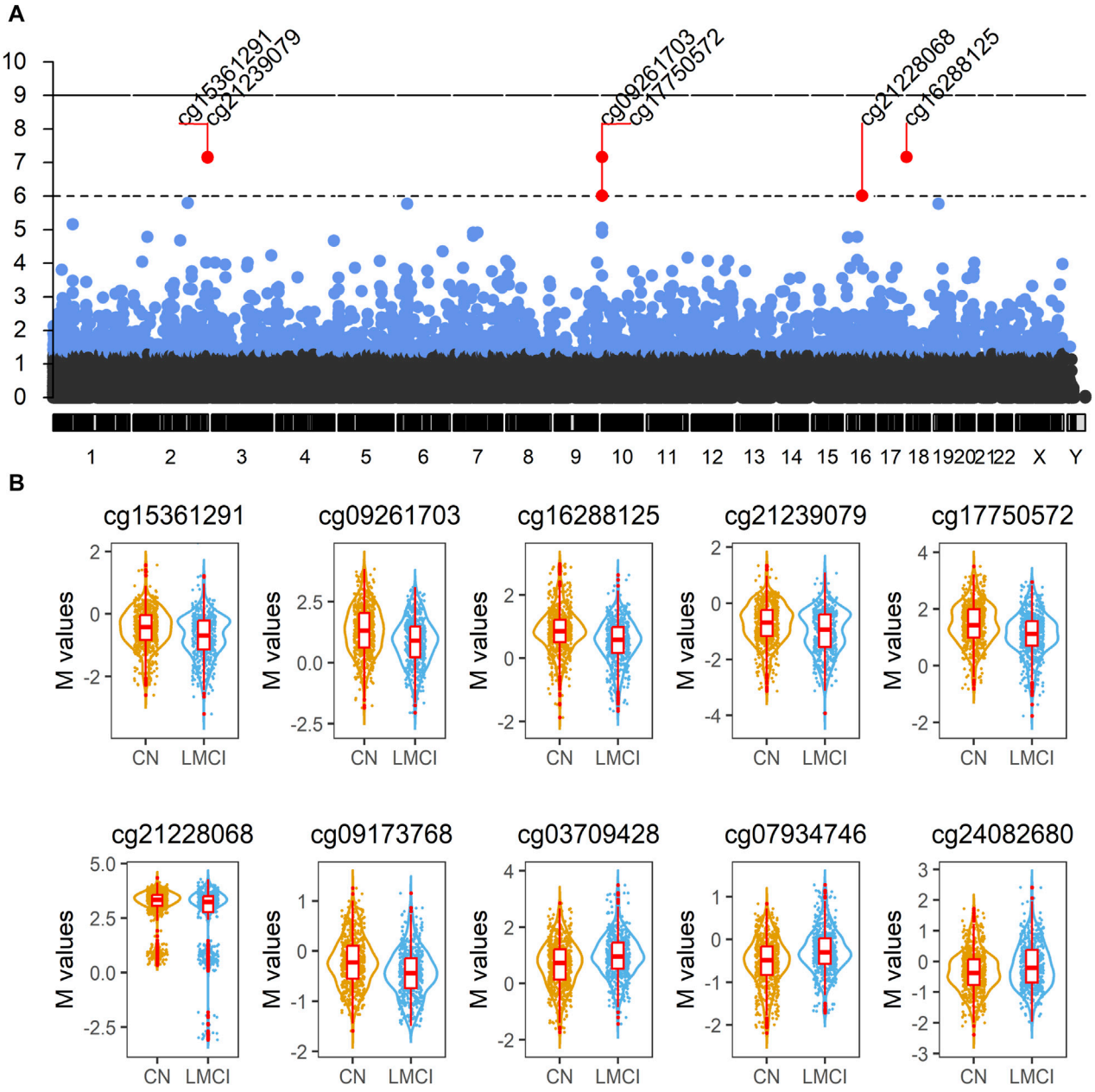

FIGURE 2
Analysis of blood methylation in late-stage mild cognitive impairment (LMCI) versus normal cognitive aging individuals (CN). **(A)** Manhattan plot compiling genome-wide methylation sites for the comparison of LMCI versus CN. Differentially methylated probes (DMPs) above short dashed line showed genome-wide significance (adjusted $p \leq 1E^{-06}$). **(B)** Representative violin plots of select top 10 significant DMPs showing increased or decreased methylation in LMCI cases compared to CN cases.

Table 2; Supplementary Table S4), namely, AC005237.4 (cg15361291, chr2: 242,003,523, adjusted $p = 6.89E^{-08}$; cg21239079, chr2: 242,003,549, adjusted $p = 7.14E^{-08}$), RP11-526P5.2 (cg09261703, chr10: 2,543,967, adjusted $p = 6.89E^{-08}$; cg17750572, chr10: 2,544,120, adjusted $p = 9.63E^{-07}$), RP11-327F22.4 (cg21228068, chr16: 50,827,518, adjusted $p = 9.63E^{-07}$), and HOXD-AS2 (cg09173768, chr2: 176,989,349, adjusted $p = 1.59E^{-06}$) were annotated by six of the top 10 DMPs. The most significant site was cg15361291, located in chr2: 242,003,523, which showed 21% lower methylation (variation = $|1-2^{-\text{logfc}}|\times100\%$) in the LMCI subjects than in the CN individuals (Table 2). The second CpG site (cg09261703), located in Chr10: 2,543,967, had 33% lower methylation (variation = $|1-2^{-\text{logfc}}|\times100\%$) in the subjects with LMCI than in the CN participants (Table 2).

3.4 DMR analysis

DMR analysis enabled identification of the regions in the genome that showed concerted changes in methylation and were deemed to have a large impact on modulating transcription. Overall, the DMRcate algorithm identified 85 DMRs as significantly

TABLE 3 List of differentially methylated regions (DMRs) ranked by Fisher's multiple comparison statistics.

Chr	Start	End	Width	No. DMPs	Min. FDR	Stouffer	HMFDR	Fisher	Mean. diff	Overlapping genes
Chr10	2,543,474	2,544,596	1,123	8	$1.30E^{-46}$	$1.13E^{-18}$	$5.07E^{-07}$	$4.33E^{-21}$	−0.0345	RP11-526P5.2
Chr2	242,002,695	242,003,549	855	4	$6.73E^{-28}$	$9.65E^{-10}$	$1.40E^{-07}$	$1.58E^{-12}$	−0.0288	SNED1; AC005237.4
Chr7	63,505,584	63,506,261	678	9	$1.57E^{-30}$	$4.87E^{-09}$	$6.13E^{-05}$	$2.34E^{-10}$	0.0252	ZNF727; RP11-3N2.13
Chr2	190,043,537	190,044,983	1,447	8	$1.78E^{-28}$	$6.38E^{-05}$	$6.75E^{-04}$	$3.01E^{-10}$	0.0145	COL5A2
Chr1	108,022,767	108,023,486	720	7	$2.20E^{-26}$	$1.86E^{-09}$	$1.52E^{-03}$	$5.72E^{-10}$	0.0262	NTNG1
Chr11	85,393,571	85,394,069	499	6	$7.68E^{-24}$	$3.49E^{-10}$	$1.32E^{-03}$	$3.73E^{-09}$	0.0308	CREBZF
Chr5	1,102,675	1,104,195	1,521	6	$1.19E^{-18}$	$5.78E^{-09}$	$1.39E^{-03}$	$5.84E^{-08}$	0.0126	SLC12A7
Chr1	63,249,197	63,249,765	569	9	$1.06E^{-26}$	$3.79E^{-02}$	$6.02E^{-05}$	$6.43E^{-08}$	0.0163	
Chr16	53,543,684	53,544,321	638	5	$2.44E^{-18}$	$1.90E^{-08}$	$6.85E^{-04}$	$1.33E^{-07}$	0.0201	
Chr15	99,789,622	99,791,336	1715	13	$3.04E^{-22}$	$3.90E^{-07}$	$3.25E^{-03}$	$2.59E^{-07}$	0.0183	TTC23

Chr, chromosome; Start, start base position of region; End, end base position of region; Width, width of region; No. DMPs, number of DMPs, within the region; Min. FDR, the minimum adjusted *p* from the CpGs constituting the significant region; Stouffer, the adjusted *p* of Stouffer's test; HMFDR, the adjusted *p* of Harmonic test; Fisher, the adjusted *p* of Fisher's test; Mean. diff, the mean methylation difference across groups in Fisher's test.

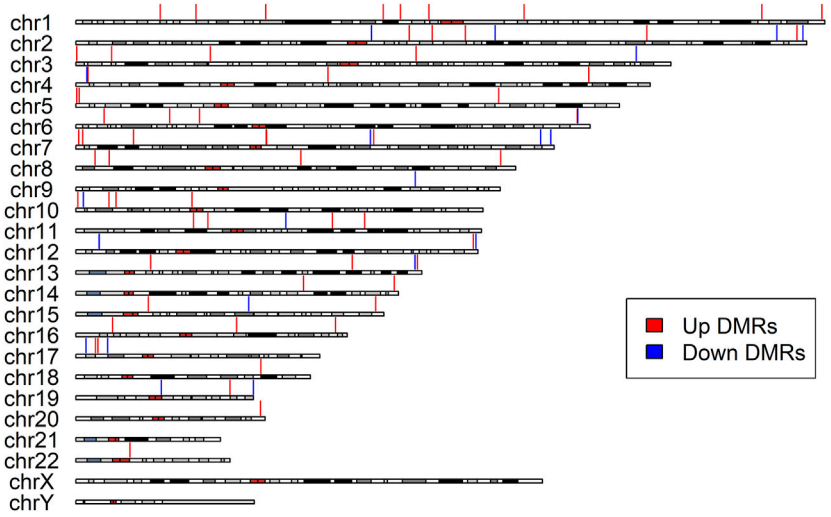

FIGURE 3
Differentially Methylated Regions (DMRs) distribution along the chromosomes. The red vertical lines indicate upregulated DMRs, while the blue vertical lines indicate downregulated DMRs. All identified DMRs are localized within autosomes; no DMRs were detected within sex chromosomes.

associated with cognitive decline in the participants with LMCI (Table 3; Supplementary Table S3). All of the DMRs in the genome were located in autosomal chromosomes (Figure 3). Among them, we identified 46 DMRs annotated to PCGs (Supplementary Table S5), such as DMRs annotated to SNED1 [chr2: 242,002,695 to 242,003,549 (4 probes), Fisher-corrected $p = 1.58E^{-12}$], ZNF727 [chr7: 63,505,584 to 63,506,261 (9 probes), Fisher-corrected $p = 2.34E^{-10}$], COL5A2 [chr2: 190,043,537 to 190,044,983 (8 probes), Fisher-corrected $p = 3.01E^{-10}$], NTNG1 [chr1: 108,022,767 to 108,023,486 (7 probes), Fisher-corrected $p = 5.72E^{-10}$], and CREBZF [chr11: 85,393,571 to 85,394,069 (6 probes), Fisher-corrected $p = 3.73E^{-09}$]. Recent studies have underlined the potential involvement of these genes in regulating immune cell function and inflammation, as well as their potential implication in the pathogenesis of various neurological disorders, such as AD and Parkinson disease (Naba et al., 2014; Cassandri et al., 2017; Krushkal et al., 2020; Barqué et al., 2021; Bu et al., 2021; Vallet et al., 2021; Arunachalam et al., 2022; Raouf Issa et al., 2022). The methylation region associated with the crucial gene TTC23, which plays a vital role in protein QC during brain development (Roubroeks et al., 2020; Vasanthakumar et al., 2020; Li et al., 2021; Lee et al., 2022), had the second highest density of significant CpG probes (13 probes; Supplementary Table S3; Supplementary Figure S4).

Moreover, DMRcate detected 12 DMRs annotated to NCGs (Supplementary Table S5), such as DMRs annotated to

TABLE 4 List of differentially methylated probes (DMPs) related with HOX family genes.

Probes	Chr	Pos	Strand	GencodeCompV12	LogFC	Ave M-value	t	*p*-value	Adjusted *p*-value
cg09173768	Chr2	176,989,349	–	HOXD9; HOXD-AS2	−0.19	−0.32	−6.83	$1.35E^{-11}$	$1.59E^{-06}$
cg15410411	Chr12	54,392,884	+	HOXC9; HOXC-AS1; HOXC5; HOXC6	−0.19	−1.16	−5.56	$3.30E^{-08}$	$3.59E^{-04}$
cg21336435	Chr12	54,398,561	–	HOXC5; HOXC6	−0.14	−0.96	−4.91	$1.04E^{-06}$	$2.90E^{-03}$
cg08254359	Chr12	54,398,518	–	HOXC5; HOXC6	−0.15	−0.59	−4.62	$4.32E^{-06}$	$6.41E^{-03}$
cg05611263	Chr12	54,425,634	–	HOXC4; HOXC5	−0.12	1.30	−4.28	$2.00E^{-05}$	$1.66E^{-02}$
cg06316886	Chr2	177,027,043	–	HOXD3	−0.13	−1.82	−4.23	$2.47E^{-05}$	$1.86E^{-02}$
cg22934308	Chr2	177,038,617	–	HOXD3; HOXD-AS1	0.14	−0.22	4.22	$2.65E^{-05}$	$1.94E^{-02}$
cg07783843	Chr2	176,997,311	+	HOXD-AS2; HOXD8	0.10	−0.56	3.91	$9.65E^{-05}$	$4.04E^{-02}$
cg14324370	Chr2	177,042,789	–	HOXD-AS1; AC009336.24	0.08	−4.23	3.88	$1.09E^{-04}$	$4.29E^{-02}$

Chr, chromosome; Pos, DNA, base position; Strand, DNA, strand; GencodeCompV12, GENCODE, Comprehensive database version 12 containing all transcripts at protein-coding loci; LogFC, log2 of fold change of M-value across groups; Ave M-value, average M–value across all samples.

AC005237.4 [chr2: 242,002,695 to 242,003,549 (4 probes), Fisher-corrected $p = 1.58E^{-12}$], RP11-3N2.13 [chr7: 63,505,584 to 63,506,261 (9 probes), Fisher-corrected $p = 2.34E^{-10}$], LINC00116 [chr2: 110,969,641 to 110,970,909 (8 probes), Fisher-corrected $p = 3.21E^{-07}$], CTC-281F24.1 [chr17: 6,557,720 to 6,559,109 (7 probes), Fisher-corrected $p = 3.75E^{-06}$], and MIR4520A [chr17: 6,557,720 to 6,559,109 (7 probes), Fisher-corrected $p = 3.75E^{-06}$]. The most significant DMR identified in this study that was associated with conversion status in the patients with LMCI was annotated to RP11-526P5.2 [chr10: 2,543,474 to 2,544,596 (8 probes), Fisher-corrected $p = 4.33E^{-21}$; Table 3; Supplementary Table S3]. Six DMPs in this region, including the second significant CpG-site cg09261703, were highly correlated and located in the upstream CpG island of the RP11-526P5.2 gene (Supplementary Figure S4).

3.5 Methylation profiles in HOX and ZNF family genes

Some of the top hit DMPs and DMRs were closely associated with HOX and ZNF family genes. We summarize the significant methylation sites of HOX and ZNF family genes in Tables 4, 5; Supplementary Table S6; Supplementary Figure S5. The results showed that nine DMPs, such as cg09173768 (chr2: 176,989,349, adjusted $p = 1.59E^{-06}$) and cg15410411 (chr2: 54,392,884, adjusted $p = 3.59E^{-04}$), were enriched in the gene regions of HOXC4, HOXC5, HOXC6, HOXC9, HOXC-AS1, HOXD3, HOXD8, HOXD9, HOXD-AS1 and HOXD-AS2. However, no significant DMRs were found in HOX family genes. In the case of ZNF family genes, 31 methylation sites, such as cg13947469 (chr7: 63,505,871, adjusted $p = 1.53E^{-05}$) and cg14768256 (chr3: 44,754,587, adjusted $p = 1.09E^{-04}$), were shown to be significant in the LMCI patients. Two DMRs overlapping with ZNF727 or ZNF502 were associated with LMCI (adjusted $p < 0.05$).

3.6 DNA methylation in genes associated with histone modification

To investigate the DNA methylation status of genes that encode the enzymes of histone modification, we summarized the DMPs and DMRs related to histone acetyltransferases (HATs), histone deacetylases (HDACs), histone methyltransferases (HMTs), histone demethylases (KDMs), protein kinases (PTKs), and protein phosphatases (PPs) in Table 6; Supplementary Figure S6. Unfortunately, we did not find any DMPs in HATs, HMTs, KDMs, PTKs, and PPs. Only five DMPs in HDAC4, HDAC6, or HDAC8, such as cg14865678 (chr2: 239,984,042, adjusted $p = 1.71E^{-02}$) and cg20784693 (chr2: 239,984,030, adjusted $p = 1.94E^{-02}$), were identified. There were no DMRs in the region overlapping HMTs, HDACs, KDMs, PTKs, and PPs.

3.7 Enriched pathways related to neurotransmission

Generalized gene set enrichment analysis with the hypergeometric test in the R package missMethyl was performed to gain biological insight from these epigenetic differences. GO terms and KEGG pathways with adjusted p values less than 0.05 were selected to annotate the PCGs of differential CpG sites (Supplementary Table S4). This selection yielded 503 GO terms (Supplementary Table S7), including 357 terms of biological processes (BP), 75 terms of cell components (CC), and 71 terms of molecular functions (MF), and 20 KEGG pathways (Supplementary Table S8). A total of 157 of the identified GO terms reached enrichment significance at an adjusted $p < 0.0001$ (99 BP, 28 CC, and 30 MF; Supplementary Table S7). The results of GO analysis showed that the DMPs annotated genes were involved in nervous system development, neurogenesis, and cell (neuron) projection pathways (adjusted $p < 0.05$, ratio values of DMPs annotated genes in the pathways ranging between 0.67 and 1;

TABLE 5 List of top 10 differentially methylated probes (DMPs) related with ZNF family genes.

Probes	Chr	Pos	Strand	GencodeCompV12	LogFC	Ave M-value	t	*p*-value	Adjusted *p*-value
cg13947469	Chr7	63,505,871	–	ZNF727; RP11-3N2.13	0.27	−1.43	6.36	$2.78E^{-10}$	$1.53E^{-05}$
cg14768256	Chr3	44,754,587	+	ZNF502	0.25	1.06	5.90	$4.82E^{-09}$	$1.09E^{-04}$
cg06088684	Chr2	180,610,608	–	ZNF385B	−0.13	2.79	−5.41	$7.44E^{-08}$	$5.83E^{-04}$
cg18831899	Chr17	5,019,056	–	ZNF232; USP6	0.16	2.03	5.33	$1.17E^{-07}$	$7.57E^{-04}$
cg09560297	Chr19	37,406,349	–	ZNF568; ZNF829	0.14	0.94	5.11	$3.65E^{-07}$	$1.52E^{-03}$
cg05769153	Chr19	53,636,398	+	ZNF415	0.20	1.75	5.04	$5.36E^{-07}$	$1.89E^{-03}$
cg05223766	Chr19	53,590,304	+	ZNF160	0.15	−2.07	4.86	$1.33E^{-06}$	$3.36E^{-03}$
cg01511534	Chr16	3,284,640	–	ZNF200	0.14	−1.72	4.80	$1.81E^{-06}$	$4.02E^{-03}$
cg16428517	Chr16	3,317,428	+	ZNF263	0.12	2.51	4.71	$2.75E^{-06}$	$4.91E^{-03}$
cg05241461	Chr19	22,816,980	–	ZNF492	0.15	−3.48	4.71	$2.82E^{-06}$	$4.99E^{-03}$

Chr, chromosome; Pos, DNA, base position; Strand, DNA, strand; GencodeCompV12, GENCODE, Comprehensive database version 12 containing all transcripts at protein-coding loci; LogFC, log2 of fold change of M-value across groups; Ave M-value, average M–value across all samples.

TABLE 6 List of differentially methylated probes (DMPs) related with HDAC family genes.

Probes	Chr	Pos	Strand	GencodeCompV12	LogFC	Ave M-value	t	*p*-value	Adjusted *p*-value
cg14865678	Chr2	239,984,042	+	HDAC4	0.13	0.83	4.27	$2.10E^{-05}$	$1.71E^{-02}$
cg20784693	Chr2	239,984,030	+	HDAC4	0.15	0.55	4.22	$2.67E^{-05}$	$1.94E^{-02}$
cg04067339	ChrX	71,760,492	–	HDAC8	0.09	−1.28	3.94	$8.76E^{-05}$	$3.85E^{-02}$
cg24616736	ChrX	48.659,713	–	HDAC6	0.10	−1.84	3.92	$9.24E^{-05}$	$3.95E^{-02}$
cg09155776	Chr2	239,984,105	–	HDAC4	0.11	−0.22	3.90	$1.03E^{-04}$	$4.18E^{-04}$

Chr, chromosome; Pos, DNA, base position; Strand, DNA, strand; GencodeCompV12, GENCODE, Comprehensive database version 12 containing all transcripts at protein-coding loci; LogFC, log2 of fold change of M-value across groups; Ave M-value, average M–value across all samples.

Figure 4; Supplementary Tables S4, S7). Parallel testing in the KEGG gene sets showed a marked enrichment in addiction disorders and neurotransmission, such as morphine addiction, the calcium signaling pathway, and GABAergic synapses (adjusted $p < 0.05$, ratio values of DMPs annotated genes in the pathways ranging between 0.73 and 0.92; Figure 4; Supplementary Tables S4, S8).

3.8 Influence of DNA methylation on gene expression

To investigate the influence of DNA methylation on the gene expression, we examined the expression levels of 28 PCGs that overlapped with DMPs or DMRs. In general, these target genes exhibited low expression abundance, that is, their average expression counts were lower than 50 (Table 7; Supplementary Table S9). As shown in Table 7, a total of 11 genes were significantly differentially expressed between the LMCI and CN individuals. Four of the DEGs were HOX or ZNF family genes, namely, HOXC9 (adjusted $p = 5.49E^{-03}$), HOXC5 (adjusted $p = 1.15E^{-02}$), ZNF415 (adjusted $p = 7.17E^{-05}$), and ZNF502 (adjusted $p = 7.17E^{-05}$). In addition, we found that the expression of HDAC8 (adjusted $p = 8.75E^{-03}$) and HDAC4 (adjusted $p = 1.03E^{-02}$) was significantly upregulated in the LMCI patients. In contrast, SNED1 and ADCYAP1, which were annotated by the top hit DMPs and DMRs, were downregulated in the LMCI patients.

3.9 Validation with proteomic profiling

The serum proteomic profile analysis of the eight proteins associated with DMPs further validated the EWAS results. The results showed that six of these proteins, namely, HDAC4, HOXC5, HOXC6, HOXC9, ZNF415, and ZNF502, were significantly differentially expressed between LMCI and CN (adjusted $p < 0.05$; Figure 5; Supplementary Table S10). Consistent with the results of the gene expression profile analysis, the expression of proteins HDAC4 (adjusted $p = 2.70E^{-02}$), HOXC5 (adjusted $p = 1.30E^{-03}$), and HOXC9 (adjusted $p = 1.46E^{-02}$) was significantly upregulated in the LMCI patients (Figure 5; Supplementary Table S10). However, the proteomic results of proteins ZNF415 and ZNF502 were opposite those of the results of the gene expression profile analysis. Both of ZNF415 and ZNF502 were also significantly upregulated in the LMCI patients (adjusted $p < 0.05$; Table 7; Figure 5; Supplementary Tables S9, S10).

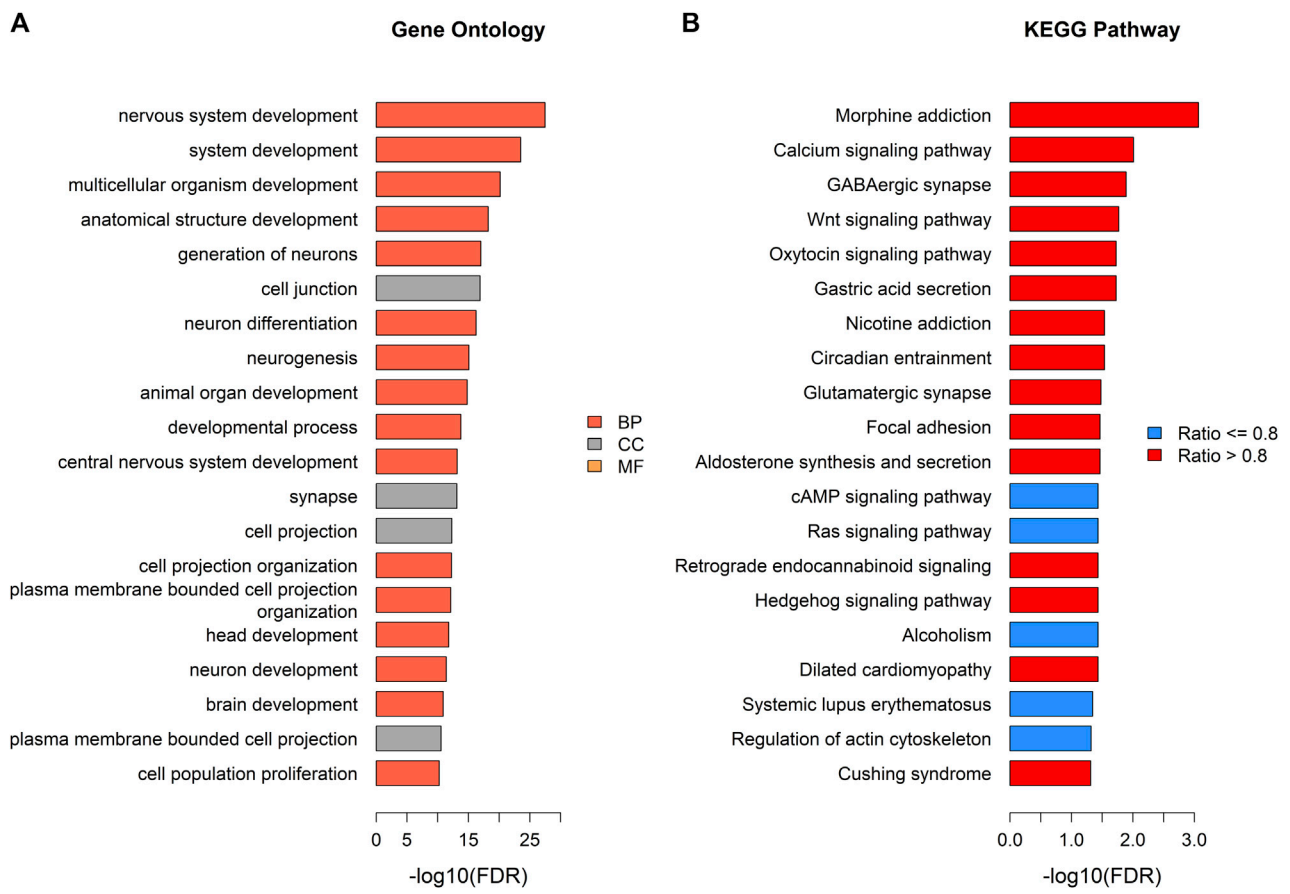

FIGURE 4
Pathway enrichment analysis of DMPs annotated genes. **(A)** Top gene ontology (GO) enrichment terms with adjusted $p < 0.05$ (tomato color bars: BP; grey color bars: CC; orange color bars: MF). **(B)** Top KEGG pathways (blue color bars: pathways with ratio of genes annotated by DMPs ≤ 0.8; red color bars: pathways with ratio of genes annotated by DMPs >0.8).

TABLE 7 Gene expression validation of candidate DMPs or DMRs related protein-coding genes (11 significant genes).

Genes	LogFC	AveExpr	t	*p*-value	Adjusted *p*-value
NTNG1	−1.34	2.31	−9.80	$2.45E^{-20}$	$6.87E^{-19}$
COL5A2	1.41	2.48	9.04	$8.75E^{-18}$	$1.23E^{-16}$
ADCYAP1	−1.06	2.72	−7.09	$6.71E^{-12}$	$6.26E^{-11}$
ZNF415	−0.75	2.63	−4.47	$1.02E^{-05}$	$7.17E^{-05}$
CYLD	−1.48	7.55	−3.63	$3.23E^{-04}$	$1.81E^{-03}$
HOXC9	0.71	3.58	3.27	$1.18E^{-03}$	$5.49E^{-03}$
HDAC8	0.71	4.43	3.08	$2.19E^{-03}$	$8.75E^{-03}$
HDAC4	0.79	4.19	2.99	$2.94E^{-03}$	$1.03E^{-02}$
HOXC5	0.64	4.15	2.92	$3.70E^{-03}$	$1.15E^{-02}$
SNED1	−0.57	3.98	−2.45	$1.47E^{-02}$	$4.12E^{-02}$
ZNF502	−0.72	5.25	−2.38	$1.80E^{-02}$	$4.57E^{-02}$

LogFC, log2 of fold change of expression counts across groups; AveExpr, the average value of log2 expression count.

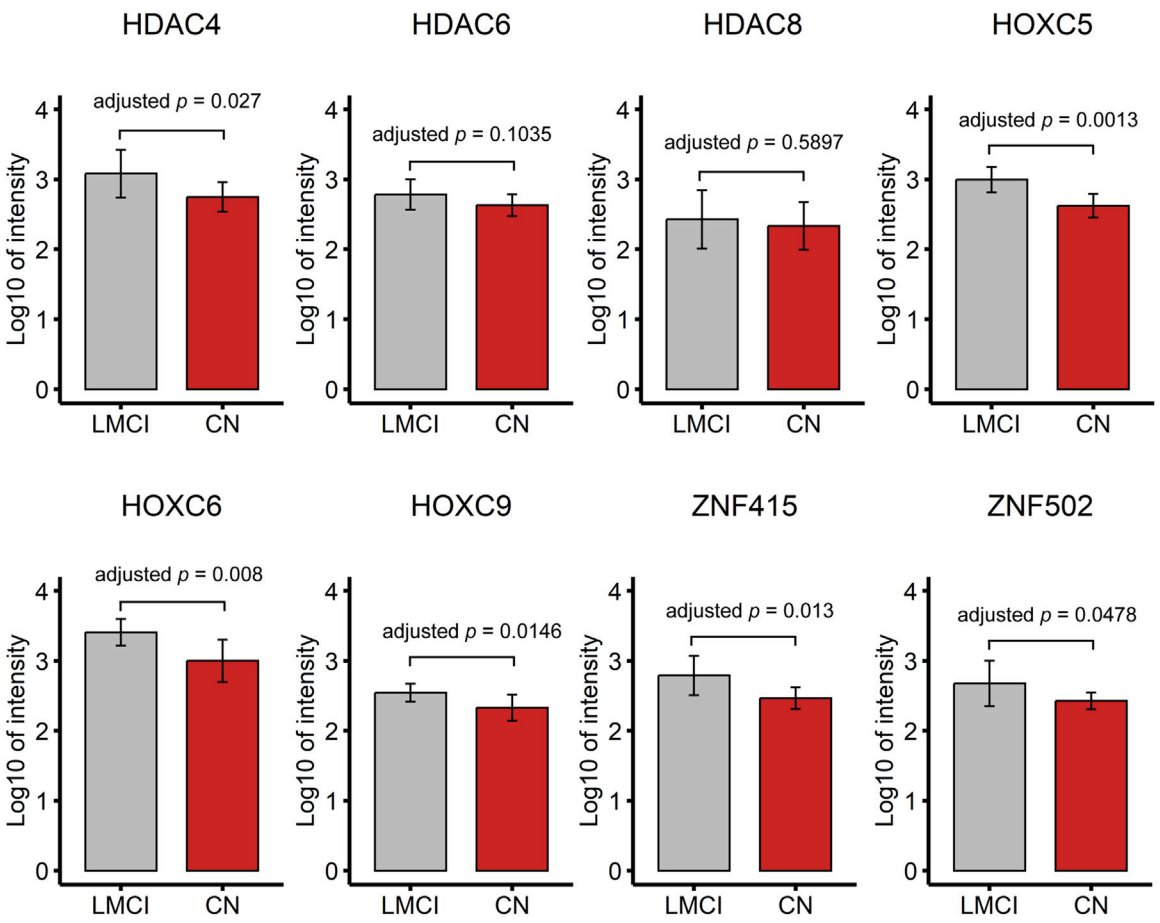

FIGURE 5
Proteomic profile of candidate DMPs or DMRs related proteins (8 candidate proteins).

3.10 Association of DNA methylation level with progression to AD

We screened the samples (756 with EMCI and 1,120 with LMCI) in the ADNI cohort to calculate the proportion of MCI progression to AD. As shown in Figure 6A; Supplementary Table S11, we found that the probability of LMCI progressing to AD was about three times higher than that of EMCI (49% vs. 17%). The average progression speed of the LMCI patients was much faster than that of the EMCI patients (26 months vs. 46 months; Figure 6B; Supplementary Table S11). Out of the 554 LMCI patients included in this study, 358 subjects (65%) had progressed to AD. The OR values from the logistic regression model indicated that HDAC6-associated DMP cg24616736 [OR = 1.67, 95% CI (1.08–2.62), p = 2.33E^{-02}], ZNF502-associated DMP cg14768256 [OR = 1.53, 95% CI (1.16–2.02), p = 2.57E^{-03}], HOXC5- and HOXC6-associated DMP cg08254359 [OR = 1.41, 95% CI (1.01–1.97), p = 4.30E^{-02}], and HOXD8-associated DMP cg07783843 [OR = 1.75, 95% CI (1.15–2.71), p = 1.04E^{-02}] were associated with increased susceptibility to AD in LMCI subjects (Figures 6C, D; Supplementary Table S12). SNED1-associated DMPs cg15361291 [OR = 0.48, 95% CI (0.36–0.65), p = 2.49E^{-06}] and cg21239079 [OR = 0.55, 95% CI (0.43–0.71), p = 5.53E^{-06}] and ZNF727-associated DMP cg13947469 [OR = 0.74, 95% CI (0.58–0.94), p = 1.33E^{-02}] showed protective associations with the risk of progression to AD from LMCI (Figures 6C, D; Supplementary Table S12). DMP cg21336435 highly correlated with cg08254359 (Supplementary Figure S5), and both of them were associated with the expression of HOXC5 and HOXC6 (Figures 6C, D; Supplementary Table S12). However, the OR of cg21336435 was not significant [OR = 1.49, 95% CI (1.00–2.23), p = 5.22E^{-02}; Figures 6C, D; Supplementary Table S12].

Two methylation sites, namely, cg24616736 (r = −0.26, p = 9.73E^{-07}) and cg13947469 (r = 0.17, p = 1.59E^{-03}) were significantly associated with progression time from LMCI to AD (Supplementary Table S13). The distribution curve of methylation signal intensity over time clearly showed that subjects with a weaker methylated signal of cg24616736 had slower progression speed (Figure 6E). Progression speed of subjects with a high unmethylated signal of cg24616736 was mainly between 96 and 120 months (Figure 6E). A similar trend was noticed in the distribution of cg21336435 (Figure 6E). Although there was no significant correlation between progression time and signal intensity of protective DMPs cg21239079 and cg15361291 (p > 0.05), we found that subjects with a high methylated signal needed more time for progression from LMCI to AD (Figure 6E). The progression speed in subjects with a high methylated signal of cg21239079 or cg15361291 mainly ranged between 84 and 120 months (Figure 6E).

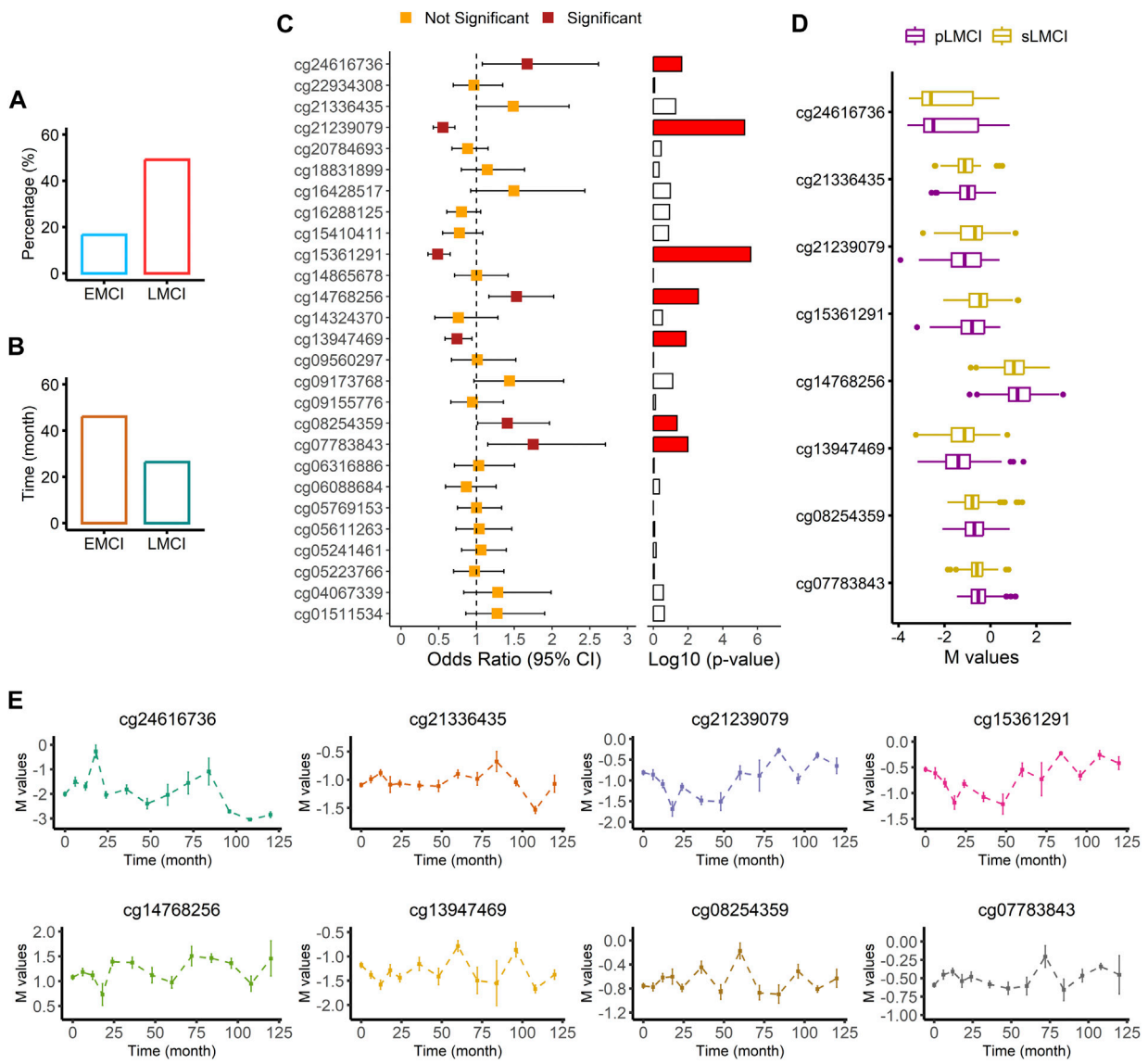

FIGURE 6
Association analysis of AD progression from LMCI. **(A)** Comparison of progression probability between EMCI and LMCI. **(B)** Comparison of progression time between EMCI and LMCI. **(C)** Odds ratio values from logistic regression with comparison between sLMCI and pLMCI. **(D)** Box plot of methylation signal intensity across groups. **(E)** Distribution curve of methylation signal intensity over time.

Among the DMPs increasing susceptibility to AD, HDAC6-associated DMP cg24616736 was significantly correlated with cognitive scores at baseline diagnosis (Figure 7; Supplementary Table S14), namely, MMSE_bl (r = −0.15, p = 5.36E^{-03}), CDRSB_bl (r = 0.12, p = 2.20E^{-02}), mPACCdigit_bl (r = −0.22, p = 1.77E^{-05}), and mPACCtrailsB_bl (r = −0.17, p = 1.23E^{-03}), and was also significantly correlated with the speed of cognitive score decline (Figure 8; Supplementary Table S14), namely, MMSE_speed (r = 0.19, p = 3.95E^{-04}), CDRSB_speed (r = 0.13, p = 1.49E^{-02}), mPACCdigit_speed (r = 0.20, p = 1.40E^{-04}), and mPACCtrailsB_speed (r = 0.20, p = 1.20E^{-04}). As shown in Figures 7, 8, ZNF502-associated DMP cg14768256 was significantly correlated with MMSE_speed (r = −0.11, p = 3.79E^{-02}), CDRSB_bl (r = −0.10, p = 4.75E^{-02}), mPACCdigit_speed (r = −0.13, p = 1.45E^{-02}), and mPACCtrailsB_speed (r = −0.13, p = 1.24E^{-02}). HOXC5- and HOXC6-associated DMP cg08254359 was significantly correlated with the cognitive decline speed (Figure 8; Supplementary Table S14), namely, mPACCdigit_speed (r = −0.12, p = 2.76E^{-02}) and mPACCtrailsB_speed (r = −0.12, p = 2.92E^{-02}). DMP cg21336435, which was highly correlated with cg08254359, was the only DMP that was significantly correlated with CDRSB_bl (r = 0.16, p = 3.20E^{-03}; Figure 7; Supplementary Table S14). There was no significant correlation between HOXD8-associated DMP cg07783843 and the cognitive scores at baseline diagnosis or the speed of cognitive score decline (p > 0.05; Figures 7, 8; Supplementary Table S14). Moreover, we found that the LMCI patients with a higher intensity of cg21239079, which was associated with SNED1, had better cognitive ability as measured by the MMSE_bl (r = 0.12, p = 2.29E^{-02}) and mPACCtrailsB_bl (r = 0.11, p = 4.37E^{-02}) scores, but also had a higher CDRSB_bl score (r = 0.17, p = 1.37E^{-03}), which

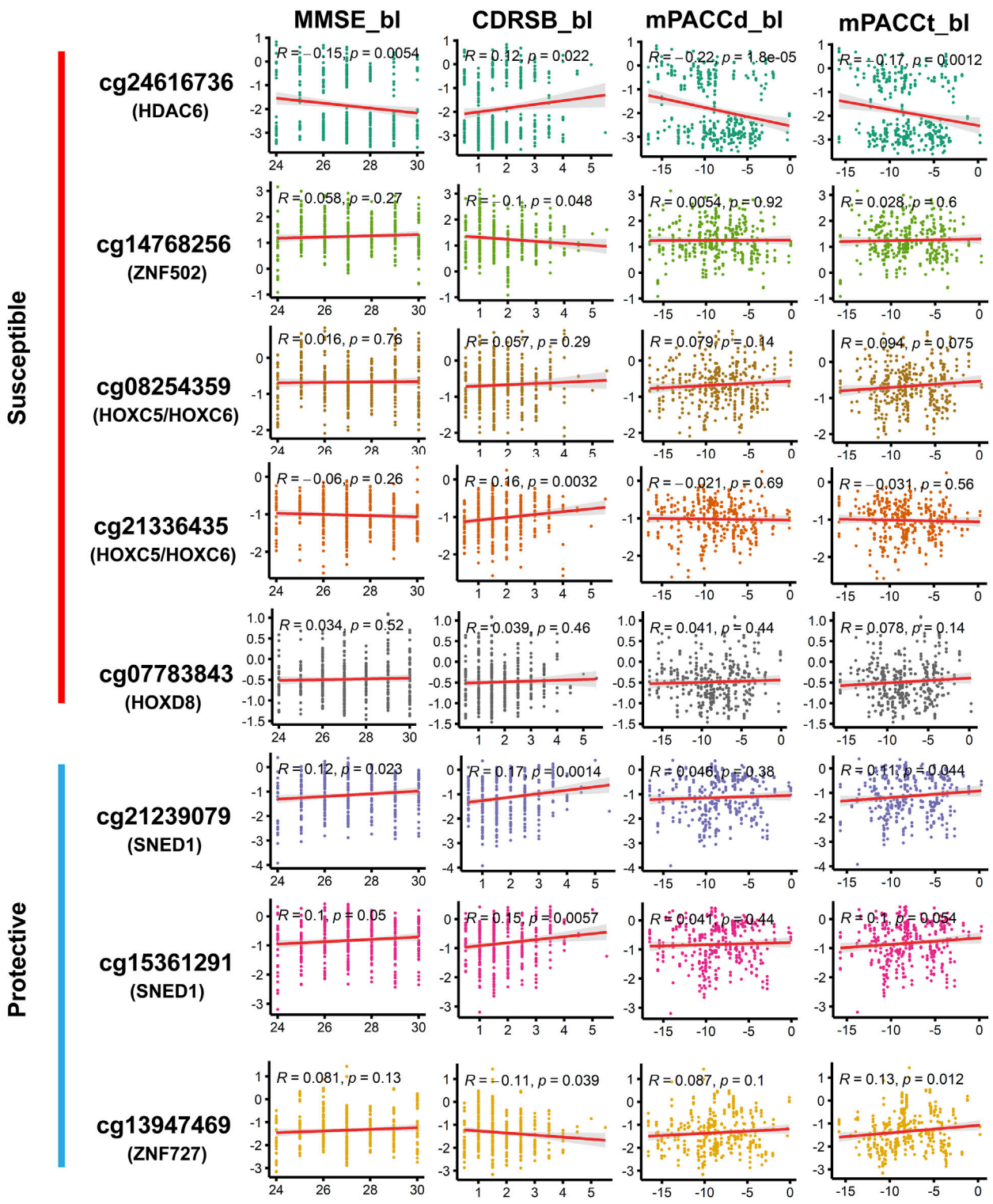

FIGURE 7
Correlation of methylation signal intensities of DMPs with the cognitive scores at baseline diagnosis. MMSE, mini-mental state examination; CDRSB, clinical dementia rating scale sum of boxes; mPACCdigit, modified preclinical Alzheimer cognitive composite that used digit symbol substitution test; mPACCtrailsB, modified preclinical Alzheimer cognitive composite that used trail-making test part B. Higher scores of MMSE, mPACCdigit, and mPACCtrailsB, represent better cognitive function. However, higher score of CDRSB represent more severe cognitive impairment. Correlation coefficients with *p*-value lower than 0.05 were considered to be significant.

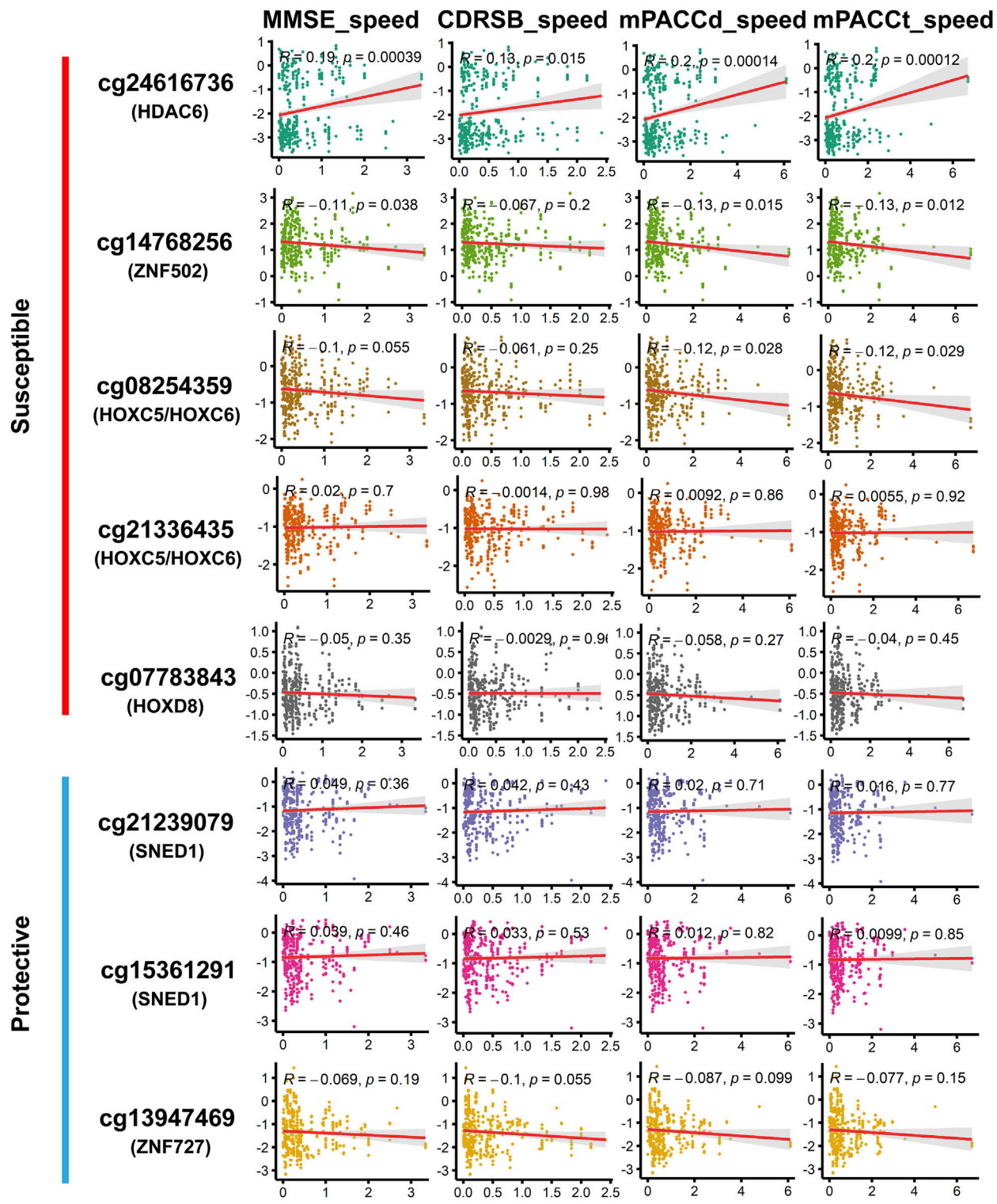

FIGURE 8
Correlation of methylation signal intensities of DMPs with the speed of cognitive decline. The speed scores were calculated as |Score $_{(\text{first diagnosis as AD})}$−Score $_{(\text{baseline diagnosis as LMCI})}$|/progression time $_{(\text{months})}$. MMSE_speed: the speed of cognitive decline based on MMSE; CDRSB_speed: the speed of cognitive decline based on CDRSB; mPACCdigit_speed: the speed of cognitive decline based on mPACCdigit; mPACCtrailsB_speed: the speed of cognitive decline based on mPACCtrailsB. Higher scores of MMSE_speed, CDRSB_speed, mPACCdigit_speed, and mPACCtrailsB_speed, represent higher speed of cognitive decline. Correlation coefficients with p-value lower than 0.05 were considered to be significant.

represents declined cognitive function (Figure 7; Supplementary Table S14). Similarly, cg15361291, another protective DMP associated with SNED1, was positively correlated with both MMSE_bl (r = 0.10, p = 4.99E^{-02}; Figure 7; Supplementary Table S14) and CDRSB_bl (r = 0.15, p = 5.68E^{-03}; Figure 7; Supplementary Table S14). ZNF727-associated DMP cg13947469 was negatively correlated with CDRSB_bl (r = −0.11, p = 3.93E^{-02}; Figure 7; Supplementary Table S14), but positively correlated with mPACCtrailsB_bl (r = 0.13, p = 1.17E^{-02}; Figure 7; Supplementary Table S14).

4 Discussion

Both patients with EMCI and LMCI generally exhibit preserved daily activities but present slight cognitive deficits (Grundman et al., 2004; Petersen, 2004; Zhang et al., 2019). Patients with LMCI show more severe impairment in episodic memory than those with EMCI, which has led to the belief that LMCI typically arises during a progression from EMCI (Aisen et al., 2010; Zhang et al., 2019). Previous studies that pooled patients with EMCI and LMCI into a single MCI group have hindered research into the pathogenic mechanisms of LMCI and the elucidation of factors that contribute to LMCI progression to AD (Jessen et al., 2014; Zhang et al., 2019; Vasanthakumar et al., 2020; Chen et al., 2022).

In this study, a total of 2,333 DMPs and 85 DMRs were found in the LMCI patients. The high-risk genes identified in previous EWAS that combined EMCI and LMCI groups into a single MCI group for comparison with CN (Lo et al., 2011; Dumurgier et al., 2017; Chouliaras et al., 2018; Roubroeks et al., 2020; Vasanthakumar et al., 2020), such as FLRT2, were not confirmed to be associated with LMCI in the present study. It is possible that LMCI patients have a higher likelihood of progression to AD than those with EMCI (Jessen et al., 2014); thus, the comparative analysis of LMCI and CN showed more similar results with the studies of AD progression from CN or MCI. Previous EWAS and molecular genetic studies have shown that the DMPs or DMRs associated with HOX and ZNF family genes are closely associated with the onset of AD or progression from MCI to AD (Cassandri et al., 2017; Smith et al., 2018; Roubroeks et al., 2020; Bu et al., 2021; Li et al., 2021; Arunachalam et al., 2022). In this study, gene expression and proteomic profile analysis confirmed that the DNA methylations in LMCI could disrupt the expression of HDAC, HOX, and ZNF family genes. These methylations were closely associated with the cognitive impairment in LMCI patients as measured by the scores of MMSE, CDRSB, mPACCdigit, and mPACCtrailsB.

In the case of HOX family genes, aberrantly expressed HOXB and HOXA genes have been validated as high-risk genes for AD (Smith et al., 2018; Roubroeks et al., 2020; Li et al., 2021; Arunachalam et al., 2022). However, few studies have directly linked HOXC genes to AD or the direct formation of MCI. Only one study has shown that HOX Antisense Intergenic RNA (HOTAIR), transcribed from the antisense strand of the HOXC locus, may be associated with central nervous system inflammation and potentially induce AD (Lu et al., 2022). In this study, we revealed that upregulated expression of HOXC5, HOXC6, and HOXC9 may be associated with the onset of LMCI. Results from EWAS and proteomic profiling showed that increased unmethylated signals of positions such as cg08254359 and cg21336435 could cause high expression levels of HOX family proteins in LMCI patients. These alterations in specific sites of HOX family genes may be related to the cognitive decline in LMCI, and further influence the progression speed from LMCI to AD. While the precise molecular biology links between HOXC genes and LMCI remain unclear, it is apparent that HOX family genes play a crucial role in the occurrence of LMCI.

Peripheral blood EWAS is helpful for identifying the changes in common methylation status across tissues, such as brain and peripheral lymphocytes. This is the reason why the GO and KEGG analyses revealed that the DMPs-associated genes were significantly enriched in the pathways of addiction disorders, neurotransmission, and neurogenesis. The results from peripheral blood EWAS may provide new insights into the link between immune dysfunction and neurodegeneration. Based on DNA methylation signals, we could estimate the composition of lymphocyte subpopulations. We found that the patients with LMCI had lower abundance of B cells and CD8$^+$ T cells and higher abundance of neutrophils (Neu) compared with the CN individuals. These findings suggest that LMCI patients exhibit signs of abnormal immune function. Most of the genes associated with DMPs were closely associated with the maintenance of both neural and immune systems. For example, SNED1, which is associated with the top hit DMPs, has been demonstrated to function as a promoter of breast cancer metastasis and amyotrophic lateral sclerosis, and its abnormal expression significantly affects the survival outcome of these patients (Naba et al., 2014; Tarr et al., 2019; Krushkal et al., 2020; Barqué et al., 2021; Vallet et al., 2021). Similarly, the HOX and ZNF family genes have been proven to influence immune function and contribute to the development of neurological system disorders, such as glioblastoma and Parkinson's disease (Cassandri et al., 2017; Bu et al., 2021; Arunachalam et al., 2022; Raouf Issa et al., 2022).

Investigation in the large population of the ADNI cohort showed that the probability of progressing to AD was about three times higher from LMCI than from EMCI (49% vs. 17%), which is consistent with the findings reported by other research groups (Jessen et al., 2014; Zhang et al., 2019; Vasanthakumar et al., 2020; Chen et al., 2022). Furthermore, we found that the average progression speed of the LMCI patients was much faster than that of the EMCI patients (26 months vs. 46 months). These results demonstrate the importance of independently exploring the pathogenesis of each stage of MCI. Progression analysis indicated that DMPs associated with HDAC6, ZNF502, HOXC5, HOXC6, and HOXD8 were associated with increased susceptibility to AD in LMCI subjects. In contrast, DMPs associated with SNED1 and ZNF727 showed protective associations with the risk of progression from LMCI to AD. In particular, DMP cg24616736, which was associated with HDAC6, showed the strongest correlation with progression time and the speed of cognitive decline in the LMCI patients. We found that both the methylation status and protein expression level of HDAC6 were different between LMCI and CN. This finding suggests that HDAC6 may be a crucial histone deacetylase in the whole process from CN to MCI and further progression to AD. Previous evidence has indicated the important role of HDAC6 in tau-mediated neurodegeneration, and HDAC6 may be involved in various neurodegenerative diseases such as AD, Parkinson disease, amyotrophic lateral sclerosis, and Huntington disease (Zhang et al., 2013; Trzeciakiewicz et al., 2020; Li et al., 2022). However, the

epigenetic regulation mechanism behind the expression of HDAC6 is not yet clear. Both LMCI and AD exhibit symptoms of cognitive decline; therefore, targeted inhibition or degradation of HDAC6 as a therapeutic approach for AD could potentially have preventive effects on the occurrence of LMCI.

This study also demonstrated the presence of an association between ZNF family genes and cognitive impairment in LMCI patients. Most of them, including ZNF502, ZNF727, ZNF415, ZNF385B, ZNF232, ZNF200, and ZC3H14, have been validated as critical genes implicated in the pathogenesis of AD (Cassandri et al., 2017; Roubroeks et al., 2020; Vasanthakumar et al., 2020; Bu et al., 2021; Li et al., 2021). However, their roles in the molecular process of cognitive decline are not yet clear. We found that methylations of ZNF727 and ZNF502 have opposite effects on the progression of LMCI to AD. Consistent with this, previous studies have shown that the function of ZNFs could be distinct in altering cerebrospinal fluid (CSF) tau/ptau levels, promoting or inhibiting neuroinflammation in different regions, protecting or exposing neurons to oxidative stress–induced apoptosis, and interfering with the differentiation potential of neural stem cells (Cassandri et al., 2017; Calderari et al., 2018; Lopez et al., 2019; Baker et al., 2020; Bu et al., 2021). ZNFs act as transcription factors that modulate the expression of crucial genes involved in cellular biochemical processes by specifically binding to DNA or RNA (Farmiloe et al., 2020). Further studies of gene expression regulation related to these candidate ZNFs may be helpful to explore the onset and progression of cognitive impairment.

To the best of our knowledge, this is the first comprehensive genome-wide DNA methylation association analysis for LMCI. This analysis serves to elucidate the mechanisms of LMCI development, and aid in the prevention of LMCI progression to AD. However, due to the absence of relevant cellular biological experiments, the functionality of the noncoding gene RP11-526P5.2, which is associated with the top DMPs, could not be validated. It is important to mention another limitation of this study, namely, we only collected the methylation data from the ADNI cohort; thus, the results may be affected by the limitations imposed by the experimental design of the ADNI study. Therefore, it is imperative to expand the sample size and validate the experimental findings using datasets from other research centers to ensure the reliability of the results.

Data availability statement

Publicly available datasets were analyzed in this study. This data can be found here: ADNI datasets are publicly available (http://adni.loni.usc.edu/).

Ethics statement

The studies involving humans were approved by the Institutional Review Boards of Alzheimer's Disease Neuroimaging Initiative (ADNI, https://adni.loni.usc.edu). The studies were conducted in accordance with the local legislation and institutional requirements. Written informed consent for participation in this study was provided by the participants' legal guardians/next of kin.

Author contributions

YZ: Conceptualization, Data curation, Formal Analysis, Methodology, Writing–original draft, Writing–review and editing. SS: Conceptualization, Data curation, Formal Analysis, Methodology, Writing–original draft.

Funding

The author(s) declare financial support was received for the research, authorship, and/or publication of this article. This research was supported by Sichuan Science and Technology Program (No. 2018HH0120), National Innovation and Entrepreneurship Training Program for College Students (S202211360089), Panzhihua University Cultivation Program (No. 035000421), and Panzhihua University Research Startup Fund (No. 035200301).

Acknowledgments

We would like to thank the participants of the ADNI projects for providing the methylation and gene expression data. We thank LetPub (www.letpub.com) for its linguistic assistance during the preparation of this manuscript.

Conflict of interest

The authors declare that the research was conducted in the absence of any commercial or financial relationships that could be construed as a potential conflict of interest.

Publisher's note

Supplementary material

The Supplementary Material for this article can be found online at: https://www.frontiersin.org/articles/10.3389/fcell.2024.1276288/full#supplementary-material

References

Aisen, P. S., Petersen, R. C., Donohue, M. C., Gamst, A., Raman, R., Thomas, R. G., et al. (2010). Clinical core of the Alzheimer's disease neuroimaging initiative: progress and plans. *Alzheimer's Dementia* 6 (3), 239–246. doi:10.1016/j.jalz.2010.03.006

Arunachalam, E., Rogers, W., Simpson, G. R., Möller-Levet, C., Bolton, G., Ismael, M., et al. (2022). HOX and PBX gene dysregulation as a therapeutic target in glioblastoma multiforme. *BMC cancer* 22 (1), 400–413. doi:10.1186/s12885-022-09466-8

Baker, J. D., Uhrich, R. L., Strovas, T. J., Saxton, A. D., and Kraemer, B. C. (2020). Targeting pathological tau by small molecule inhibition of the poly (A): MSUT2 RNA–protein interaction. *ACS Chem. Neurosci.* 11 (15), 2277–2285. doi:10.1021/acschemneuro.0c00214

Barqué, A., Jan, K., De La Fuente, E., Nicholas, C. L., Hynes, R. O., and Naba, A. (2021). Knockout of the gene encoding the extracellular matrix protein SNED1 results in early neonatal lethality and craniofacial malformations. *Dev. Dyn.* 250 (2), 274–294. doi:10.1002/dvdy.258

Bu, S., Lv, Y., Liu, Y., Qiao, S., and Wang, H. (2021). Zinc finger proteins in neuro-related diseases progression. *Front. Neurosci.* 15, 760567. doi:10.3389/fnins.2021.760567

Calderari, S., Ria, M., Gérard, C., Nogueira, T. C., Villate, O., Collins, S. C., et al. (2018). Molecular genetics of the transcription factor GLIS3 identifies its dual function in beta cells and neurons. *Genomics* 110 (2), 98–111. doi:10.1016/j.ygeno.2017.09.001

Cassandri, M., Smirnov, A., Novelli, F., Pitolli, C., Agostini, M., Malewicz, M., et al. (2017). Zinc-finger proteins in health and disease. *Cell death Discov.* 3 (1), 17071–17112. doi:10.1038/cddiscovery.2017.71

Chen, Y., Qian, X., Zhang, Y., Su, W., Huang, Y., Wang, X., et al. (2022). Prediction models for conversion from mild cognitive impairment to alzheimer's disease: a systematic review and meta-analysis. *Front. Aging Neurosci.* 14, 840386. doi:10.3389/fnagi.2022.840386

Chouliaras, L., Pishva, E., Haapakoski, R., Zsoldos, E., Mahmood, A., Filippini, N., et al. (2018). Peripheral DNA methylation, cognitive decline and brain aging: pilot findings from the Whitehall II imaging study. *Epigenomics* 10 (5), 585–595. doi:10.2217/epi-2017-0132

Dumurgier, J., Hanseeuw, B. J., Hatling, F. B., Judge, K. A., Schultz, A. P., Chhatwal, J. P., et al. (2017). Alzheimer's disease biomarkers and future decline in cognitive normal older adults. *J. Alzheimer's Dis.* 60 (4), 1451–1459. doi:10.3233/JAD-170511

Farias, S. T., Mungas, D., Reed, B. R., Harvey, D., and DeCarli, C. (2009). Progression of mild cognitive impairment to dementia in clinic-vs community-based cohorts. *Archives neurology* 66 (9), 1151–1157. doi:10.1001/archneurol.2009.106

Farmiloe, G., Lodewijk, G. A., Robben, S. F., van Bree, E. J., and Jacobs, F. M. (2020). Widespread correlation of KRAB zinc finger protein binding with brain-developmental gene expression patterns. *Philosophical Trans. R. Soc. B* 375 (1795), 20190333. doi:10.1098/rstb.2019.0333

Fortin, J.-P., Triche, T. J., Jr, and Hansen, K. D. (2017). Preprocessing, normalization and integration of the Illumina HumanMethylationEPIC array with minfi. *Bioinformatics* 33 (4), 558–560. doi:10.1093/bioinformatics/btw691

Grundman, M., Petersen, R. C., Ferris, S. H., Thomas, R. G., Aisen, P. S., Bennett, D. A., et al. (2004). Mild cognitive impairment can be distinguished from Alzheimer disease and normal aging for clinical trials. *Archives neurology* 61 (1), 59–66. doi:10.1001/archneur.61.1.59

Houseman, E. A., Accomando, W. P., Koestler, D. C., Christensen, B. C., Marsit, C. J., Nelson, H. H., et al. (2012). DNA methylation arrays as surrogate measures of cell mixture distribution. *BMC Bioinforma.* 13 (1), 86–16. doi:10.1186/1471-2105-13-86

Jack, C. R., Jr, Bernstein, M. A., Fox, N. C., Thompson, P., Alexander, G., Harvey, D., et al. (2008). The Alzheimer's disease neuroimaging initiative (ADNI): MRI methods. *J. Magnetic Reson. Imaging Official J. Int. Soc. Magnetic Reson. Med.* 27 (4), 685–691. doi:10.1002/jmri.21049

Jessen, F., Wolfsgruber, S., Wiese, B., Bickel, H., Mösch, E., Kaduszkiewicz, H., et al. (2014). AD dementia risk in late MCI, in early MCI, and in subjective memory impairment. *Alzheimer's Dementia* 10 (1), 76–83. doi:10.1016/j.jalz.2012.09.017

Krushkal, J., Silvers, T., Reinhold, W. C., Sonkin, D., Vural, S., Connelly, J., et al. (2020). Epigenome-wide DNA methylation analysis of small cell lung cancer cell lines suggests potential chemotherapy targets. *Clin. epigenetics* 12, 93–28. doi:10.1186/s13148-020-00876-8

Lee, M., Joehanes, R., McCartney, D. L., Kho, M., Hüls, A., Wyss, A. B., et al. (2022). Opioid medication use and blood DNA methylation: epigenome-wide association meta-analysis. *Epigenomics* 14 (23), 1479–1492. doi:10.2217/epi-2022-0353

Li, Q. S., Vasanthakumar, A., Davis, J. W., Idler, K., Nho, K., Waring, J., et al. (2021). Association of peripheral blood DNA methylation levels with Alzheimer's disease progression. *Alzheimer's Dementia* 17, e052477. doi:10.1002/alz.052477

Li, Y., Lin, S., Gu, Z., Chen, L., and He, B. (2022). Zinc-dependent deacetylases (HDACs) as potential targets for treating Alzheimer's disease. *Bioorg. Med. Chem. Lett.* 76, 129015. doi:10.1016/j.bmcl.2022.129015

Lo, R. Y., Hubbard, A. E., Shaw, L. M., Trojanowski, J. Q., Petersen, R. C., Aisen, P. S., et al. (2011). Longitudinal change of biomarkers in cognitive decline. *Archives neurology* 68 (10), 1257–1266. doi:10.1001/archneurol.2011.123

Lopez, J. A. S., González, H. M., and Léger, G. C. (2019). Alzheimer's disease. *Handb. Clin. neurology* 167, 231–255. doi:10.1016/B978-0-12-804766-8.00013-3

Lu, J., Liu, L., Chen, J., Zhi, J., Li, J., Li, L., et al. (2022). The involvement of lncRNA HOTAIR/miR-130a-3p axis in the regulation of voluntary exercise on cognition and inflammation of Alzheimer's disease. *Am. J. Alzheimer's Dis. Other Dementias®* 37, 15333175221091424. doi:10.1177/15333175221091424

Lunnon, K., Smith, R., Hannon, E., De Jager, P. L., Srivastava, G., Volta, M., et al. (2014). Methylomic profiling implicates cortical deregulation of ANK1 in Alzheimer's disease. *Nat. Neurosci.* 17 (9), 1164–1170. doi:10.1038/nn.3782

Madrid, A., Hogan, K. J., Papale, L. A., Clark, L. R., Asthana, S., Johnson, S. C., et al. (2018). DNA hypomethylation in blood links B3GALT4 and ZADH2 to Alzheimer's disease. *J. Alzheimer's Dis.* 66 (3), 927–934. doi:10.3233/JAD-180592

McGirr, A., Nathan, S., Ghahremani, M., Gill, S., Smith, E. E., and Ismail, Z. (2022). Progression to dementia or reversion to normal cognition in mild cognitive impairment as a function of late-onset neuropsychiatric symptoms. *Neurology* 98 (21), e2132–e2139. doi:10.1212/WNL.0000000000200256

Naba, A., Clauser, K. R., Lamar, J. M., Carr, S. A., and Hynes, R. O. (2014). Extracellular matrix signatures of human mammary carcinoma identify novel metastasis promoters. *elife* 3, e01308. doi:10.7554/eLife.01308

Petersen, R. C. (2004). Mild cognitive impairment as a diagnostic entity. *J. Intern. Med.* 256 (3), 183–194. doi:10.1111/j.1365-2796.2004.01388.x

Petersen, R. C., Doody, R., Kurz, A., Mohs, R. C., Morris, J. C., Rabins, P. V., et al. (2001). Current concepts in mild cognitive impairment. *Archives neurology* 58 (12), 1985–1992. doi:10.1001/archneur.58.12.1985

Raouf Issa, A., Ac Menzies, J., Padmanabhan, A., and Alonso, C. R. (2022). A novel post-developmental role of the Hox genes underlies normal adult behavior. *Proc. Natl. Acad. Sci.* 119 (49), e2209531119. doi:10.1073/pnas.2209531119

Roubroeks, J. A., Smith, A. R., Smith, R. G., Pishva, E., Ibrahim, Z., Sattlecker, M., et al. (2020). An epigenome-wide association study of Alzheimer's disease blood highlights robust DNA hypermethylation in the HOXB6 gene. *Neurobiol. Aging* 95, 26–45. doi:10.1016/j.neurobiolaging.2020.06.023

Smith, R. G., Hannon, E., De Jager, P. L., Chibnik, L., Lott, S. J., Condliffe, D., et al. (2018). Elevated DNA methylation across a 48-kb region spanning the HOXA gene cluster is associated with Alzheimer's disease neuropathology. *Alzheimer's Dementia* 14 (12), 1580–1588. doi:10.1016/j.jalz.2018.01.017

Tábuas-Pereira, M., Baldeiras, I., Duro, D., Santiago, B., Ribeiro, M. H., Leitão, M. J., et al. (2016). Prognosis of early-onset vs. late-onset mild cognitive impairment: comparison of conversion rates and its predictors. *Geriatrics* 1 (2), 11. doi:10.3390/geriatrics1020011

Tarr, I. S., McCann, E. P., Benyamin, B., Peters, T. J., Twine, N. A., Zhang, K. Y., et al. (2019). Monozygotic twins and triplets discordant for amyotrophic lateral sclerosis display differential methylation and gene expression. *Sci. Rep.* 9 (1), 8254. doi:10.1038/s41598-019-44765-4

Tian, Y., Morris, T. J., Webster, A. P., Yang, Z., Beck, S., Feber, A., et al. (2017). ChAMP: updated methylation analysis pipeline for Illumina BeadChips. *Bioinformatics* 33 (24), 3982–3984. doi:10.1093/bioinformatics/btx513

Trzeciakiewicz, H., Ajit, D., Tseng, J.-H., Chen, Y., Ajit, A., Tabassum, Z., et al. (2020). An HDAC6-dependent surveillance mechanism suppresses tau-mediated neurodegeneration and cognitive decline. *Nat. Commun.* 11 (1), 5522. doi:10.1038/s41467-020-19317-4

Vallet, S. D., Davis, M. N., Barqué, A., Thahab, A. H., Ricard-Blum, S., and Naba, A. (2021). Computational and experimental characterization of the novel ECM glycoprotein SNED1 and prediction of its interactome. *Biochem. J.* 478 (7), 1413–1434. doi:10.1042/BCJ20200675

Vasanthakumar, A., Davis, J. W., Idler, K., Waring, J. F., Asque, E., Riley-Gillis, B., et al. (2020). Harnessing peripheral DNA methylation differences in the Alzheimer's Disease Neuroimaging Initiative (ADNI) to reveal novel biomarkers of disease. *Clin. epigenetics* 12, 84–11. doi:10.1186/s13148-020-00864-y

Zhang, L., Sheng, S., and Qin, C. (2013). The role of HDAC6 in Alzheimer's disease. *J. Alzheimer's Dis.* 33 (2), 283–295. doi:10.3233/JAD-2012-120727

Zhang, T., Zhao, Z., Zhang, C., Zhang, J., Jin, Z., and Li, L. (2019). Classification of early and late mild cognitive impairment using functional brain network of resting-state fMRI. *Front. Psychiatry* 10, 572. doi:10.3389/fpsyt.2019.00572

frontiers | Frontiers in Cardiovascular Medicine

TYPE Systematic Review
PUBLISHED 26 February 2024
DOI 10.3389/fcvm.2024.1323423

OPEN ACCESS

EDITED BY
Peng Zhang,
Institute of ENT and Shenzhen Key Laboratory of ENT, China

REVIEWED BY
Satyesh K Sinha,
University of California, Los Angeles, United States
George Lisi,
Brown University, United States
Shannon Moonah,
University of Florida, United States

*CORRESPONDENCE
Atiyeh M. Abdallah
✉ aabdallah@qu.edu.qa

RECEIVED 17 October 2023
ACCEPTED 14 February 2024
PUBLISHED 26 February 2024

CITATION
Fouda H, Ibrahim WN, Shi Z, Alahmadi F, Almohammadi Y, Al-Haidose A and Abdallah AM (2024) Impact of the *MIF* -173G/C variant on cardiovascular disease risk: a meta-analysis of 9,047 participants.
Front. Cardiovasc. Med. 11:1323423.
doi: 10.3389/fcvm.2024.1323423

Impact of the *MIF* -173G/C variant on cardiovascular disease risk: a meta-analysis of 9,047 participants

Hamas Fouda[1], Wisam N. Ibrahim[1], Zumin Shi[2], Fahad Alahmadi[3], Yousef Almohammadi[4], Amal Al-Haidose[1] and Atiyeh M. Abdallah[1]*

[1]Department of Biomedical Sciences, College of Health Sciences, QU Health, Qatar University, Doha, Qatar, [2]Human Nutrition Department, College of Health Sciences, QU Health, Qatar University, Doha, Qatar, [3]Pediatric Department, College of Medicine, Taibah University, King Faisal Specialist Hospital, Al-Madinah, Saudi Arabia, [4]Pediatric Department, Security Forces Medical Centre, Al-Madinah, Saudi Arabia

Introduction: Many factors contribute to the risk of cardiovascular disease (CVD), an umbrella term for several different heart diseases, including inflammation. Macrophage migration inhibitory factor (MIF) is an important immune modulator that has been shown to be involved in the pathogenesis of different heart diseases, so understanding pathogenic variants of the *MIF* gene is important for risk stratification. We therefore conducted a meta-analysis to investigate whether the *MIF* -173G/C (rs755622) polymorphism is associated with CVD.

Methods: The PubMed, Science Direct, and Embase databases were searched from inception to June 2023 for case-control studies of the *MIF* -173G/C polymorphism and its relationship to any type of CVD. Correlations between the *MIF* -173G/C polymorphism and CVD were estimated by pooling the odds ratios (ORs) with 95% confidence intervals in allelic, dominant, and recessive models using random-effects meta-analysis.

Results: A total of 9,047 participants (4141 CVD cases and 4906 healthy controls) from 11 relevant studies were included. In the total population, there was no significant association between the *MIF* -173G/C (rs755622) polymorphism and the risk of developing CVD in the three different models. In a stratified analysis by ethnicity, the allelic model (C vs G) was significantly associated with CVD in the Arab and Asian populations (OR = 0.56, CI 0.42 -0.75 and OR = 1.28, CI 1.12 -1.46, respectively); the dominant model (CC+CG vs GG) was significantly associated with CVD in the Arab population (OR = 0.42, CI 0.30 -0.61); while the recessive model (GG+GC vs CC) was associated with CVD susceptibility in the Arab population (OR = 3.84, CI 1.57 -9.41). There were no significant associations between the *MIF* -173 G/C polymorphism and CVD risk in the European population. Conclusion, the *MIF* -173G/C polymorphism is associated with CVD in some populations.

Systematic Review Registration: https://www.crd.york.ac.uk/PROSPERO/, PROSPERO (CRD42023441139).

KEYWORDS

cardiovascular disease, macrophage migration inhibitory factor, polymorphism, meta-analysis, Arab, Asian, European

1 Introduction

Macrophage migration inhibitory factor (MIF) is an immune cytokine with pro-inflammatory, enzymatic, and hormonal functions implicated the pathogenesis of inflammatory and neoplastic diseases. MIF has various functions including in leukocyte recruitment, regulation of immune responses, inflammation, counter-regulation of glucocorticoid activity, and cellular proliferation (1). It is expressed in several immune cell types including T cells, neutrophils, monocytes/macrophages, and eosinophils and also in pituitary cells, epithelial cells, smooth muscle cells, and cardiomyocytes (2, 3), suggesting that it can have diverse roles in various pathophysiological processes (4, 5). MIF is known to play a critical role in both innate and acquired immune responses and it upregulates the expression of pro-inflammatory cytokines (6, 7). In addition, MIF is implicated in cardiovascular diseases (CVD), acting as a reliable biomarker of disease severity and being readily detectable in the blood and at sites of inflammation (8). MIF may therefore have significant impact on the prognosis of CVD patients through its ability to modulate the disease phenotype.

CVD is a common and leading cause of mortality and morbidity worldwide (9, 10). Recognizing CVD as a serious concern for global health, the WHO launched the 25×25 Action Plan in 2013 to reduce premature mortality due to non-communicable diseases by 25% by 2025 (11). The 2015 Global Burden of Diseases study estimated that there are 422.7 million CVD cases and 17.59 million CVD deaths worldwide (10). Furthermore, its prevalence is increasing, mostly due to population growth and aging populations, with especially high prevalences in South and East Asia due to their large and rapidly growing populations. Conversely, CVD mortality rates decreased by ~15% between 1990 and 2015 in some high-income and some middle-income countries (11), while mortality rates have plateaued in high-income regions such as Western Europe, North America, and Australia. Overall, middle-to-low-income countries appear to be disproportionately burdened by CVD mortality. Additionally, CVD occurs approximately 7–10 years later in females than in males, although it remains a major cause of death in females over 65 years. For instance, recent data from the National Health and Nutrition Examination revealed that the prevalence of MI has increased in females aged between 35 and 45 years over the past two decades while decreasing in similarly aged males (12). Deaths due to CVD are most amenable to rapid intervention, and preventing deaths from CVD requires reliable data on CVD risk factors to inform effective treatment and prevention. Individual predisposition to CVD is determined by both environmental and genetic risk factors, the most prevalent environmental factors being hypertension, hypercholesteremia, diabetes, obesity, smoking, stress, gender, ethnic origin, and a sedentary lifestyle (13–15).

CVD is an umbrella term for different heart diseases including coronary artery disease (CAD), myocardial infarction (MI), heart failure (HF), coronary artery abnormalities (CAA), acute coronary syndrome (ACS), and rheumatic heart disease (RHD) (Figure 1). CHD is defined as the narrowing of the coronary arteries leading to a reduced luminal diameter and hence a decrease in blood flow, and it is the most common cause of MI (16). Hypertension and hypercholesteremia accelerate atherosclerotic plaque development and formation due to endothelial injury, which increases endothelial permeability and allows plasma components to infiltrate (17). Plaque hemorrhage ultimately activates thrombus formation initiated by platelet aggregation. Furthermore, cholesterol and triglycerides contribute to plaque formation, both positively and negatively (18). Prolonged and silent atherosclerosis and plaque formation involve chronic inflammatory reactions that influence immune cell, platelet, and complement recruitment to the site of injury (18). Recent

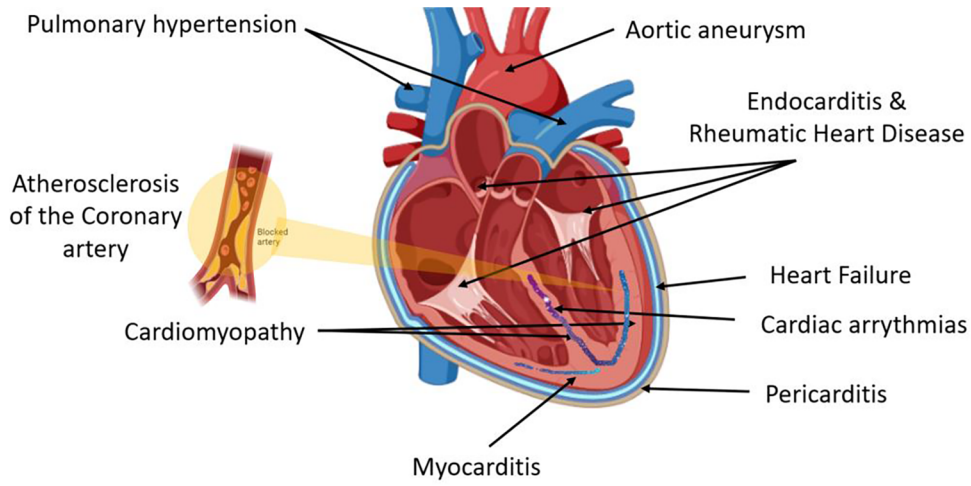

FIGURE 1
Cardiovascular disease (CVD) is an umbrella term for different heart diseases that include abnormalities of the pericardial layer (e.g., pericarditis and pericardial effusion), myocardial layer [e.g., myocarditis, cardiomyopathy, coronary artery disease (CAD), myocardial infarction (MI), heart failure (HF), coronary artery abnormalities (CAA), acute coronary syndrome (ACS)], the endocardial layer [e.g., valvular heart diseases including endocarditis and rheumatic heart disease (RHD)], abnormalities of the cardiac conductive system including all cardiac arrythmias, and lastly arterial abnormalities such as hypertension and aneurysm.

compelling evidence highlights a central role for macrophage proliferation within atherosclerotic lesions in driving disease progression. These macrophages, initially immune cells, undergo multiplication, contributing significantly to the pool of foam cells within arterial walls (19). As part of this process, myocardium-produced MIF is highly associated with the development of various CVDs (20), and there is increasing evidence that MIF plays a major role in atheroma formation and CVD progression.

MIF is a short gene (<0.7 kb) at 22q11.2 composed of three short exons of 107, 172, and 66 base pairs (21). The *MIF* promoter harbors two polymorphisms that have a regulatory effect on gene transcription (22): the -974 CATT tetranucleotide repeat, which exists in 5–8 repeats (rs5844572), and the -173 G-to-C polymorphism (rs755622). The $CATT_5$ repeat is associated with low *MIF* expression compared with the $CATT_6$, $CATT_7$, and $CATT_8$ repeat alleles. By contrast, -173C allele is associated with high *MIF* gene expression (23). Both polymorphisms have been reported to be associated with different autoimmune and inflammatory diseases. A meta-analysis of 23 articles from different populations representing 5,559 cases and 7,335 controls reported an association between the -173G/C polymorphism and susceptibility to a wide range of different autoimmune diseases (24). Karakaya et al. reported an association between the *MIF* -173C allele and erythema nodosum in Löfgren syndrome patients but not sarcoidosis, indicating a role for MIF after the sarcoid inflammatory response has begun (25). Interestingly, MIF demonstrated a specific role in the recruitment and accumulation of inflammatory macrophages in an animal model of polymicrobial sepsis (26). Moreover, MIF was found to play an important role as a stress molecule counteracting the immunosuppressive effect of glucocorticoids in renal inflammation (27), and MIF deficiency suppressed apoptosis and protected the liver from ischemia-reperfusion injury (28). Conversely, MIF has been shown to play a protective role in Parkinson's disease (29).

Therefore, there is evidence that MIF is associated with CVD, with an association between the *MIF* -173C/G polymorphism and CVD reported in some but not all populations. To clarify this association, here we conducted a meta-analysis based on a systematic literature review to confirm whether *MIF* -173G/C (rs755622) is associated with the risk of developing CVD.

2 Materials and methods

2.1 Study design and objectives

This review followed Preferred Reporting Items for Systematic Review and Meta-Analysis (PRISMA) guidelines (Figure 2) (30) and was registered in the International Prospective Register of Systematic Reviews (PROSPERO; CRD42023441139) database. A PICO strategy was used to guide the study design: population, patients with CVD; intervention, association between the *MIF* -173G/C variant and CVD; and primary outcome, the association between *MIF* -173G/C and CVD.

2.2 Search strategy

The PubMed, Science Direct, and Embase databases were searched from inception of these databases to June 2023 using the

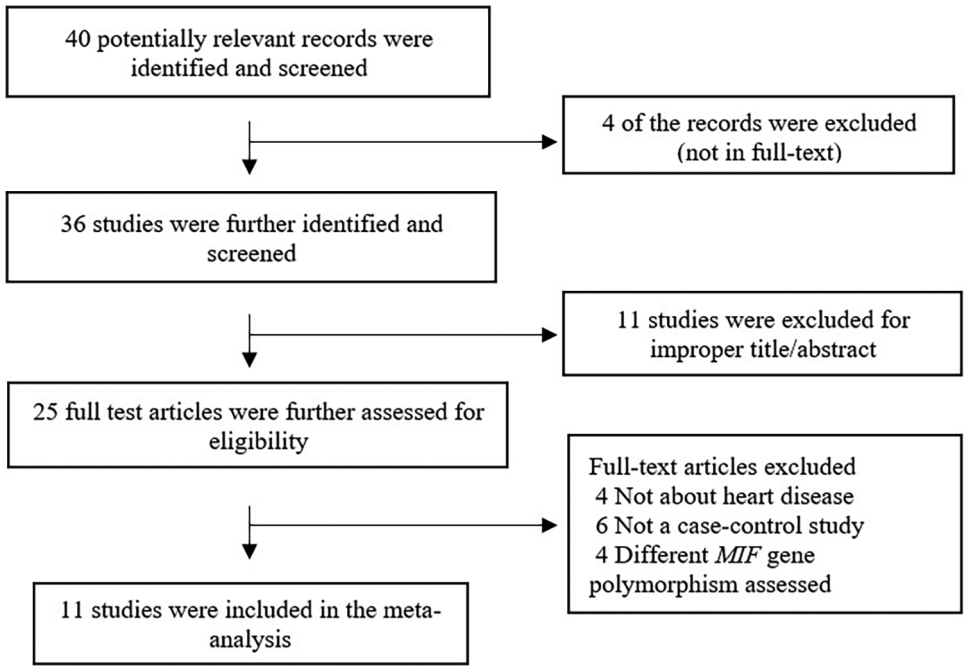

FIGURE 2
Flow chart of the literature review.

following terms: macrophage migration inhibitory factor or *MIF* [TEXT WORD] and cardiovascular disease or coronary artery disease [TEXT WORD] or cardiomyopathy [TEXT WORD] or cardiac surgery [TEXT WORD] or HF [TEXT WORD] or rheumatic heart disease [TEXT WORD] or kawasaki disease [TEXT WORD], MI [TEXT WORD] or intracoronary thrombosis [TEXT WORD] or acute coronary syndrome [TEXT WORD] or sudden cardiac death [TEXT WORD]. In addition, the reference lists of compatible articles and conferences were reviewed. Two authors individually screened each article by title and abstract and then evaluated the full text to fully assess eligibility for inclusion.

2.3 Inclusion and exclusion criteria

The inclusion criteria were: (1) all conditions affecting the heart or blood vessels were included as CVD; (2) evaluated *MIF* -173 G/C polymorphisms and cardiovascular risk; (3) case-control or nested case-control design; (4) included the genotypes for the *MIF* -173G/C gene polymorphism in CVD cases and controls; and (5) the study reported that the distribution of genotypes among controls was in Hardy-Weinberg equilibrium (HWE). Exclusion criteria were: (1) failed to provide detailed data in the abstract and review; (2) the study was a duplicate; (3) failed to report the genotype frequency; and (4) the controls failed to meet HWE.

2.4 Data extraction and models

The author's details, date of publication, region of study, population ethnicity, number of genotypes analyzed, and the total number of cases and controls were recorded from each article. Two authors individually extracted the required data for each study article, and any disagreement was resolved by consensus or by consultation with a senior author.

Three different genetic models were used to assess the association between the genetic variant and the outcome: the dominant model (Model 1) was defined as the presence of the common allele (CC + CG vs. GG); the recessive genetic model (Model 2) was the presence of rare allele (GG + GC vs. CC); and the allelic model assessed the association between the alleles (C vs. G) and the outcome, regardless of whether it was dominant or recessive.

2.5 Quality assessment

Quality was assessed using the Newcastle-Ottawa quality assessment scale (NOS) for case-control studies. Data quality was judged based on comparability, selection, and outcome of interest for case-control study articles and was noted using a "star system". To compare study quality, star counts were totaled (Table 1). Data validity was assessed by senior authors based on the provided criteria.

2.6 Statistical analysis

All statistical analyses were performed in STATA v17 (StataCorp, College Station, TX, United States). Heterogeneity between studies was assessed with the I^2 statistic. The pooled odds ratio (OR) with 95% CI in the forest plot was analyzed using a random-effects model [restricted maximum likelihood (REML) method] with the subgroup option in Stata. Begg's funnel plot was used to qualitatively assess the risk of publication bias. All analyses were performed using Stata 18. A p-value <0.05 (two-sided) was considered statistically significant in all analyses.

3 Results

3.1 Study characteristics

Figure 1 summarizes the search process. Forty articles were found in the initial search, 29 of which were excluded after applying exclusion criteria. Eleven articles met the inclusion criteria and were used in the meta-analysis, representing 4,906 controls and 4,141 cases.

The characteristics of the included articles are summarized in Table 1. Of the included studies, three were performed in Arab populations, six in Asian populations, and two in European

TABLE 1 Characteristics of studies included in the meta-analysis.

No	Reference	Country	Ethnicity	CVD type	Case number	Control number	Genotyping	Newcastle-Ottawa score
1	Idouz et al. 2019 (32)	Morocco	Arab	Dilated cardiomyopathy (DCM)	53	50	TaqMan	6/7
2	El-Mahdy et al. 2021 (33)	Egypt	Arab	Heart failure	90	60	PCR-RFLP	6/7
3	Abdallah et al. 2016 (34)	Saudi Arabia	Arab	Rheumatic heart disease	124	202	TaqMan	6/7
4	Simonini et al. 2008 (35)	Italy	European	Kawasaki disease	69	60	PCR-RFLP	6/7
5	Tereshchenko et al. 2009 (36)	Czech	European	Myocardial infarction	219	137	TaqMan	5/7
	Tereshchenko et al. 2009 (36)	Russian	European	Myocardial infarction	240	174	PCR-SSP	
6	Luo et al. 2016 (37)	Chinese Kazakh	Asian	Coronary artery disease	320	603	TaqMan	4/7
7	Ji et al. 2015 (38)	Chinese Han	Asian	Coronary heart disease	70	186	PCR	3/7
8	Luo et al. 2021 (39)	Chinese Han	Asian	Coronary artery disease	1,176	1,120	TaqMan	5/7
9	Du et al. 2020 (40)	Chinese	Asian	Acute coronary syndrome	699	1,153	TaqMan	5/7
10	Zhang et al. 2022 (41)	Chinese	Asian	Acute coronary syndrome	963	932	50-Plex SNPscan	6/7
11	Qian & Ripeng 2018 (31)	Chinese	Asian	Coronary heart disease	118	229	PCR-RFLP	3/7
				Total	4,141	4,906		

populations (31–41). All included studies were cross-sectional case-control studies that included the necessary data to calculate the possible association between the *MIF* -173G/C polymorphism and CVD. One study was published in Chinese, while the remaining studies were published in English.

The individual studies' quality was appraised utilizing the Newcastle-Ottawa Scale (NOS) scoring system. According to the NOS results, 73% of the included studies achieved a score of 5 or higher out of 7 on the NOS scale, indicating an overall good level of quality (Table 1).

3.2 Quantitative data synthesis

The distribution of the *MIF* -173 genotype in CVD is shown in Table 2, and the meta-analysis results are shown in Table 3. There was no significant impact of the *MIF* -173G/C polymorphism and the risk of CVD in the three models assessed: Model 1 (dominant): CC + CG vs. GG (Figure 3), Model 2 (recessive): GG + GC vs. CC (Figure 4), and Model 3 (allelic): C vs. G (Figure 5).

In the stratified analysis by ethnicity, Model 1 (CC + CG vs. GG) and Model 2 (GG + GC vs. CC) demonstrated significant associations between the *MIF* -173G/C polymorphism and CVD in the Arab population (OR = 0.42, CI 0.30 to 0.61, $p < 0.001$ and OR = 3.84, CI 1.57 to 9.41, $p < 0.001$) (Figures 3, 4) but not in the European and Asian populations. Model 3 (C vs. G) also demonstrated a significant association between the *MIF* -173G/C polymorphism and the risk of CVD in the Arab population (OR = 0.56, CI 0.42 to 0.75, $p < 0.001$) (Figure 5) and in the Asian population (OR = 1.28, CI 1.12 to 1.46, $p < 0.001$) but not in the European population.

3.3 Publication bias analyses

Begg's funnel plot and Egger's test were performed to assess publication bias (Figure 6). For all three models, there was no

TABLE 2 Genotypes and allele frequencies *of MIF* -173G/C genes in CVD patients and controls.

Study	Case					Control						
	GG	GC	CC	G	C	GG	GC	CC	G	C	Sample size	HWE (P)
Idouz et al. 2019 (32)	29	18	6	76	30	11	39	0	61	39	53/50	0.01
El-Mahdy et al. 2021 (33)	51	36	3	87	39	24	30	6	54	36	90/60	0.15
Abdallah et al. 2016 (34)	95	26	3	216	32	122	64	16	308	96	124/202	0.07
Simonini et al. 2008 (35)	46	19	14	111	47	46	12	2	104	16	69/60	0.30
Tereshchenko et al. 2009 (36)	163	47	9	373	65	103	31	3	237	37	219/137	0.71
Tereshchenko et al. 2009 (36)	164	73	3	401	79	126	42	6	294	54	240/174	0.30
Luo et al. 2016 (37)	153	140	27	446	194	367	205	31	939	267	320/603	0.73
Ji et al. 2015 (38)	46	14	10	106	34	136	44	6	316	56	70/186	0.31
Luo et al. 2021 (39)	688	411	77	1,787	565	703	373	44	1,779	461	1,176/1,120	0.53
Du et al. 2020 (40)	396	272	31	1,064	334	727	382	44	1,836	470	699/1,153	0.48
Zhang et al. 2022 (41)	586	317	60	1,489	437	559	337	36	1,455	409	963/932	0.09
Qian & Ripeng 2018 (31)	71	26	21	168	68	142	73	14	357	101	118/229	0.27

HWE, Hardy-Weinberg equilibrium; MIF, macrophage migration inhibitory factor; CVD, cardiovascular disease.

TABLE 3 Summary of different meta-analysis results.

Study	Sample size			Test of association			Heterogeneity		
	Case	Control	Number of studies	OR (95% CI)	Z	*p*-value	X^2	*p*-value	I^2 (%)
CC + CG vs. GG									
Overall	4,279	5,069	12	1.03 [0.73 to 1.46]	0.19	0.85	0.30	0.00	91.2
Arab	267	312	3	0.42 [0.30 to 0.61]	−4.60	0.00	0.00	0.32	0.00
European	528	371	3	1.30 [0.92 to 1.85]	1.48	0.14	0.02	0.19	24.2
Asian	3,484	4,386	6	1.24 [0.98 to 1.57]	1.82	0.07	0.06	0.00	76.8
GG + GC vs. CC									
Overall	4,279	5,069	12	0.86 [0.52 to 1.43]	−0.58	0.56	0.53	0.00	81.2
Arab	267	312	3	3.84 [1.57 to 9.41]	2.94	0.00	0.00	0.66	0.00
European	528	371	3	0.63 [0.13 to 3.15]	−0.56	0.57	1.50	0.02	74.2
Asian	3,484	4,386	6	0.67 [0.46 to 0.97]	−2.12	0.03	0.14	0.01	68.1
C vs. G									
Overall	4,279	5,069	12	1.13 [0.90 to 1.43]	1.04	0.30	0.13	0.00	87.9
Arab	267	312	3	0.56 [0.42 to 0.75]	−3.83	0.00	0.00	0.59	0.0
European	528	371	3	1.42 [0.82 to 2.47]	1.24	0.21	0.18	0.03	76
Asian	3,484	4,386	6	1.28 [1.12 to 1.46]	3.60	0.00	0.01	0.04	59

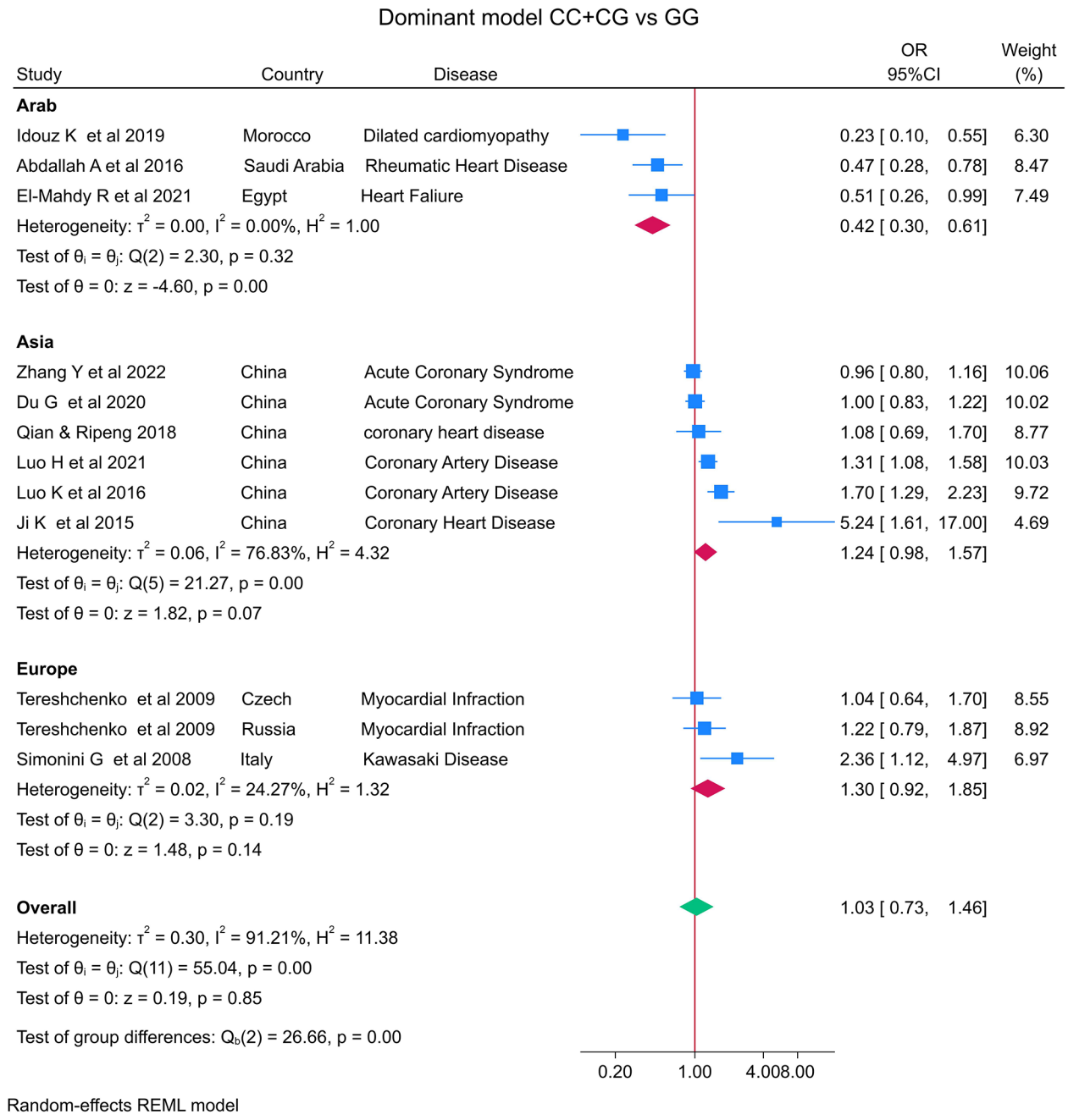

FIGURE 3
Forest plot of cardiovascular disease risk associated with the *MIF* -173 G/C polymorphism in Model 1 (CC + CG vs. GG) in Arab, Asian, and European ethnicities.

obvious asymmetry and there was no evidence of publication bias for Model 1 ($p = 0.851$), Model 2 ($p = 0.154$), or Model 3 ($p = 0.687$).

4 Discussion

In this meta-analysis, we aimed to comprehensively review and quantify the literature to establish whether the *MIF* -173G/C (rs755622) polymorphism is associated with a risk of CVD development. By meta-analyzing eleven studies representing 4,279 cases and 5,069 controls, we found no significant association between the *MIF* -173G/C polymorphism and the risk of CVD in the overall study population in the three models assessed: CC + CG vs. GG (OR = 1.03), GG + GC vs. CC (OR = 0.86), and C vs. G allele (OR = 1.13). In addition, due to overall heterogeneity and variability in study outcomes between different studies, we conducted a subgroup analysis of the different ethnicities, which revealed that the *MIF* -173G/C polymorphism is significantly associated with a decreased risk of CVD in the Arab population but not the Asian or European populations in the CC

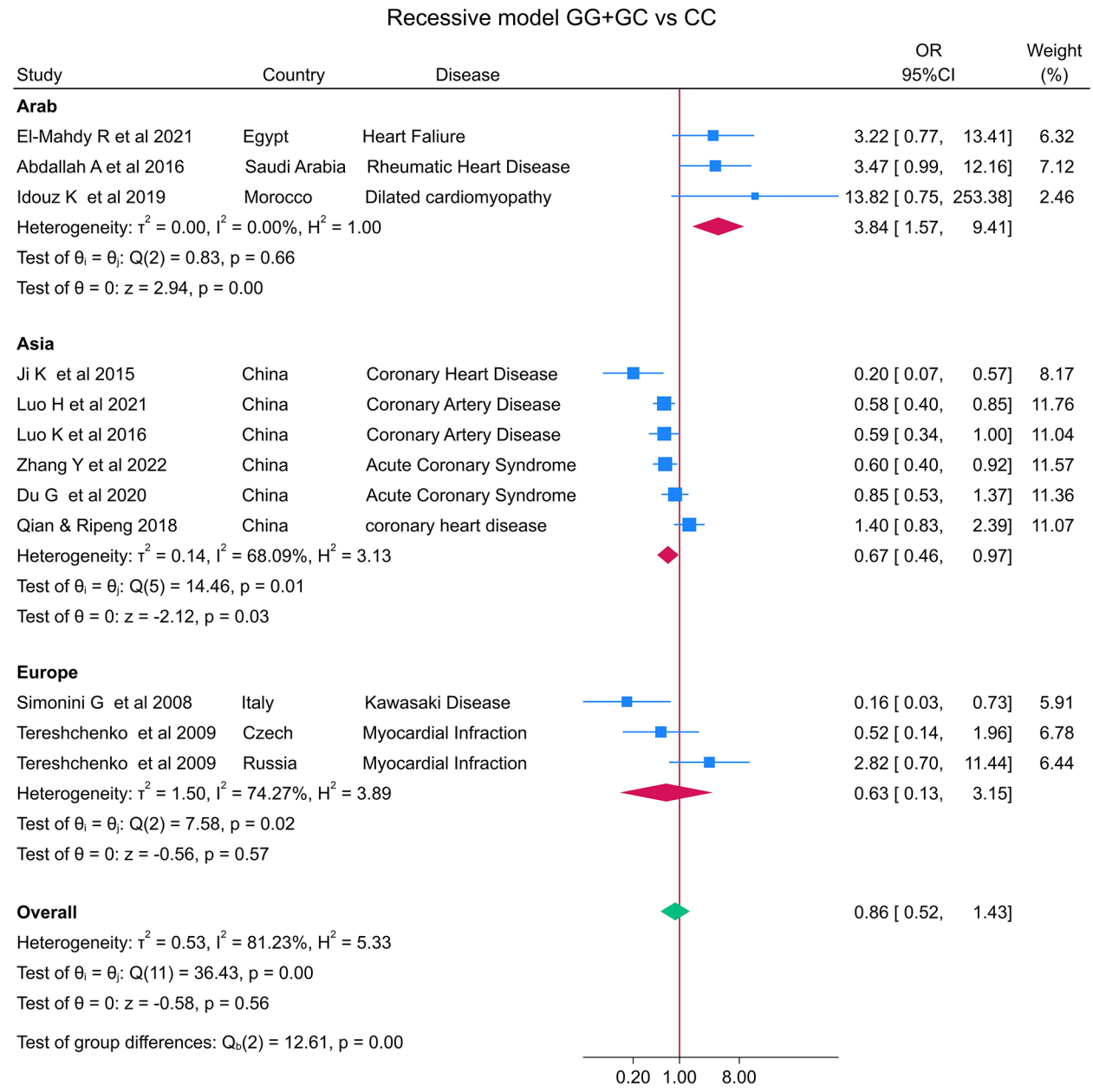

FIGURE 4
Forest plot of cardiovascular disease risk associated with the *MIF* -173 G/C polymorphism in model 2 (GG + GC vs. CC) in Arab, Asian, and European ethnicities.

+ CG vs. GG model. In the second GG + GC vs. CC model, there was again a significant association between the *MIF* -173G/C polymorphism and the risk of CVD in the Arab population but not the Asian or European populations. Finally, for the C vs. G allele model, a significant association was observed in the Arab population (OR = 0.56) and the Asian population (OR = 1.28) but not the European population for the *MIF* -173G/C polymorphism and CVD risk. Our findings are similar to other meta-analyses of *MIF*, where the C allele was found to be more common within CAD patients (42) and those with chronic kidney diseases (43). However, in systemic lupus erythematosus, while serum MIF levels were associated with the disease, a meta-analysis found no association between the -173G/C polymorphism and the disease (44).

In atherosclerosis, macrophages play a pivotal role, undergoing proliferation and apoptosis. Macrophage proliferation contributes to plaque inflammation, while apoptosis, if excessive, may lead to plaque instability (45). MIF influences macrophage functions, promoting recruitment and inhibiting migration. This interplay is crucial in atherosclerotic plaque development. Within plaques, activated macrophages release pro-inflammatory signals and transform into foam cells by engulfing oxidized LDL cholesterol.

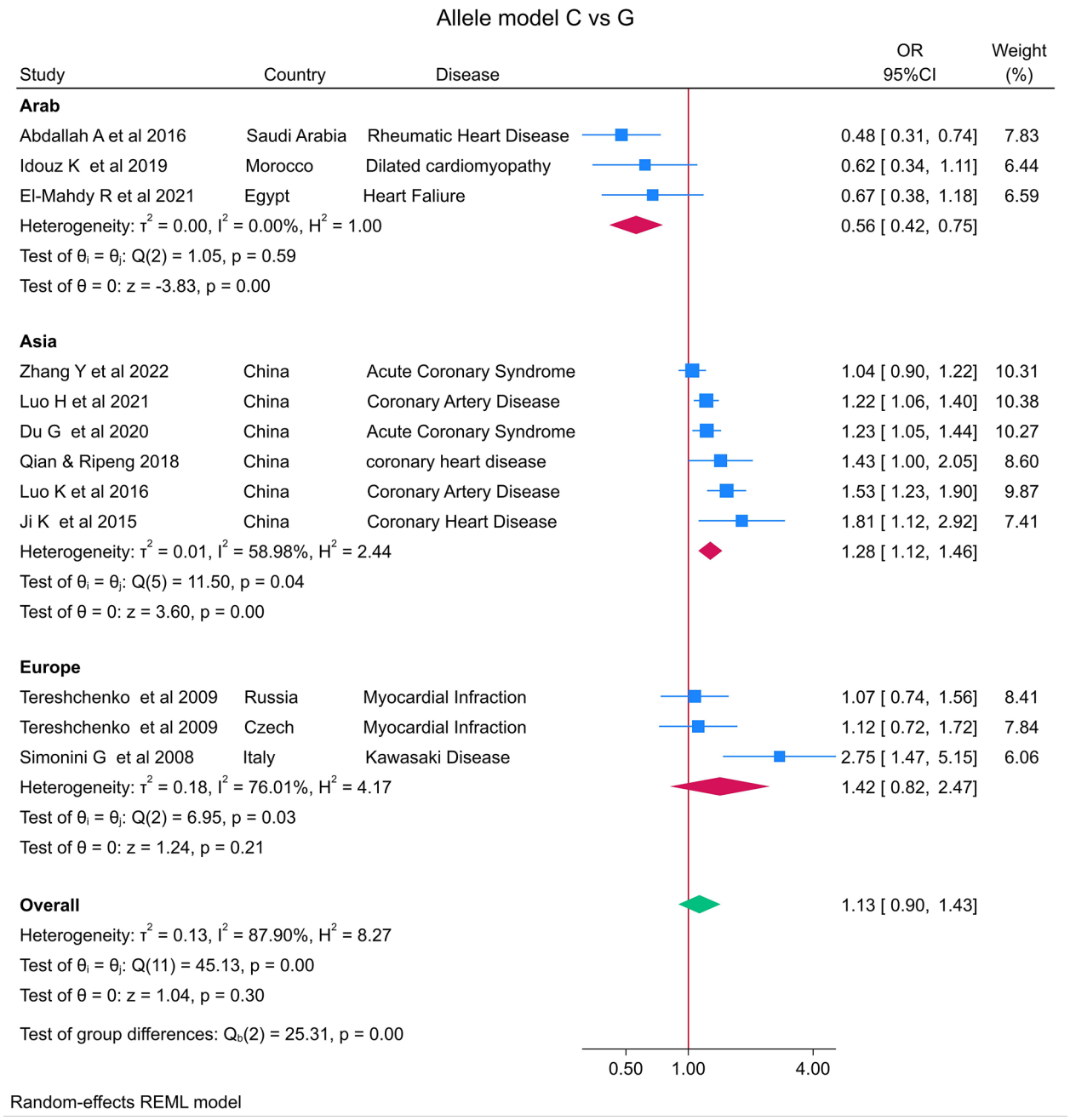

FIGURE 5
Forest plot of cardiovascular disease risk associated with the *MIF* -173 G/C polymorphism in model 3 (C vs. G) alleles in Arab, Asian, and European ethnicities.

The balance between macrophage dynamics and MIF's influence determines the progression and severity of atherosclerosis. Blockade of MIF reduces the aortic inflammatory response and is associated with reduction in aortic plaque and foam cell formation (46). In addition to its direct effects on inflammation and plaque stability, MIF interacts intricately with CXCL4L1, leading to the formation of prothrombotic and proinflammatory MIF-CXCL4L1 heterocomplexes (47, 48). These heterocomplexes have been implicated in promoting endothelial dysfunction, thrombosis, and exacerbation of inflammatory responses within the vascular environment (49). The presence of the -173 polymorphism in the MIF gene may modulate the formation or activity of these heterocomplexes, potentially influencing the progression and severity of CAD. Consequently, understanding the interplay between MIF protein levels, genetic variations, and the formation of MIF-CXCL4L1 heterocomplexes is crucial for deciphering the multifaceted molecular mechanisms underlying CAD and

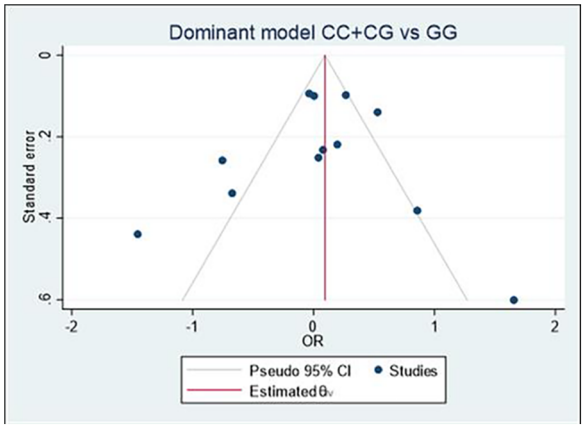

FIGURE 6
Begg's funnel plot of the MIF -173 polymorphism and CVD for all models; Model 1: CC + CG vs. GG, Model 2: GG + GC vs. CC, and Model 3: C vs. G. Egger's test was used to provide statistical evidence of funnel plot symmetry for the three models, and no evidence of publication bias was found in Model 1 ($p = 0.851$), Model 2 ($p = 0.154$), and Model 3 ($p = 0.687$).

devising targeted therapeutic strategies aimed at disrupting these detrimental interactions (50).

Studies of patients with MI have demonstrated dual functions for the *MIF* polymorphism depending on disease severity and the patient's age. For instance, when cardiac ischemia is brief, *MIF* secreted by cardiomyocytes is cardioprotective through activation of AMP-activated protein kinase (AMPK) (51). Phosphorylation of AMPK stimulates glucose uptake through glucose transporter-4 (GLUT4). Conversely, when myocardial ischemia is prolonged, MIF activates immune cells, thereby increasing inflammation and cardiac remodeling by utilizing myofibroblasts to promote matrix protein synthesis (51). Similarly, Abdallah et al. (34) reported a similar dual function for *MIF* in RHD patients, with a lower frequency of the *MIF* -173C allele in RHD patients compared with controls and in those with later disease onset. Their findings suggested that MIF may help to clear pathogens and apoptotic cells during the early stages of RHD, perhaps protecting cardiomyocytes and delaying valvular damage. Conversely, after repetitive rheumatic insults, MIF may accelerate the recruitment of inflammatory cells and pro-inflammatory mediators, increasing regional inflammation and cardiac tissue damage. Similar studies on other diseases have also demonstrated that *MIF* is age-dependent. For instance, Das et al. (52) reported that adults expressing the low MIF ($CATT_5$) allele were more susceptible to Gram-negative bacterial infections, while Lehmann et al. (53) found that adults expressing high levels of *MIF* polymorphisms were protected from sepsis mortality. In animal models, the protective role of MIF was lost in aged animals after ischemic heart injury, with low *MIF* expression impairing AMPK activation (54). These data suggest that it is important to consider the patient's age and disease stage when analyzing *MIF* polymorphisms.

Sex has also been reported to be associated with *MIF* polymorphisms. The MONICA/KORA Augsburg study concluded that female carriers of the *MIF* -173C polymorphism were at higher risk of coronary heart disease (55). This result was later confirmed in two studies of Chinese populations (37, 38). In inflammatory diseases, *MIF* -173 was found to be a disease severity marker for male multiple sclerosis patients (56), while the minor homozygous genotype for both the 974 CATT repeat and the -173G/C polymorphism were reported to protect female patients from major depressive disorder (57). However, another study showed that the *MIF* -173C allele is a susceptibility factor for depression in type 2 diabetes patients (58). These data suggest that these two polymorphisms are sex-specific disease modifiers.

There are several limitations to our meta-analysis. First, we identified relatively few studies for inclusion, and independent validation is now needed, especially for different ancestries. The number of studies for certain diseases and demographic subgroups was small, and the control group in one study was not in HWE. This precluded meaningful subgroup analysis with specific genotypes. In addition, several records without available original data were excluded from the final analysis. The chance of publication bias is high, as studies with statistically significant results are more likely to be published. The lack of representation of certain ethnicities leads to a reduction in the overall heterogeneity of the study samples, so the results require cautious interpretation. The influence of the MIF -173G/C variant on CVD may be affected by genetic, lifestyle, or environmental factors that were inconsistently measured across studies. This lack of consistent measurement may have led to underreporting of these phenomena in the context of MIF variants and CVD within the scope of this meta-analysis. Finally, variations in diagnostic methodology and criteria for CVD can contribute to inconsistencies, compromising the data integrity of published results. Consequently, these discrepancies may restrict the relevance of this meta-analysis.

In conclusion, our meta-analysis suggests that the *MIF* -173G/C polymorphism is not significantly associated with the risk of cardiovascular disease in the overall population. In subgroup analysis by ethnicity, the polymorphism was associated with a decreased risk of CVD in the Arab population. Future meta-analyses should consider the dual effect of *MIF* and the other promoter polymorphisms as well as disease status, sex, and patient age.

Data availability statement

The original contributions presented in the study are included in the article/Supplementary Material, further inquiries can be directed to the corresponding author.

Author contributions

HF: Data curation, Methodology, Writing – original draft. WI: Formal Analysis, Investigation, Resources, Supervision, Validation, Writing – review & editing. ZS: Methodology, Formal Analysis,

Writing – review & editing. FA: Validation, Visualization, Writing – review & editing. YA: Validation, Visualization, Writing – review & editing. AA: Validation, Writing – review & editing, Funding acquisition, Project administration, Resources. AA: Resources, Validation, Conceptualization, Investigation, Supervision, Writing – review & editing.

Funding

The author(s) declare financial support was received for the research, authorship, and/or publication of this article.

This publication was supported by Qatar University, internal grant no. QUCP-CHS-2022-551. The findings achieved herein are solely the responsibility of the authors.

Conflict of interest

The authors declare that the research was conducted in the absence of any commercial or financial relationships that could be construed as a potential conflict of interest.

Publisher's note

References

1. Sumaiya K, Langford D, Natarajaseenivasan K, Shanmughapriya S. Macrophage migration inhibitory factor (MIF): a multifaceted cytokine regulated by genetic and physiological strategies. *Pharmacol Ther*. (2022) 233:108024. doi: 10.1016/j.pharmthera.2021.108024

2. Kasama T, Ohtsuka K, Sato M, Takahashi R, Wakabayashi K, Kobayashi K. Macrophage migration inhibitory factor: a multifunctional cytokine in rheumatic diseases. *Arthritis*. (2010) 2010:1–10. doi: 10.1155/2010/106202

3. Daryadel A, Grifone RF, Simon H-U, Yousefi S. Apoptotic neutrophils release macrophage migration inhibitory factor upon stimulation with tumor necrosis factor-α. *J Biol Chem*. (2006) 281:27653–61. doi: 10.1074/jbc.M604051200

4. Mitchell RA, Metz CN, Peng T, Bucala R. Sustained mitogen-activated protein kinase (MAPK) and cytoplasmic phospholipase A2 activation by macrophage migration inhibitory factor (MIF). *J Biol Chem*. (1999) 274:18100–6. doi: 10.1074/jbc.274.25.18100

5. Mitchell RA, Liao H, Chesney J, Fingerle-Rowson G, Baugh J, David J, et al. Macrophage migration inhibitory factor (MIF) sustains macrophage proinflammatory function by inhibiting p53: regulatory role in the innate immune response. *Proc Natl Acad Sci USA*. (2002) 99:345–50. doi: 10.1073/pnas.012511599

6. Rossi AG, Haslett C, Hirani N, Greening AP, Rahman I, Metz CN, et al. Human circulating eosinophils secrete macrophage migration inhibitory factor (MIF). Potential role in asthma. *J Clin Invest*. (1998) 101:2869–74. doi: 10.1172/JCI1524

7. Morand EF, Leech M, Bernhagen J. MIF: a new cytokine link between rheumatoid arthritis and atherosclerosis. *Nat Rev Drug Discov*. (2006) 5:399–411. doi: 10.1038/nrd2029

8. Yu C-M, Lau C-P, Lai KW-H, Huang X-R, Chen W-H, Lan HY. Elevation of plasma level of macrophage migration inhibitory factor in patients with acute myocardial infarction. *Am J Cardiol*. (2001) 88:774–7. doi: 10.1016/S0002-9149(01)01850-1

9. Omran AR. The epidemiologic transition: a theory of the epidemiology of population change: the epidemiologic transition. *Milbank Q*. (2005) 83:731–57. doi: 10.1111/j.1468-0009.2005.00398.x

10. Roth GA, Johnson C, Abajobir A, Abd-Allah F, Abera SF, Abyu G, et al. Global, regional, and national burden of cardiovascular diseases for 10 causes, 1990 to 2015. *J Am Coll Cardiol*. (2017) 70:1–25. doi: 10.1016/j.jacc.2017.04.052

11. World Health Organization. *Global Action Plan for the Prevention and Control of Noncommunicable Diseases 2013–2020*. Geneva: World Health Organization (2013). Available online at: https://apps.who.int/iris/handle/10665/94384 (accessed May 21, 2023).

12. Rodgers JL, Jones J, Bolleddu SI, Vanthenapalli S, Rodgers LE, Shah K, et al. Cardiovascular risks associated with gender and aging. *J Cardiovasc Dev Dis*. (2019) 6:19. doi: 10.3390/jcdd6020019

13. Hajar R. Risk factors for coronary artery disease: historical perspectives. *Heart Views*. (2017) 18:109–14. doi: 10.4103/HEARTVIEWS.HEARTVIEWS_106_17

14. Abdallah AM, Abu-Madi M. The genetic control of the rheumatic heart: closing the genotype-phenotype gap. *Front Med*. (2021) 8:611036. doi: 10.3389/fmed.2021.611036

15. Abdallah AM, Alnuzha A, Al-Mazroea AH, Eldardear AE, AlSamman AY, Almohammadi Y, et al. IL10 promoter polymorphisms are associated with rheumatic heart disease in Saudi Arabian patients. *Pediatr Cardiol*. (2016) 37:99–105. doi: 10.1007/s00246-015-1245-y

16. Bräuninger H, Krüger S, Bacmeister L, Nyström A, Eyerich K, Westermann D, et al. Matrix metalloproteinases in coronary artery disease and myocardial infarction. *Basic Res Cardiol*. (2023) 118:18. doi: 10.1007/s00395-023-00987-2

17. Andreou I, Antoniadis AP, Shishido K, Papafaklis MI, Koskinas KC, Chatzizisis YS, et al. How do we prevent the vulnerable atherosclerotic plaque from rupturing? Insights from in vivo assessments of plaque, vascular remodeling, and local endothelial shear stress. *J Cardiovasc Pharmacol Ther*. (2015) 20:261–75. doi: 10.1177/1074248414555005

18. Libby P. Inflammation during the life cycle of the atherosclerotic plaque. *Cardiovasc Res*. (2021) 117:2525–36. doi: 10.1093/cvr/cvab303

19. Amin MN, Siddiqui SA, Ibrahim M, Hakim ML, Ahammed MS, Kabir A, et al. Inflammatory cytokines in the pathogenesis of cardiovascular disease and cancer. *SAGE Open Med*. (2020) 8:2050312120965752. doi: 10.1177/2050312120965752

20. Tilstam PV, Qi D, Leng L, Young L, Bucala R. MIF family cytokines in cardiovascular diseases and prospects for precision-based therapeutics. *Expert Opin Ther Targets*. (2017) 21:671–83. doi: 10.1080/14728222.2017.1336227

21. Esumi N, Budarf M, Ciccarelli L, Sellinger B, Kozak CA, Wistow G. Conserved gene structure and genomic linkage for D-dopachrome tautomerase (DDT) and MIF. *Mamm Genome*. (1998) 9:753–7. doi: 10.1007/s003359900858

22. Calandra T, Roger T. Macrophage migration inhibitory factor: a regulator of innate immunity. *Nat Rev Immunol*. (2003) 3:791–800. doi: 10.1038/nri1200

23. Leng L, Siu E, Bucala R. Genotyping two promoter polymorphisms in the MIF gene: a -794 CATT5-8 microsatellite repeat and a -173 G/C SNP. *Methods Mol Biol*. (2020) 2080:67–84. doi: 10.1007/978-1-4939-9936-1_7

24. Du X, Li R, Song S, Ma L, Xue H. The role of MIF-173G/C gene polymorphism in the susceptibility of autoimmune diseases. *Mediat Inflamm*. (2020) 2020:7825072. doi: 10.1155/2020/7825072

25. Karakaya B, van Moorsel CHM, van der Helm-van Mil AHM, Huizinga TWJ, Ruven HJT, van der Vis JJ, et al. Macrophage migration inhibitory factor (MIF) -173 polymorphism is associated with clinical erythema nodosum in Löfgren's syndrome. *Cytokine*. (2014) 69:272–6. doi: 10.1016/j.cyto.2014.05.020

26. Tilstam PV, Schulte W, Holowka T, Kim B-S, Nouws J, Sauler M, et al. MIF but not MIF-2 recruits inflammatory macrophages in an experimental polymicrobial sepsis model. *J Clin Invest*. (2021) 131:e127171. doi: 10.1172/JCI127171

27. Kong Y-Z, Chen Q, Lan H-Y. Macrophage migration inhibitory factor (MIF) as a stress molecule in renal inflammation. *Int J Mol Sci*. (2022) 23:4908. doi: 10.3390/ijms23094908

28. Chen S, Yu Q, Song Y, Cui Z, Li M, Mei C, et al. Inhibition of macrophage migration inhibitory factor (MIF) suppresses apoptosis signal-regulating kinase 1 to protect against liver ischemia/reperfusion injury. *Front Pharmacol*. (2022) 13:951906. doi: 10.3389/fphar.2022.951906

29. Basile MS, Battaglia G, Bruno V, Mangano K, Fagone P, Petralia MC, et al. The dichotomic role of macrophage migration inhibitory factor in neurodegeneration. *Int J Mol Sci*. (2020) 21:3023. doi: 10.3390/ijms21083023

30. Page MJ, Moher D, Bossuyt PM, Boutron I, Hoffmann TC, Mulrow CD, et al. PRISMA 2020 explanation and elaboration: updated guidance and exemplars for reporting systematic reviews. *Br Med J*. (2021) 372:n160. doi: 10.1136/bmj.n160

31. Qian L, Yin R. Macrophage migration inhibitory factor promoter polymorphisms (-173G/C): relationship with coronary atherosclerotic disease subjects. *J Med Res*. (2018) (12):32–5.

32. Idouz K, Drighil A, Naour O, Moundir C, Hakeem MA, Ali Bah R, et al. Protective role of macrophage migration inhibitory factor −173 G > C (rs755622) gene polymorphism in pediatric patients with dilated cardiomyopathy. *Gene Rep*. (2019) 16:100455. doi: 10.1016/j.genrep.2019.100455

33. El-Mahdy RI, Saleem TH, Essam OM, Algowhary M. Functional variants in the promoter region of macrophage migration inhibitory factor rs755622 gene (MIF G173C) among patients with heart failure: association with echocardiographic indices and disease severity. *Heart Lung*. (2021) 50:92–100. doi: 10.1016/j.hrtlng.2020.07.015

34. Abdallah AM, Al-Mazroea AH, Al-Harbi WN, Al-Harbi NA, Eldardear AE, Almohammadi Y, et al. Impact of MIF gene promoter variations on risk of rheumatic heart disease and its age of onset in Saudi Arabian patients. *Front Immunol*. (2016) 7:98. doi: 10.3389/fimmu.2016.00098

35. Simonini G, Corinaldesi E, Falcini F, Massai C, De Martino M, Cimaz R. Macrophage migration inhibitory factor gene polymorphisms in an Italian cohort of patients with Kawasaki disease. *Pediatr Rheumatol*. (2008) 6:1. doi: 10.1186/1546-0096-6-S1-P256

36. Tereshchenko IP, Petrkova J, Mrazek F, Lukl J, Maksimov VN, Romaschenko AG, et al. The macrophage migration inhibitory factor (MIF) gene polymorphism in Czech and Russian patients with myocardial infarction. *Clin Chim Acta*. (2009) 402:199–202. doi: 10.1016/j.cca.2008.12.034

37. Luo J-Y, Xu R, Li X-M, Zhou Y, Zhao Q, Liu F, et al. MIF Gene polymorphism rs755622 is associated with coronary artery disease and severity of coronary lesions in a Chinese Kazakh population: a case–control study. *Medicine (Baltimore)*. (2016) 95: e2617. doi: 10.1097/MD.0000000000002617

38. Ji K, Wang X, Li J, Lu Q, Wang G, Xue Y, et al. Macrophage migration inhibitory factor polymorphism is associated with susceptibility to inflammatory coronary heart disease. *BioMed Res Int*. (2015) 2015:1–6. doi: 10.1155/2015/315174

39. Luo J-Y, Fang B-B, Du G-L, Liu F, Li Y-H, Tian T, et al. Association between MIF gene promoter rs755622 and susceptibility to coronary artery disease and inflammatory cytokines in the Chinese han population. *Sci Rep*. (2021) 11:8050. doi: 10.1038/s41598-021-87580-6

40. Du G-L, Luo J-Y, Wang D, Li Y-H, Fang B-B, Li X-M, et al. MIF gene rs755622 polymorphism positively associated with acute coronary syndrome in Chinese Han population: case–control study. *Sci Rep*. (2020) 10:140. doi: 10.1038/s41598-019-56949-z

41. Zhang J-Y, Zhao Q, Liu F, Li D-Y, Men L, Luo J-Y, et al. Genetic variation of migration inhibitory factor gene rs2070766 is associated with acute coronary syndromes in Chinese population. *Front Genet*. (2022) 12:750975. doi: 10.3389/fgene.2021.750975

42. Li D-Y, Zhang J-Y, Chen Q-J, Liu F, Zhao Q, Gao X-M, et al. MIF -173G/C (rs755622) polymorphism modulates coronary artery disease risk: evidence from a systematic meta-analysis. *BMC Cardiovasc Disord*. (2020) 20:300. doi: 10.1186/s12872-020-01564-4

43. Tziastoudi M, Pissas G, Raptis G, Cholevas C, Eleftheriadis T, Dounousi E, et al. A systematic review and meta-analysis of pharmacogenetic studies in patients with chronic kidney disease. *IJMS*. (2021) 22:4480. doi: 10.3390/ijms22094480

44. Bae S-C, Lee YH. Circulating macrophage migration inhibitory factor levels and its polymorphisms in systemic lupus erythematosus: a meta-analysis. *Cell Mol Biol (Noisy-le-grand)*. (2017) 63:74–9. doi: 10.14715/cmb/2017.63.10.12

45. Schelemei P, Wagner E, Picard FSR, Winkels H. Macrophage mediators and mechanisms in cardiovascular disease. *FASEB J*. (2024) 38:e23424. doi: 10.1096/fj.202302001R

46. Burger-Kentischer A, Göbel H, Kleemann R, Zernecke A, Bucala R, Leng L, et al. Reduction of the aortic inflammatory response in spontaneous atherosclerosis by blockade of macrophage migration inhibitory factor (MIF). *Atherosclerosis*. (2006) 184:28–38. doi: 10.1016/j.atherosclerosis.2005.03.028

47. Yan Y, Thakur M, Van Der Vorst EPC, Weber C, Döring Y. Targeting the chemokine network in atherosclerosis. *Atherosclerosis*. (2021) 330:95–106. doi: 10.1016/j.atherosclerosis.2021.06.912

48. Leberzammer J, Von Hundelshausen P. Chemokines, molecular drivers of thromboinflammation and immunothrombosis. *Front Immunol*. (2023) 14:1276353. doi: 10.3389/fimmu.2023.1276353

49. Brandhofer M, Hoffmann A, Blanchet X, Siminkovitch E, Rohlfing A-K, El Bounkari O, et al. Heterocomplexes between the atypical chemokine MIF and the CXC-motif chemokine CXCL4L1 regulate inflammation and thrombus formation. *Cell Mol Life Sci*. (2022) 79:512. doi: 10.1007/s00018-022-04539-0

50. Li B, Li W, Li X, Zhou H. Inflammation: a novel therapeutic target/direction in atherosclerosis. *CPD*. (2017) 23:1216–27. doi: 10.2174/1381612822666161230142931

51. Dayawansa NH, Gao X-M, White DA, Dart AM, Du X-J. Role of MIF in myocardial ischaemia and infarction: insight from recent clinical and experimental findings. *Clin Sci*. (2014) 127:149–61. doi: 10.1042/CS20130828

52. Das R, Subrahmanyan L, Yang IV, van Duin D, Levy R, Piecychna M, et al. Functional polymorphisms in the gene encoding macrophage migration inhibitory factor are associated with gram-negative bacteremia in older adults. *J Infect Dis*. (2014) 209:764–8. doi: 10.1093/infdis/jit571

53. Lehmann LE, Book M, Hartmann W, Weber SU, Schewe J-C, Klaschik S, et al. A MIF haplotype is associated with the outcome of patients with severe sepsis: a case control study. *J Transl Med*. (2009) 7:100. doi: 10.1186/1479-5876-7-100

54. Ma H, Wang J, Thomas DP, Tong C, Leng L, Wang W, et al. Impaired macrophage migration inhibitory factor–AMP-activated protein kinase activation and ischemic recovery in the senescent heart. *Circulation*. (2010) 122:282–92. doi: 10.1161/CIRCULATIONAHA.110.953208

55. Herder C, Illig T, Baumert J, Müller M, Klopp N, Khuseyinova N, et al. Macrophage migration inhibitory factor (MIF) and risk for coronary heart disease: results from the MONICA/KORA Augsburg case-cohort study, 1984–2002. *Atherosclerosis*. (2008) 200:380–8. doi: 10.1016/j.atherosclerosis.2007.12.025

56. Benedek G, Meza-Romero R, Jordan K, Zhang Y, Nguyen H, Kent G, et al. MIF and D-DT are potential disease severity modifiers in male MS subjects. *Proc Natl Acad Sci USA*. (2017) 114:E8421–9. doi: 10.1073/pnas.1712288114

57. Swoboda C, Deloch L, von Zimmermann C, Richter-Schmidinger T, Lenz B, Kornhuber J, et al. Macrophage migration inhibitory factor in major depressive disorder: a multilevel pilot study. *Int J Mol Sci*. (2022) 23:15460. doi: 10.3390/ijms232415460

58. Hamidi AK, Arzaghi SM, Qorbani M, Khatami F, Ebrahimi M, Bandarian F, et al. MIF 173 G > C variation was associated with depressive disorder in type 2 diabetes in an Iranian population. *Psychoneuroendocrinology*. (2019) 104:243–8. doi: 10.1016/j.psyneuen.2019.03.011

Frontiers in
Cardiovascular Medicine

Innovations and improvements in cardiovascular treatment and practice

Focuses on research that challenges the status quo of cardiovascular care, or facilitates the translation of advances into new therapies and diagnostic tools.

Discover the latest Research Topics

See more →

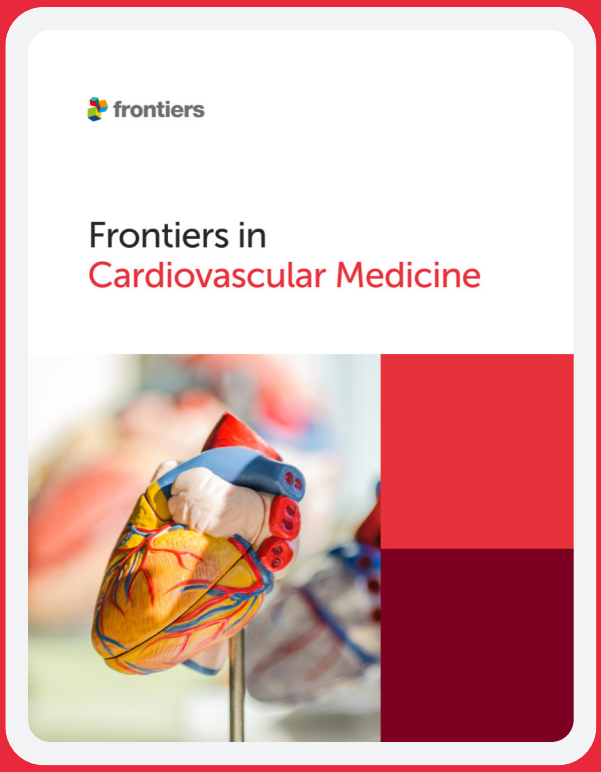

Frontiers

Avenue du Tribunal-Fédéral 34
1005 Lausanne, Switzerland
frontiersin.org

Contact us

+41 (0)21 510 17 00
frontiersin.org/about/contact